Anillo ACT 172099

Registro Fósil y Evolución de Vertebrados

Paleontología de Vertebrados

Origen de las Aves Y Neornithes

Sergio Soto Acuña
Paleontólogo de Vertebrados

Red Paleontológica U-Chile, Laboratorio de Ontogenia y Filogenia, Facultad de Ciencias, Universidad de Chile: sesotacu@ug.uchile.cl

Clase Aves

Las Aves son Reptiles

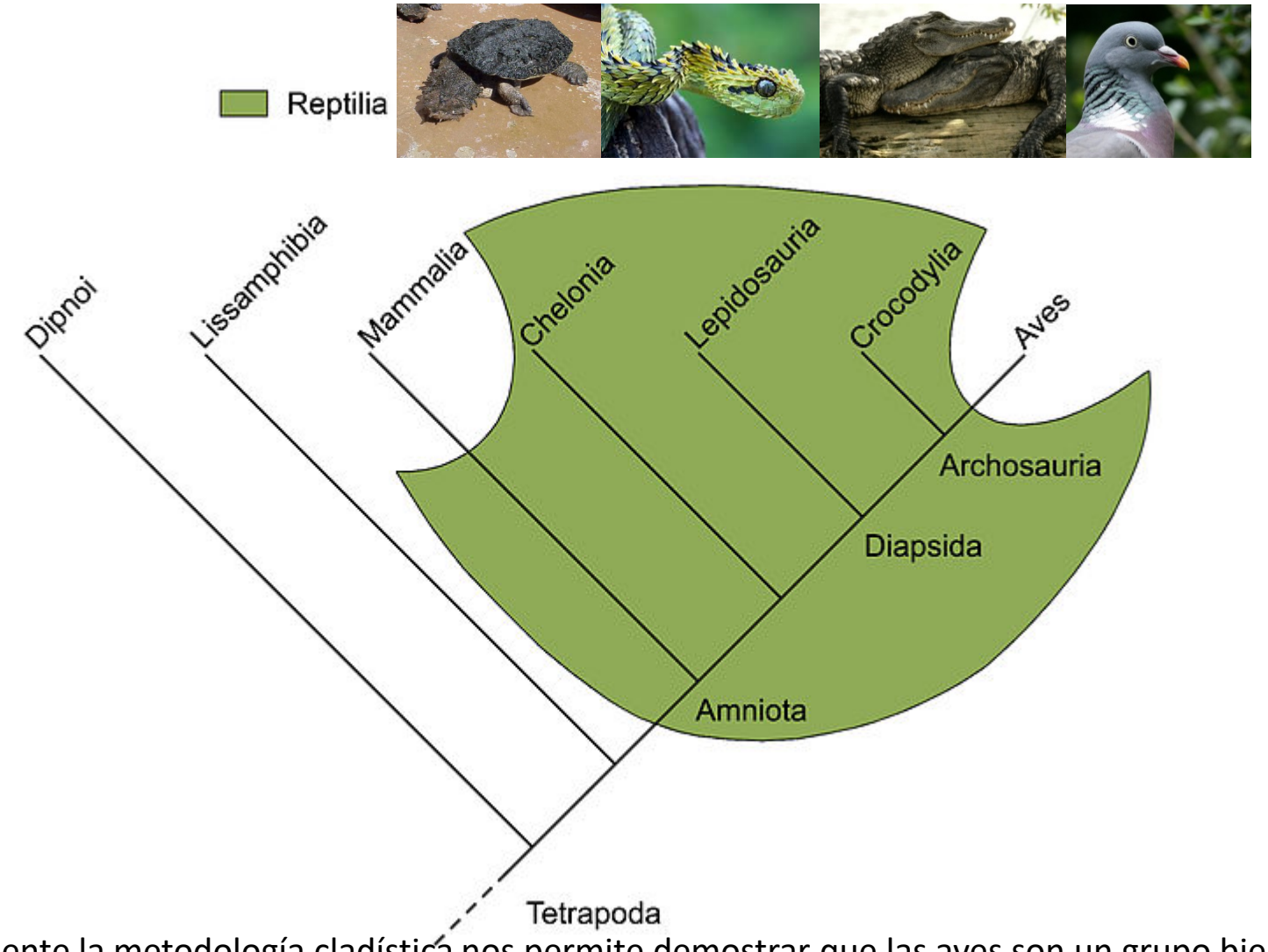

Actualmente la metodología cladística nos permite demostrar que las aves son un grupo bien anidado dentro de los reptiles.

Archosauria

Definición:

Clado que incluye al ancestro común más reciente entre cocodrilos y aves, más todos sus descendientes.

Archosauria

Definición:

Clado que incluye al ancestro común más reciente entre cocodrilos y aves, más todos sus descendientes.

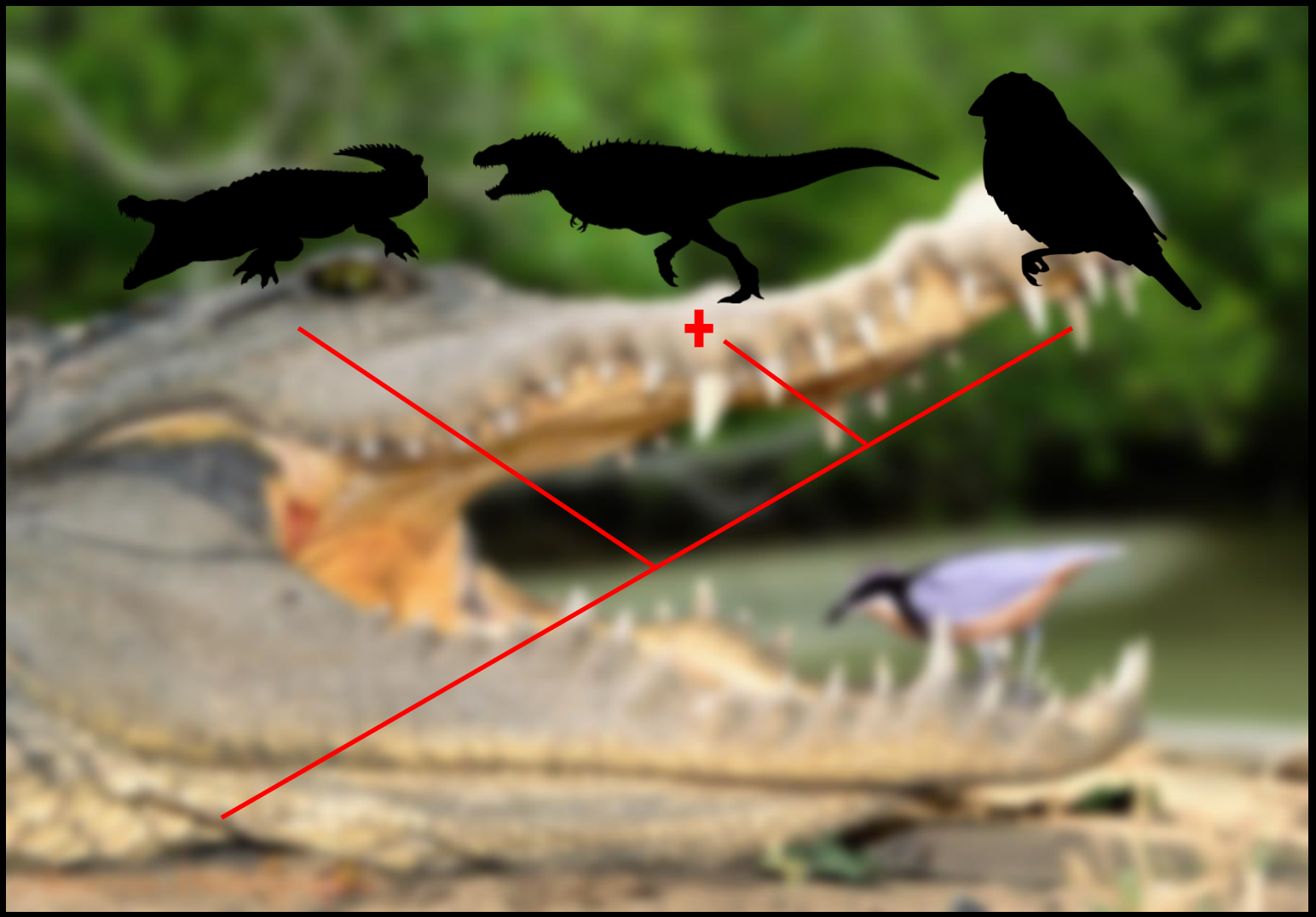

Dinosauria

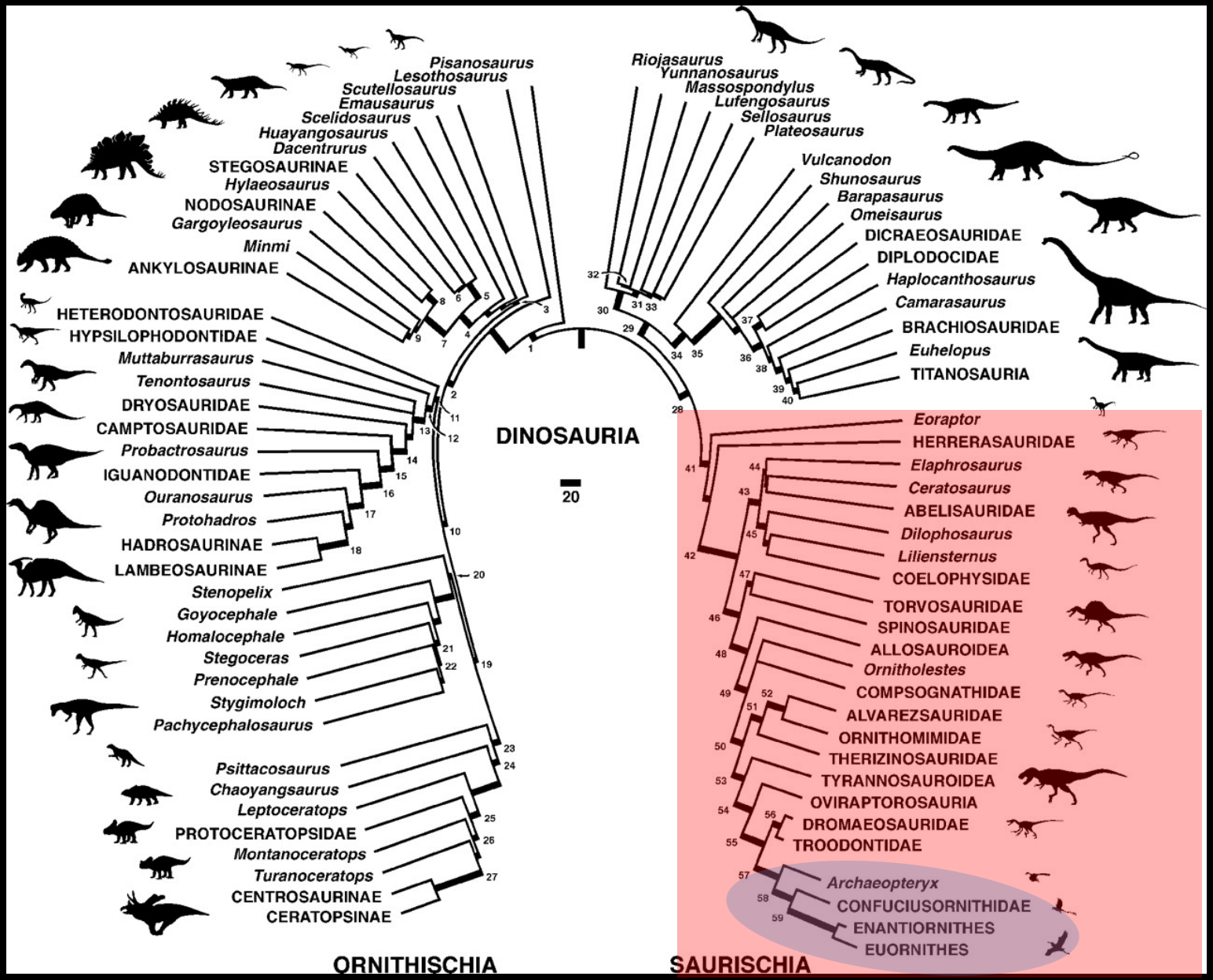

Sereno 1999

Aves: Dinosaurios vivientes

El esqueleto de las aves modernas (Neornithes) ha sufrido una serie de modificaciones respecto a la condición ancestral presente en dinosaurios terópodos. El esqueleto poscraneal se caracteriza por presentar una serie de fusiones y/o pérdida de elementos óseos en porciones del esqueleto axial y apendicular en el fenotipo adulto (Baumel y Witmer, 1993), lo que en algunos casos dificulta la homología entre estos huesos con otros amniotas (Burke y Feduccia, 1997; Martin et al., 1980).

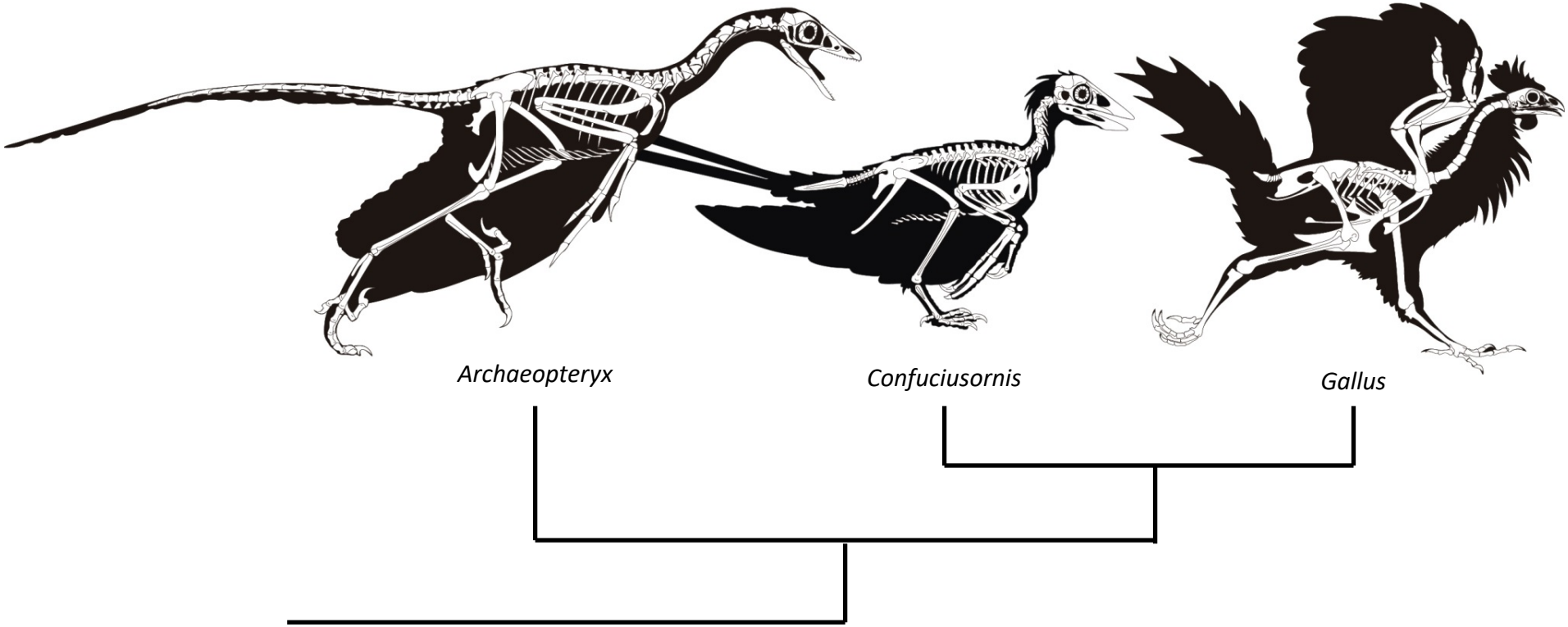

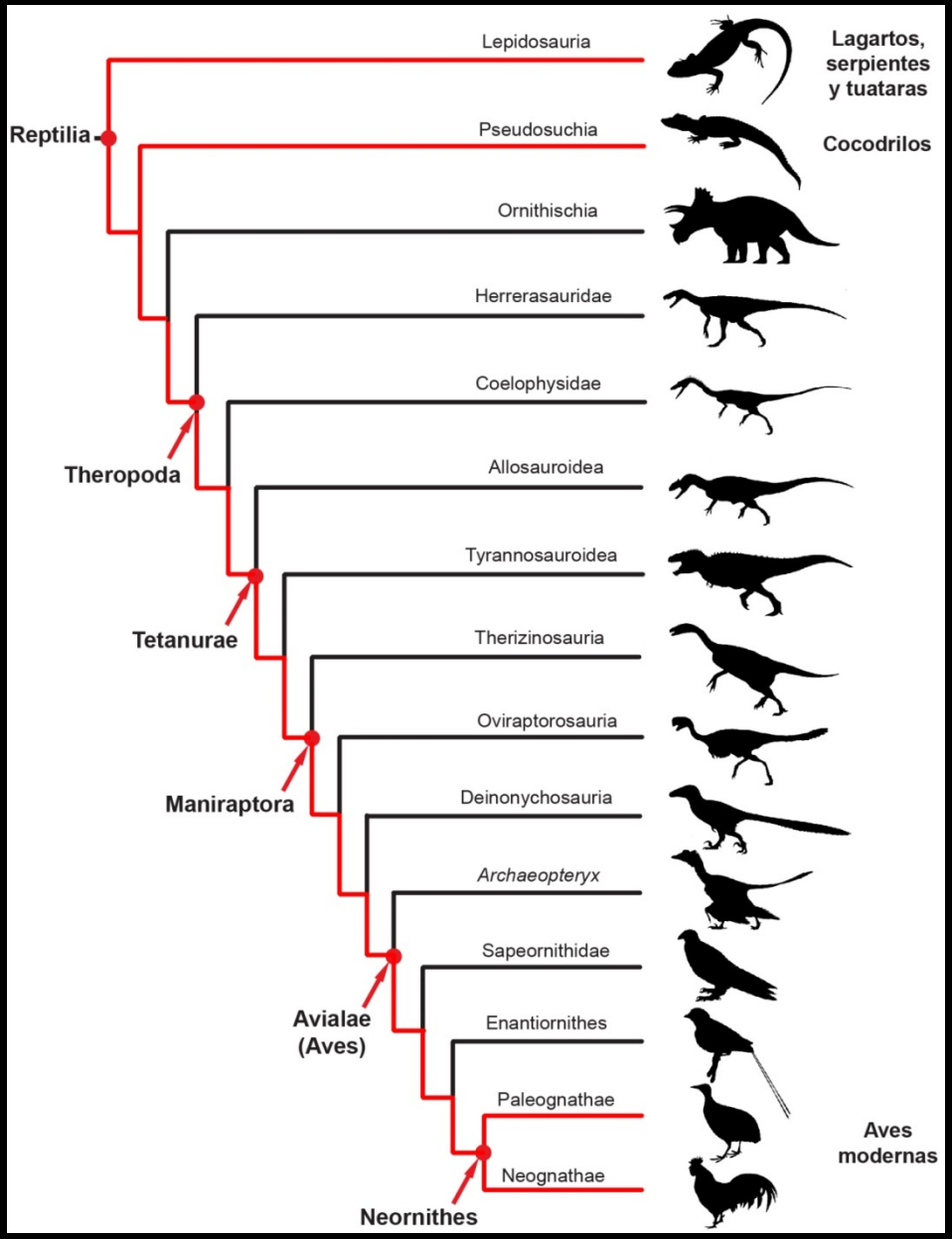
Lepidosauria
Lagartos, serpientes y tuataras
Reptilia
Pseudosuchia
Cocodrilos
Ornithischia
Herrerasauridae
Coelophysidae
Theropoda
Allosauroidea
Tyrannosauroidea
Tetanurae
Therizinosauria
Oviraptorosauria
Maniraptora
Deinonychosauria
Archaeopteryx
Sapeornithidae
Avialae (Aves)
Enantiornithes
Paleognathae
Aves modernas
Neognathae
Neornithes

Pero..¿Qué es un ave?

***Archaeopteryx*, la primera ave**

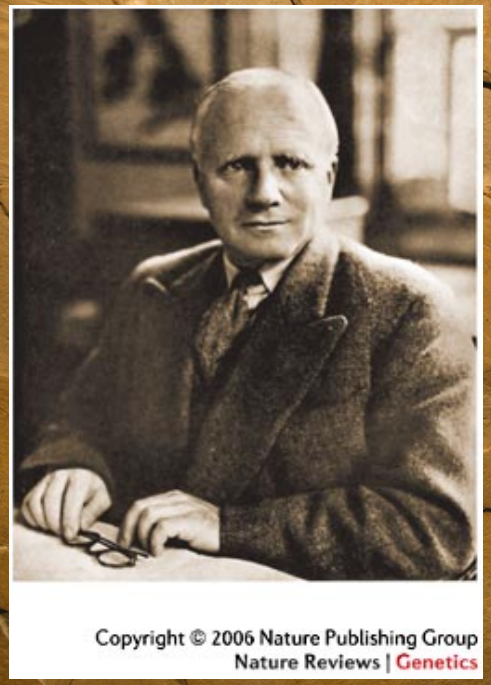

Gavin de Beer

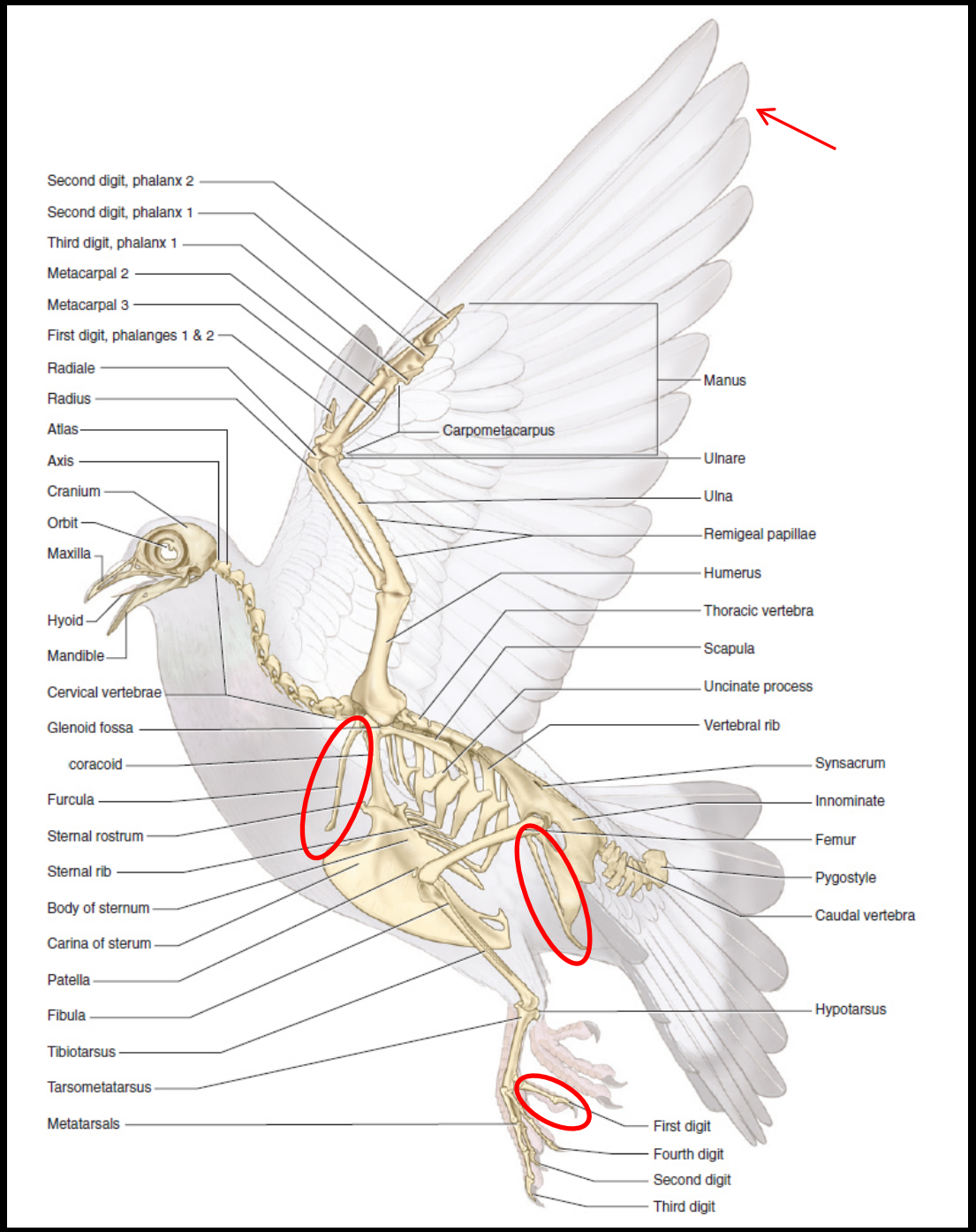

Fúrcula, el hueso de la suerte

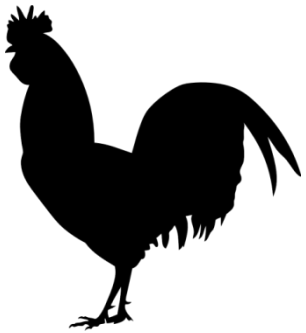

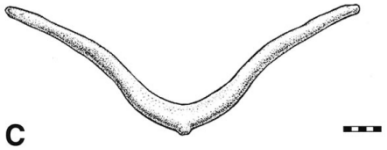

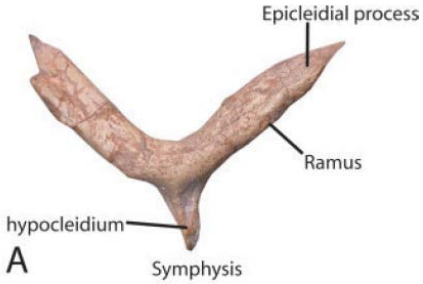

Coelophysis

Oviraptor

Archaeopteryx

Gansus

Origen y evolución de la Fúrcula

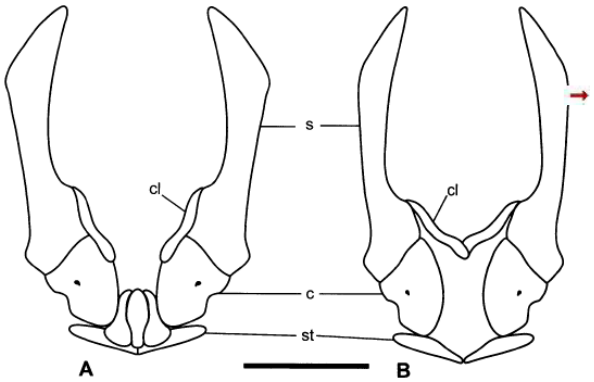

FIGURE 2. Reconstructions of the pectoral girdle of *Plateosaurus engelhardti* in anterior view. **A**, non-bracing model, redrawn from Paul (1987). **B**, preferred reconstruction based on BP/1/5241. **Abbreviations**: see Fig 1. Note that there is little evidence for the episternal elements in shown in A, and they are omitted from our reconstruction. Scale bar equals 20 cm.

Yates y Vasconcelos, 2005

Figure 5. Alleged left clavicle from the ornithischian dinosaur *Leptoceratops gracilis* (Canadian Museum of Nature [NMC] 8889) in two views. Various ornithischian and sauropodomorphan dinosaurs are reported to have clavicle-like elements as components of the pectoral apparatus. However, the identification of these elements remains ambiguous. See text for details. Scale bar, 20 mm.

Vickaryous y Hall 2009

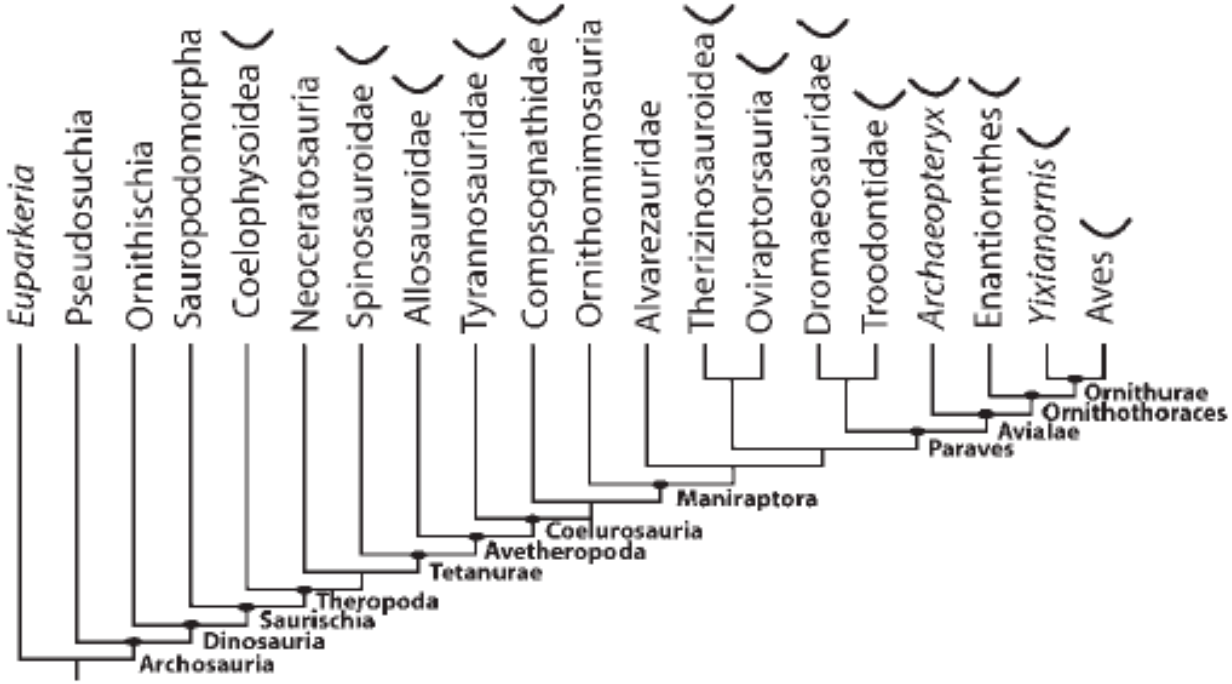

Nesbitt et al., 2009

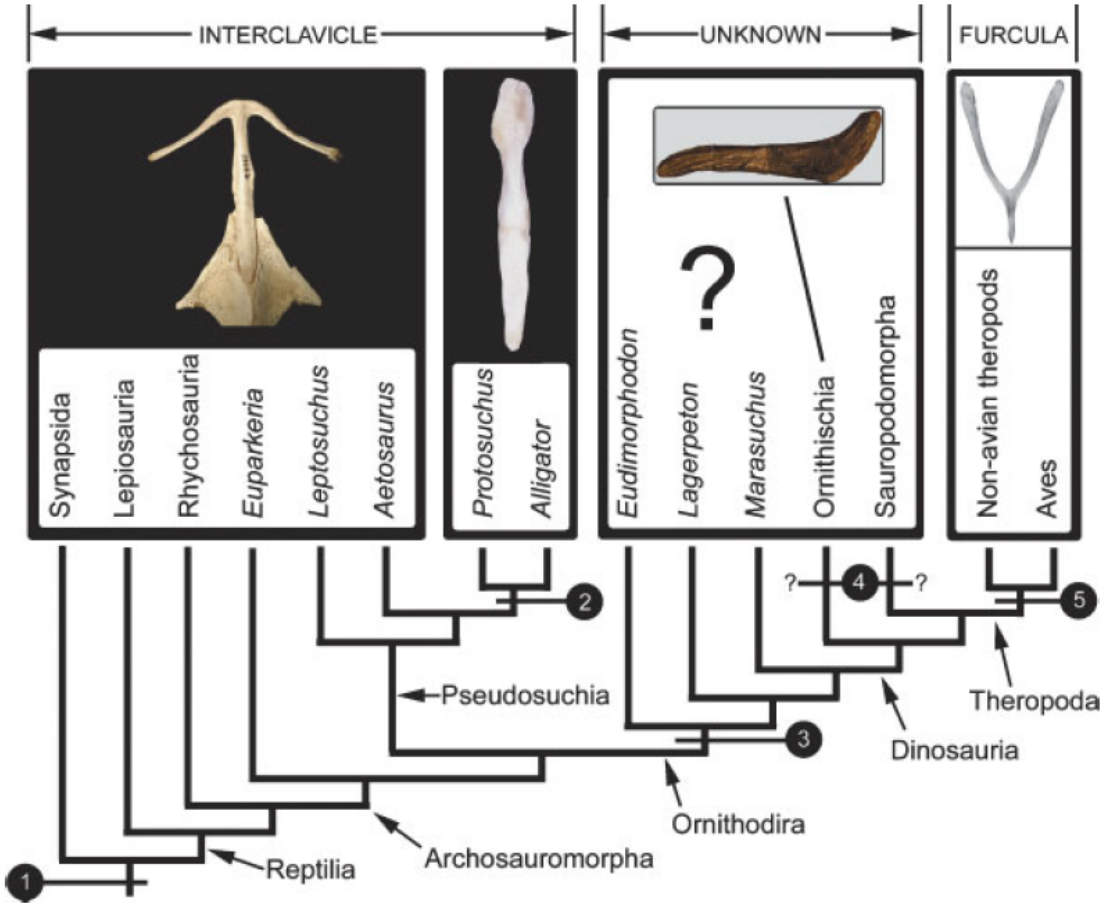

Figure 4. Phylogenetic distribution of the interclavicle and furcula. Amniote phylogeny based on the work of Hill (2005) and Irmis et al. (2007). Nodes: (1) An unpaired, mid-ventrally positioned interclavicle with lateral processes is plesiomorphic for crown-group amniotes (e.g., *Varanus komodoensis*); (2) Among deeply nested pseudosuchian archosauromorphs, the lateral processes are lost yielding a flattened bar-like element (e.g., *Alligator mississippiensis*); (3) The pectoral apparatus of basal ornithodirans is incompletely known, and it remains unclear which if any mid-ventral dermal element was present; (4) Among some ornithischian and sauropodomorph dinosaurs, paired bar-like pectoral elements have been reported (e.g., *Leptoceratops gracilis*; Canadian Museum of Nature [NMC] 8889). Although previously interpreted as clavicles, the identity of these elements is herein considered equivocal; (5) In theropods, the mid-ventral position of the pectoral apparatus is occupied by a chevron or "Y"-shaped furcula (e.g., *Gallus gallus*).

Vickaryous y Hall 2009

Persistencia de Interclavicular en dinosaurios?

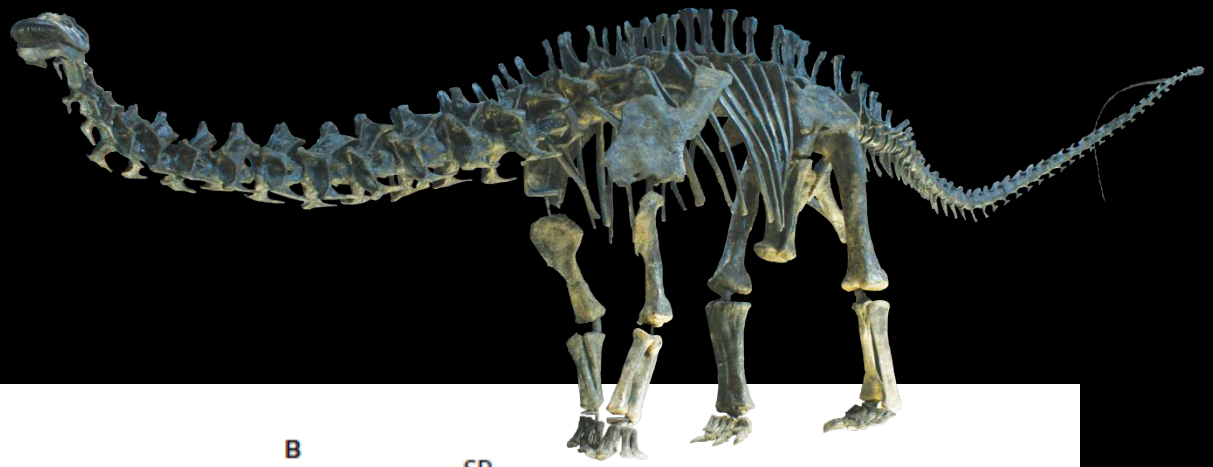

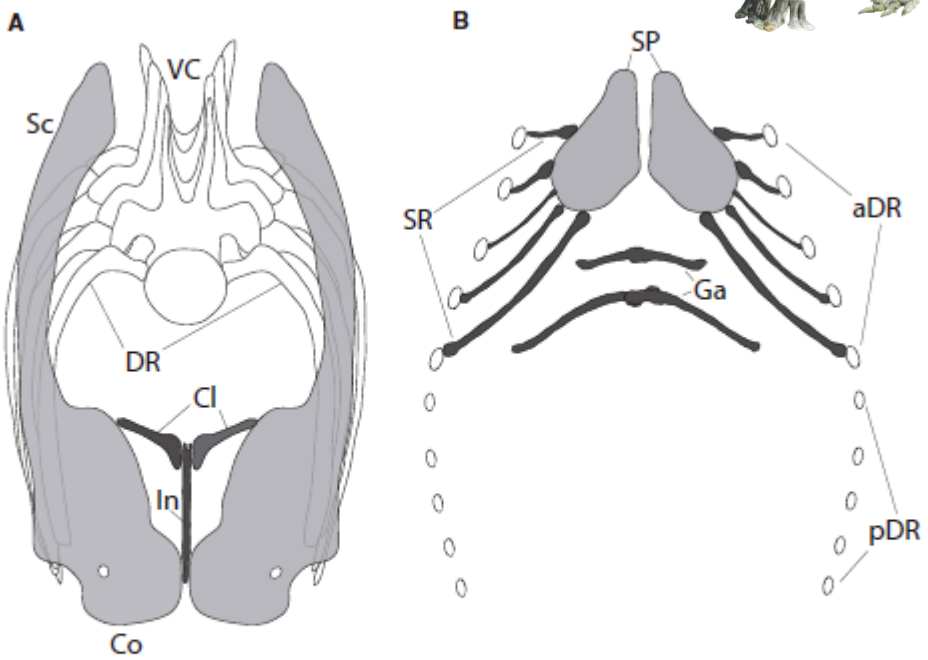

Fig. 12 Reconstruction of the pectoral girdle and the chest region of an indeterminate diplodocid sauropod, based on the finds reported. Light grey elements represent pectoral girdle elements not discussed in the paper, dark grey elements mark the bones identified as chest bone morphotypes in this paper. Anterior (a) and ventral (b) view. Abbreviations: aDR, anterior dorsal ribs; Cl, clavicle (morphotype B); Co, coracoid; DR, dorsal rib; Ga, gastralia (morphotype D); In, interclavicle (morphotype A); pDR, posterior dorsal ribs; Sc, scapula; SP, sternal plates; SR, sternal ribs (morphotypes C and E); VC, vertebral column. Modified from Schwarz et al. (2007a; a) and Filla & Redman (1994; b).

Tschopp & Mateus, 2012

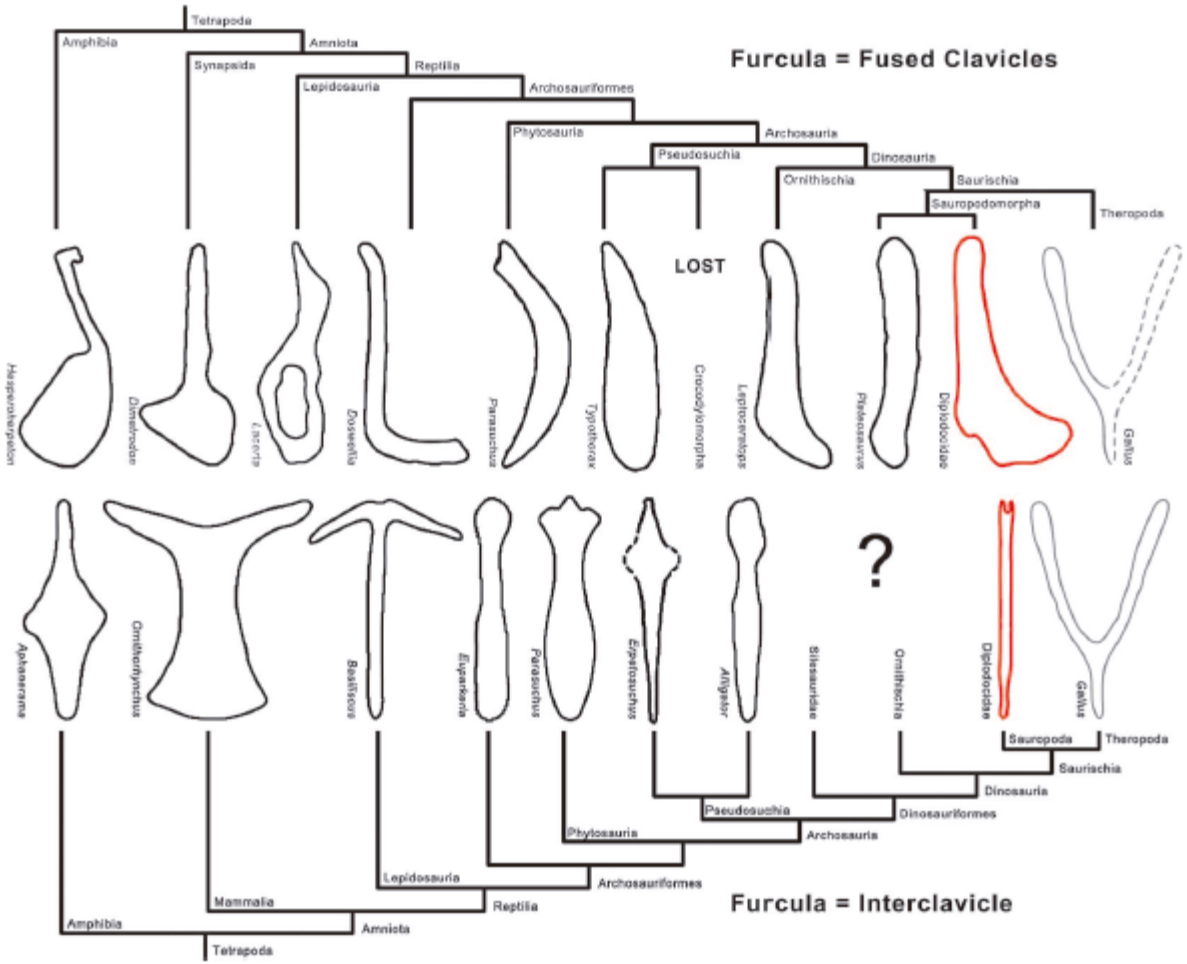

Fig. 13 Evolution of the furcula, comparison between the two hypotheses. Note the gap within Dinosauriformes in the furcula-interclavicle hypothesis. Line drawings scaled to same size. Eaton & Stewart (1960: *Hesperoherpeton*); Chatterjee (1978: *Parasuchus*); Klima (1987: *Ornithorhynchus*); Rieppel (1992: *Lacerta*); Steyer et al. (2000: *Aphanerama*); Benton & Walker (2002: *Erpetosuchus*); Martz (2002: *Typothorax*); Vickaryous & Hall (2006: Dimetrodon; 2010: *Alligator, Basilicus, Gallus, Leptoceratops*); Remes (2008: *Euparkeria*); Dilkes & Sues (2009: *Doswellia*).

Tschopp & Mateus, 2012

Origen del Hallux (Dígito Perchador)

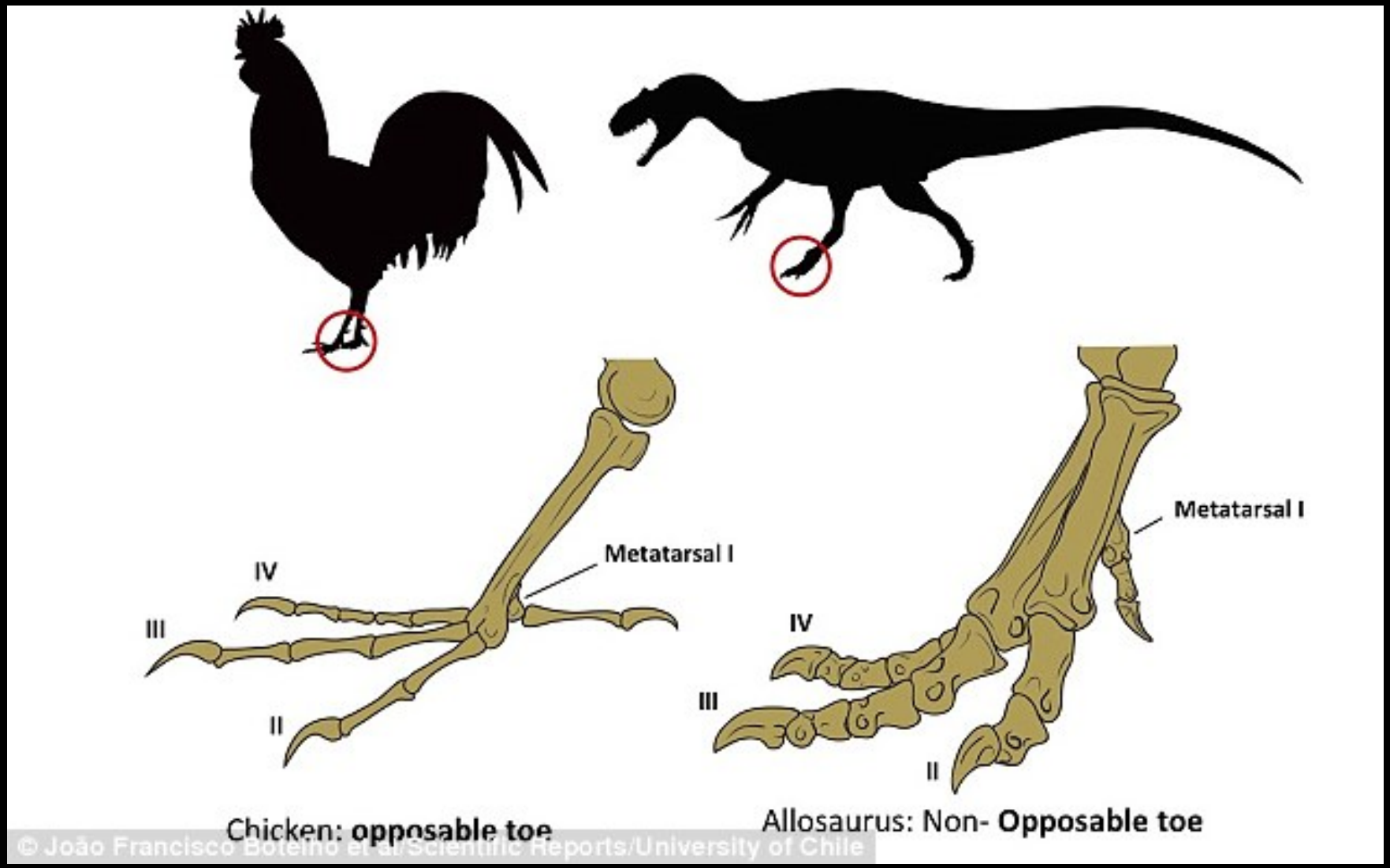

Origen del Hallux (Dígito Perchador)

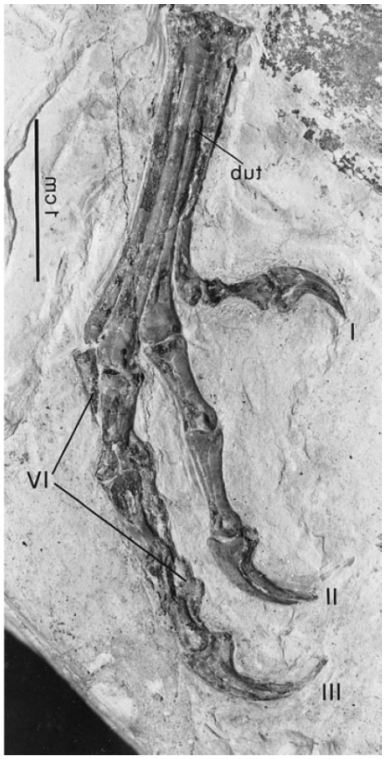

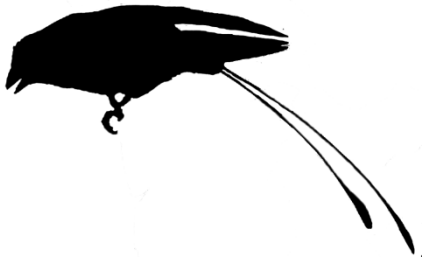

Epidendrosaurus

Archaeopteryx

Confuciusornis

Posición distal del Dígito Perchador

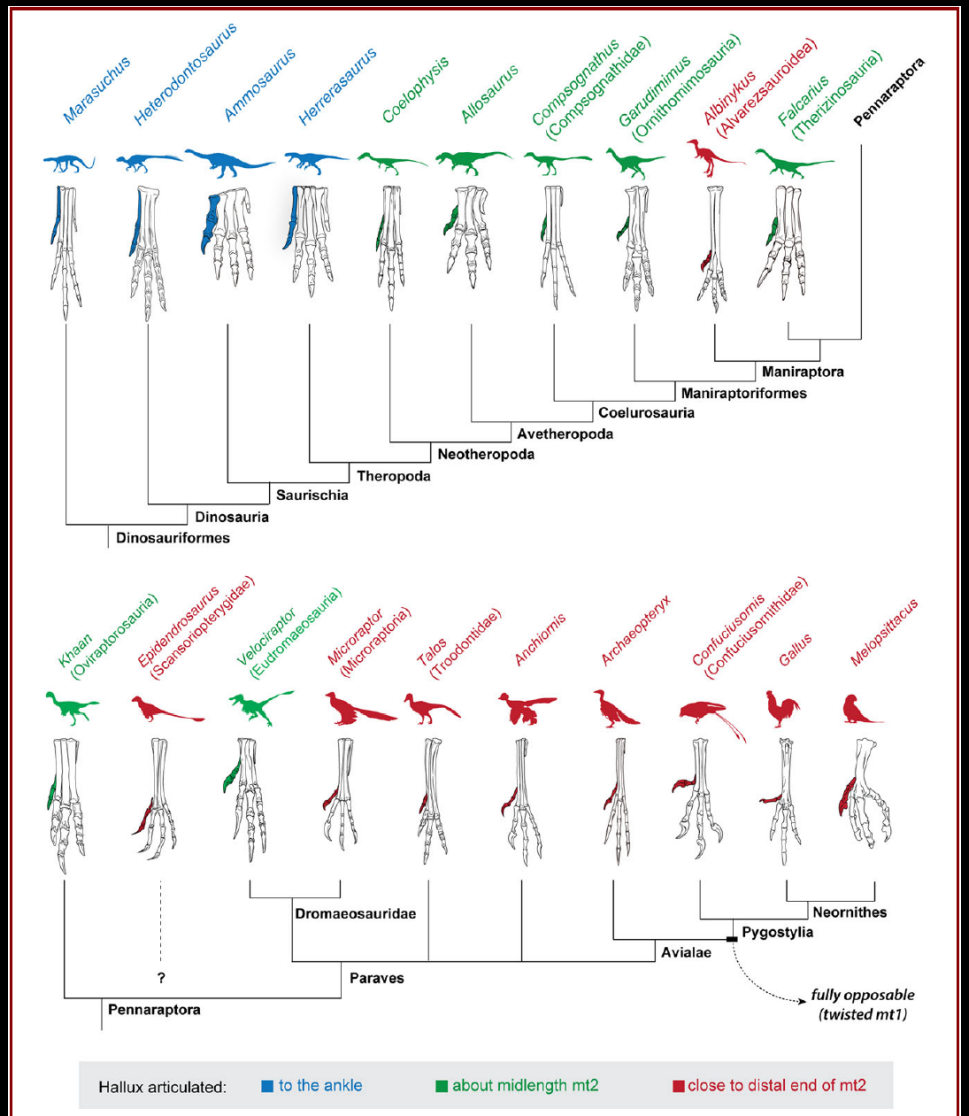

Figure 5. The evolution of hallux position in theropods. The ancestral state for Dinosauria is a hallux shorter than other toes, but proximally connected to distal tarsals (blue). In Neotheropoda, mt1 reduced, losing its proximal epiphysis, and articulated at the mid-shaft position of mt2 in non-Maniraptora (green). In several Maniraptora clades (such as Alvarezsauridae, Troodontidae, *Anchiornis*, Avialae, and some Dromaeosauridae), mt1 articulates closer to the distal end of mt2 (red).

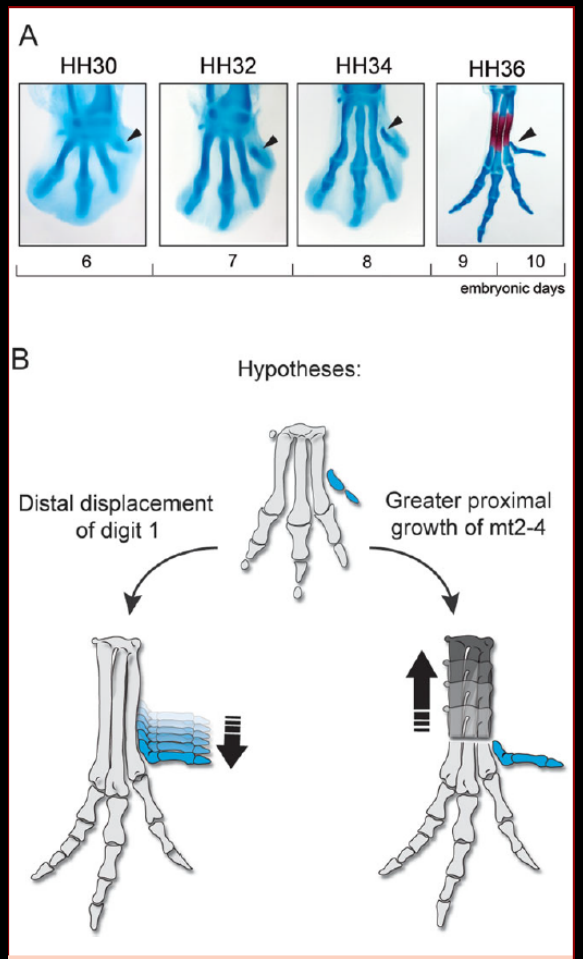

Figure 1. The development of digit 1 position in birds. (A) Embryonic development of the chicken foot shows a proximally placed mt1 at HH30 (day 6 of incubation), at about mid-length of mt2 between HH32 and HH34 (days 7 and 8), and reaching its final distal position at HH36 (day 10). (B) Two hypotheses are proposed for the development of the distal position of the hallux: either the hallux moves to a more distal position, or mt2-4 grow more towards proximal, creating the illusion that the hallux moves toward distal.

Boteho et al., 2016

Torsión del Dígito Perchador

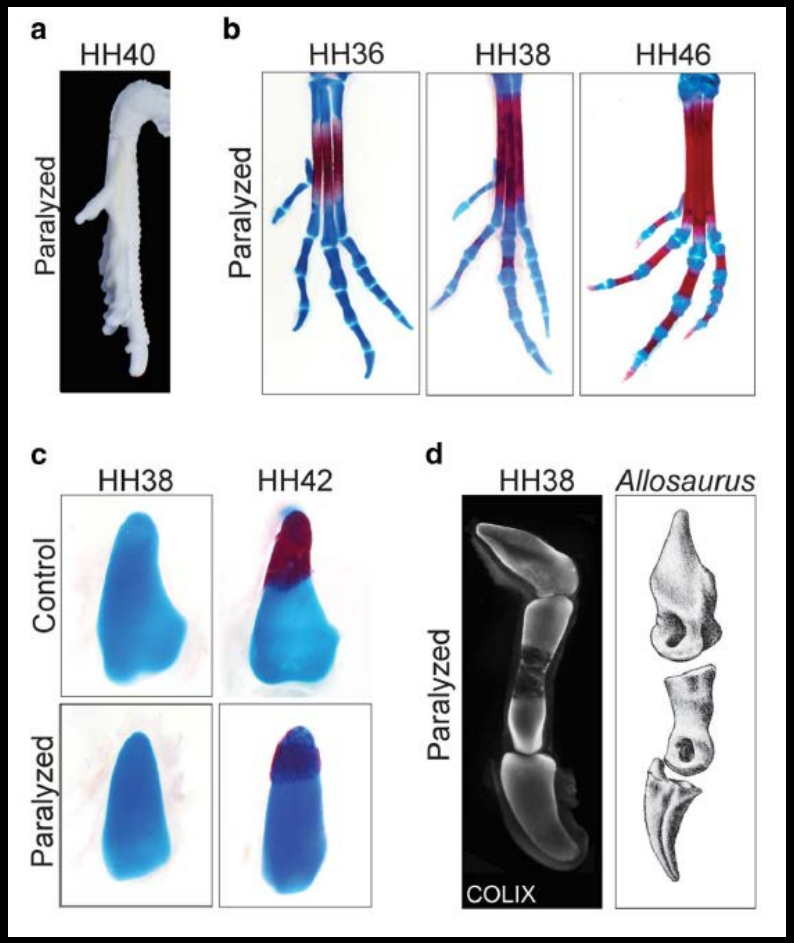

Figure 6. Paralyzed embryos fail to develop an opposable hallux: (**a**) Paralyzed chicken embryos at HH40 showing the maintenance of the medial orientation of the hallux; (**b**) Paralyzed chicken embryos exhibit the hallux articulated to the ventral Mt2 but not opposable; (**c**) Mt1 of paralyzed chicken embryos are straight, as opposed to control embryos; (**d**) Mt1 of paralyzed embryos at HH38 immunostained for COLIX resembles the non-twisted Mt1 of early tetanuran dinosaurs, as *Allosaurus*. (See SI, Movie 2).

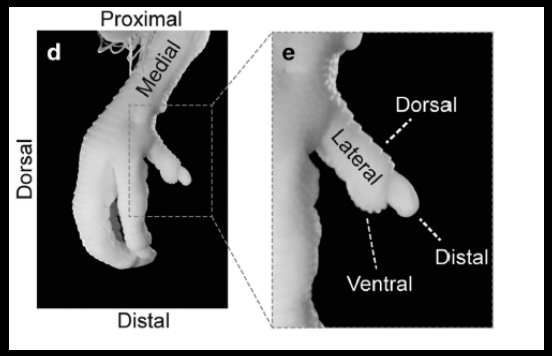

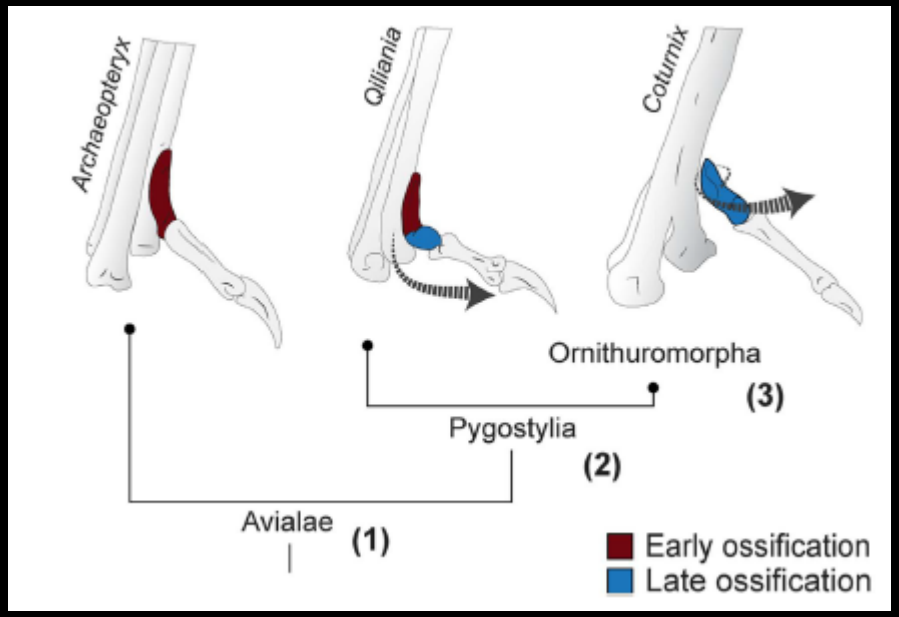

Figure 7. The evolutionary transition to a twisted Mt1. In Intermediate forms like the early short-tailed *Quiliania*, Mt1 has a non-twisted proximal end, but an offset ("bent") distal end (arrow). Because Mt1 in modern birds matures from proximal to distal, we suggest that in (**1**) non-Pygostylian birds, Mt1 would have matured before the onset of muscular activity; (**2**) Maturation of Mt1 was delayed in pygostylia, allowing its distal bending by embryonic muscular activity; (**3**) Ornithuromorpha further delayed maturation of Mt1, allowing full torsion of its long axis by embryonic muscular activity.

Boteho et al., 2015

Retroversión del Pubis

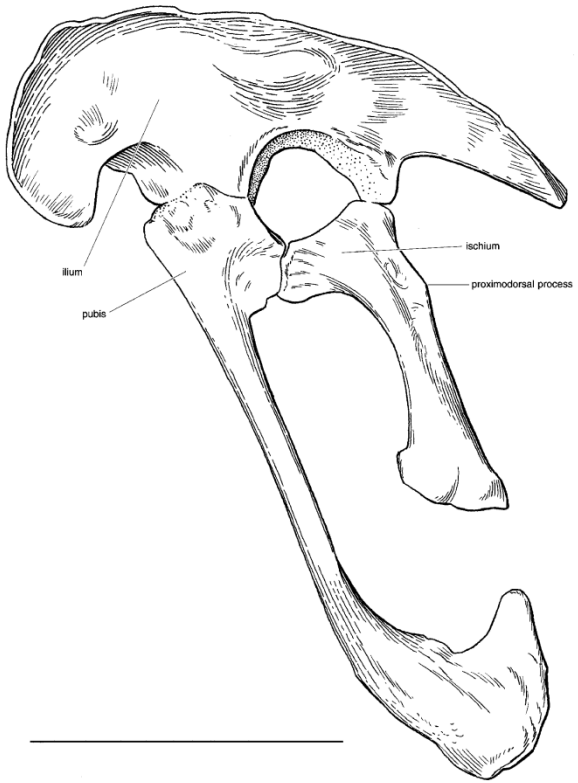

Figure 4. *Bambiraptor feinbergi* n. gen. and n. sp., holotype (FIP 001), pelvic girdle in lateral view. Scale bar: 5 cm (new).

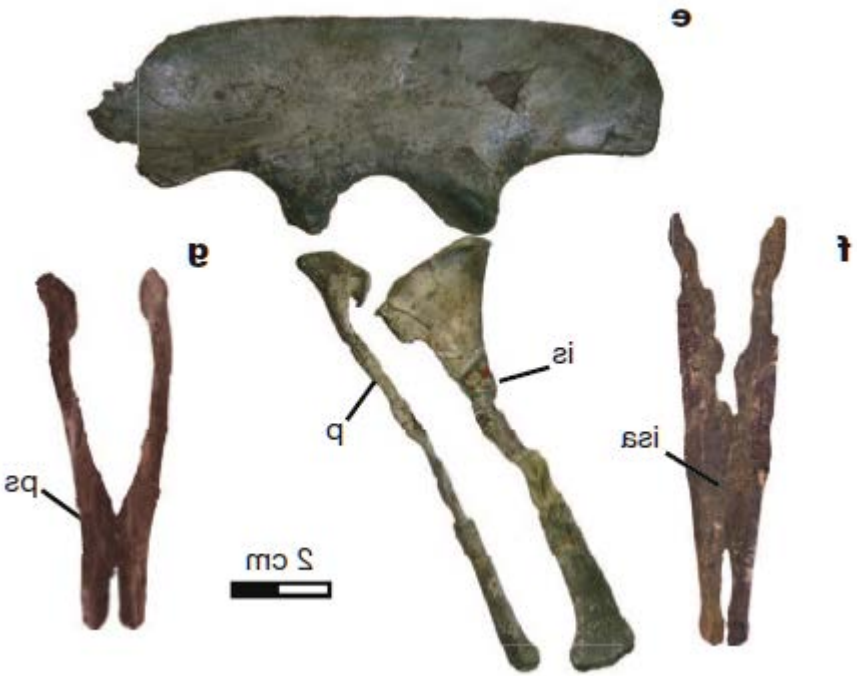

Bambiraptor

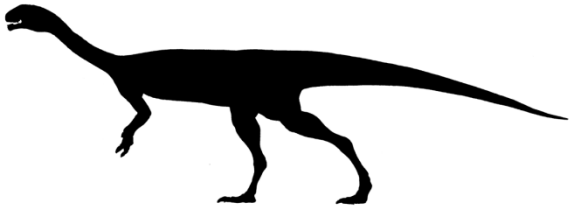

Chilesaurus

Integumento: presencia de protoplumas y plumas

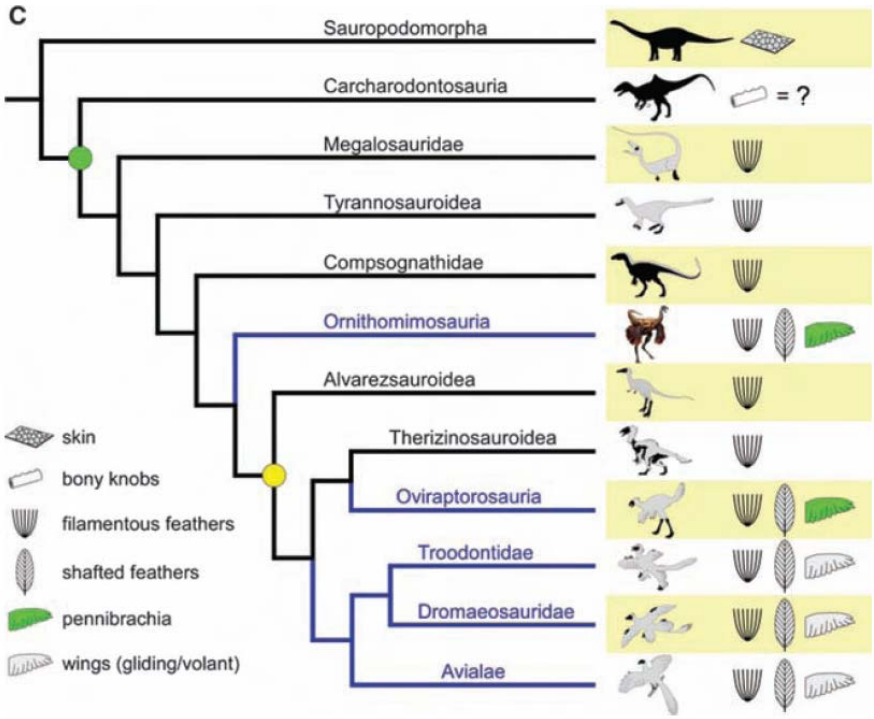

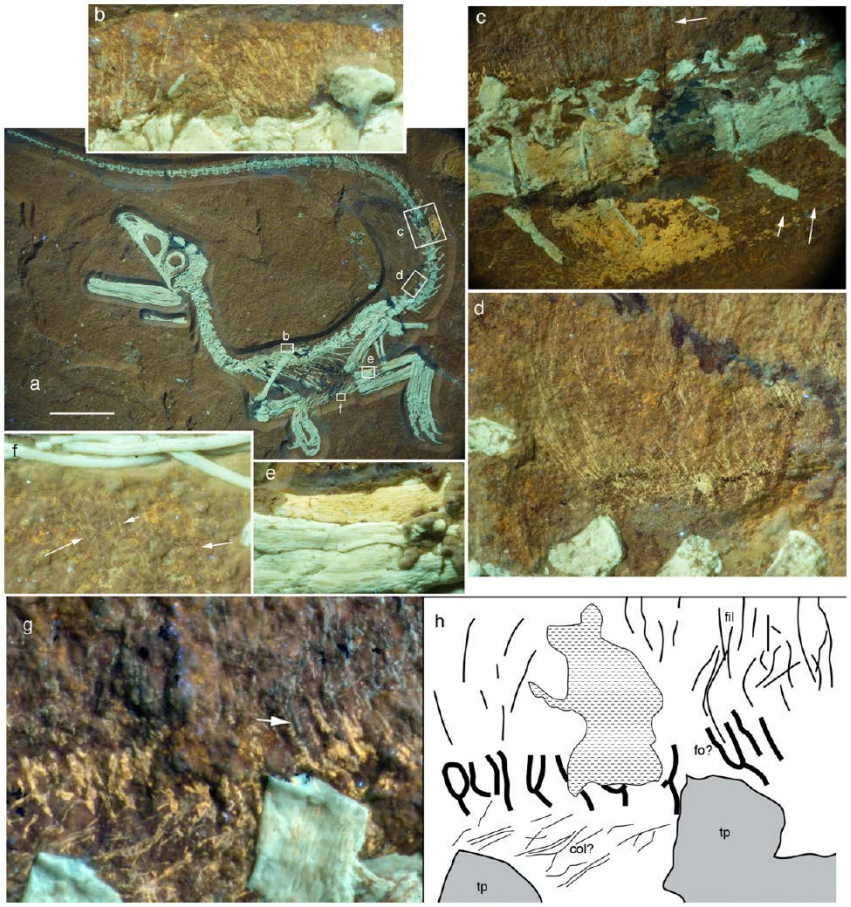

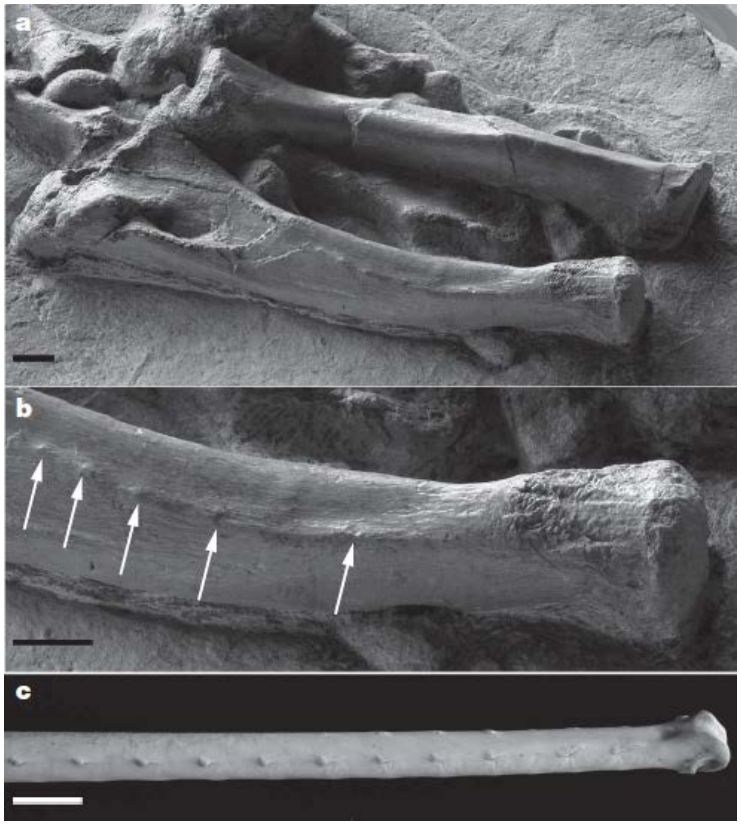

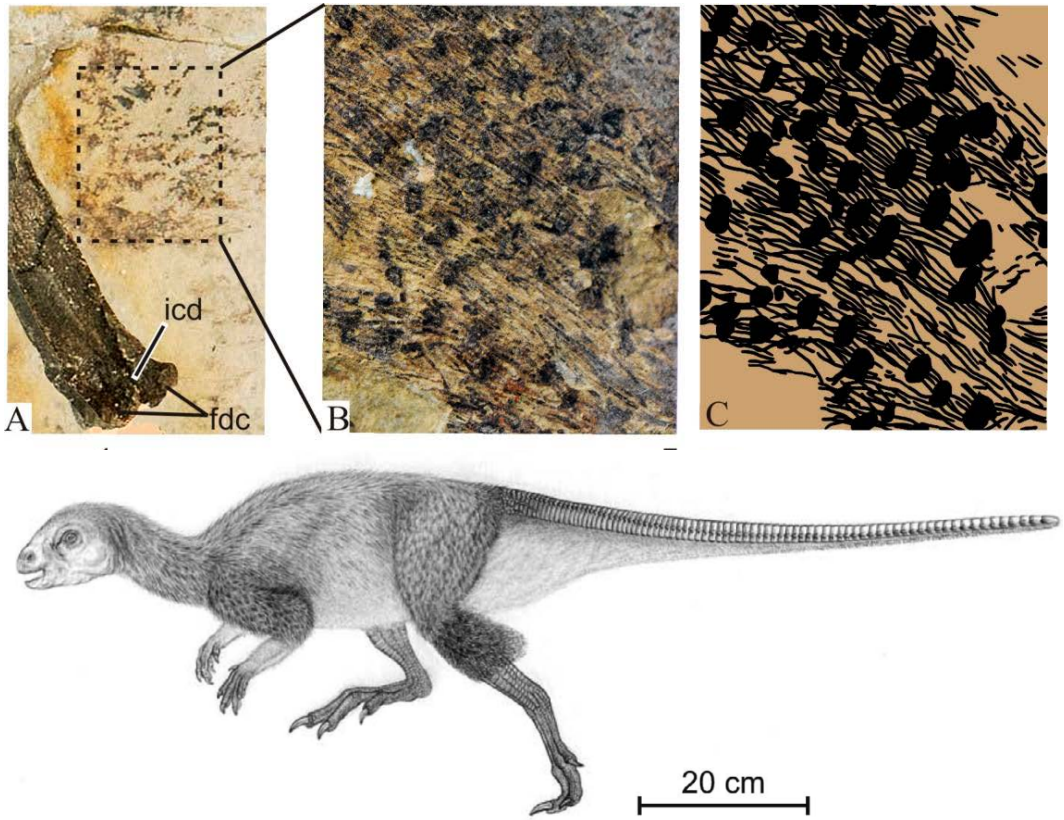

Concavenator

Kulindadromeus

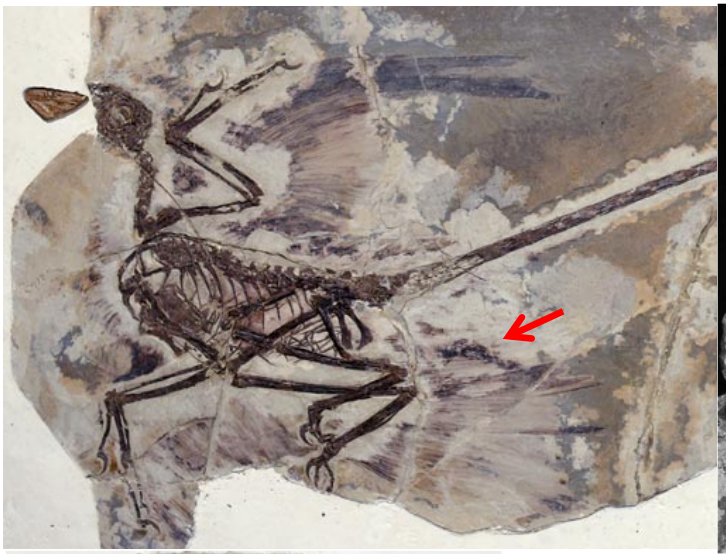


a

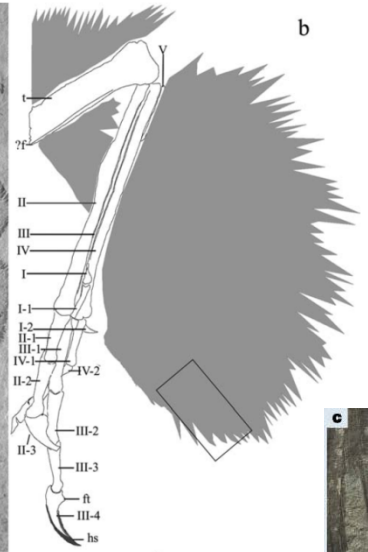
b
y
t
?f
II
III
IV
I
I-1
I-2
II-1
III-1
IV-1
IV-2
II-2
III-2
II-3
III-3
ft
III-4
hs

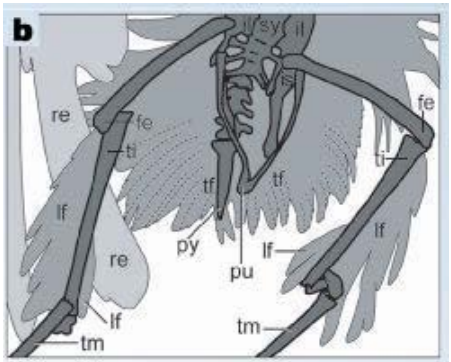
b
sy
il
re
fe
ti
tf
tf
ti
fe
lf
lf
lf
re
py
pu
tm
lf
tm

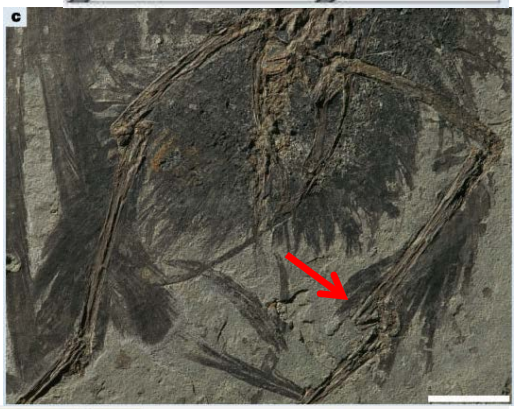
c

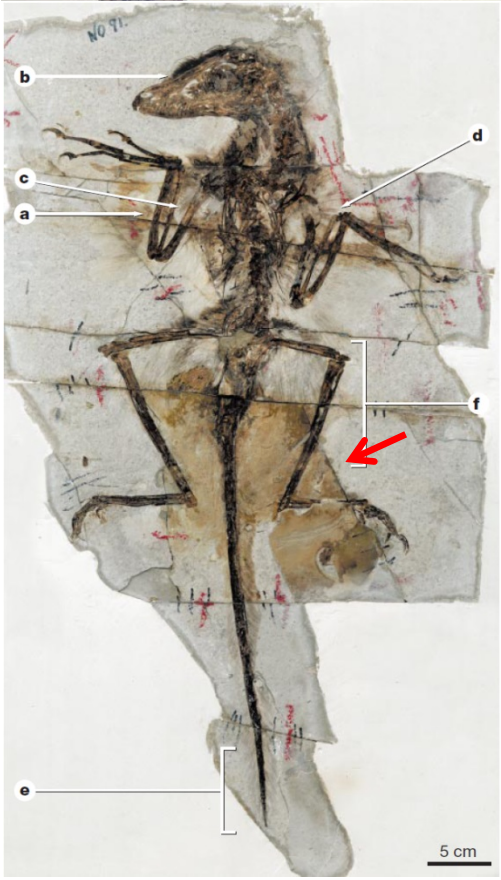
b
d
c
a
f
e
5 cm

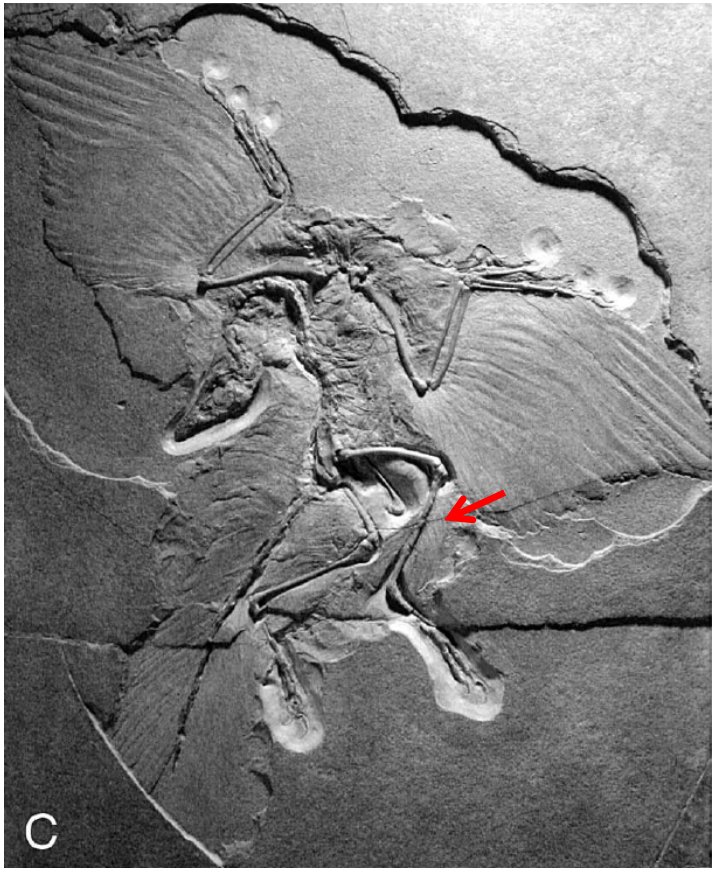
C

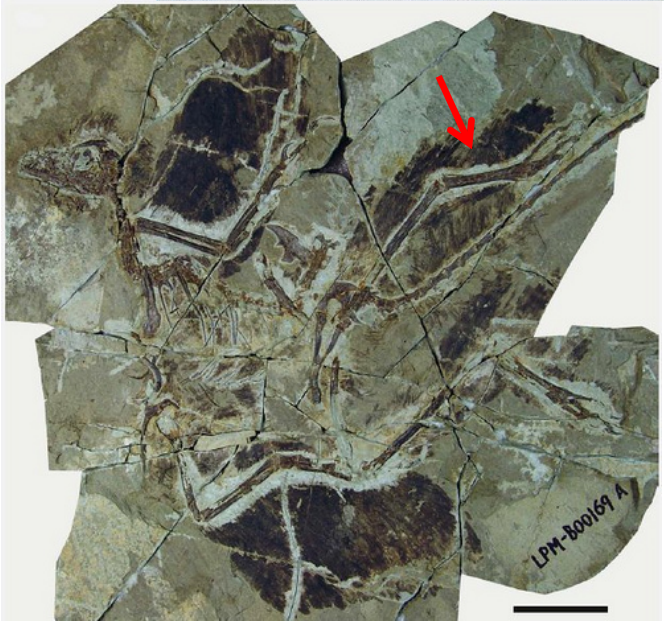
LPM-B00169 A

Alometría en el miembro anterior: ¿Origen del ala?

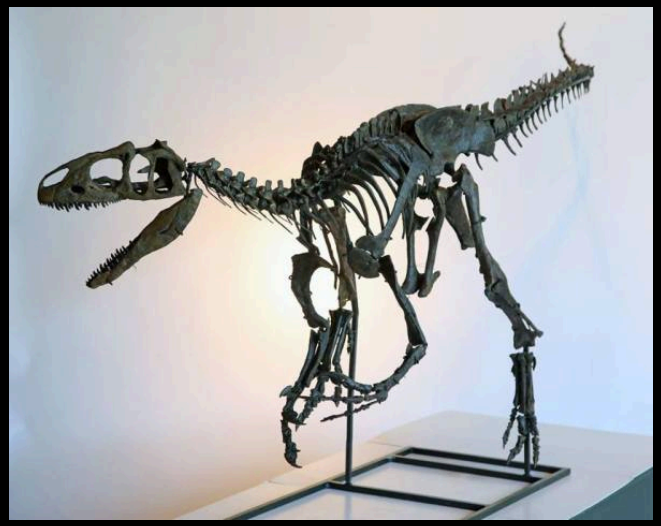

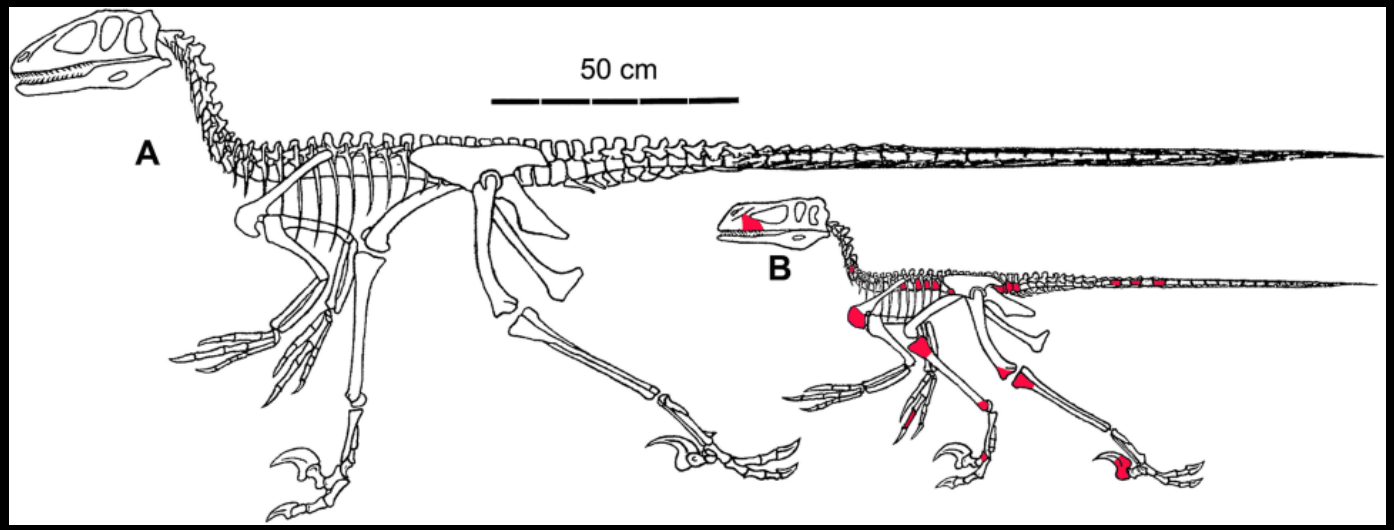

Parsons & Parsons, 2015

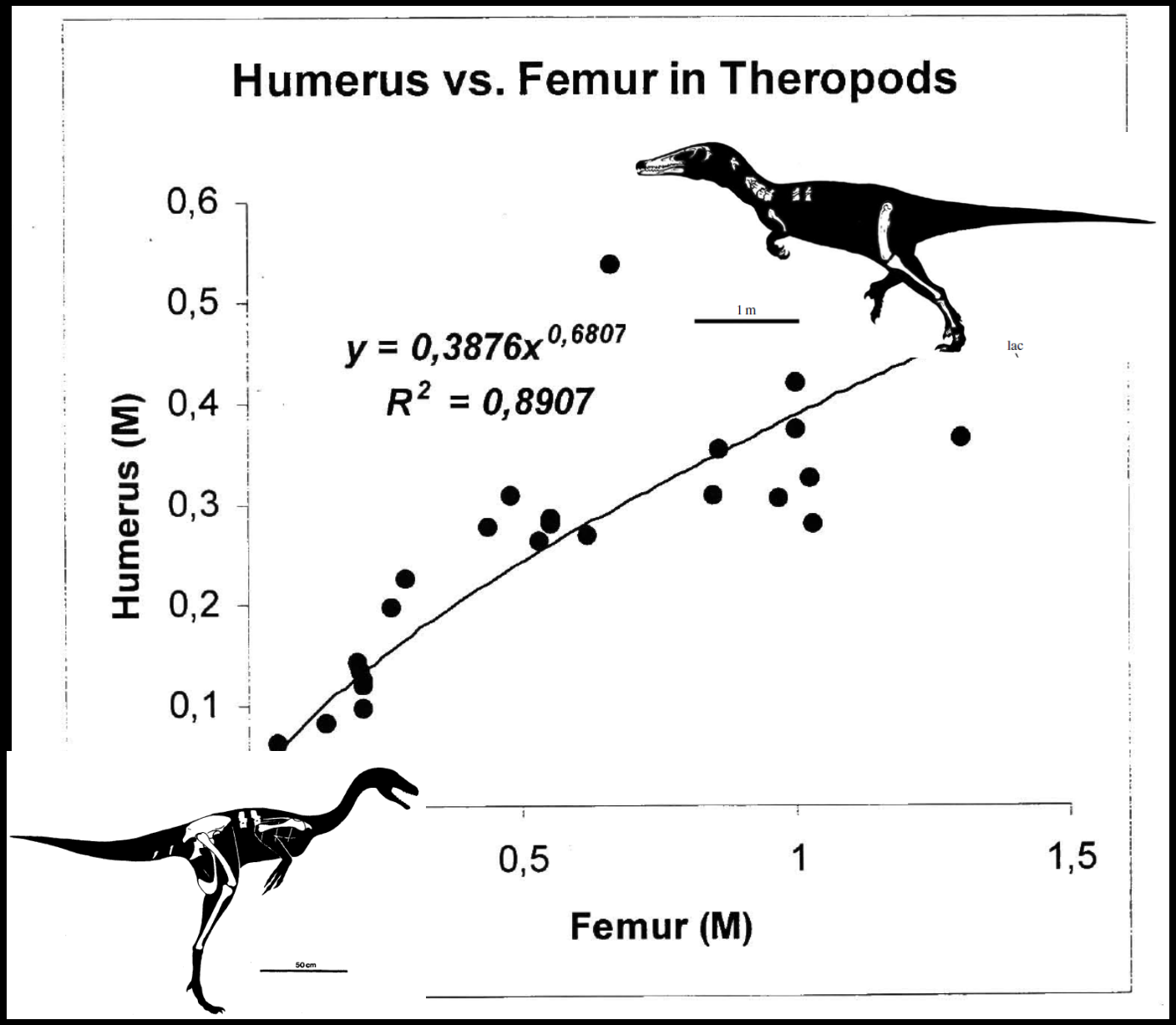
Humerus vs. Femur in Theropods
0,6
0,5
0,4
0,3
0,2
0,1
Humerus (M)
y = 0,3876x^0,6807
R^2 = 0,8907
1 m
lac
0,5
1
1,5
Femur (M)
50 cm

Vargas, 1999

Paraves

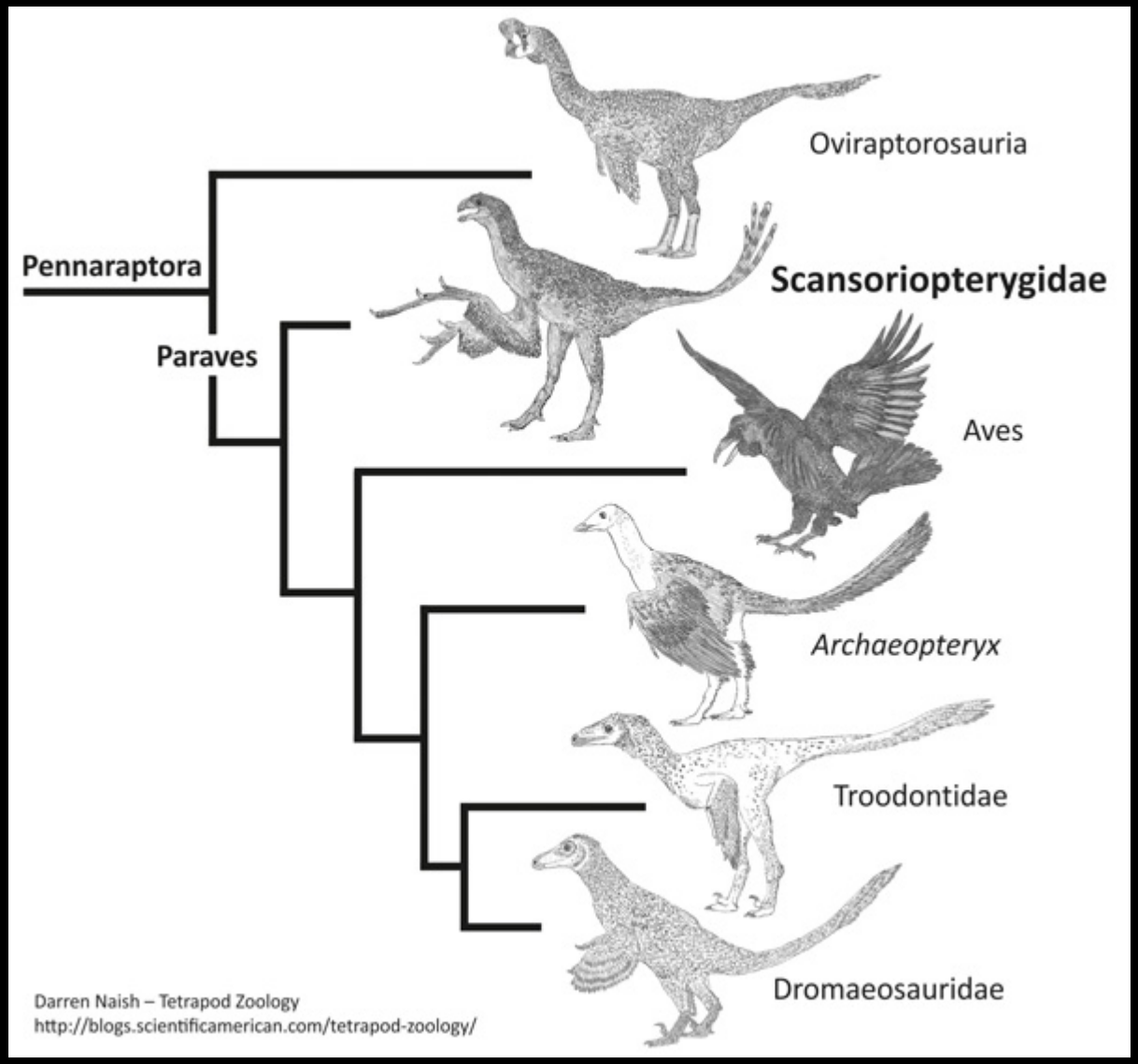
Oviraptorosauria
Pennaraptora
Scansoriopterygidae
Paraves
Aves
Archaeopteryx
Troodontidae
Dromaeosauridae
Darren Naish – Tetrapod Zoology
http://blogs.scientificamerican.com/tetrapod-zoology/

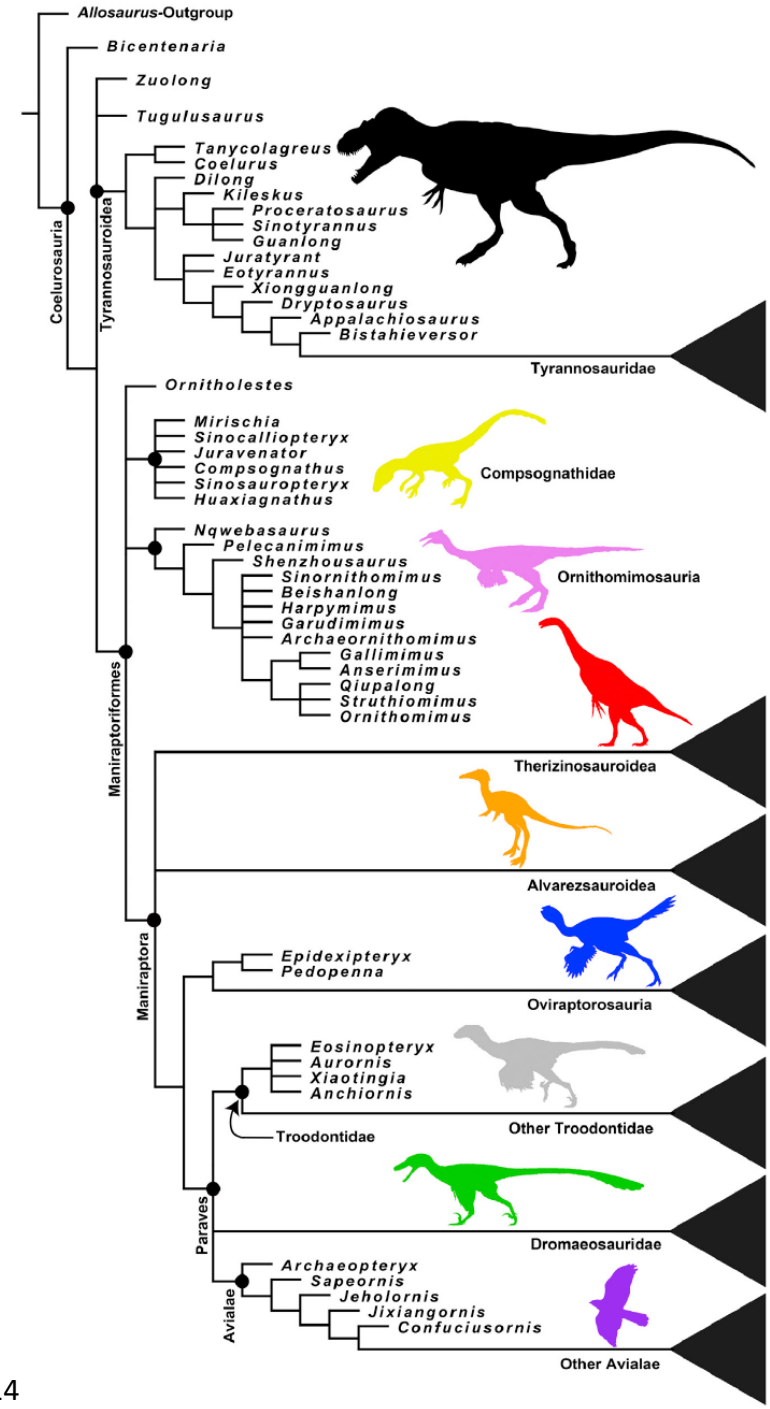

Brusatte et al., 2014

Scansoriopterygidae:
dinosaurios arborícolas?

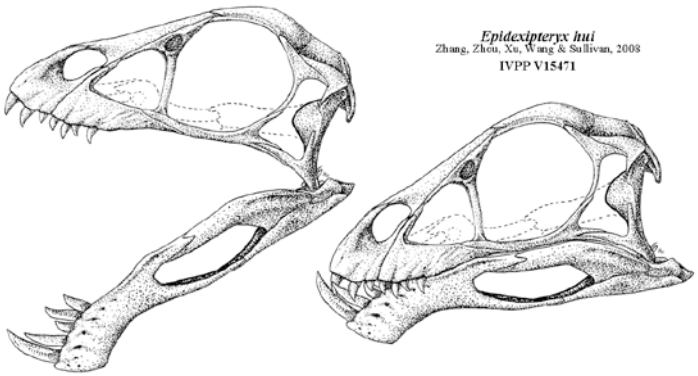

Epidexipteryx hui
Zhang et al 2008

Epideendrosaurus ninchengensis
Zhang et al 2002

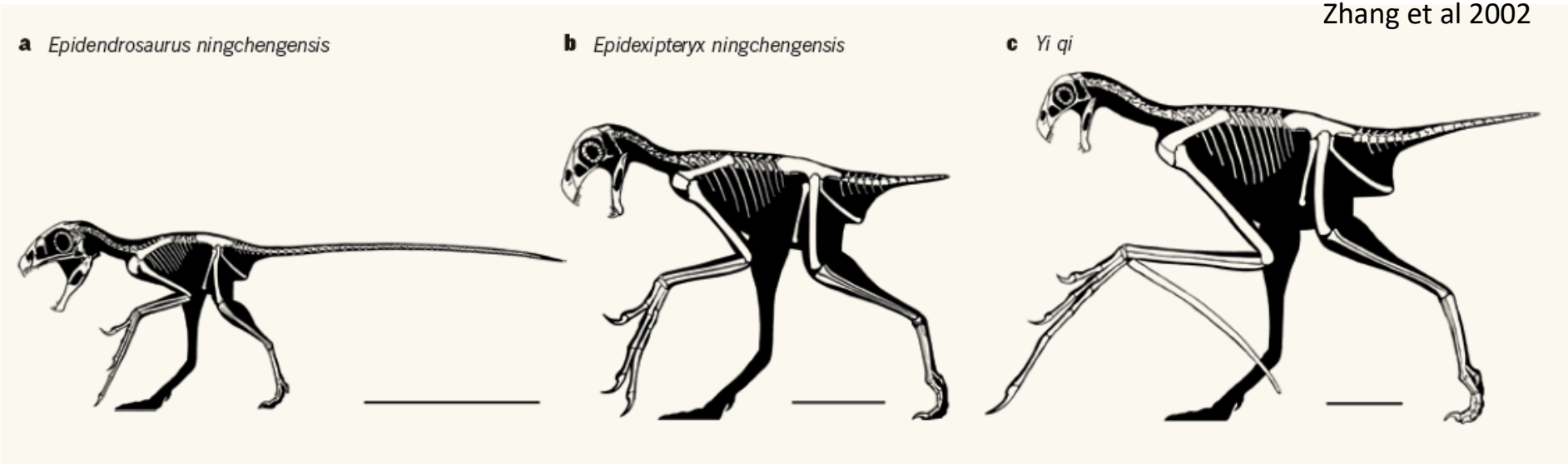

Yi qi

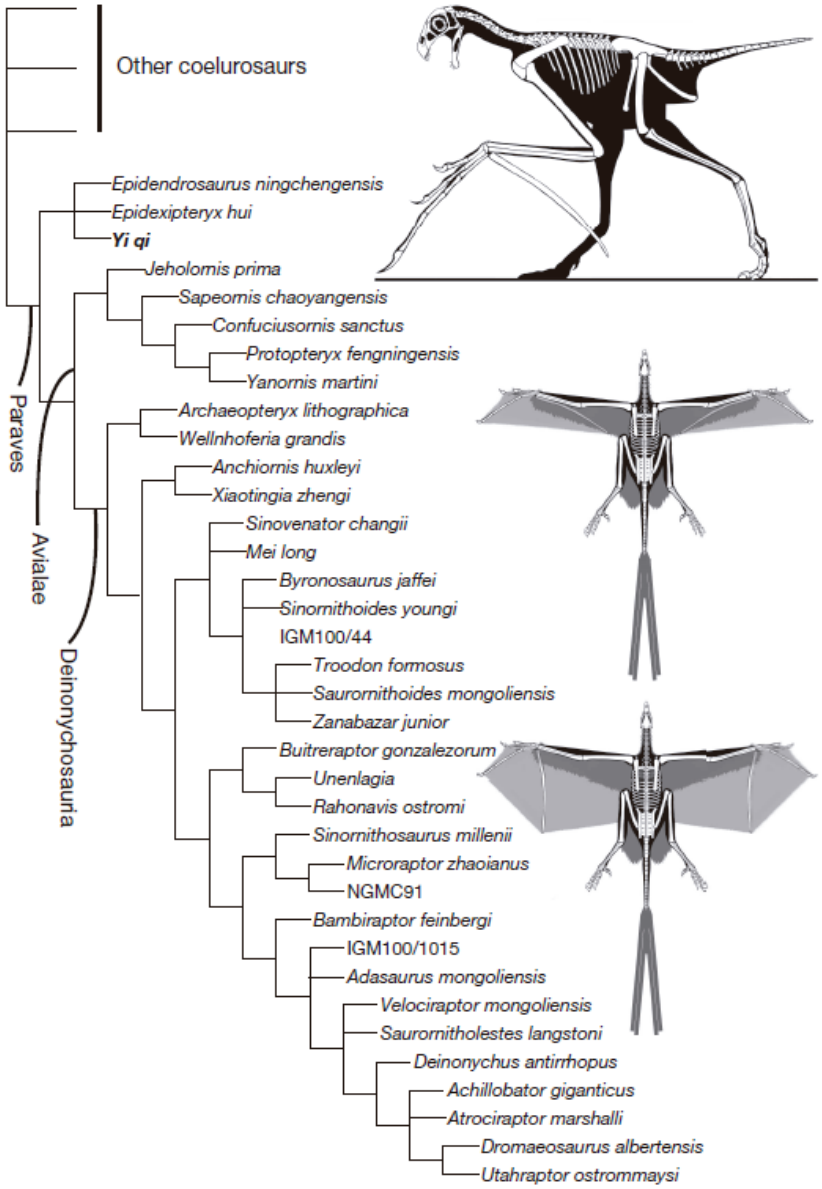
Other coelurosaurs
Epidendrosaurus ningchengensis
Epidexipteryx hui
Yi qi
Jeholornis prima
Sapeornis chaoyangensis
Confuciusornis sanctus
Protopteryx fengningensis
Yanornis martini
Archaeopteryx lithographica
Wellnhoferia grandis
Anchiornis huxleyi
Xiaotingia zhengi
Sinovenator changii
Mei long
Byronosaurus jaffei
Sinornithoides youngi
IGM100/44
Troodon formosus
Saurornithoides mongoliensis
Zanabazar junior
Buitreraptor gonzalezorum
Unenlagia
Rahonavis ostromi
Sinornithosaurus millenii
Microraptor zhaoianus
NGMC91
Bambiraptor feinbergi
IGM100/1015
Adasaurus mongoliensis
Velociraptor mongoliensis
Saurornitholestes langstoni
Deinonychus antirrhopus
Achillobator giganticus
Atrociraptor marshalli
Dromaeosaurus albertensis
Utahraptor ostrommaysi
Paraves
Avialae
Deinonychosauria


c

Deinonychosauria:

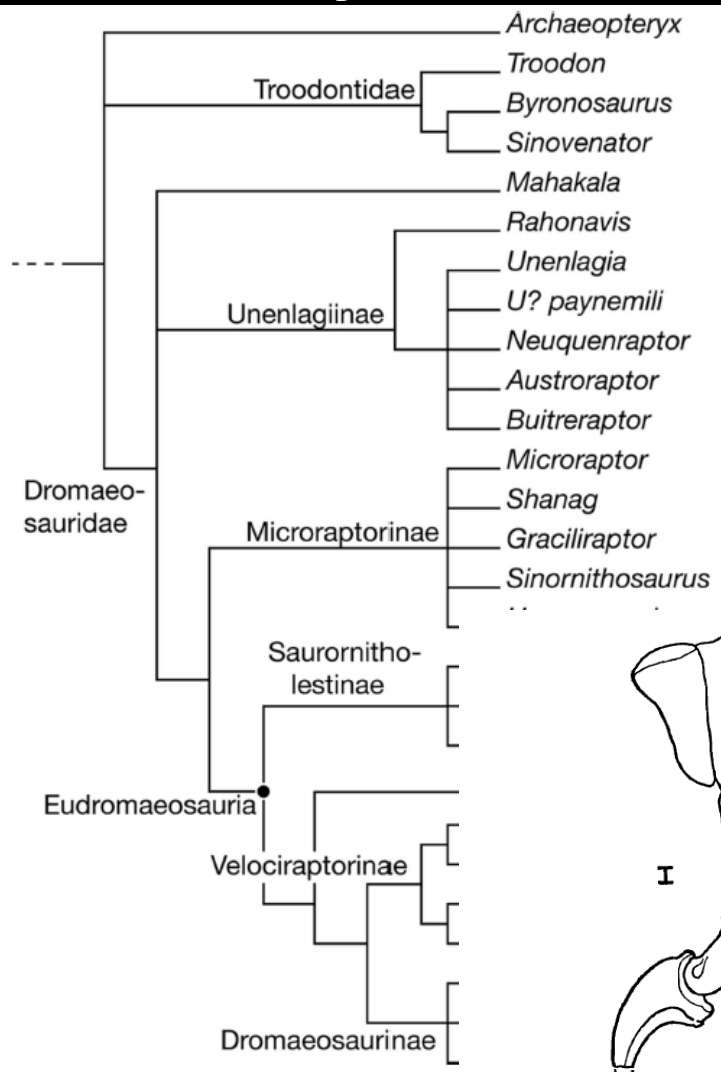

Fig. 3. Strict consensus of 5,292 most pars
phylogenetic analysis of 23 in-group taxa, 4 o
ters. *H. elizabethae* was found to be part of th
length = 223, consistency index = 0.5430, rete
consistency index = 0.3791.

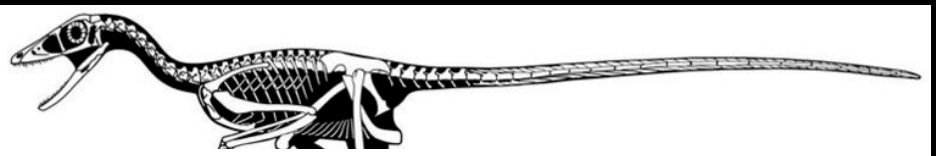

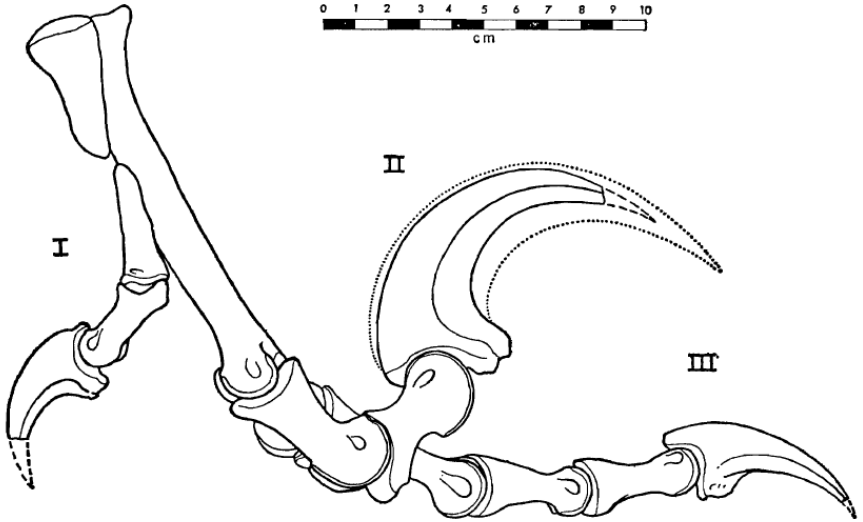

FIG. 74. Left pes of *Deinonychus antirrhopus* (YPM 5205) in internal aspect. Notice the extreme contrast in the form of the second and third unguals. The dotted line represents a conservative estimate of the size and shape of the horny claw carried by the ungual.

inonychus antirrhopus

Deinonychosauria: Troodontidae

Clado más inclusivo que contiene a Troodon formosus, pero no a Velociraptor mongoliensis. Maniraptores gráciles, con dientes aserrados, manos raptoriales y garra hipertrofiada en el dígito II pedal. Grandes órbitas.

Sinapomorfías:

- Numerosos dientes maxilares empacados anteriromente, al igual que los dientes en el dentario
- Fenestra premaxilar desaparece en Troodontidos derivados
- Canal en cara labial del dentario con foraminas neurovasculares

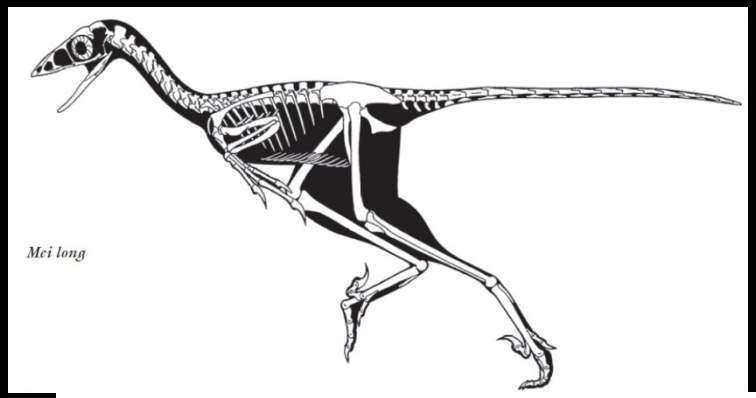

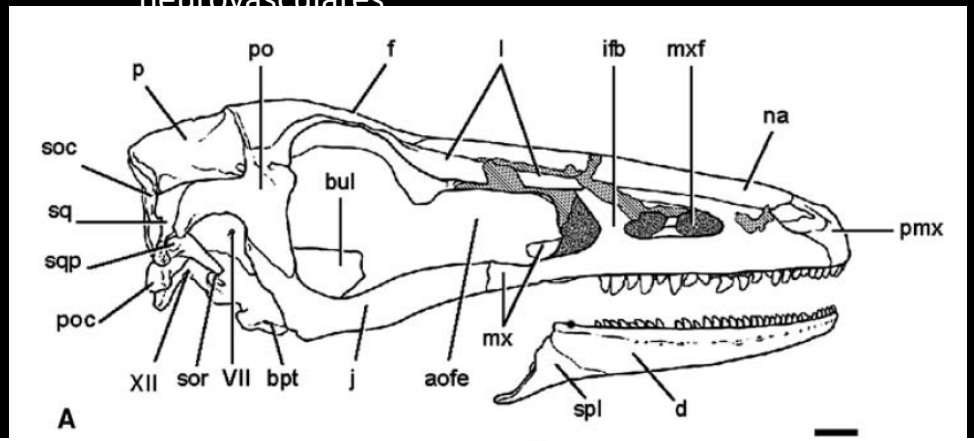

“Anchiornithidae”:
Primera radiación pre-aviana

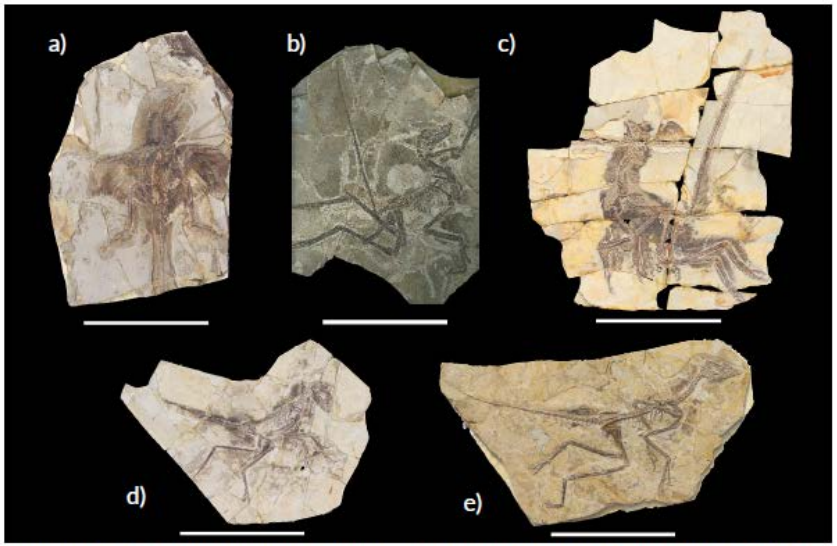

Figure 1 – Paravians from the Jurassic Tiaojishan Formation of Liaoning Province, China. a) YFGP-T5199. b) YFGP-T5200. c) YFGP-T5201. d) *Eosinopteryx brevipenna*. e) *Aurornis xui*. Scale bar is 20 cm.

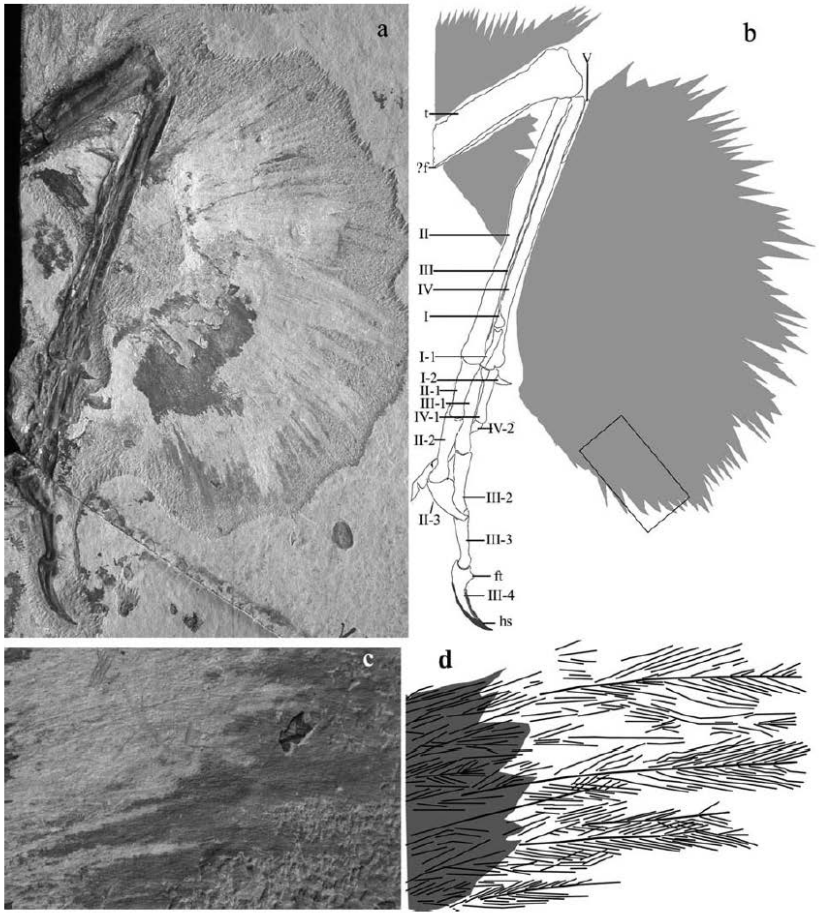

Fig. 1 The holotype of *Pedopenna daohugouensis* (Institute of Vertebrate Paleontology & Paleoanthropology, Beijing V12721): photograph (**a**) and line-drawing (**b**) of the partial leg and associated feathers, photograph (**c**) and line-drawing (**d**) of the feathers attached to the distal metatarsals showing the rachis and the parallel barbs. *Inset* in **b** indicates the positions of **c** and **d**. *Scale bar*=10 mm. *?f* Fibula, *ft* flexor tubercle, *hs* horny sheath, *I–V* metatarsal I–V, *I-1 to IV-2* pedal phalanx I-1 to IV-2, *t* tibia

Xiatingia zhengi

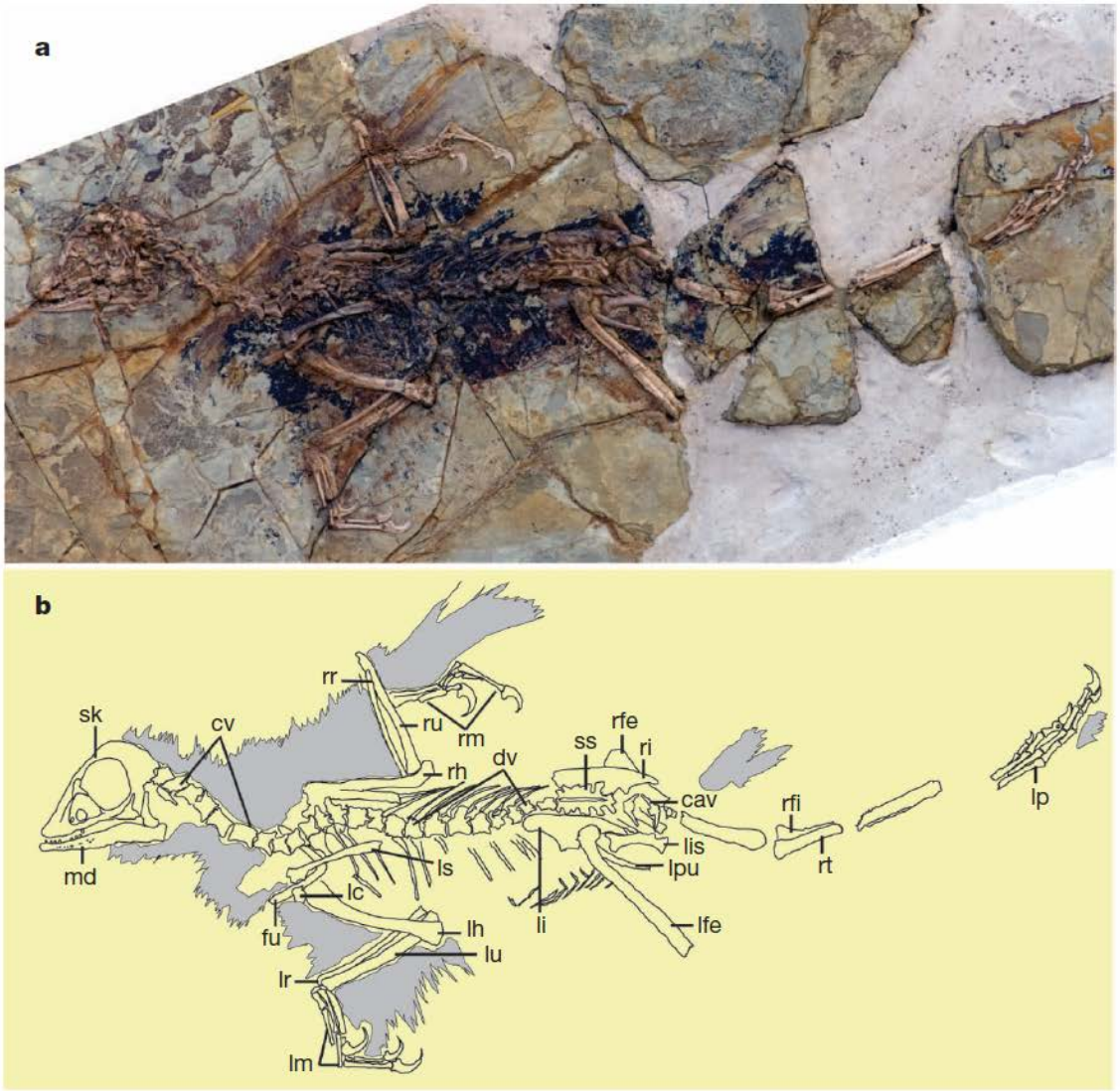

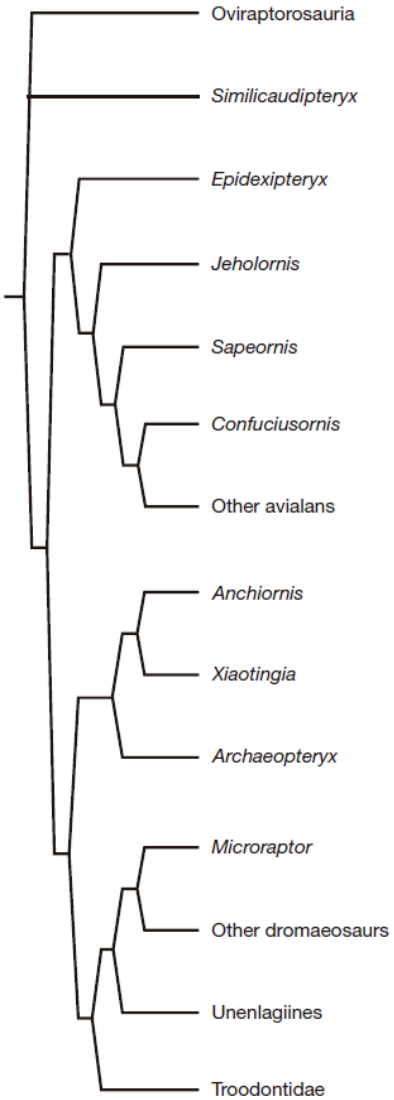

Xu et al., 2011

Figure 1 | *Xiaotingia zhengi* holotype (STM 27-2). **a**, **b**, Photograph (**a**) and line drawing (**b**). Integumentary structures in **b** are coloured grey. cav, caudal vertebra; cv, cervical vertebra; dv, dorsal vertebra; fu, furcula; lc, left coracoid; lfe, left femur; lh, left humerus; li, left ilium; lis, left ischium; lm, left manus; lp, left pes; lpu, left pubis; lr, left radius; ls, left scapula; lu, left ulna; md, mandible; rfe, right femur; rfi, right fibula; rh, right humerus; ri, right ilium; rm, right manus; rr, right radius; rt, right tibiotarsus; ru, right ulna; sk, skull; ss, synsacrum.

Anchiornis huxleyi

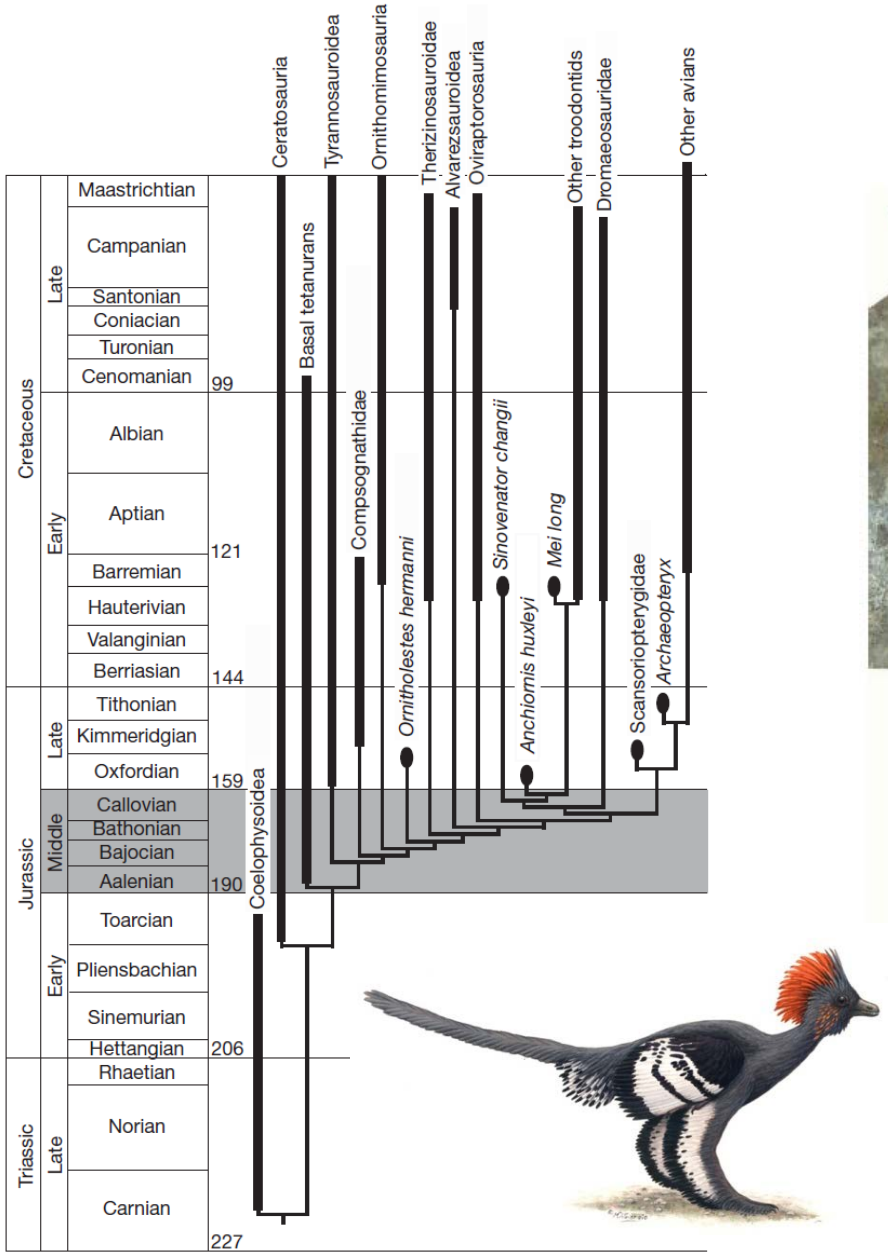

Figure 4 | Temporally calibrated phylogeny of the Theropoda. (See Supplementary Information for details.) The known temporal durations (solid bars) of the major theropod groups, based on well-corroborated fossil occurrences, indicate that the major tetanuran theropod groups diverged rapidly in the Middle Jurassic to earliest Late Jurassic.

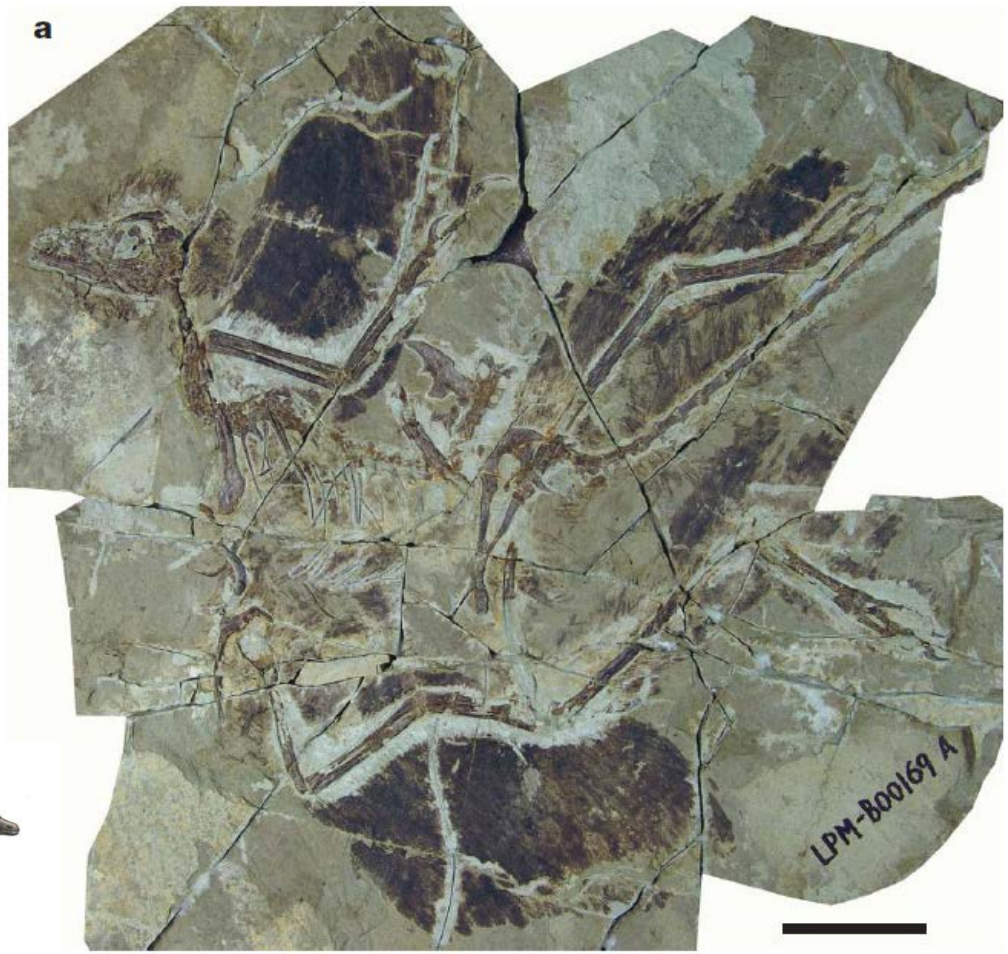

Xu et al, 2009; Hu et al, 2009

Eosinopteryx brevipenna

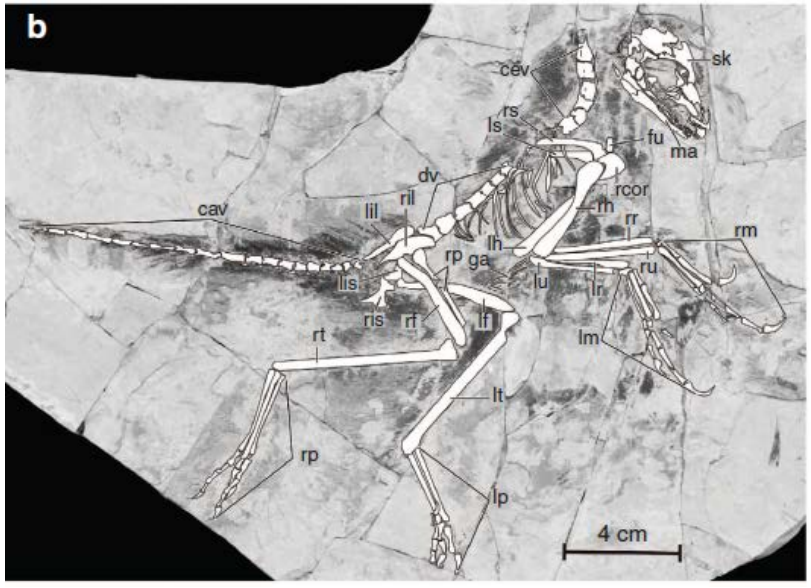

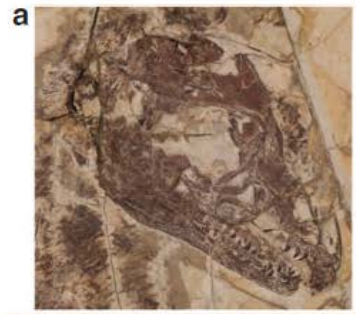

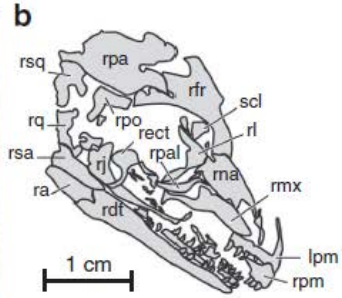

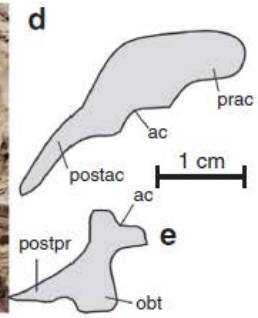

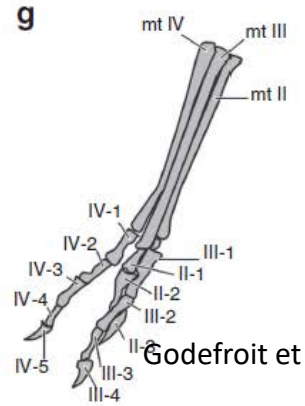

Godefroit et al., 2013

1 cm

Aurornis xui

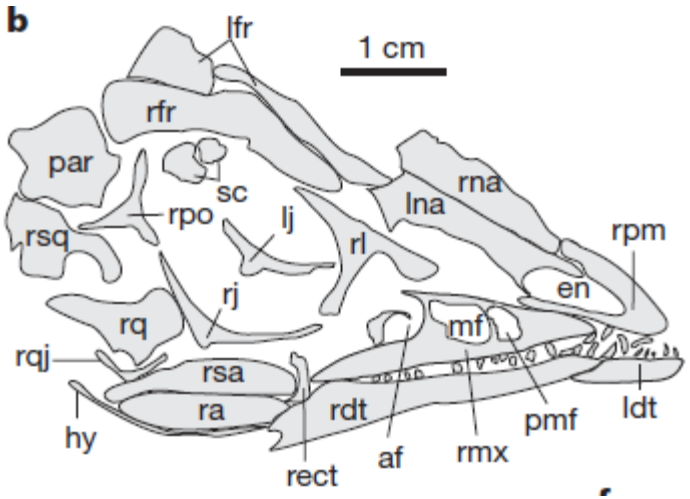

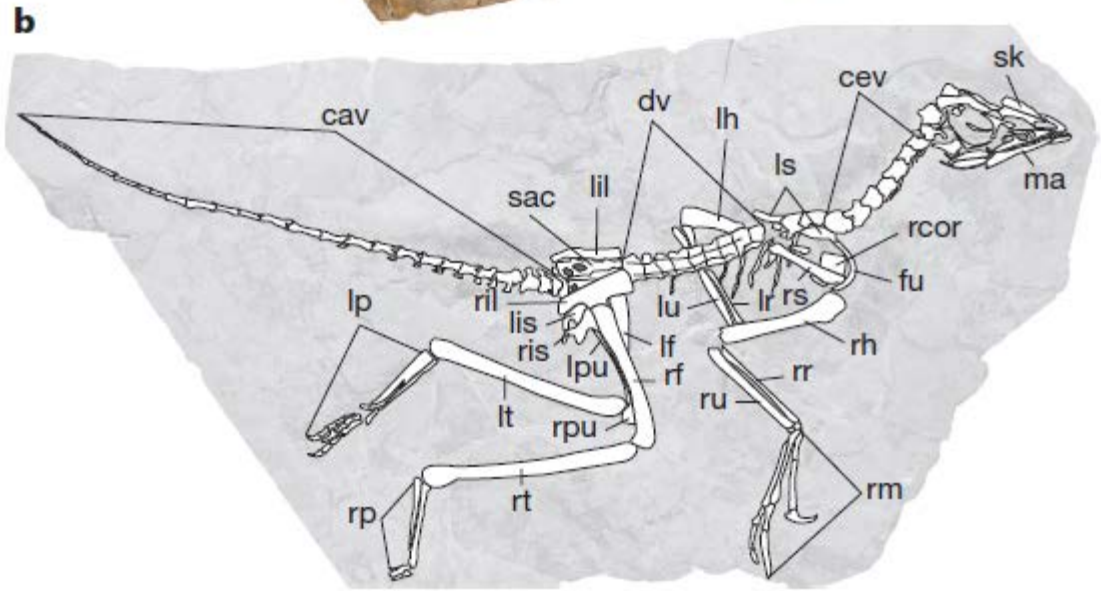

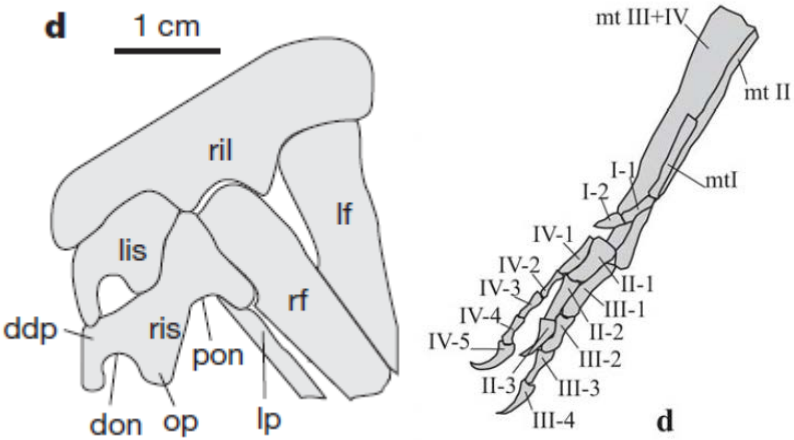

Godefroit et al., 2013b

Serikornis sungei

Léfevfre et al., 2017

Léfevfre et al., 2017

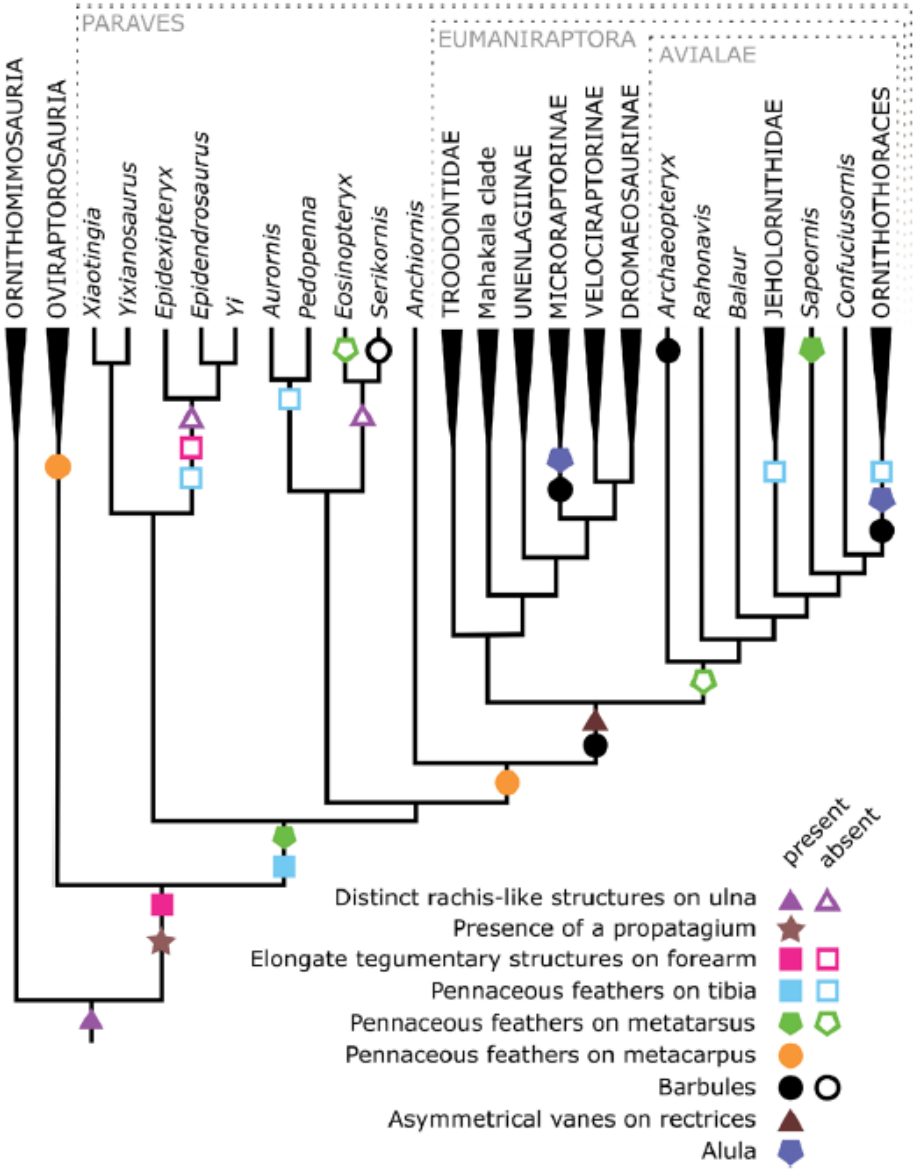

Fig. 8 Strict consensus tree resulting from the phylogenetic analysis (length = 5743, consistency index = 0.2614, retention index = 0.7386). Major evolutions in the history of birds are mapped on the paraves clade. The complete tree is presented as supplemental fig. S11

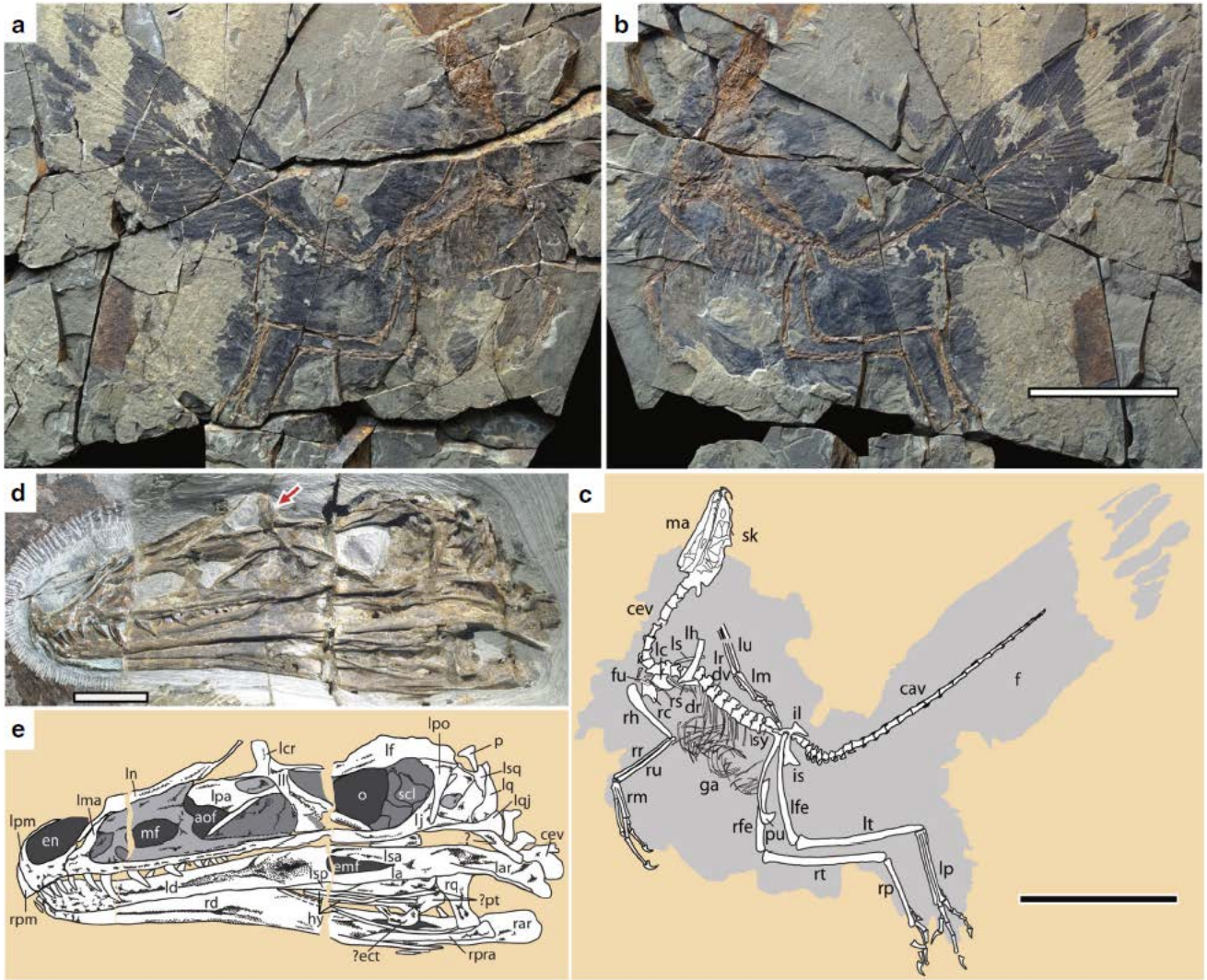

Fig. 1 *Caihong juji* holotype specimen (PMoL-B00175). Photographs of the slab (**a**) and counter slab (**b**) and line drawing (**c**) of the specimen based on both slabs. Photograph (**d**) and line drawing (**e**) of a composite of the rostrum of the skull and mandible exposed on the counter slab and the post-rostrum cranium exposed on the slab. Arrows indicate lacrimal crests. Question mark indicates uncertain identification. Scale bars: 10 cm **a–c**, 1 cm **d** and **e**. aof antorbital fenestra, cav caudal vertebra, cev cervical vertebra, dr dorsal rib, dv dorsal vertebra, ect ectopterygoid, emf external mandibular fenestra, en external naris, f feather, fu furcula, ga gastralia, hy hyoid, il ilium, is ischium, la left angular, lar left articular, lc left coracoid, lcr lacrimal crest, ld left dentary, lf left, frontal, lfe left femur, lh left humerus, lj left jugal, ll left lacrimal, lma left maxilla, lm left manus, ln left nasal, lp left pes, lpa left palatine, lpo left postorbital, lq left quadrate, lqj left quadratojugal, lr left radius, ls left scapula, lsp left splenial, lsa left surangular, lsq left squamosal, lt left tibiotarsus, lu left ulna, ma mandible, mf maxillary fenestra, o orbit, p parietal, pm premaxilla, pt pterygoid, pu pubis, rar right articular, rc right coracoid, rd right dentary, rfe right femur, rh right humerus, rm right manus, rp right pes, rpra right prearticular, rq right quadrate, rr right radius, rs right scapula, rt right tibiotarsus, ru right ulna, scl sclerotic bones, sk skull, sy synsacrum

Hu et al., 2018


Other coelurosaurs
Oviraptorosauria
Scansoriopterygidae
Avialae
Archaeopteryx
Wellnhoferia
Xiaotingia
Caihong
Anchiornis
Eosinopteryx
Aurornis
Troodontidae
Dromaeosauridae

Hu et al., 2018

Hipótesis filogenéticas e Paraves

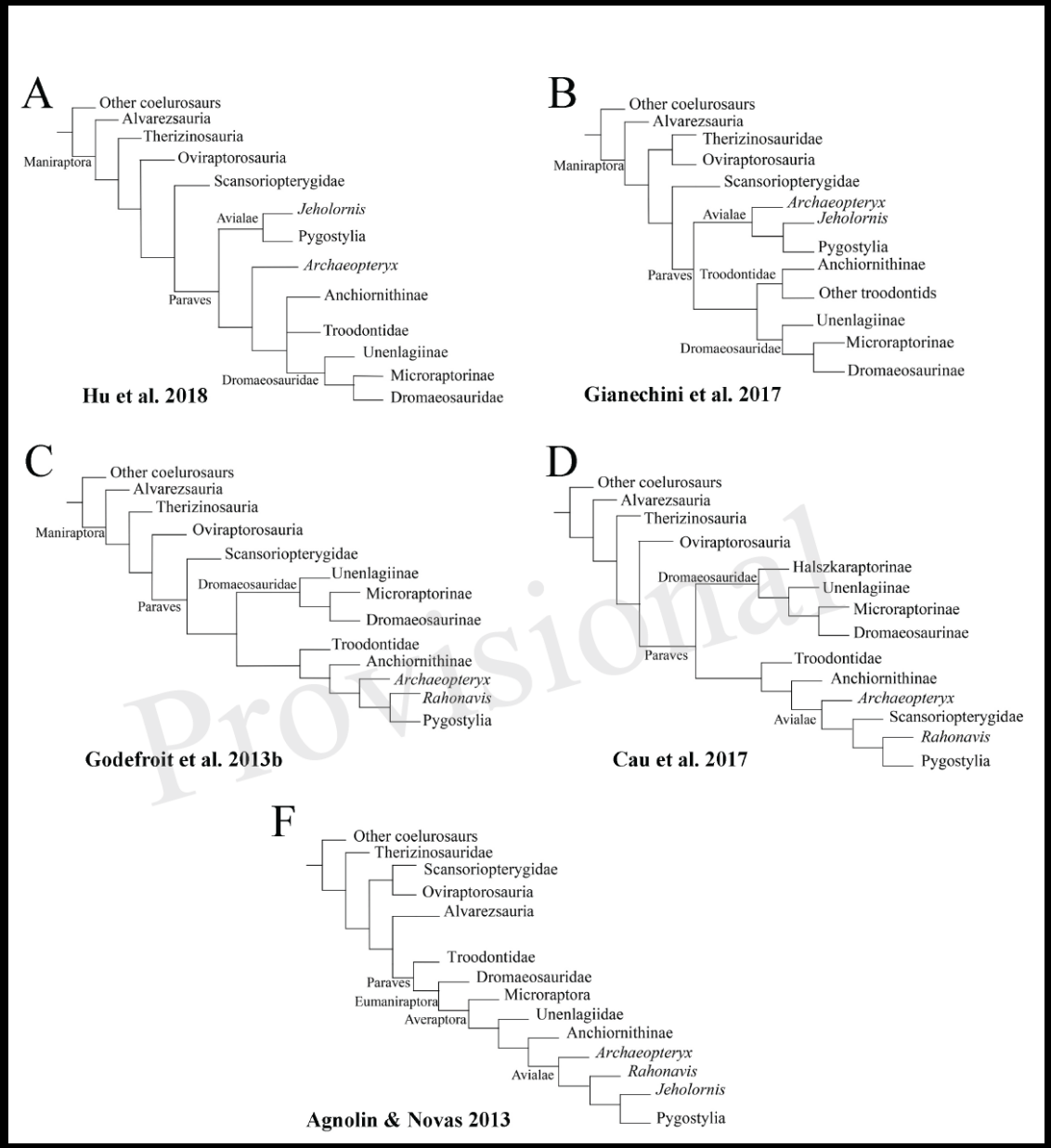

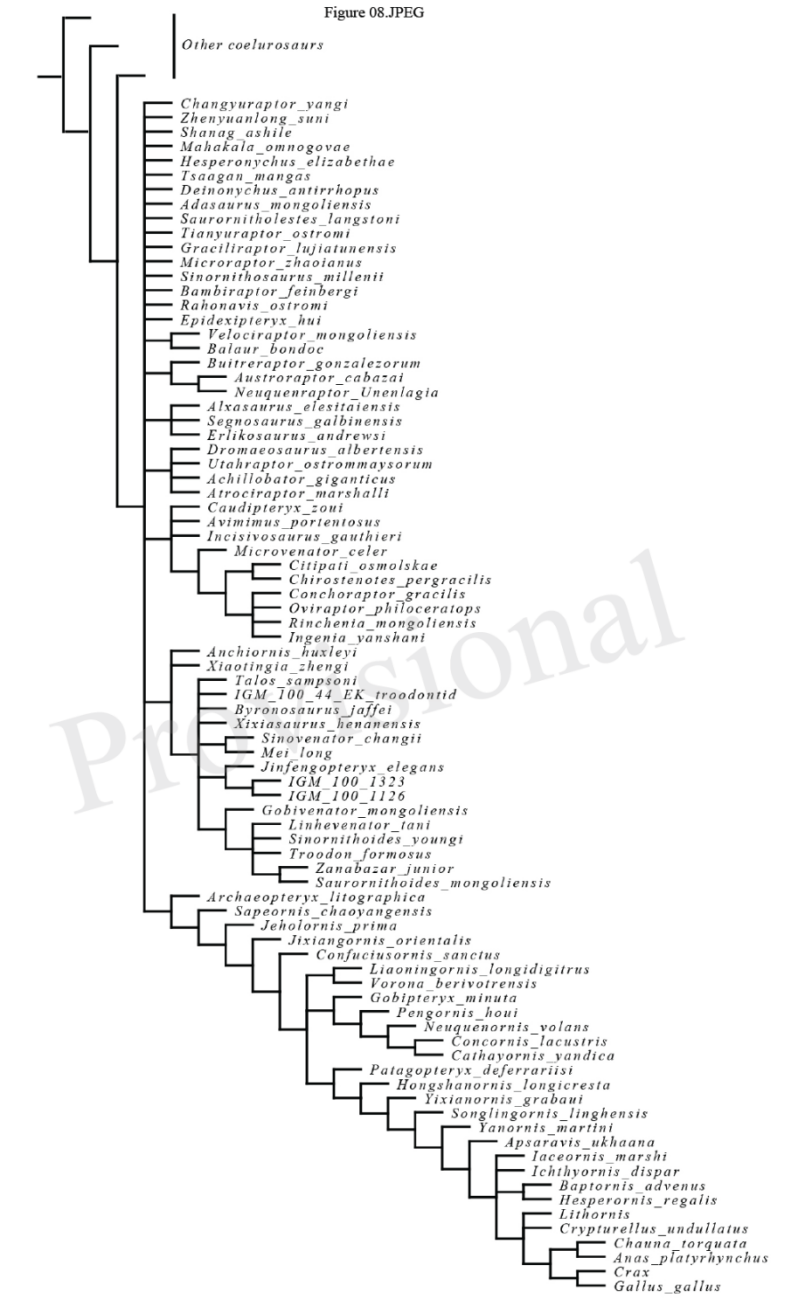

FIGURE 8. Strict consensus tree showing phylogenetic relationships of paravians, based on modified TWiG data matrix.

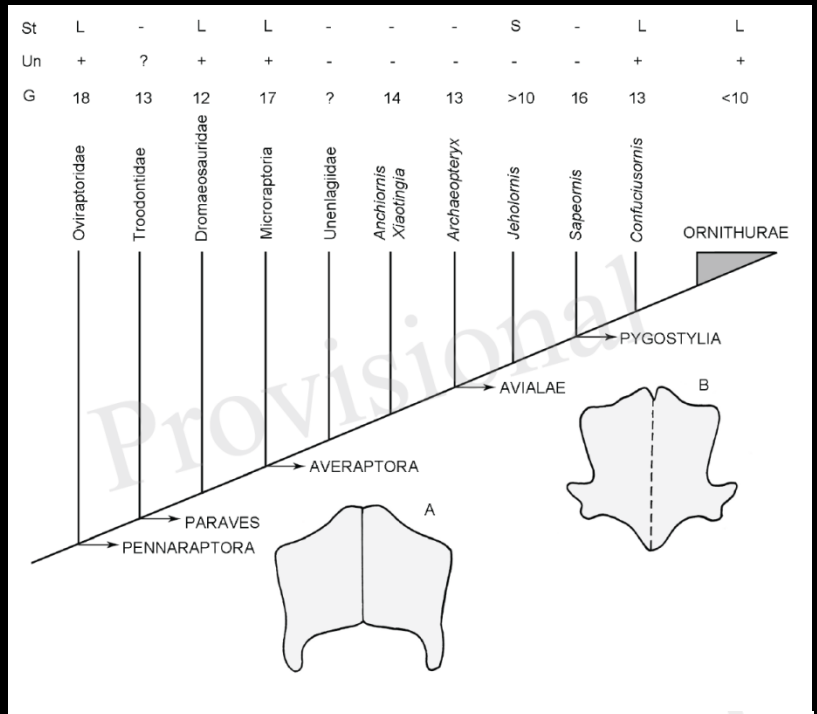

FIGURE 9. Simplified cladogram showing the phylogenetic relationships of derived coelurosaurs following the proposal of Agnolin and Novas (2013). The figure indicates the number of gastral pairs (G), presence or absence of uncinate process (Un) and relative development of the sternum (St) in avian-line theropods. **A**-**B**, gross morphology of the sternum of: **A** the dromaeosaurid *Linheraptor exquisitus*, **B** the pygostylian *Eoconfuciusornis zhengi* (modified from Zheng et al. 2012).

Abbreviations. **G**, number of pairs of gastralia, **L**, present and large, **S**, present but small; **St**, Sternum; **Un**, Uncinate process; **?**, uncertain condition; +, presence; -, absence.

Definición Cladística del grupo Aves (Avialae):

Definición de nodo (Padian, 2001; Padian, 2004): Clado más inclusivo que contiene a *Archaeopteryx* (“primera ave”), *Columba livia* (Paloma común), su ancestro común más reciente y todos sus descendientes.

Archaeopterygidae:
Archaeopteryx lithographica

(crown group Aves)

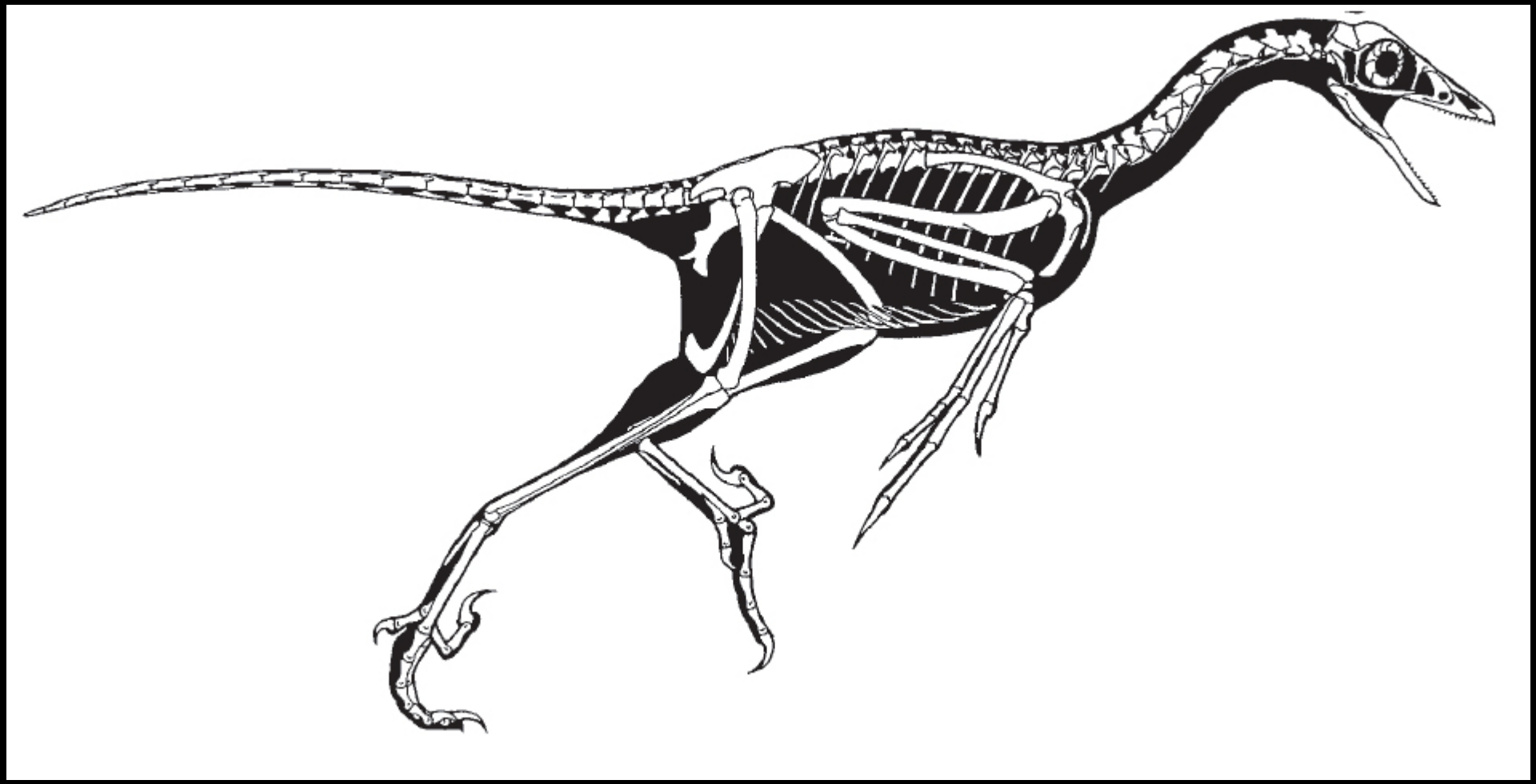


London Specimen


Berlin Specimen


Maxberg Specimen

Haarlem Specimen


Eichstätt Specimen


Solnhofen Specimen


Munich Specimen


Bürgermeister-Müller Specimen

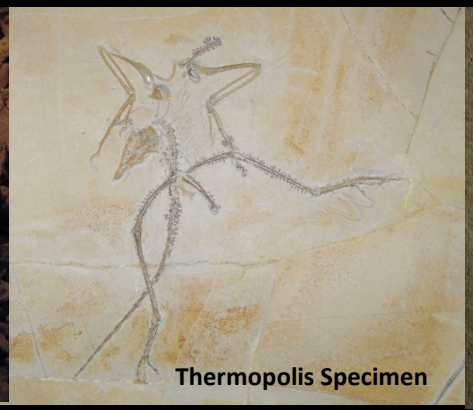
Thermopolis Specimen

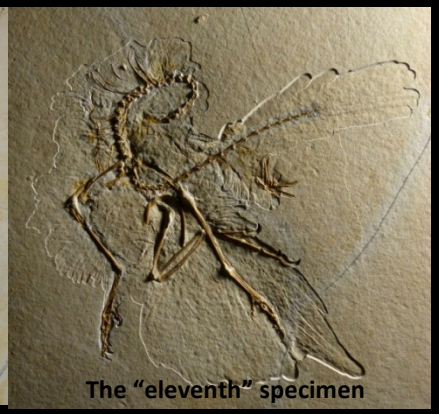
The “eleventh” specimen

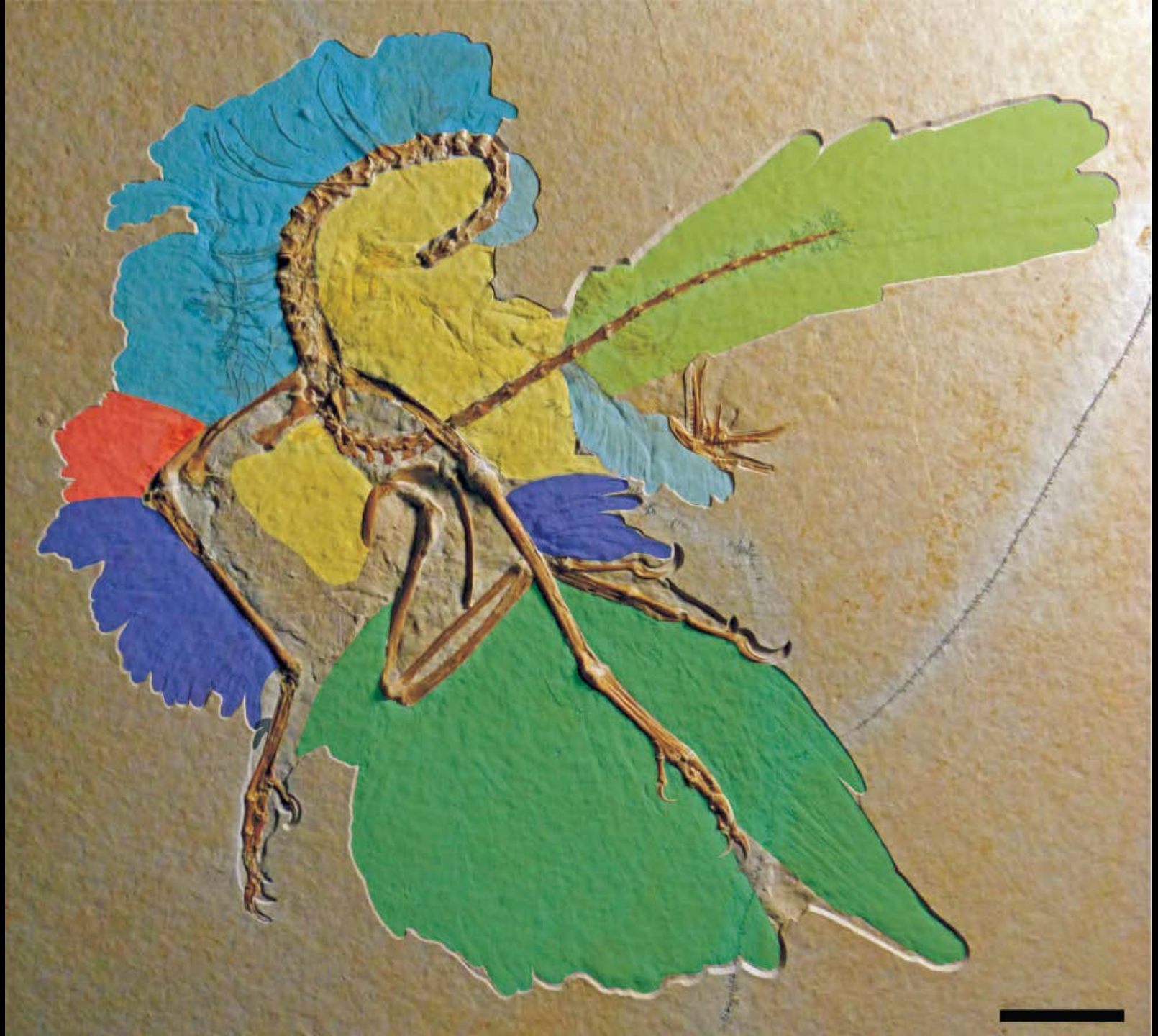

Filogenia de Aves Mesozoicas

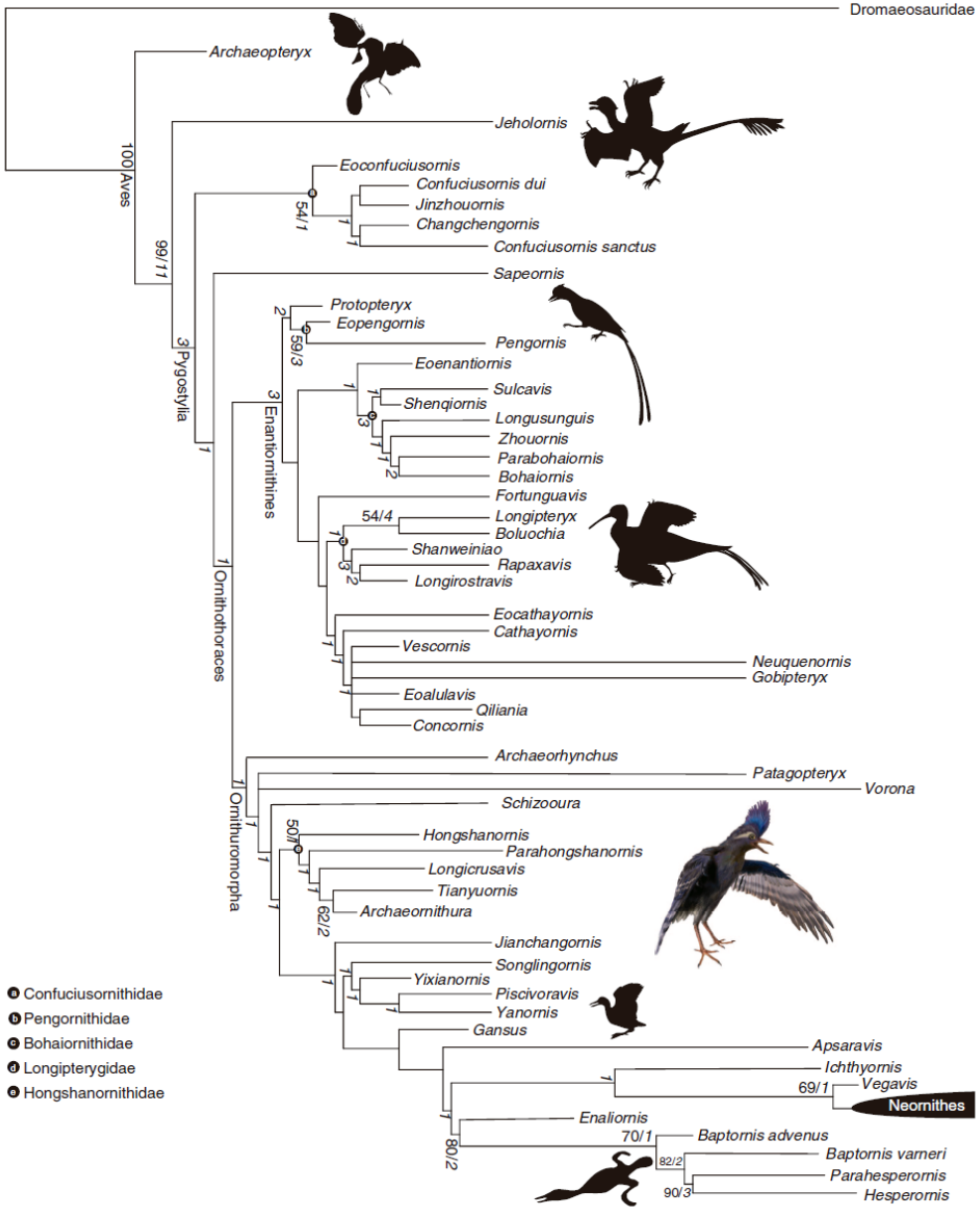

Figure 5 | Cladogram showing the systematic position of *Archaeornithura meemannae* among Mesozoic birds. Bootstrap and bremer values are labelled to the corresponding nodes in normal and bold italic formats, respectively.

Balaur bondoc

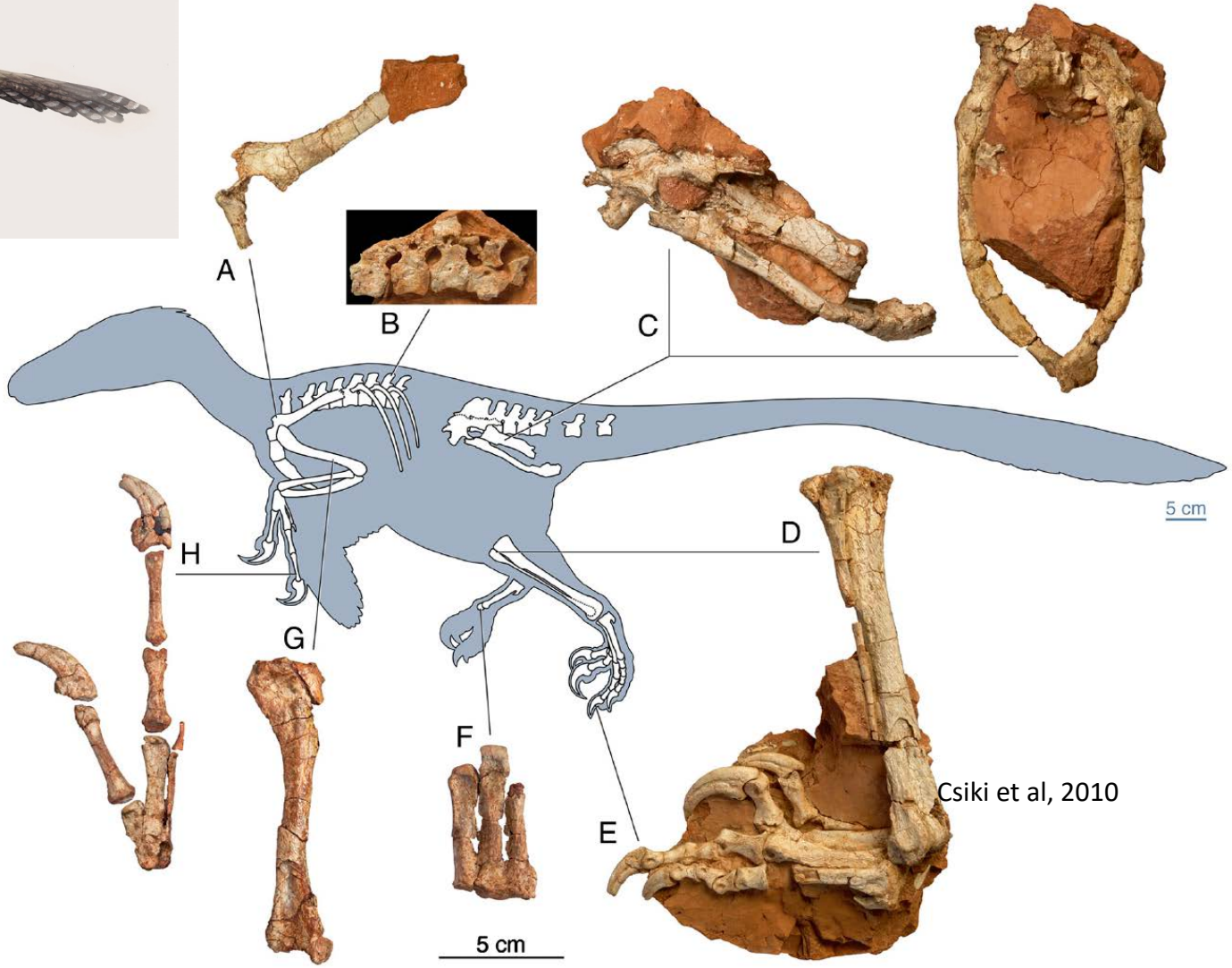

Csiki et al, 2010

Fig. 1. Skeletal anatomy of *Balaur bondoc*. Reconstruction of the holotype with photos of individual bones. (*A*) Left scapulocoracoid (lateral view). (*B*) Middorsal vertebrae (lateral view). (*C*) Pelvis (left lateral and anterior views). (*D*, *E*) Left hindlimb and pes. (*F*) Right tarsometatarsus (extensor view). (*G*) right humerus (posterior view). (*H*) Right carpometacarpus and manual digits (extensor view). Scale bar at right refers to skeletal reconstruction and at bottom to all bones.

Aves basales: Jeholornithiformes

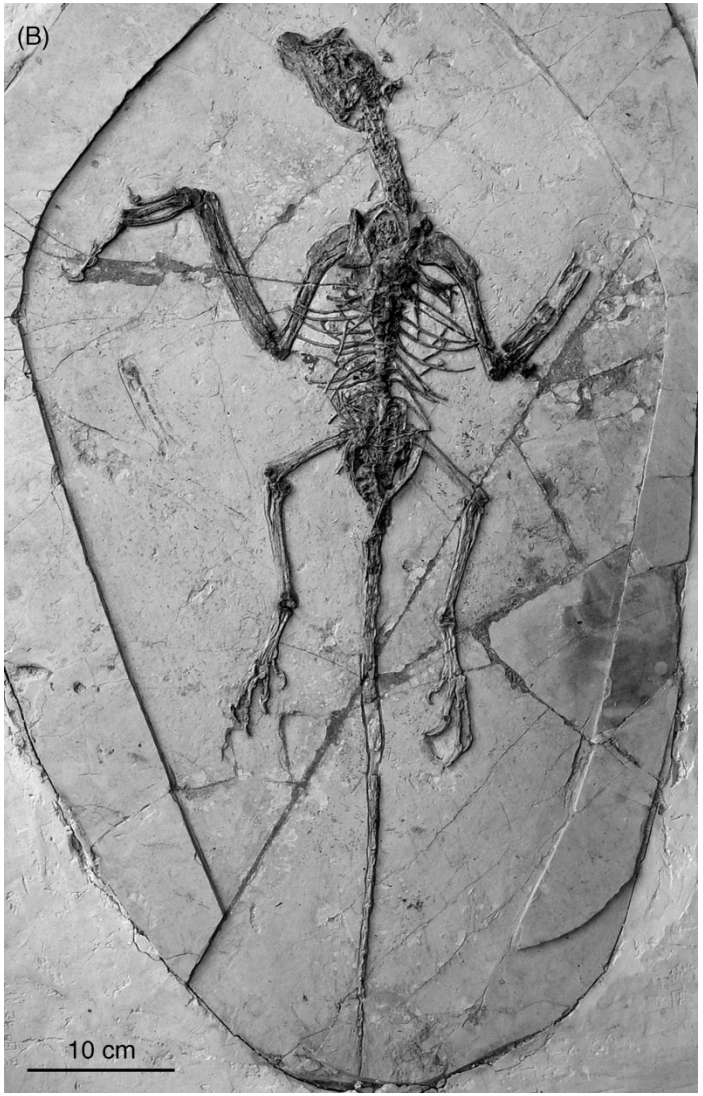

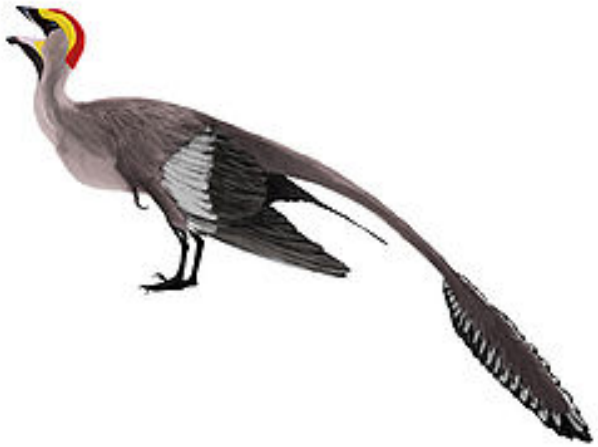

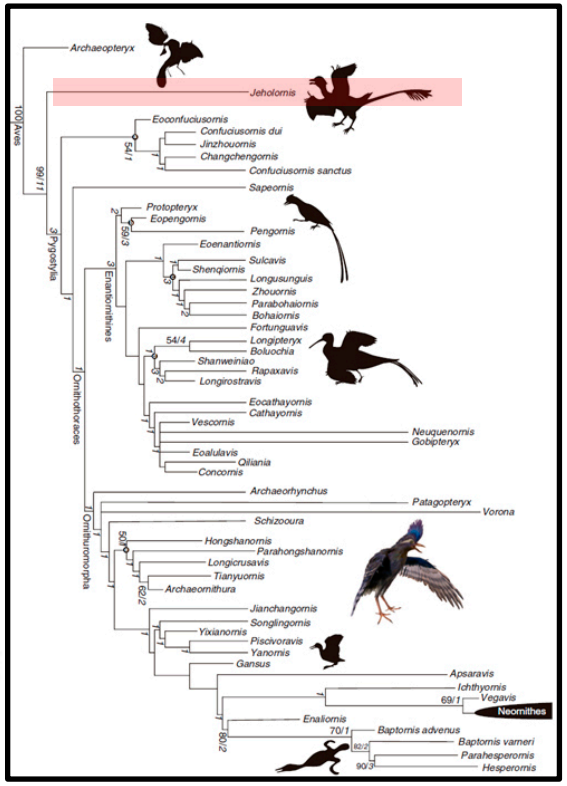

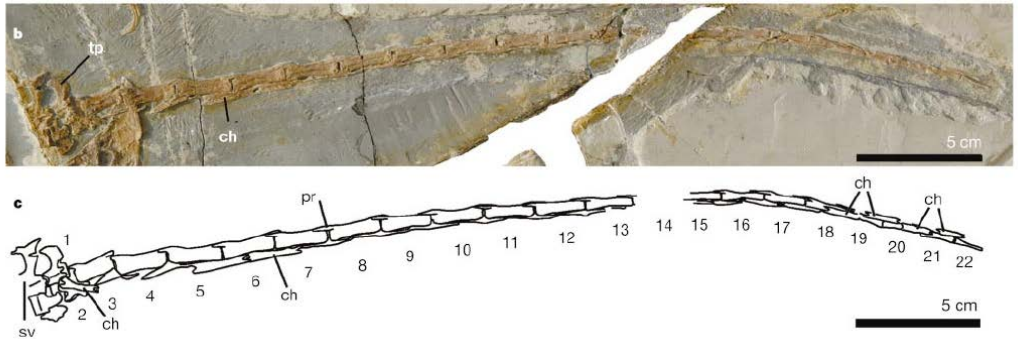

Figure 1 Complete holotype of *Jeholornis prima* gen. et sp. nov. (IVPP V13274). **a**, Skeleton. **b**, Caudal vertebrae. **c**, Line drawing of the caudal vertebrae. ch, chevron; co, coracoid; cv, cervical vertebra; dv, dorsal vertebra; fe, femur; fi, fibula; fu, furcula; ga, gastralia; hu, humerus; hy, hyoid bone; il, ilium; is, ischium; ma, mandible; mcIII, metacarpal III; ov, ovule; pr, prezygopophysis; pu, pubis; ra, radius; sc, scapula; sk, skull; st, sternum; sv, sacral vertebra; ta, tail; ti, tibia; tm, tarsometatarsus; tp, transverse process; ul, ulna; un, unguals; 1–22, caudal vertebrae 1–22.

Aparición muñeca aviana: osificación del Pisiforme

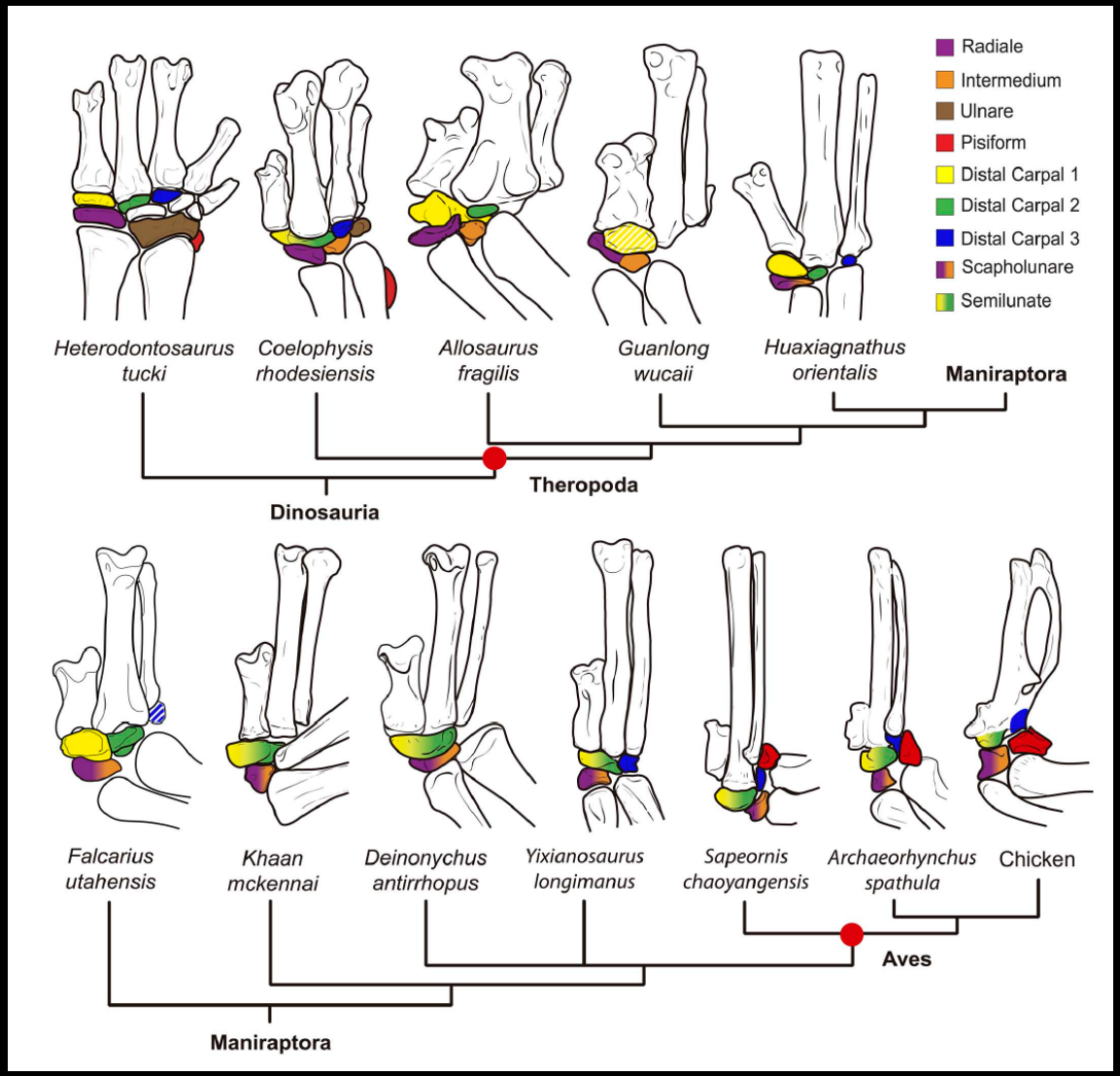

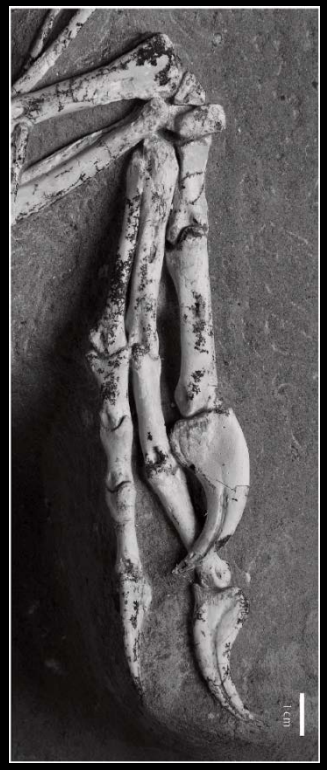

Khaan

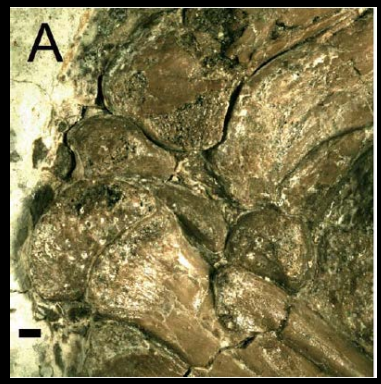

Sapeornis

Archaeopteryx

Boteho et al., 2014

Aparición del sistema digestivo moderno: El buche

Fig. 2 Relationships between specimens preserving evidence of the morphology of the alimentary canal: *Caudipteryx* (Oviraptorosauria) IVPP V12430 preserves gizzard stones; *Jeholornis* (Aves) IVPP V13352 preserves seeds indicative of a crop; *Sapeornis* (Pygostylia) STM15-15 preserves both seeds in the crop and gizzard stones; *Yanornis* (Ornithuromorpha) STM9-15 preserves fish in the crop and ventriculus. The crop is either a synapomorphy of Aves or *Jeholornis* + all more derived birds. *Dashed line* indicates no data. [Color for online/pdf only]

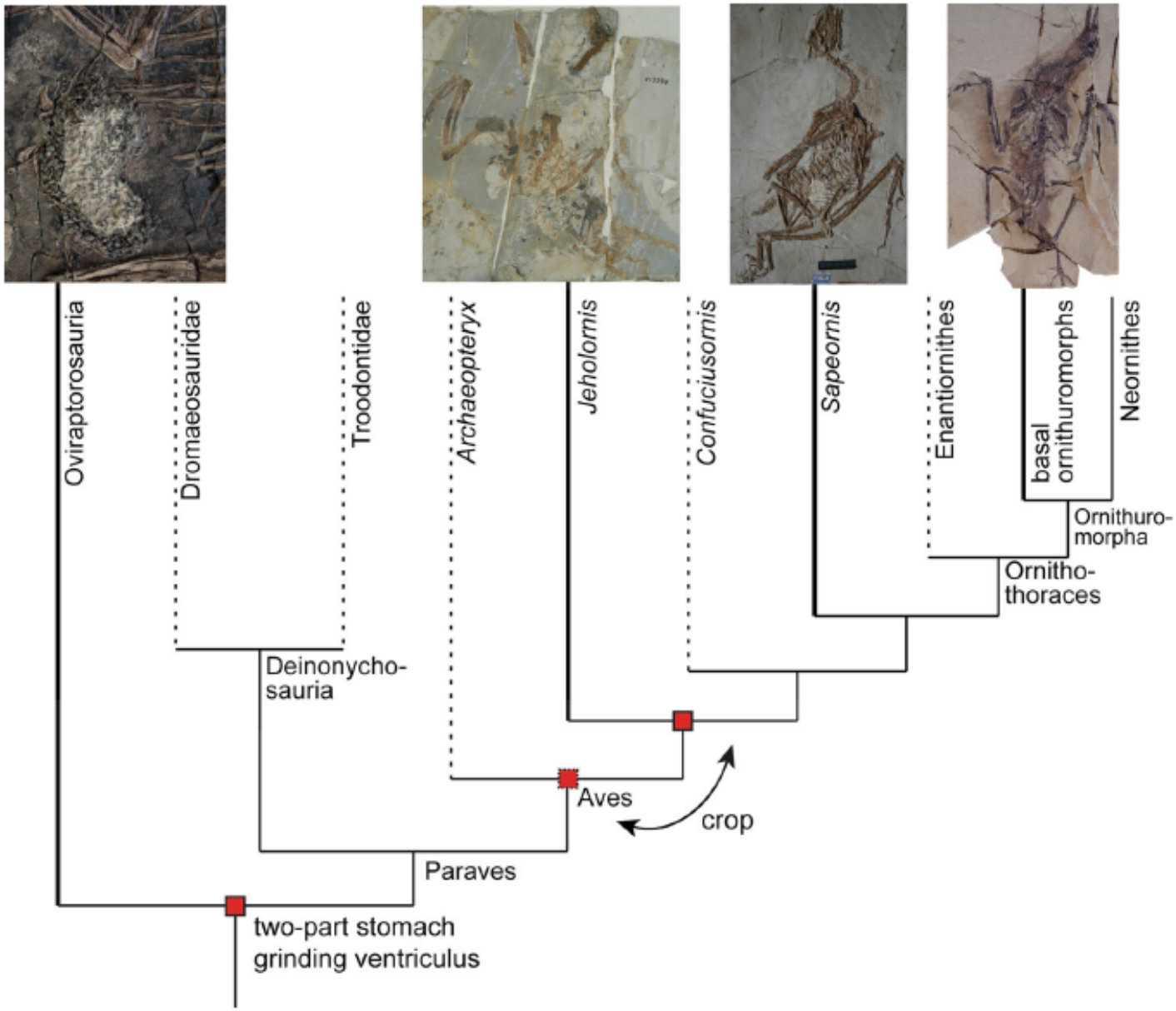

Pérdida del ovario derecho

Fig. 3 A simplified cladogram of archosaur relationships showing data regarding reproductive system. A single ovary is regarded as an autapomorphy of Aves. *Bold dashed lines* indicate indirect evidence from preserved eggs that suggest two functional ovaries and oviducts; *normal dashed lines* indicate absence of evidence. Crocodylia is represented by *Alligator mississippiensis*—note that mature follicles are nearly equal in size (one of two ovaries; image provided by L. Guillette and reproduced with permission); *Jeholornis* is represented by STM2-51; Enantiornithes is represented by an indeterminate specimen STM10-12; Neornithes is represented by *Gallus*—note the strong degree of follicular hierarchy in the maturing follicles (image provided by A. Johnson and reproduced with permission) [Color for online/pdf only]

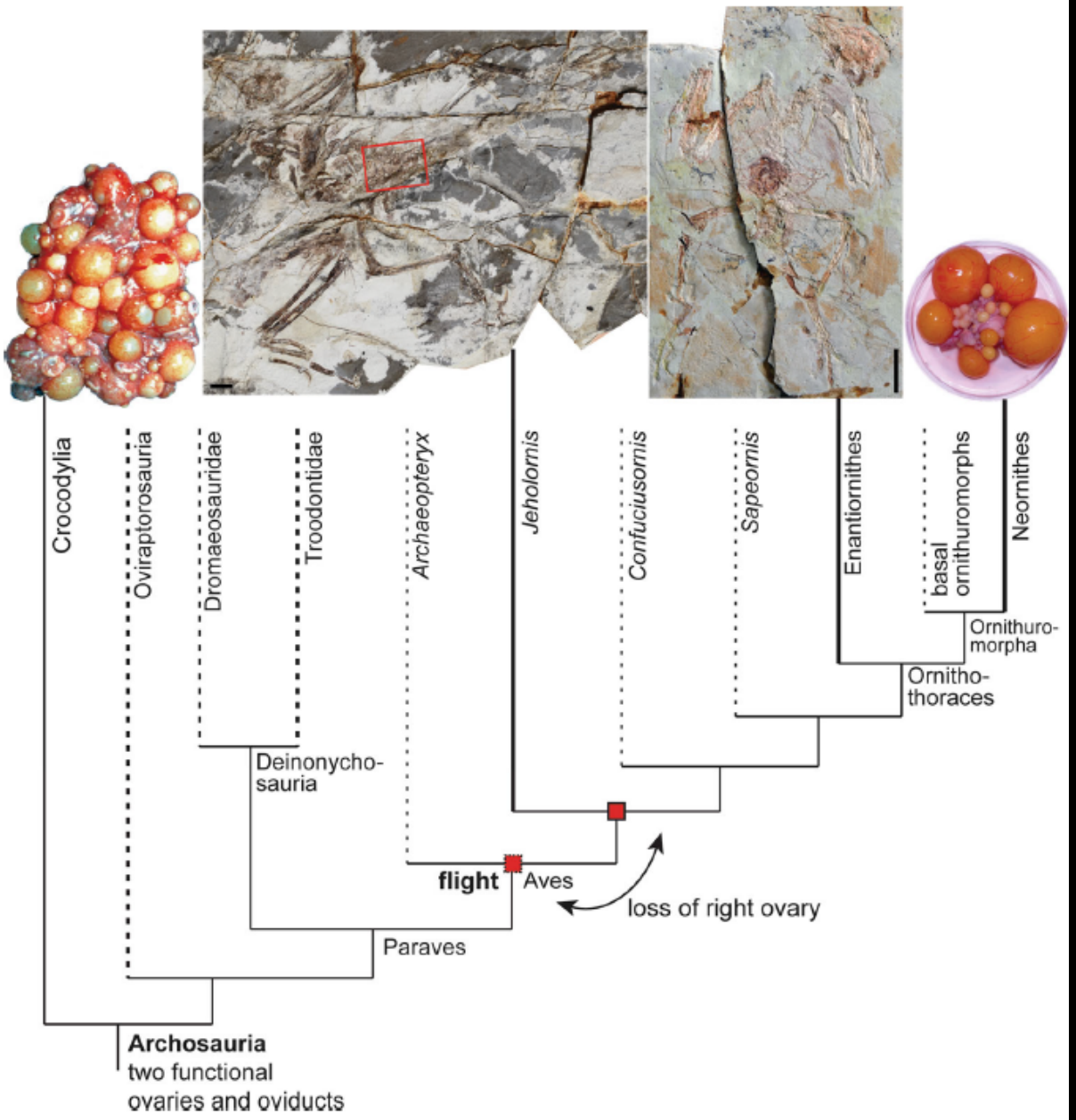


b
c
d

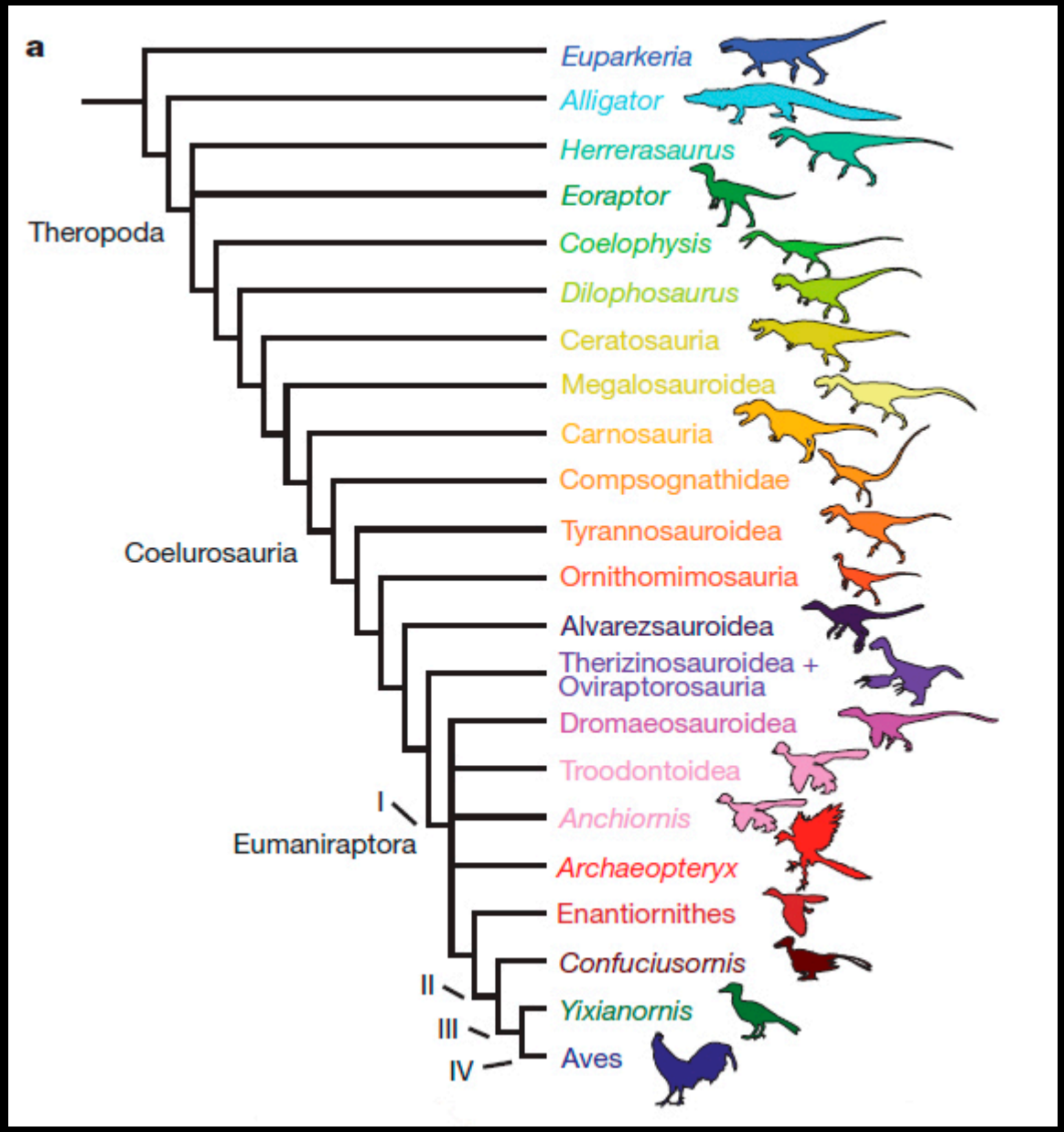
a
Euparkeria
Alligator
Herrerasaurus
Eoraptor
Theropoda
Coelophysis
Dilophosaurus
Ceratosauria
Megalosauroidea
Carnosauria
Compsognathidae
Tyrannosauroidea
Coelurosauria
Ornithomimosauria
Alvarezsauroidea
Therizinosauroidea +
Oviraptorosauria
Dromaeosauroidea
Troodontoidea
I
Anchiornis
Eumaniraptora
Archaeopteryx
Enantiornithes
Confuciusornis
II
Yixianornis
III
Aves
IV

Fig. 1 Simplified cladogram of derived maniraptoran relationships depicting relative sternal ossification patterns, which indicate there are no shared sternal features at the base of the avian clade. *Dashed line* indicates where sternal plates are absent. *Light grey* indicates Late Cretaceous; *darker grey* indicates Tertiary. [Color for online/pdf only]

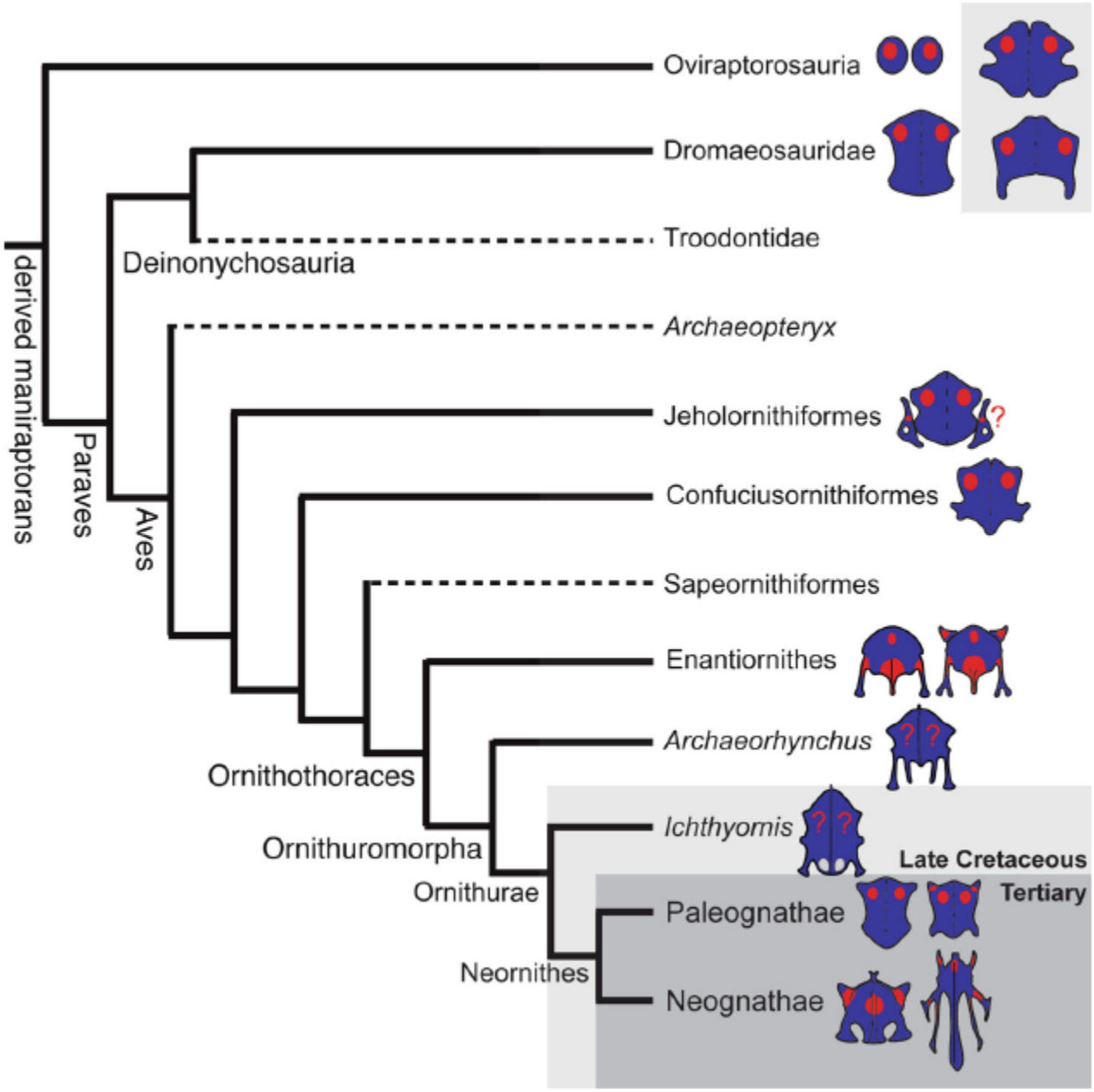

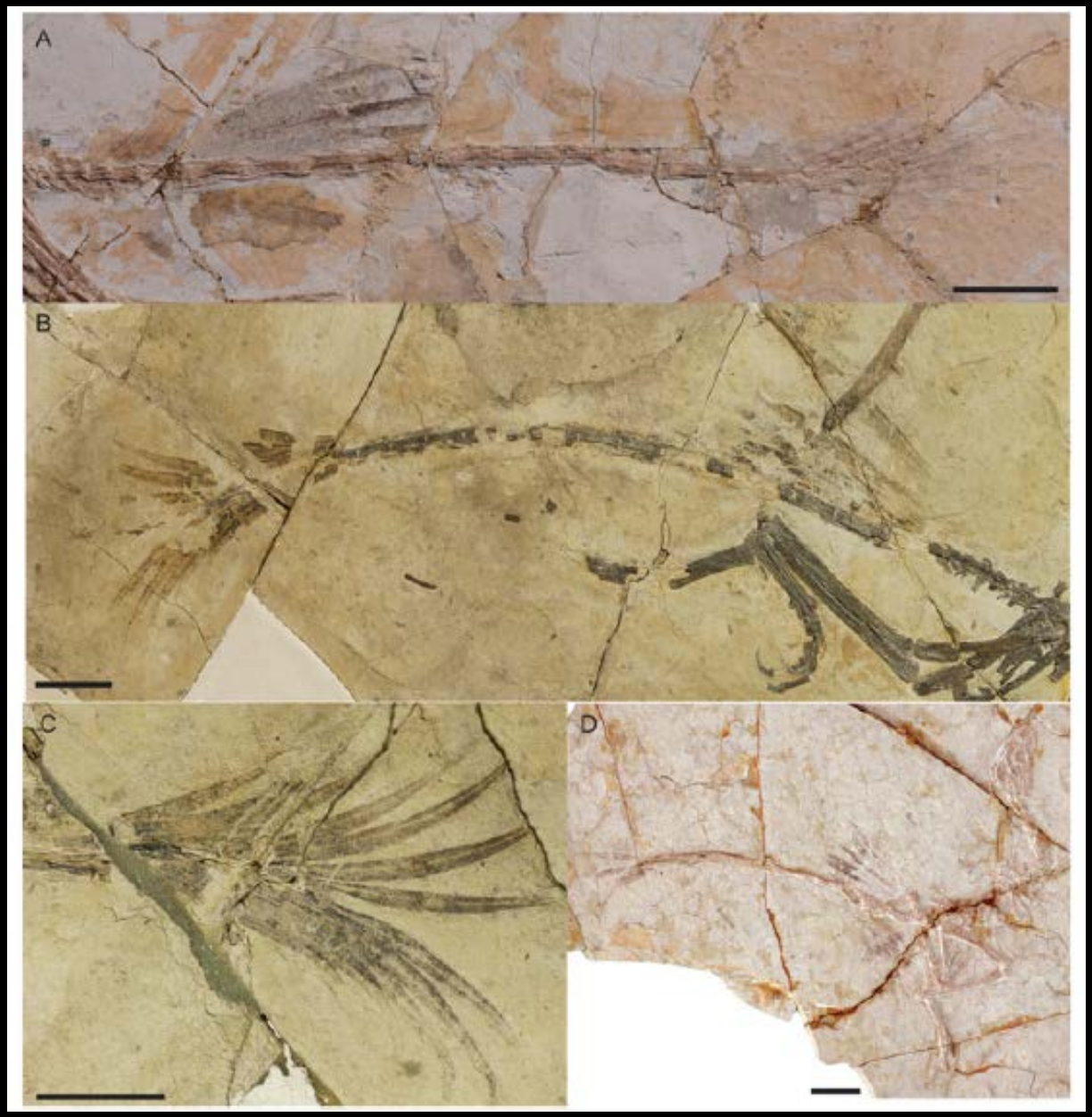
A
B
C
D

Aparición del Pigostilo

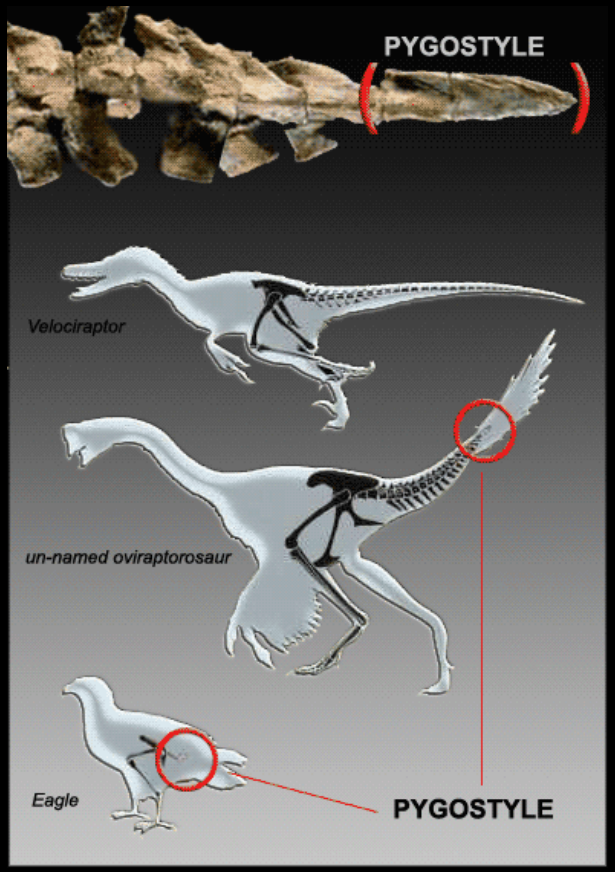

La transición de cola larga a pigostilo? *Zhongornis haoae*

Fig. 3.8 Holotype of the Yixian F
(B) DNHM D2456. (Photograph l

l: (A) DNHM D

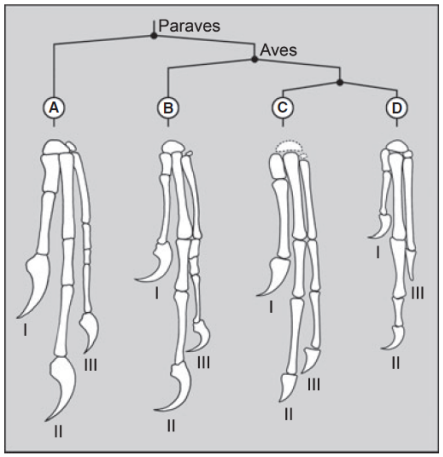

TEXT-FIG. 5. Comparative hands of the dromaeosaurid *Deinonychus* (A), *Archaeopteryx* (B), *Zhongornis* (C), and the enantiornithine bird *Longipteryx* (D). The hand of *Zhongornis* shows an intermediate phalangeal formula between 2-3-4-x-x (*Archaeopteryx* and most non-avian tetanuran theropods) and 2-3-1-x-x (typical of basal ornithothoracine birds: enantiornithines and primitive ornithuromorphs) (Chiappe 2007).

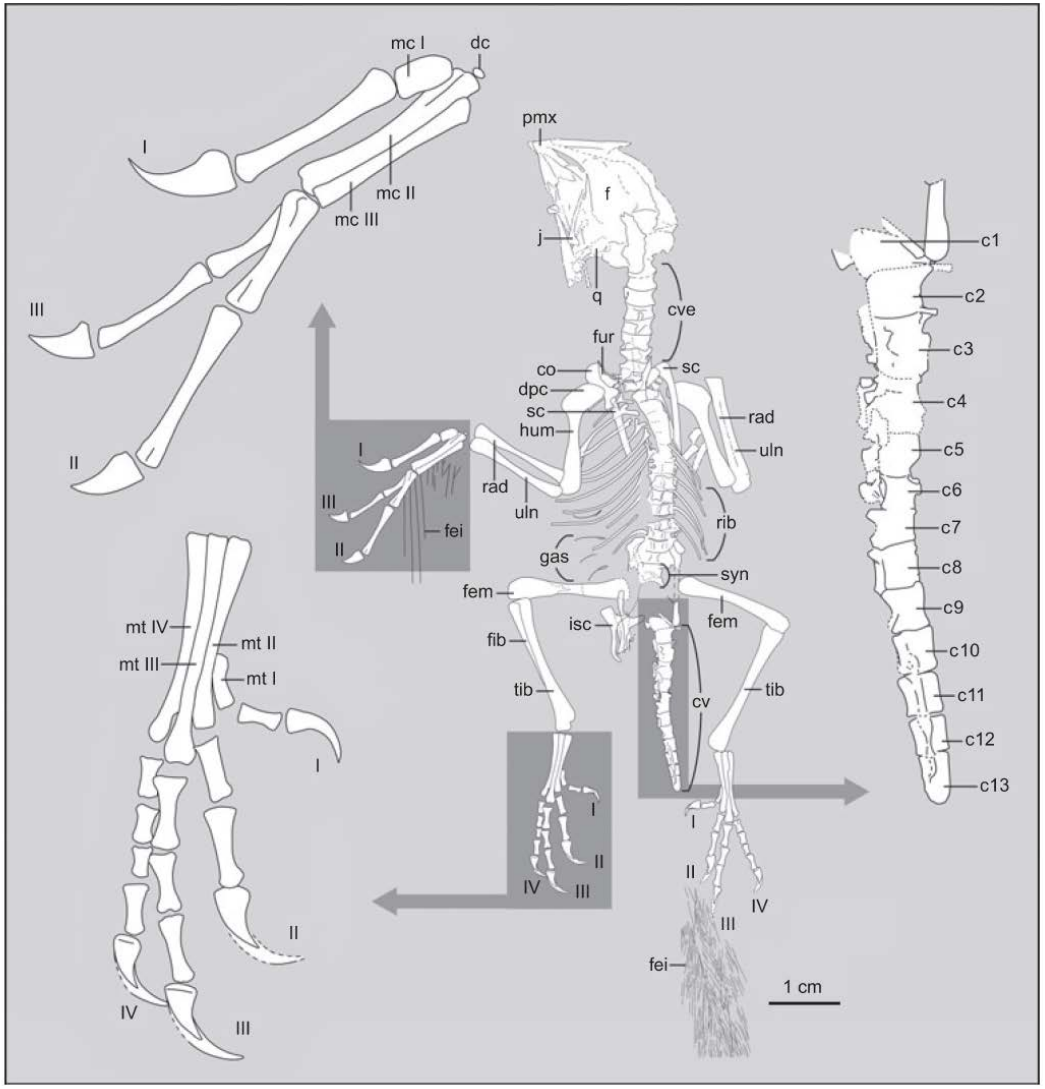

TEXT-FIG. 2. Interpretive drawing of slab (some portions added from information contained in counterslab) with close-ups of the manus, foot and caudal vertebrae. Abbreviations: co, coracoid; cv, caudal vertebrae (c1–c13); cve, cervical vertebrae; dc, distal carpal; dpc, deltopectoral crest; dv, dorsal vertebrae; gas, gastralia; f, frontal; fei, feather impressions; fem, femur; fib, fibula; fur, furcula; hum humerus; isc, ischium; j, jugal; mcI–III, metacarpals I–III; mtI–IV, metatarsals I–IV; pmx, premaxilla; q, quadrate; rad, radius; rib, thoracic ribs; sc, scapula; syn, synsacrum; tib, tibia; uln, ulna; I–IV, digits (manual or pedal) I–IV.

Confuciusornithidae

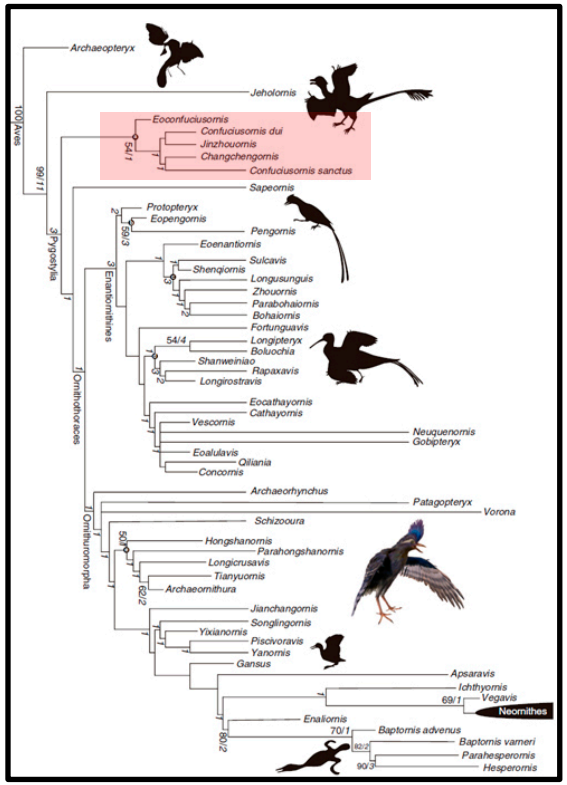

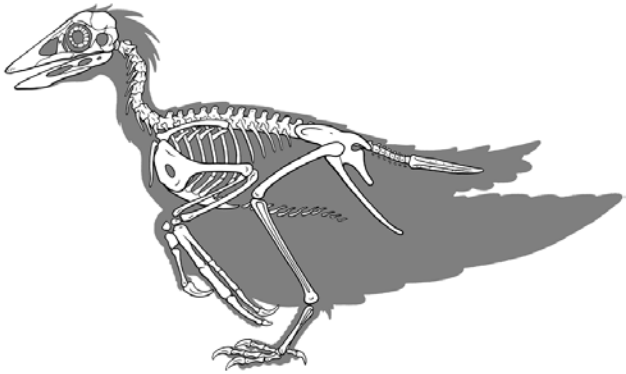

Clado que contiene al ancestro común más reciente de *Confuciusornis sanctus* y *Changchengornis hengdaoziensis* más todos sus descendientes. (Chiappe et al, 1999)

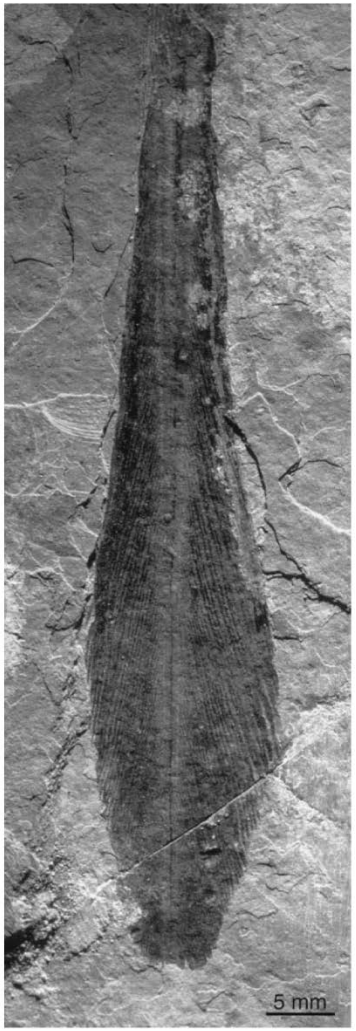

Fig. 49. Detail of distal end of the left elongate tail feathers of *Confuciusornis sanctus* (GMV-2150). Note the symmetrical rachis and barbed vanes.

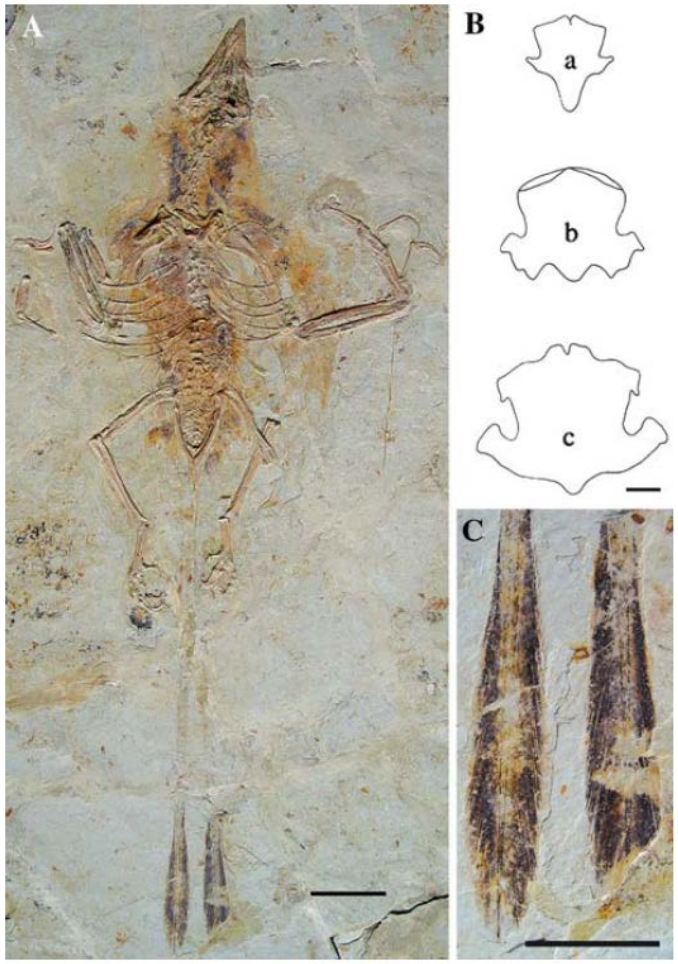

Fig. 1 **a** Holotype of *Confuciusornis feducciai* sp. nov., *scale bar* 5 cm; **b** comparison of sterna in *C. dui* (*a*) (Hou et al. 1999), *C. sanctus* (*b*) (Martin et al. 1998) and *C. feducciai* (*c*), *scale bar* 1 cm; **c** distal tail feathers of *C. feducciai*, *scale bar* 3 cm

Mosaico de rasgos: cráneo diápsido

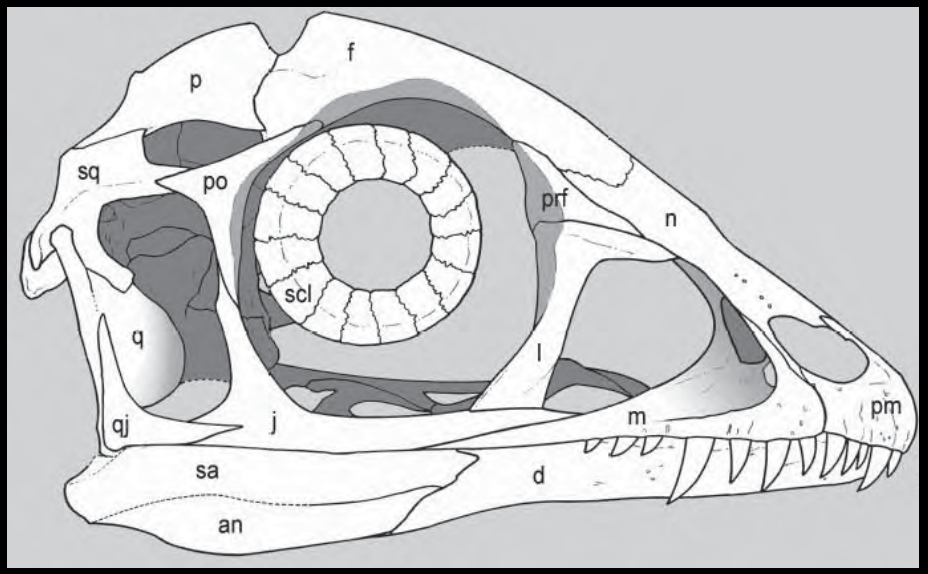

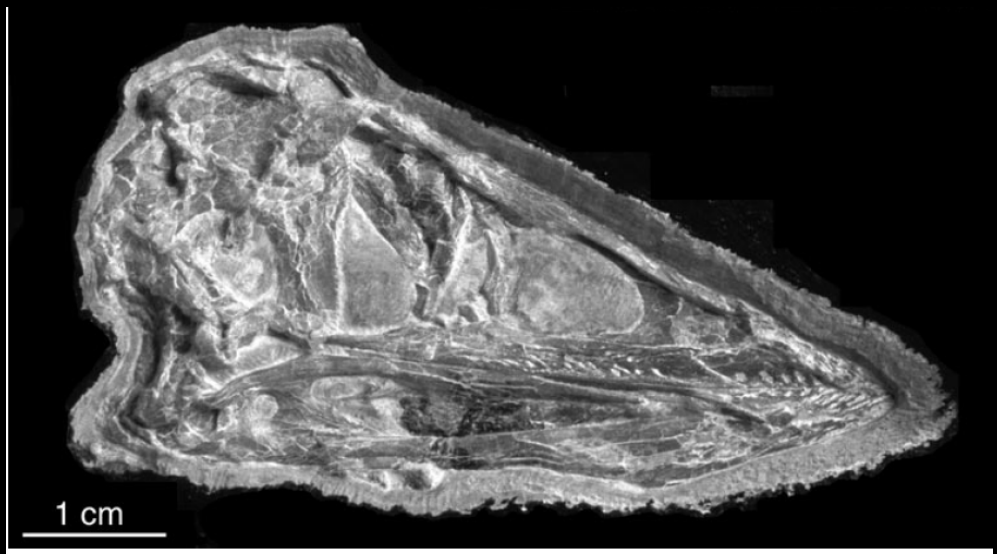

Scipionyx

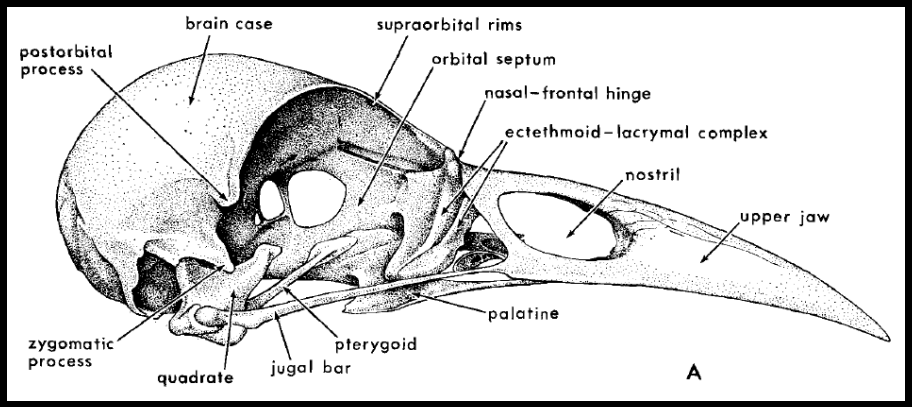

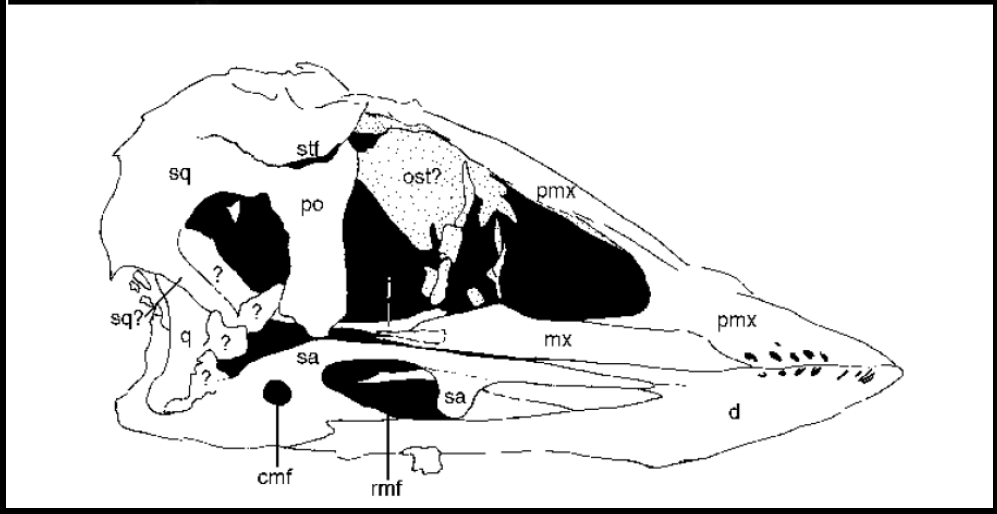

Corvus

Confuciusornis

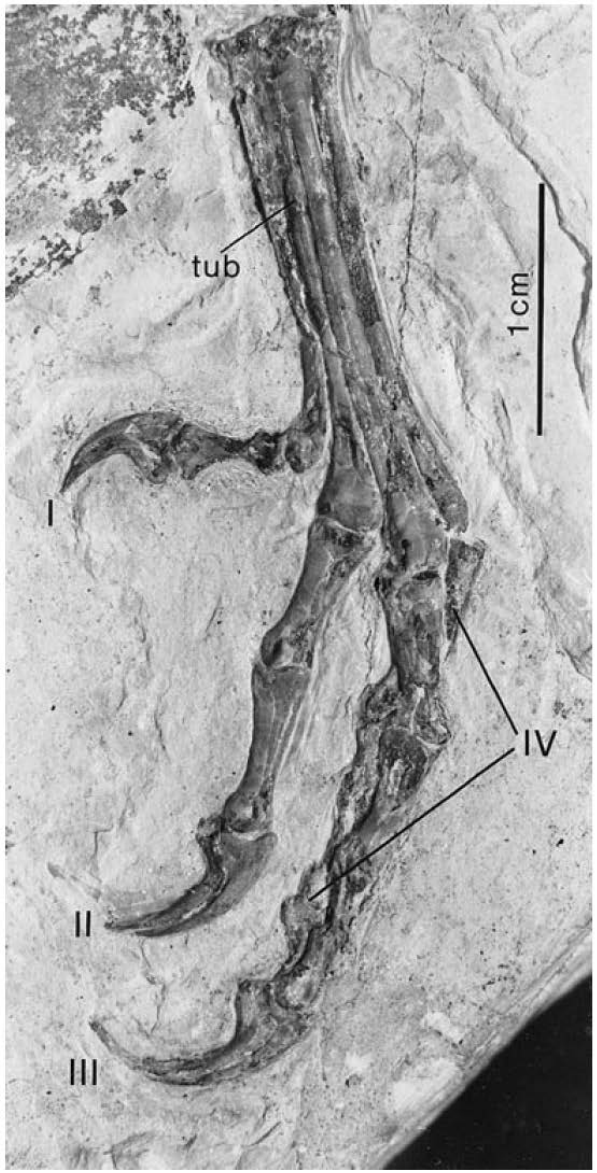

Fig. 44. Detail of left tarsometatarsus and foot of *Confuciusornis sanctus* (GMV-2130), dorsal view. See Anatomical Abbreviations for definition of labels.

Fig. 24. Detail of the synsacrum, free caudal vertebrae, pygostyle, and pelvis of *Confuciusornis sanctus* (GMV-2131), ventral view.

Fig. 33. Detail of pectralia and caudal end of the sternum of *Confuciusornis sanctus* (GMV-2152). See Anatomic

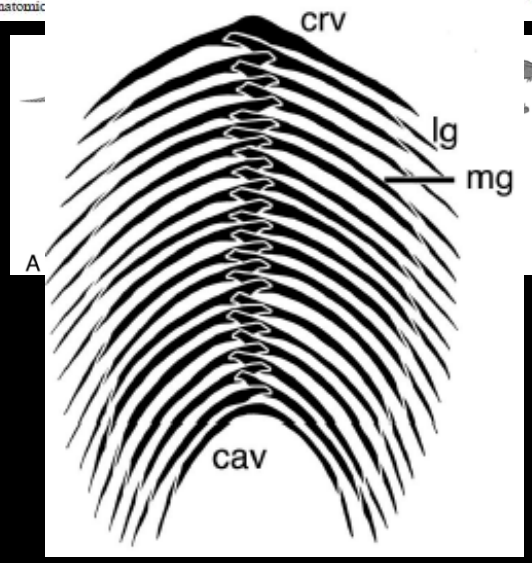

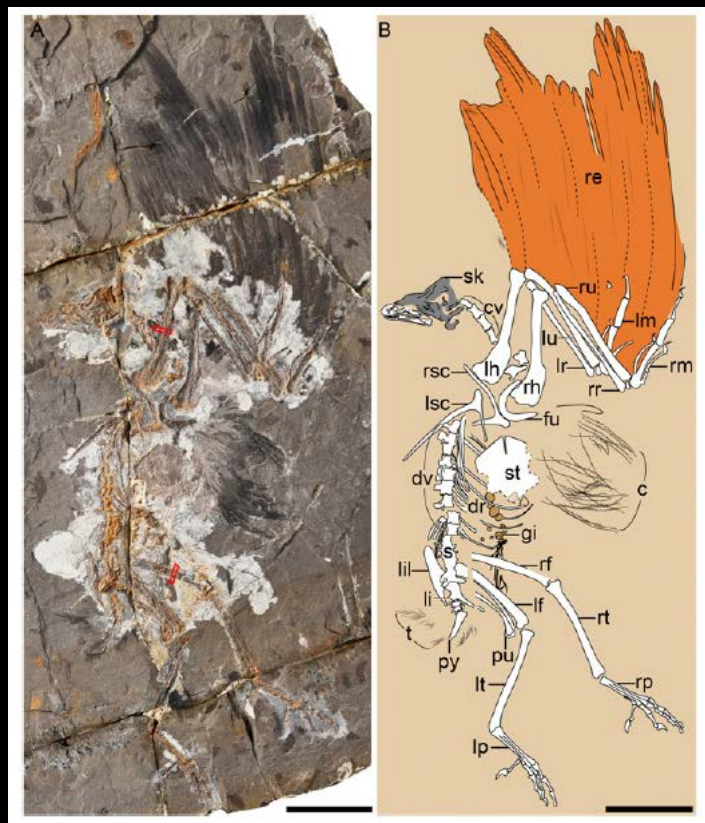

Fig. 1. *J. perplexus* gen. et sp. nov., IVPP V24194. (*A*) Photograph of main slab. (*B*) Composed line drawing. Red-outline boxes denote the locations of histological samples. c, covert feathers; cv, cervical vertebrae; dr, dorsal ribs; dv, dorsal vertebrae; fu, furcula; gi, gizzard; lf, left femur; lh, left humerus; li, left ischium; lil, left ilium; lm, left manus; lp, left pes; lr, left radius; lsc, left scapulocoracoid; lt, left tibiotarsus; lu, left ulna; pu, pubis; py, pygostyle; re, remiges; rf, right femur; rh, right humerus; rm, right manus; rp, right pes; rr, right radius; rsc, right scapulocoracoid; rt, right tibiotarsus; ru, right ulna; s, synsacrum; sk, skull; st, sternum; t, tail feathers. (Scale bar, 5 cm.)

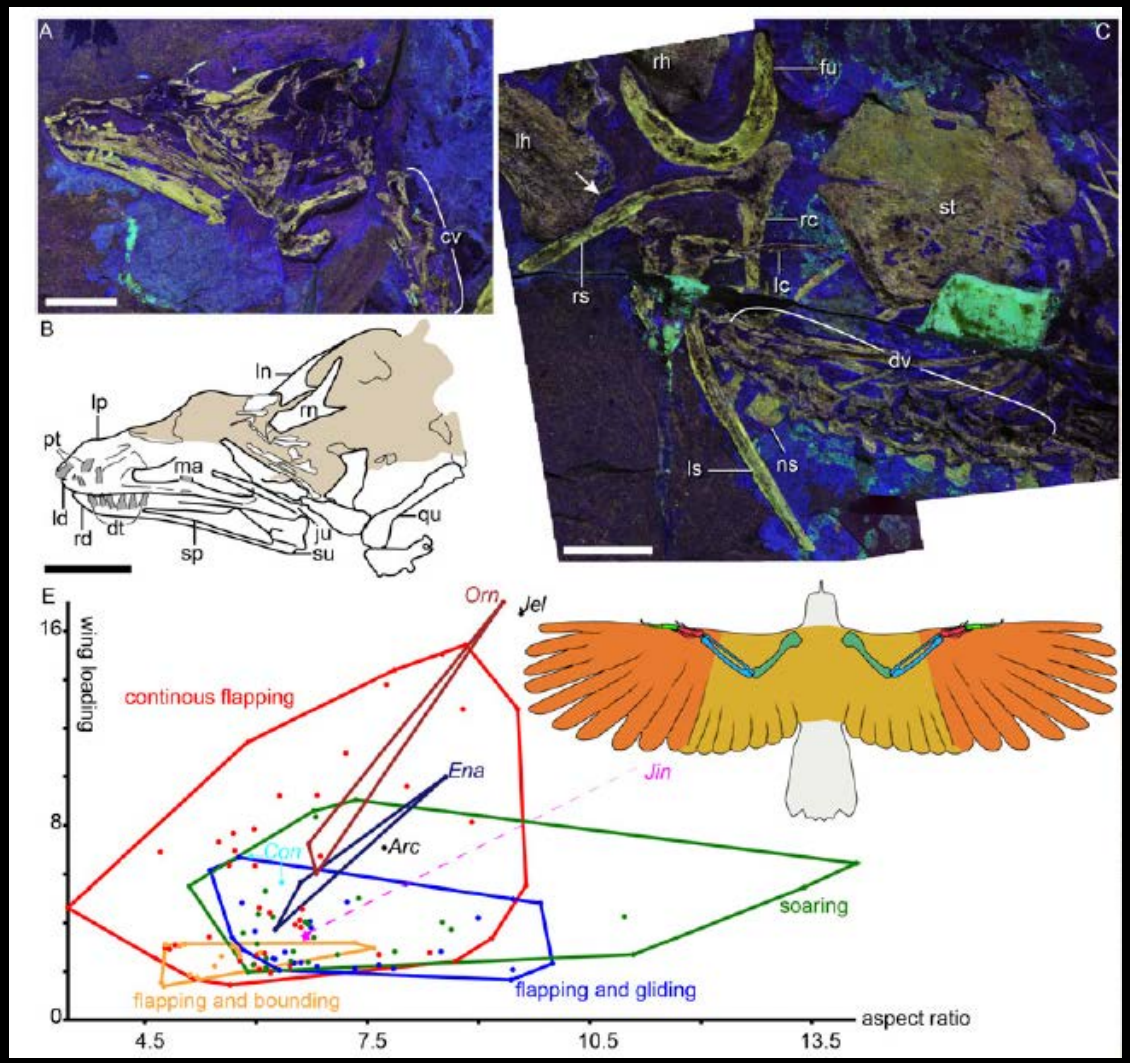

Wang et al 2018

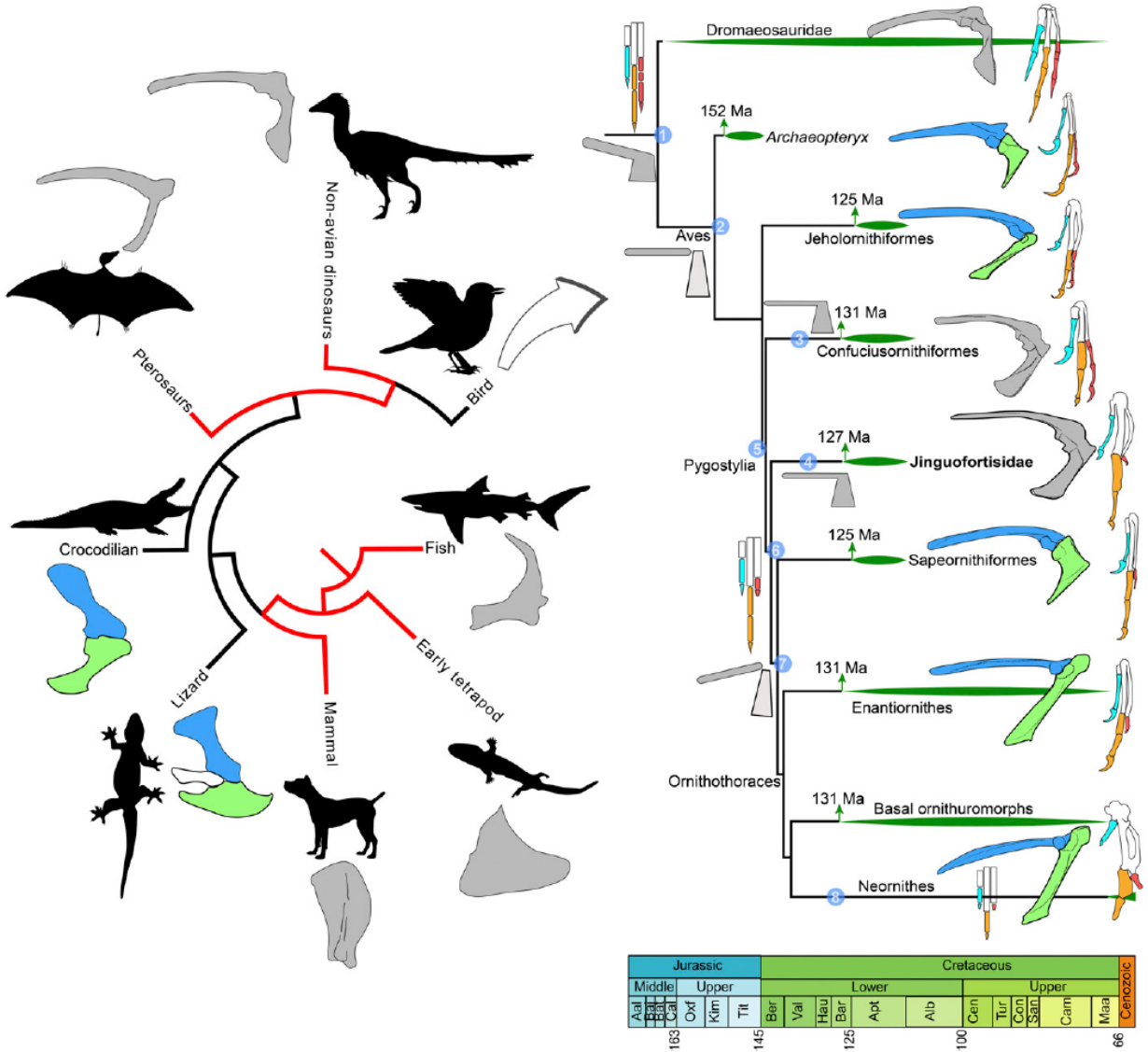

Fig. 3. Changes to the scapula and coracoid in vertebrates with a focus on basal avian clades. A simplified tree of vertebrates (*Left*) shows the scapula (colored in blue) and coracoid (in green) fused into a scapulocoracoid (in gray) in most major tetrapod clades (see *SI Appendix*, *SI Text*, for details). Simplified cladogram of basal Aves (*Right*) shows the changes to the shoulder girdle and manus (see *SI Appendix*, Fig. S8, for complete phylogenetic result). Thick green lines near each clade denote temporal range with the first-appearance datum denoted. Major changes to the shoulder girdle and manus across basal avian phylogeny are summarized: (1) in most nonavian theropods, the scapula and coracoid are fused into a scapulocoracoid at an obtuse angle, and they have a manual phalangeal formula of 2–3-4; (2) scapula and coracoid become separated and form an angle of ~90°; (3, 4) independent evolution of a fused scapulocoracoid in the Confuciusornithiformes and Jinguofortisidae; (6) minor digit is reduced resulting in a manual phalangeal formula of 2–3-2; (7) scapula and coracoid are decoupled and form an acute angle with further manual digit reduction evolving in derived ornithuromorphs; (8) alternatively, it is equally parsimonious that a fused scapulocoracoid evolved at the base of Pygostylia and was lost in pygostylians crownward of Jinguofortisidae (5).

Wang et al 2018

Origen del “vuelo moderno”: Ornithothoraces

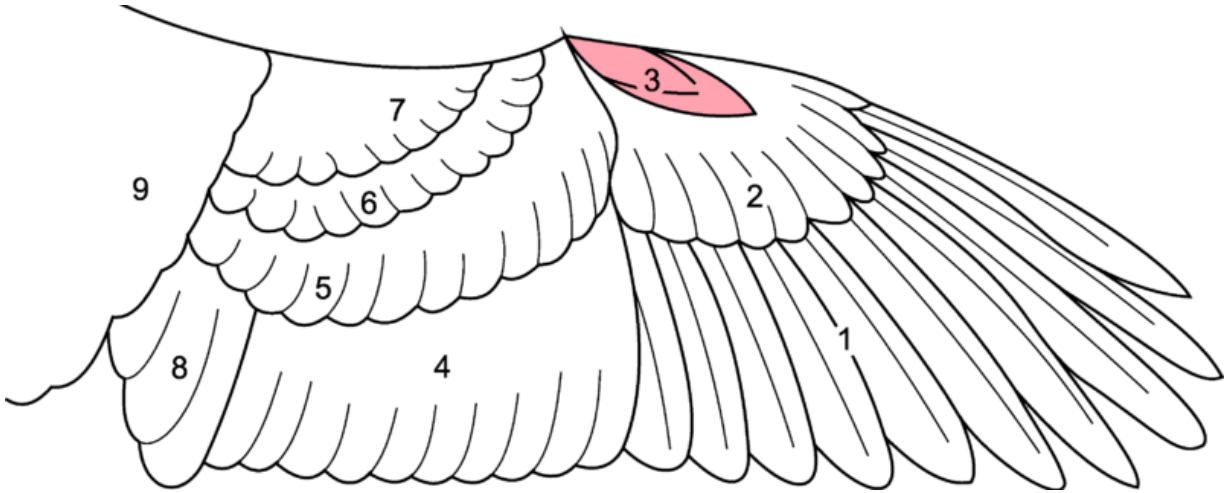

Protopteryx

Archaeornithura

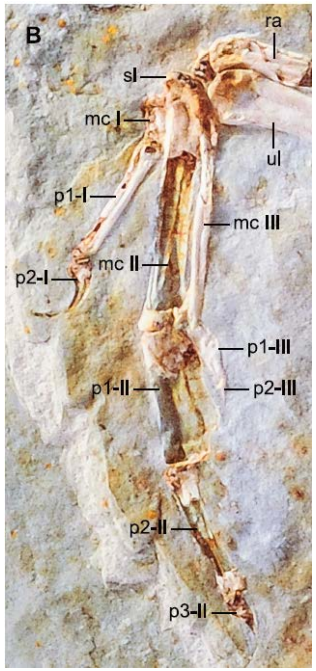

Hongshanornis

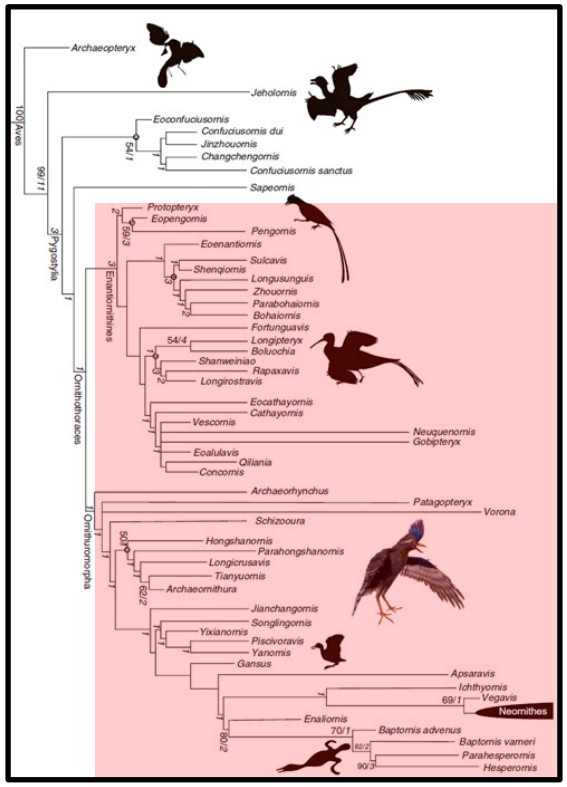

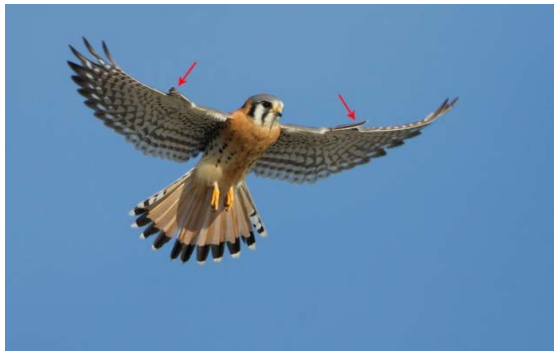

Falco

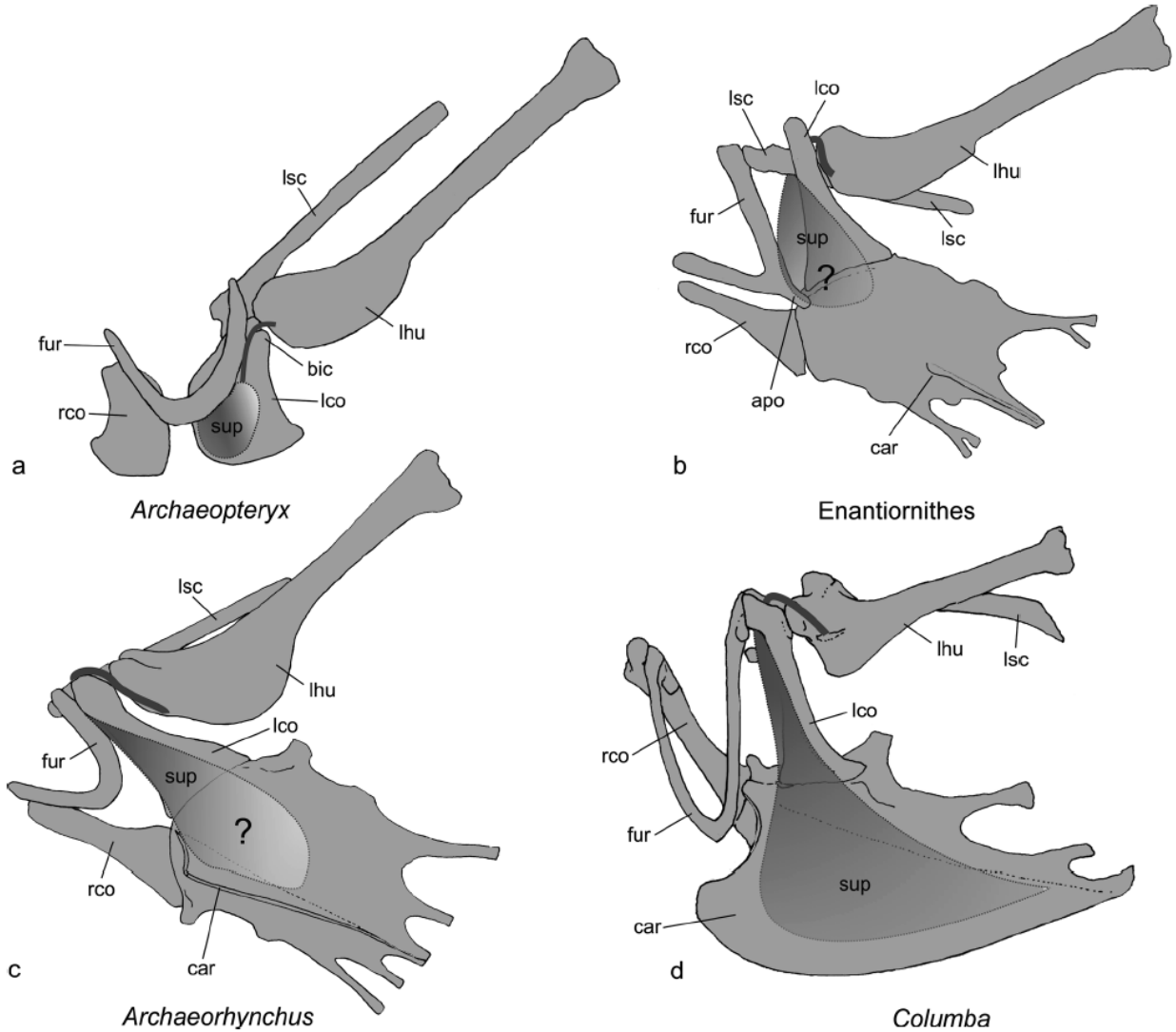

Fig. 1 Schematic reconstructions of the pectoral girdle bones and the supracoracoideus muscle with its tendon of **a** the Late Jurassic *Archaeopteryx* (reconstruction based on Thermopolis specimen described by Mayr et al. 2007), **b** the Early Cretaceous enantiornithine *Rapaxavis* (reconstruction based on DNHM-D2522, figured by Chiappe and Meng 2016), **c** the Early Cretaceous ornithuromorph *Archaeorhynchus* (reconstruction based on specimens figured by Wang and Zhou 2017), and **d** an extant bird (*Columba*). The hypothetical size and position of the supracoracoideus muscle of *Archaeopteryx* was inferred from a reconstruction of this muscle in the dromaeosaur *Saurornitholestes* (Jasinoski et al. 2006: fig. 6a). The humeri are shown in an extremely supinated position. *apo* apophysis of furcula, *bic* biceps tubercle, *car* carina sterni, *fur* furcula, *lco* left coracoid, *lhu* left humerus, *lsc* left scapula, *rco* right coracoid, *sup* musculus supracoracoideus. Not to scale

Mayr 2017

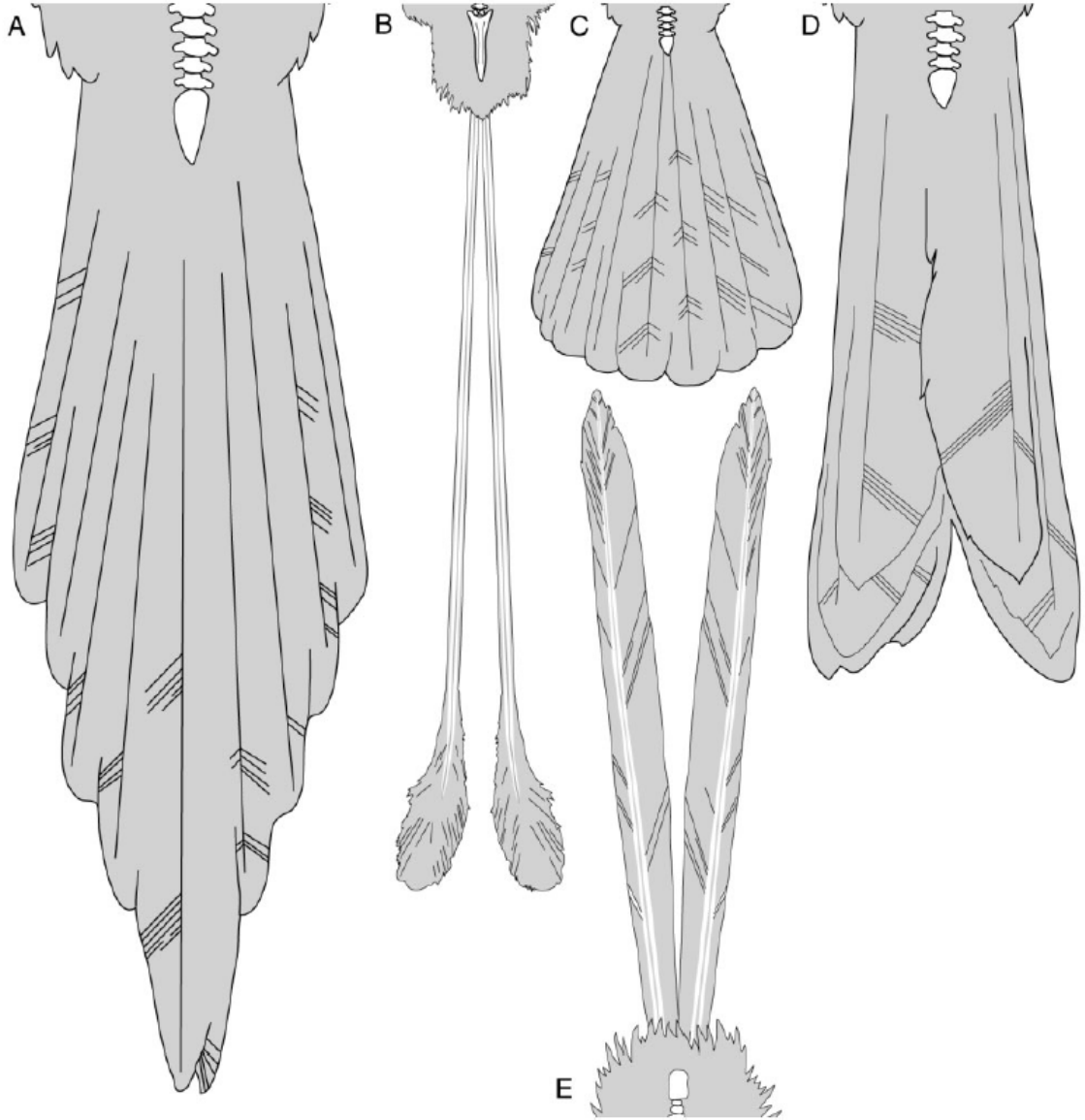

Figure 5. Reconstructions of the known tail morphologies in Jehol pygostylians. A, graded fan of pennaceous feathers in *Sapeornis* (based on STM16-18). B, paired rachis-dominated'racket-plumes' in enantiornithine *Dapingfangornis* (morphologically similar to the tail feathers of *Confuciusornis*). C, fan-shaped tail of pennaceous feathers in ornithuromorph *Hongshanornis*. D, forked tail (presumably formed by asymmetrical pennaceous feathers) in ornithuromorph *Schizooura*. E, paired fully pennaceous rachis dominated feathers in *Eopengornis*. Not drawn to exact scale.

“Las aves opuestas”: Enantiornithes

Protopteryx

Rapaxavis

Pengornis

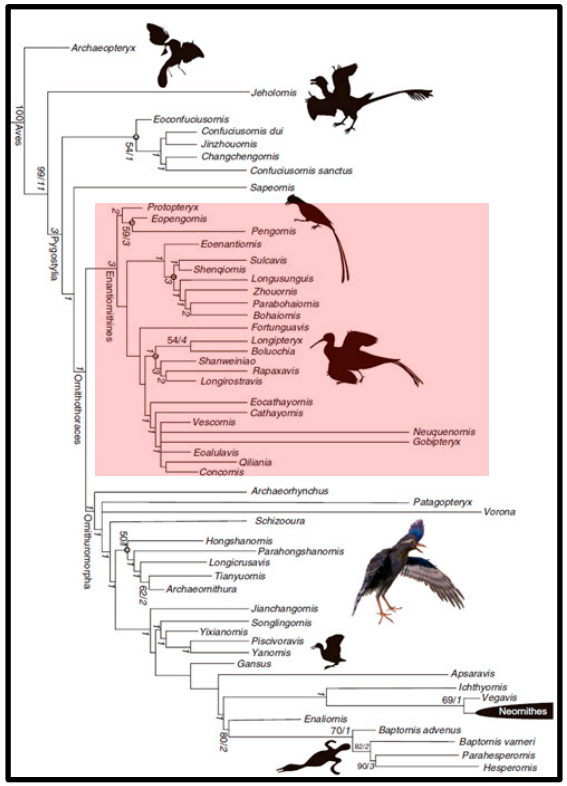

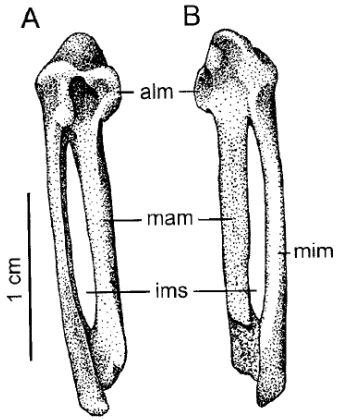

Figure 11.10. Carpometacarpus of *E. leali* (PVL-4049) from the Late Cretaceous of El Brete (Argentina). A, ventral view. B, dorsal view. Abbreviations: alm, alular metacarpal; ims, intermetacarpal space; mam, major metacarpal; mim, minor metacarpal.

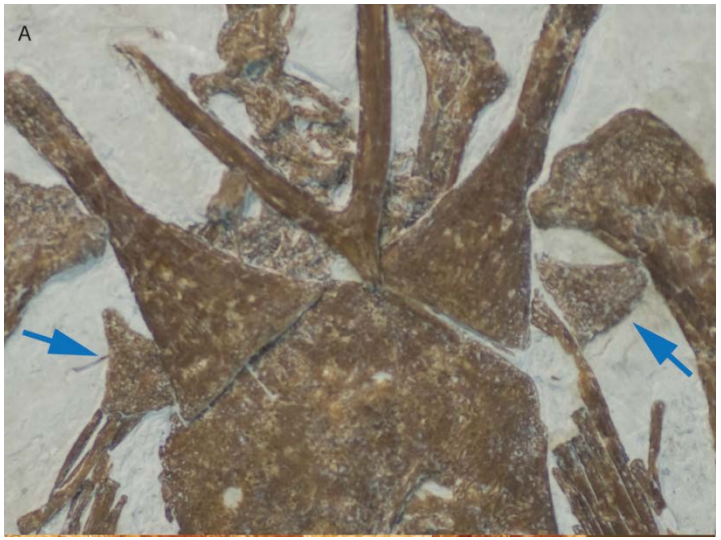

Novedades evolutivas:

- Metacarpo III (**minor metacarpal**) de mayor longitud que metacarpo II (**major metacarpal**)
- Fúrcula en forma de Y
- Presencia de plumas “racket-plume” en la cola

Diferente estrategia de crecimiento

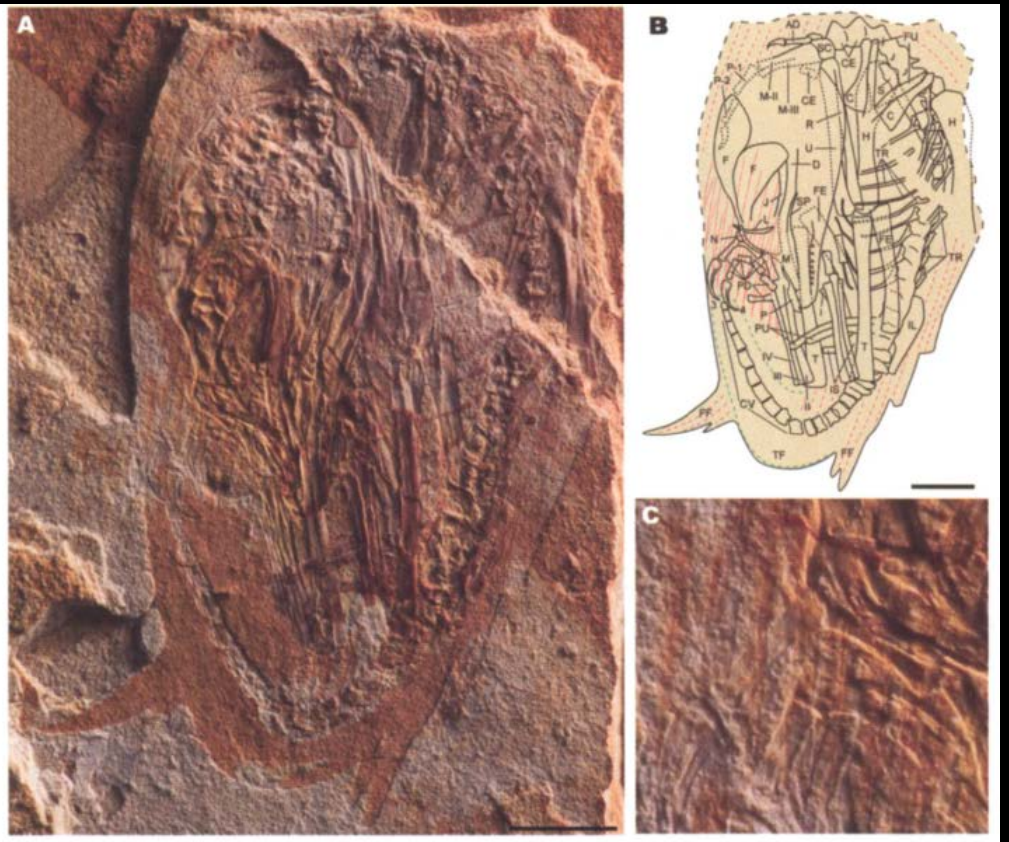

Fig. 1. (A) Photograph of a Lower Cretaceous avian embryo from Liaoning, China (Institute of Vertebrate Paleontology and Paleoanthropology no. V14238). (B) A line drawing of the fossil shown in (A). Red lines indicate wing feather sheets, and the green line shows imprints of tail feather anlagen. (C) A close-up view of long wing feather sheets near the pedal claws. Scale bars, 5 mm. AD, alular digit; C, coracoid; CE, cervical vertebra; CV, caudal vertebra; D, dentary; F, frontal; FE, femur; FF, wing feather sheets; FU, furcula; H, humerus; IL, ilium; IS, ischium; J, jugal; L, lachrymal; M, maxilla; M-II, metacarpal II; M-III, metacarpal III; N, nasal; PD, pedal digits; P, premaxilla; PU, pubis; P-1, first phalanx of the major digit; P-2, second phalanx of the major digit; R, radius; S; scapula; SC, semilunate carpal; SP, splenial; T, tibia; TF, tail feather sheets; TR, thoracic rib; U, ulna; 3 and 4, pedal digits III and IV; and I to IV, metatarsals I to IV.

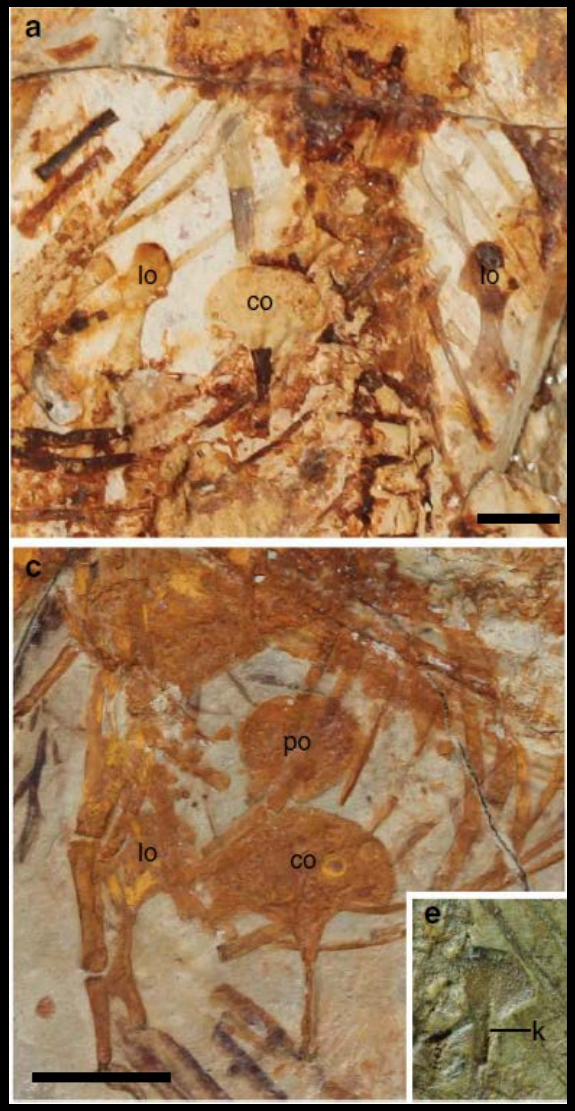

Ornithuromorpha

- Es el clado más inclusivo que contiene a la perdiz chilena (*Nothoprocta perdicaria*), pero no contiene a Enantiornithes.

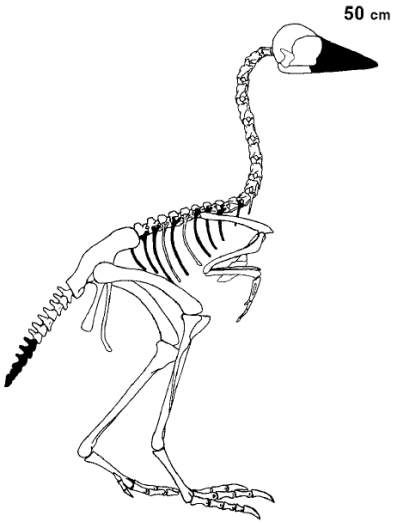

Patagopteryx

Ichthyornis

Nothoprocta

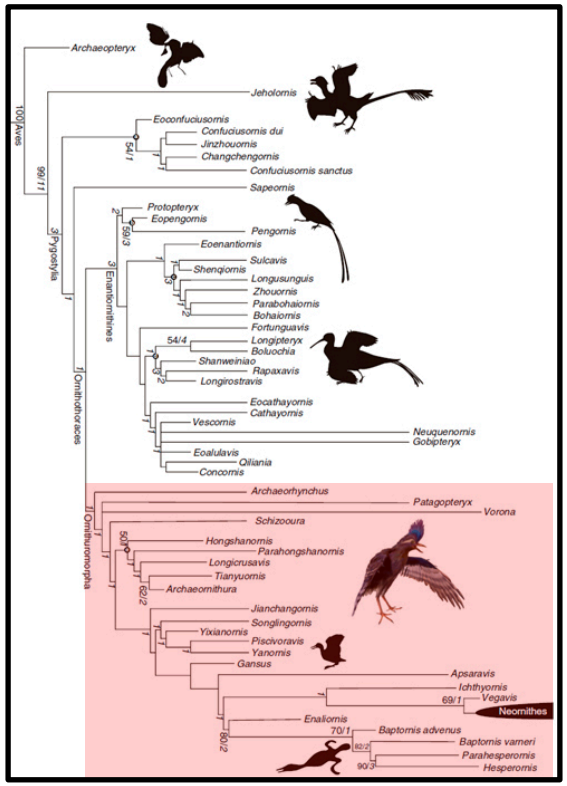

Novedades evolutivas en el esqueleto

- Pérdida de Postorbital
- Proceso procoracoides y esternal en coracoides
- Escápula curva
- Quilla bien desarrollada
- Hipotarso primitivo
- Pigostilo reducido
- Fúrcula en forma de U


A

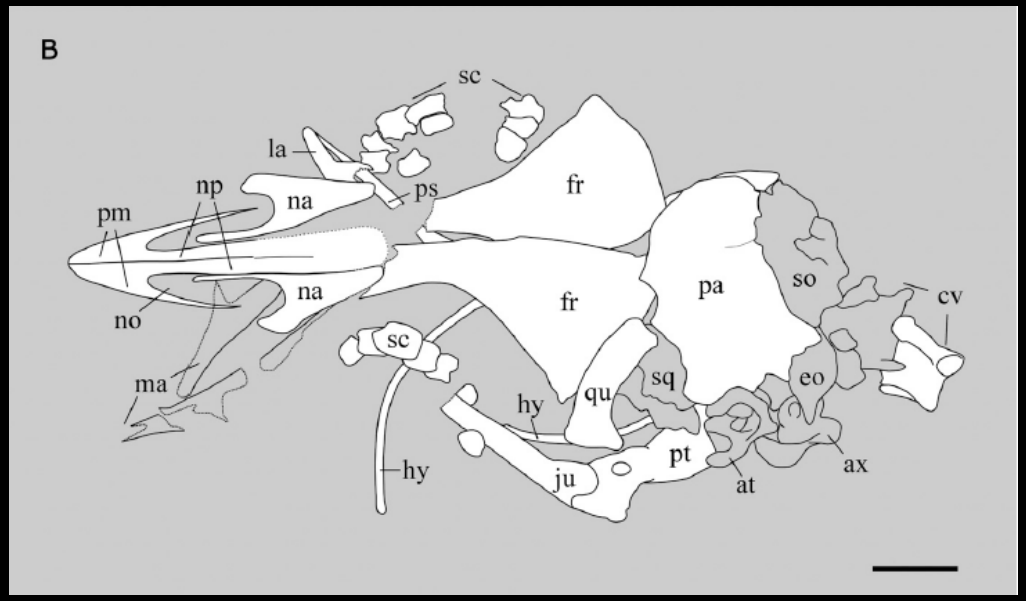
B
sc
la
ps
fr
np
na
pm
pa
so
cv
na
fr
no
sc
sq
eo
ma
qu
hy
pt
ax
hy
ju
at

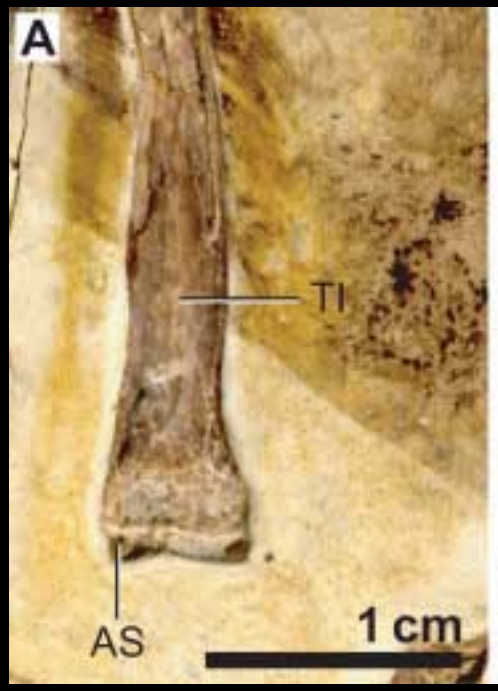
A
TI
AS
1 cm

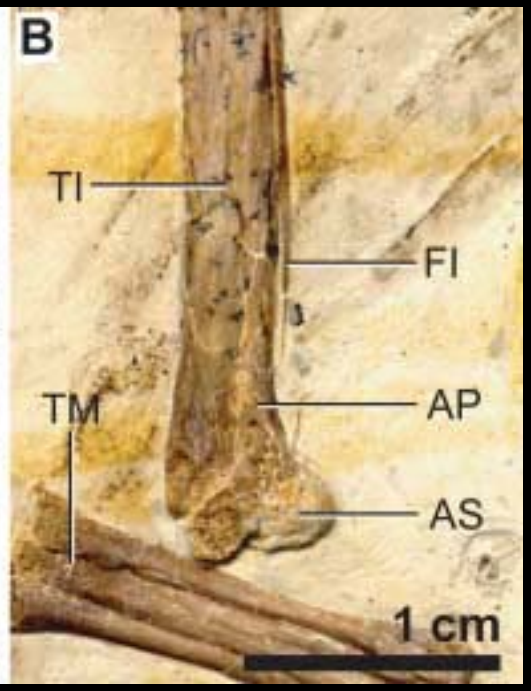
B
TI
FI
TM
AP
AS
1 cm

EL ornithuromorfo más antiguo: *Archaeornithura*

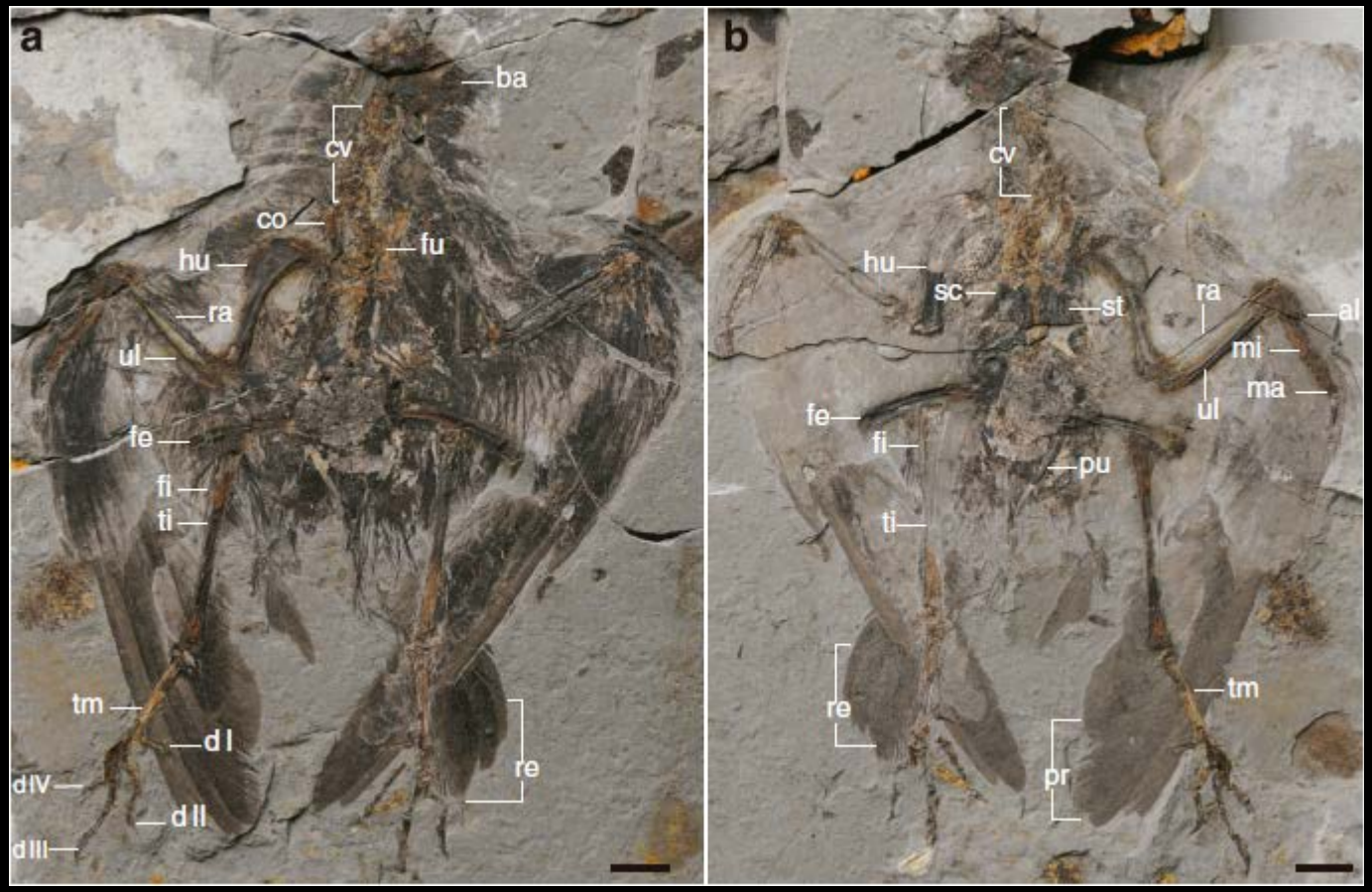

Songlingornithidae

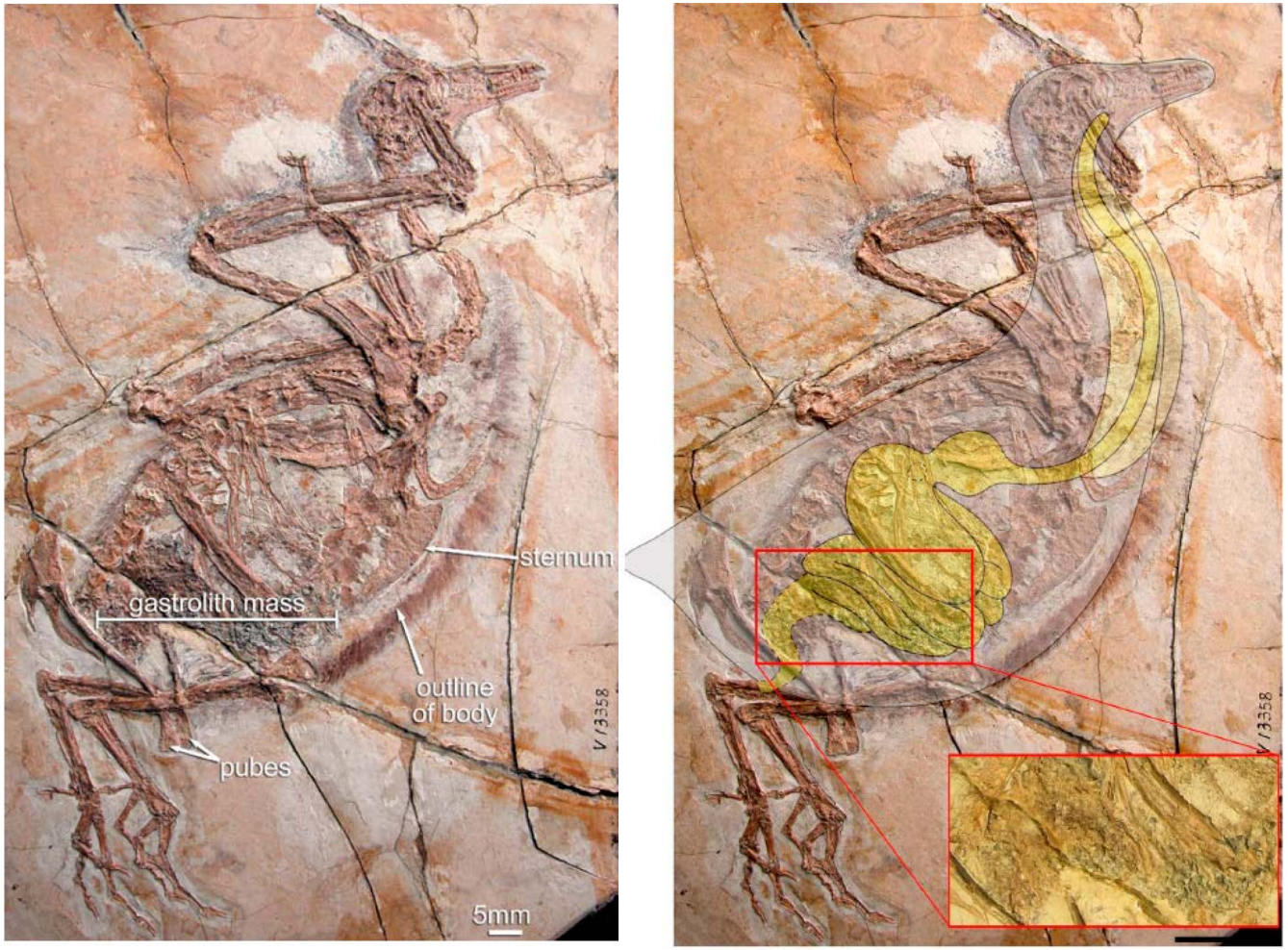

Fig. 2 A new specimen (IVPP V13358) of the fish-eating bird *Yanornis martini*, showing the grit mass in the abdominal region

Yanornis martini

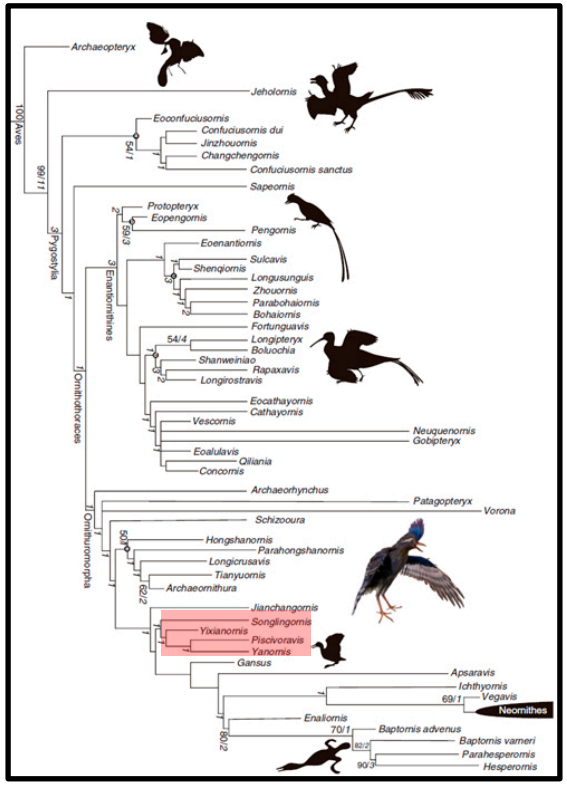

Fig. 11 Skeletal reconstruction of *Yixianornis grabaui* by G. S. Paul.


A
B
C


B

Hoshangornithidae

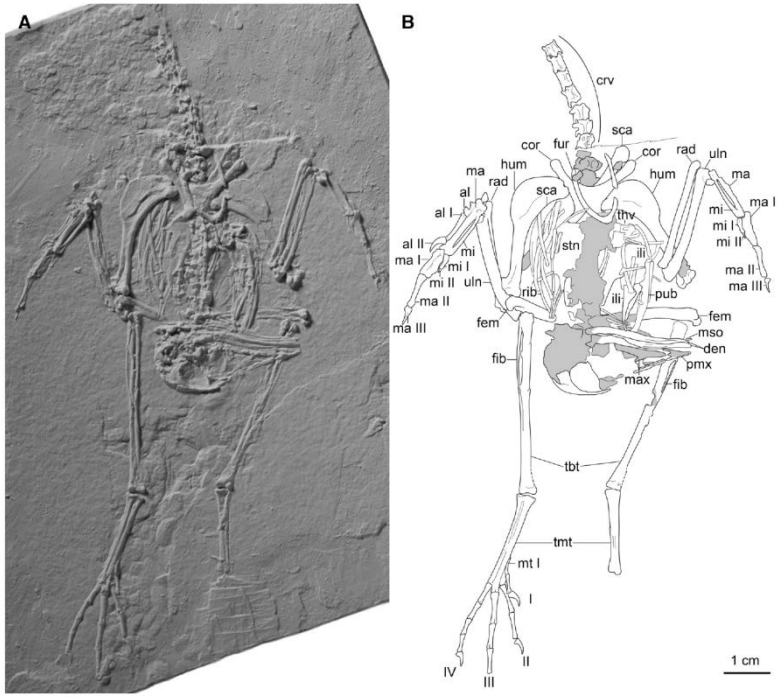

FIGURE 4. Cast of slab B of PKUP V1069, holotype of *Longicrusavis houi*, gen. et sp. nov. **A**, photograph and **B**, camera lucida drawing. The cast was dusted with magnesium to highlight the bones.

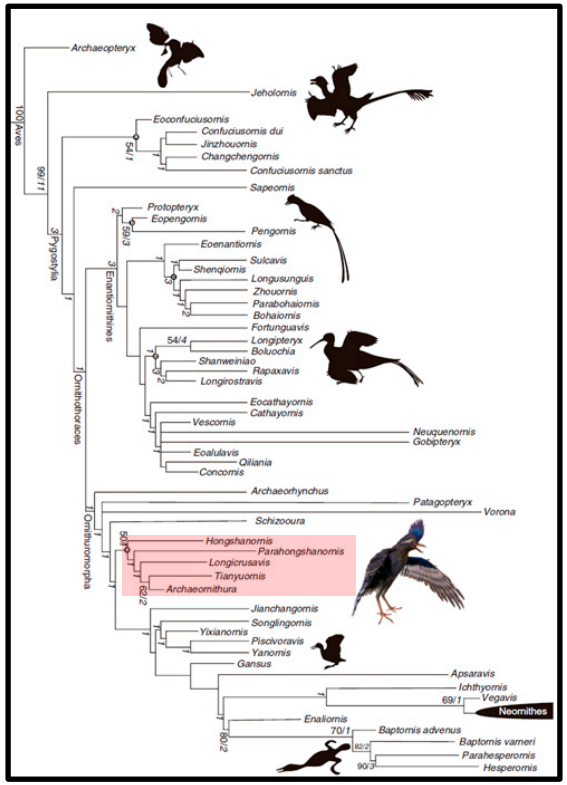

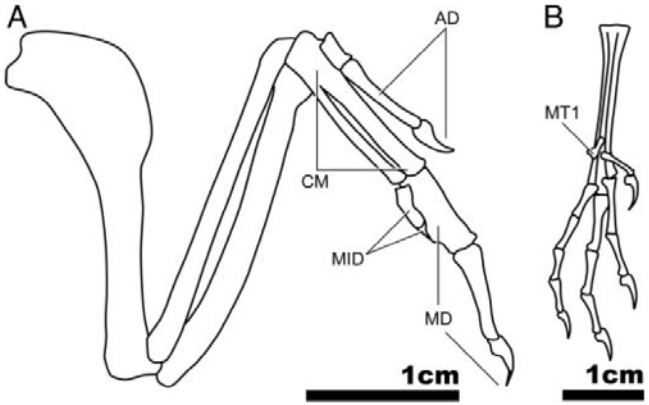

Fig. 5. Line drawing of the left wing (*A*) and left foot (*B*) of *Hongshanornis longicresta* gen. et sp. nov. (IVPP V14533). AD, alular digit; CM, carpometacarpus; MD, major digit; MID, minor digit; MT1, metatarsal I.

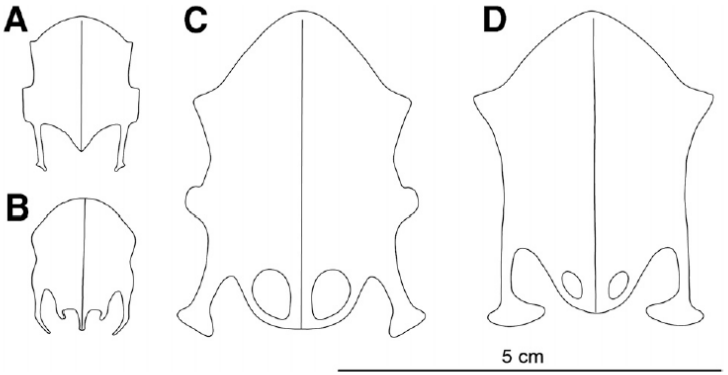

FIGURE 6. Comparative drawings of the sterna of Early Cretaceous ornithuromorphs from the Jehol Biota, China. **A**, PKUP V1069, holotype of *Longicrusavis houi*, gen. et sp. nov.; **B**, *Hongshanornis longicresta*; **C**, *Yixianornis grabaui*; **D**, *Yanornis martini*.

Aves basales acuáticos: *Gansus*

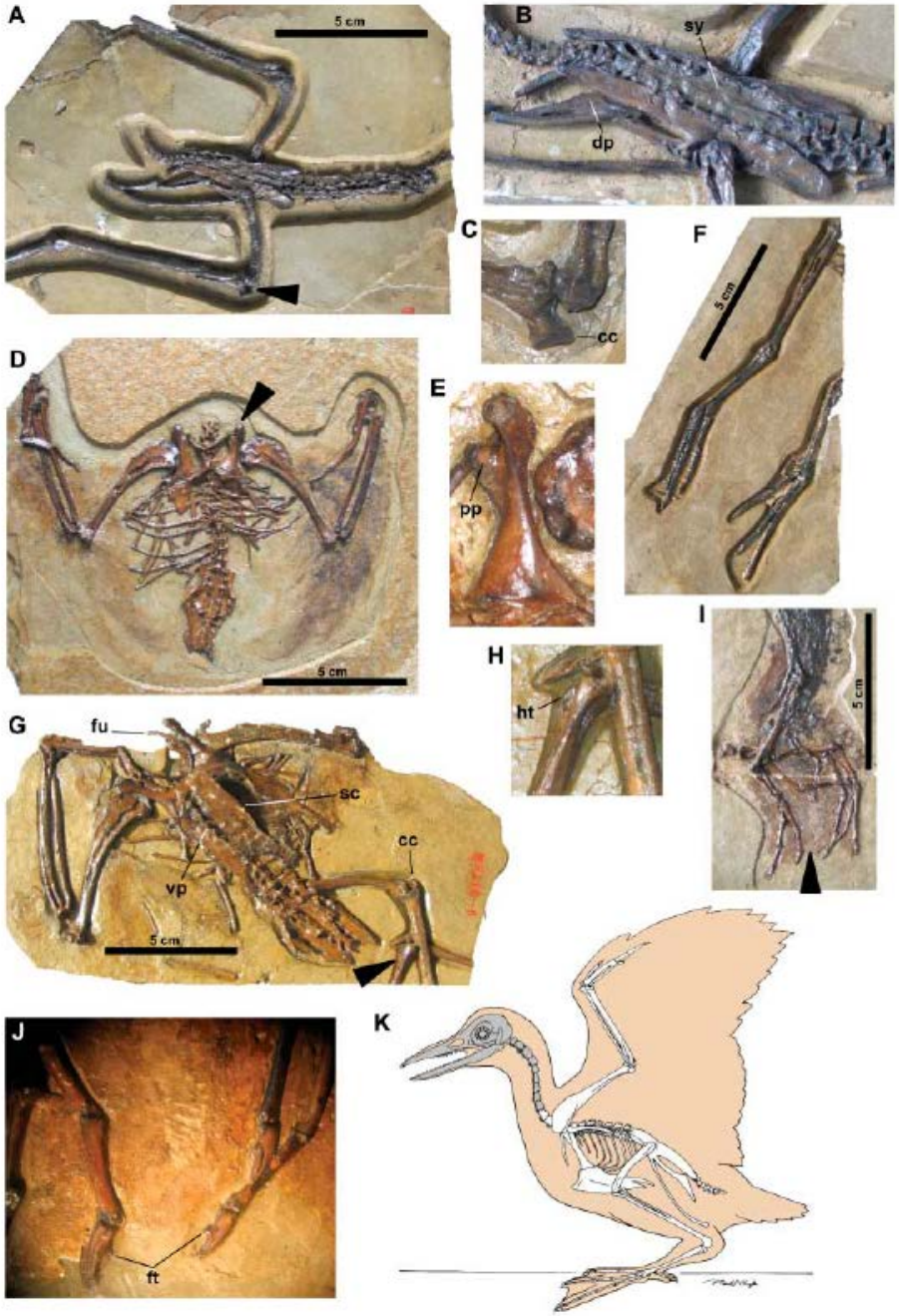

Gansus yumenensis

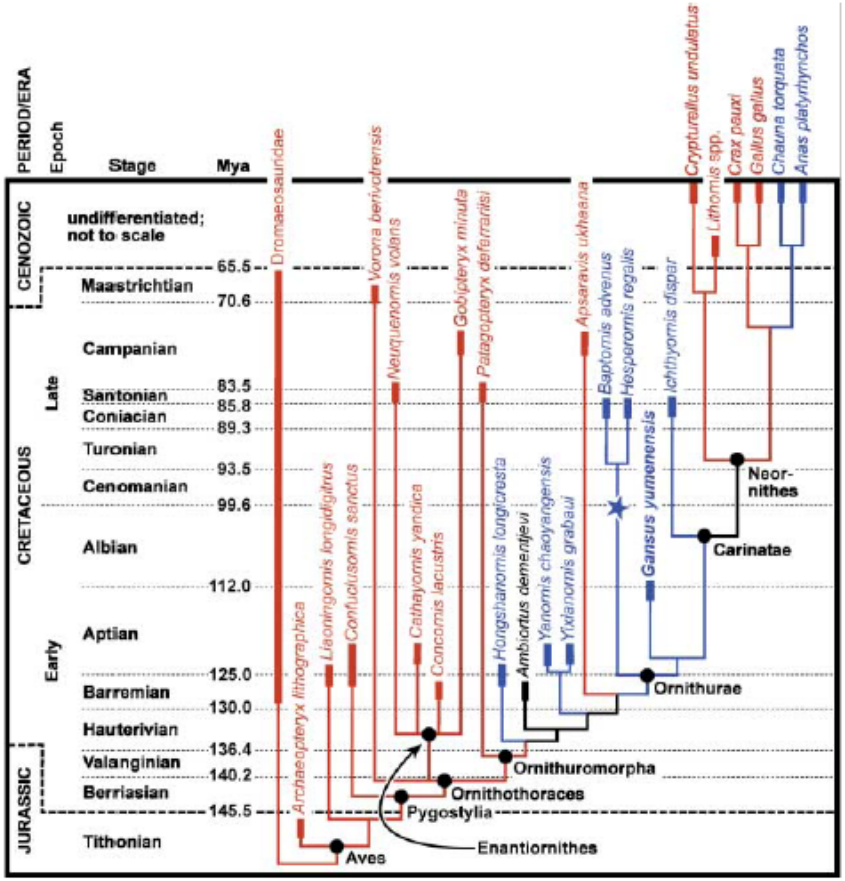

Fig. 3. Phylogenetic position of *G. yumenensis* (50% majority-rule consensus tree) based on holotype and new referred specimens; time scale is per (*28*). Thin line segments represent ghost lineages; thick line segments represent known ranges of terminal taxa. Clades are denoted by black circles (see supporting online material for clade definitions). The star represents the temporal position of *Enaliornis* spp. Colors indicate known or inferred ecologies as follows: brown, terrestrial/arboreal; blue, aquatic/amphibious; black, equivocal. Note the sequence of amphibious taxa basal to the Neornithes. Depicted divergence times are intended as approximations only, based on the oldest occurrence of an included species and subsequent divergences. Mya, million years ago.

Hesperornithiformes

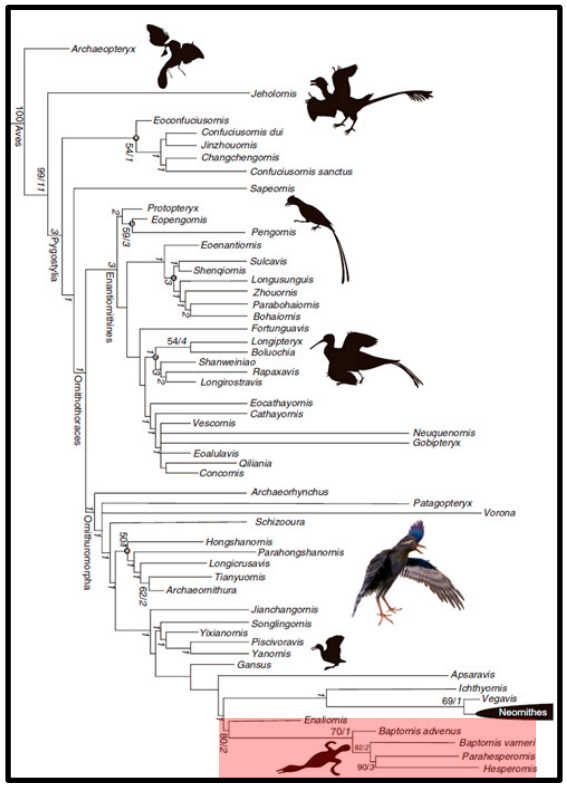

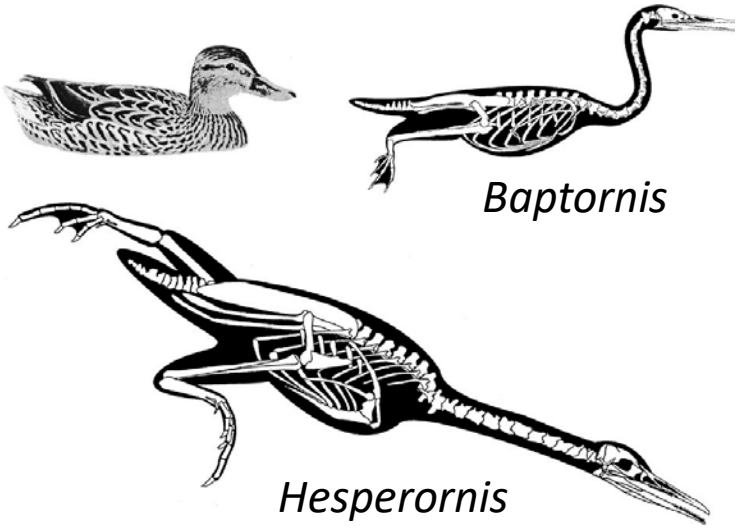

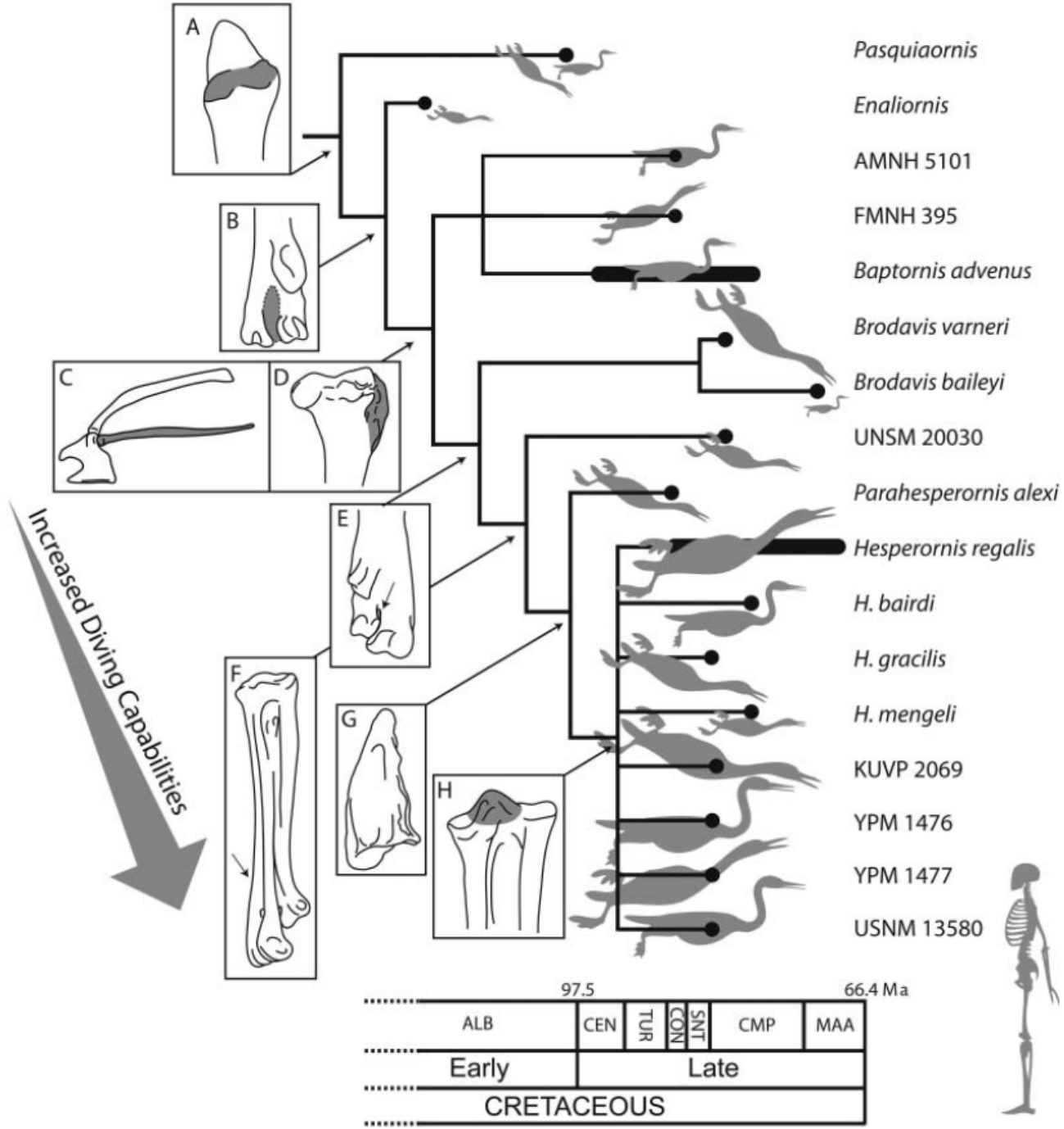
A
B
C
D
E
F
G
H
Increased Diving Capabilities
Pasquiaornis
Enaliornis
AMNH 5101
FMNH 395
Baptornis advenus
Brodavis varneri
Brodavis baileyi
UNSM 20030
Parahesperornis alexi
Hesperornis regalis
H. bairdi
H. gracilis
H. mengeli
KUVP 2069
YPM 1476
YPM 1477
USNM 13580
97.5
66.4 Ma
ALB
CEN
TUR
CON
SNT
CMP
MAA
Early
Late
CRETACEOUS

Carinatae

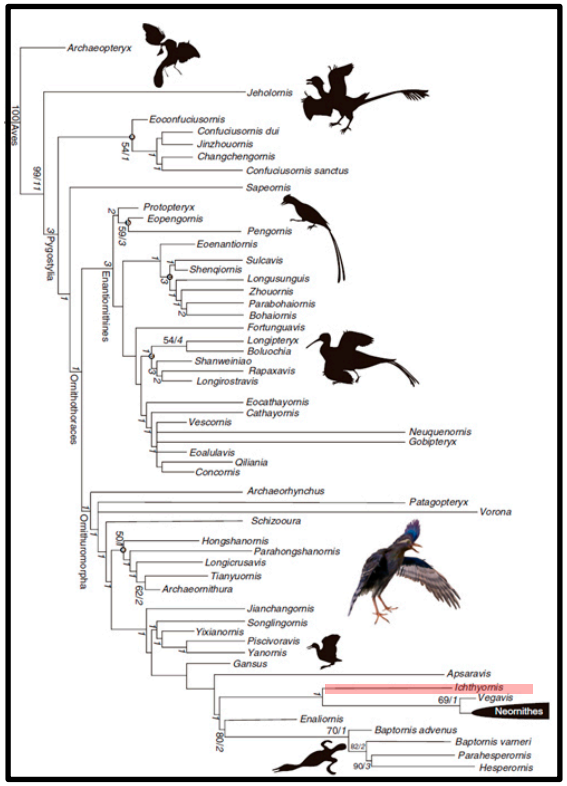

Ichthyornis

Fig. 66. Two silhouette reconstructions of *Ichthyornis dispar* by Gregory Paul showing the relative

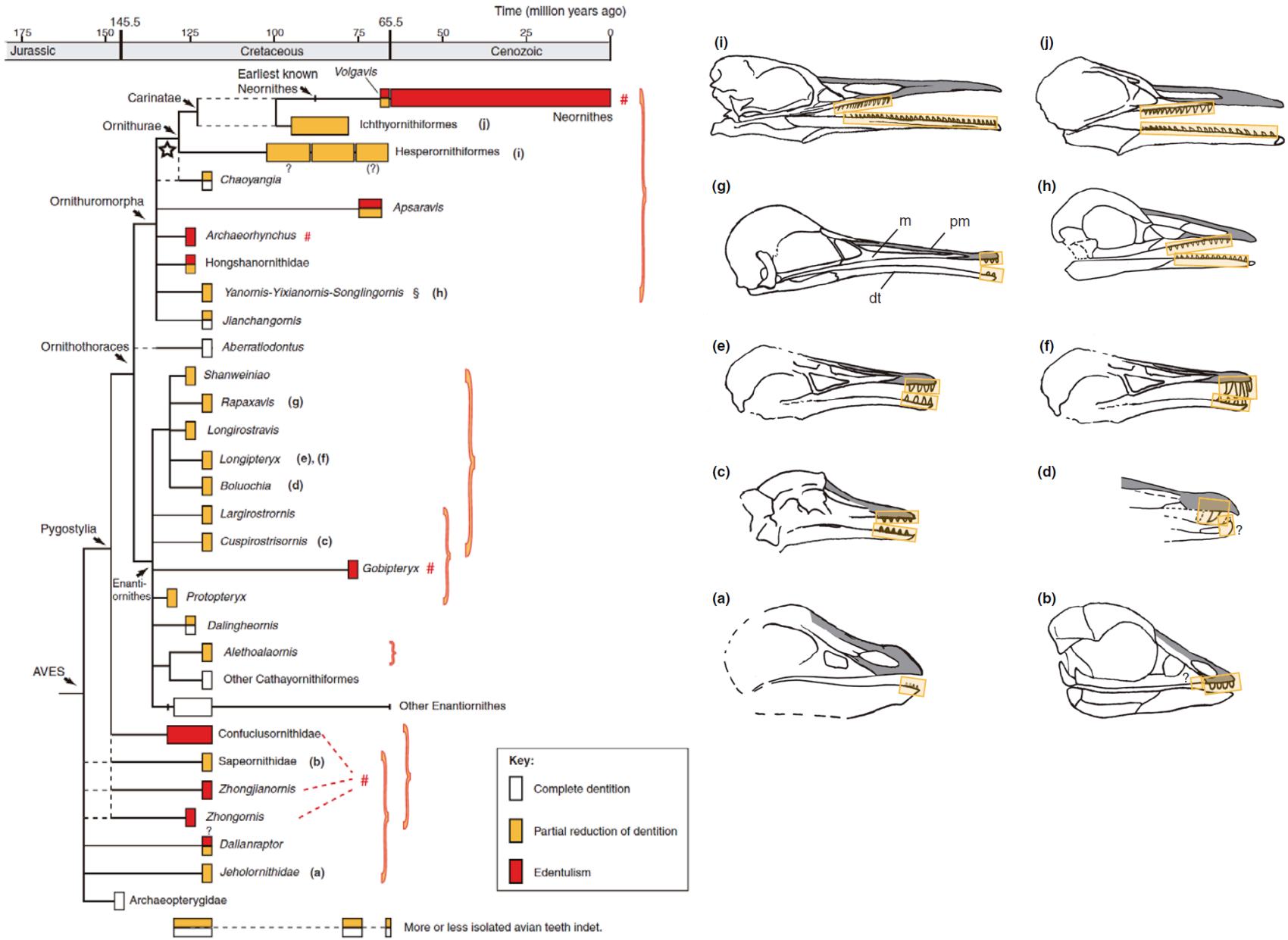

Figure 2. Examples of patterns of partial dentition reduction in birds, illustrated by different Cretaceous species (showing right side only). Toothed parts of jaws are highlighted in orange and the premaxillary in grey. Lettering refers to Figure 1. (a) *Jeholornis prima*, (b) *Sapeornis chaoyangensis*, (c) *Cuspirostrisornis houi*, (d) *Boluochia zhengi*, (e) *Longipteryx chaoyangensis*, (f) *Longipteryx* sp. [3], (g) *Rapaxavis pani*, (h) *Yanornis martini*, (i) *Hesperornis regalis*, (j) *Ichthyornis dispar*. Abbreviations: d, dentary; m, maxillary; pm, premaxillary. Other patterns are known (see the supplementary material online). Based on data and references in the supplementary material online.

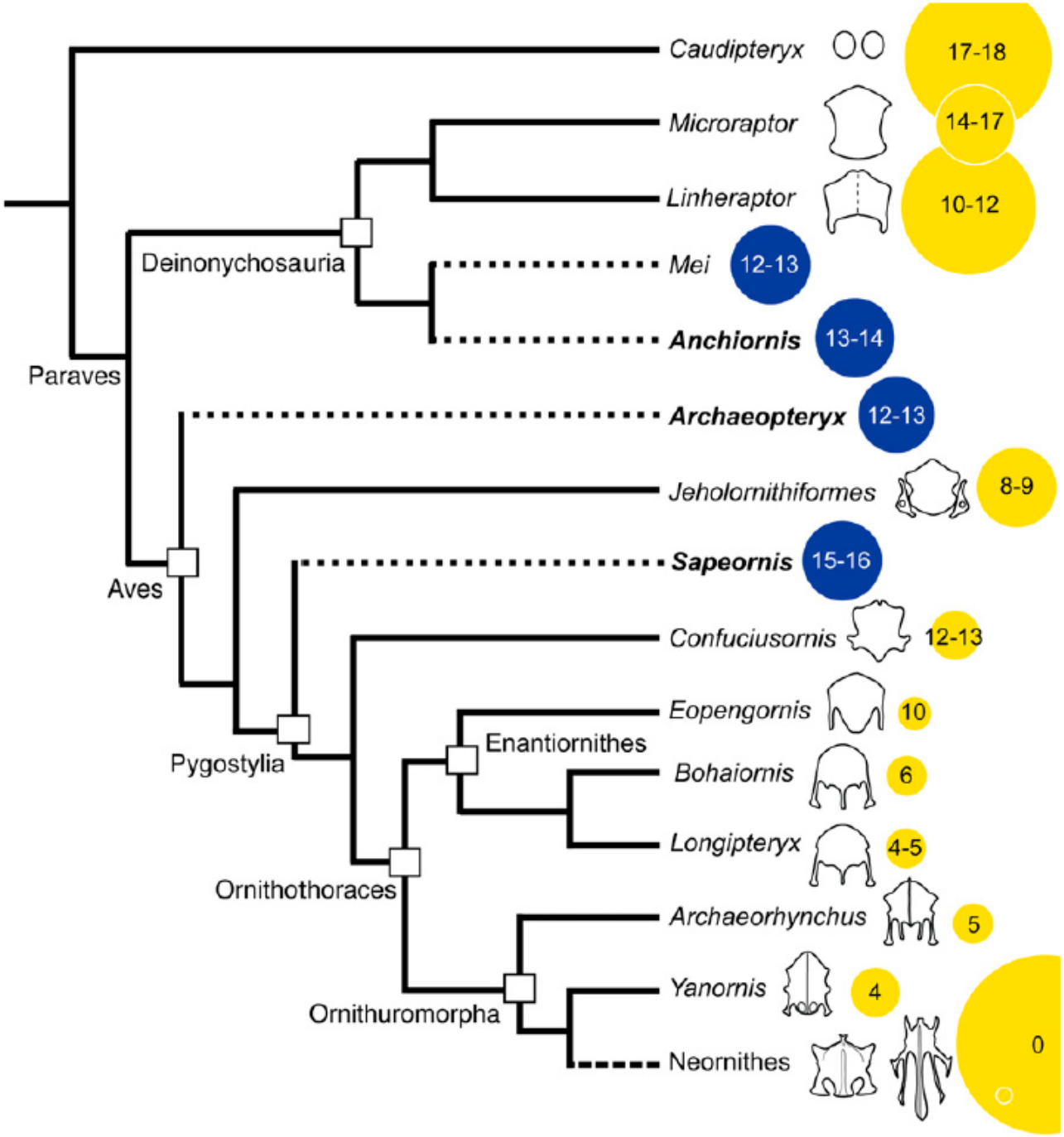
Caudipteryx
17-18
Microraptor
14-17
Linheraptor
10-12
Deinonychosauria
Mei
12-13
Anchiornis
13-14
Paraves
Archaeopteryx
12-13
Jeholornithiformes
8-9
Sapeornis
15-16
Aves
Confuciusornis
12-13
Eopengornis
10
Enantiornithes
Pygostylia
Bohaiornis
6
Longipteryx
4-5
Ornithothoraces
Archaeorhynchus
5
Yanornis
4
Ornithuromorpha
Neornithes
0

Neornithes

(crown group birds)






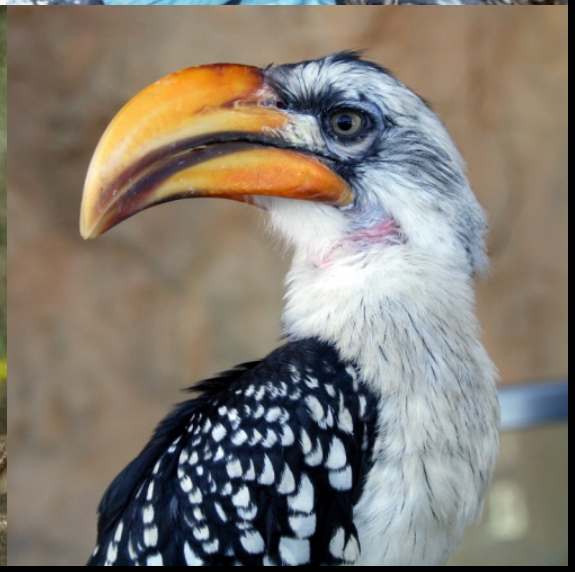

Neornithes

- Grupo de **aves vivientes,** consiste en el clado menos inclusivo que contiene a la perdiz chilena (*Nothoprocta perdicaria*) y la paloma (*Columba livia*)

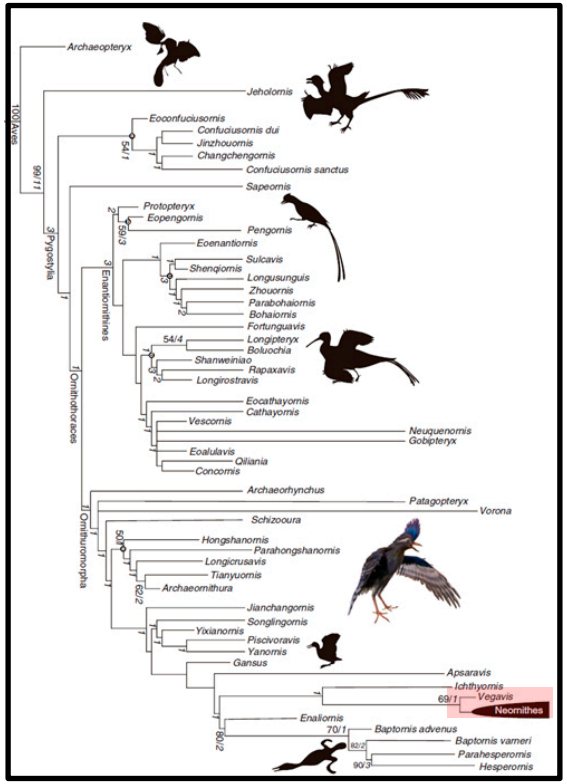

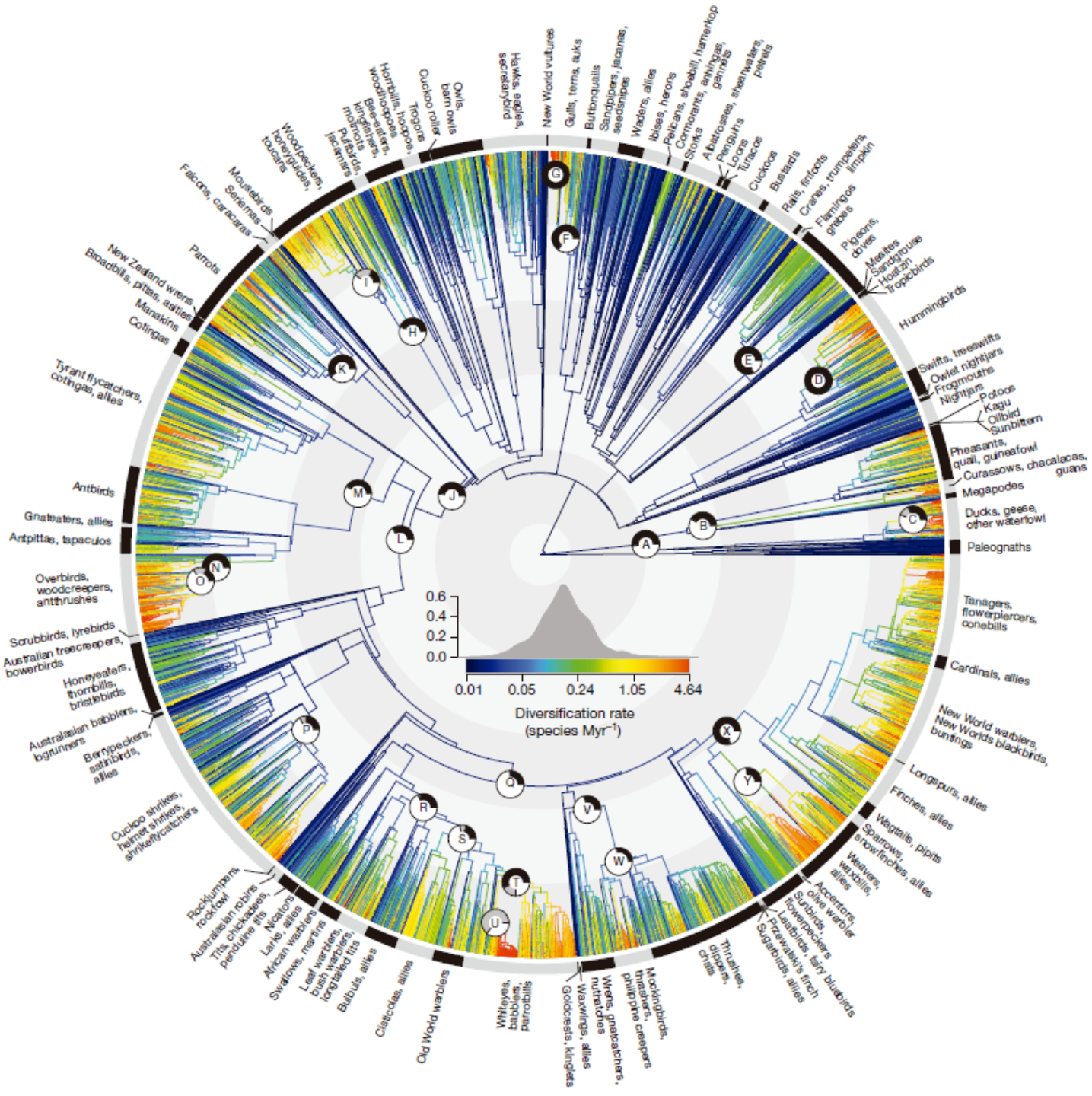
Hawks, eagles, allies
New World vultures
Gulls, terns, auks
Buttonquails
Sandpipers, jacanas, seedsnipes
Waders, allies
Ibises, herons
Pelicans, shoebill, hamerkop
Cormorants, anhingas, gannets
Storks
Albatrosses, shearwaters, petrels
Penguins
Loons
Turacos
Cuckoos
Bustards
Rails, finfoots
Cranes, trumpeters, limpkin
Flamingos
grebes
Pigeons, doves
Mesites
Sandgrouse
Hoatzin
Tropicbirds
Hummingbirds
Swifts, treeswifts
Owlet nightjars
Frogmouths
Nightjars
Potoos
Kagu
Oilbird
Sunbittern
Pheasants, quail, guineafowl
Curassows, chacalacas, guans
Megapodes
Ducks, geese, other waterfowl
Paleognaths
Tanagers, flowerpiercers, conebills
Cardinals, allies
New World warblers, New Worlds blackbirds, buntings
Longspurs, allies
Finches, allies
Wagtails, pipits
Sparrows, snow finches, allies
Weavers, waxbills, allies
Accentors, olive warbler
Sunbirds, flowerpeckers
Leatbirds, fairy bluebirds
Prawabiki's finch
Sugarbirds, allies
Thrushes, dippers, chats
Mockingbirds, thrashers, philippine creepers
Wrens, gnatcatchers, nuthatches
Wagtails, allies
Goldcrests, kinglets
Whiteyes, babblers, parrotbills
Old World warblers
Cisticolas, allies
Bulbuls, allies
Leaf warblers, bush warblers, longtailed tits
Swallows, martins
African warblers
Larks, allies
Nicators
Tits, chickadees, penduline tits
Australasian robins
Rockjumpers, rockfowl
Cuckoo shrikes, helmet shrikes, shrikefly catchers
Australian babblers, logrunners
Berrypeckers, satinbirds, allies
Honeyeaters, thornbills, bristlebirds
Australian treecreepers, bowerbirds
Scrubbirds, lyrebirds
Overbirds, woodcreepers, antthrushes
Antpittas, tapaculos
Gnateaters, allies
Antbirds
Tyrant flycatchers, cotingas, allies
Cotingas
Manakins
Broadbills, pittas, asities
New Zealand wrens
Parrots
Falcons, caracaras
Secretarybirds
Mousebirds
Woodpeckers, honeyguides, toucans
Puffbirds, jacamars
Motmots
Kingfishers, bee-eaters, woodhoopoes
Hornbills, hoopoe, trogons
Cuckoo roller
Owls, barn owls
A
B
C
D
E
F
G
H
I
J
K
L
M
N
O
P
Q
R
S
T
U
V
W
X
Y
0.6
0.4
0.2
0.0
0.01
0.05
0.24
1.05
4.64
Diversification rate
(species Myr^{-1})

Altricialidad y modos de vida

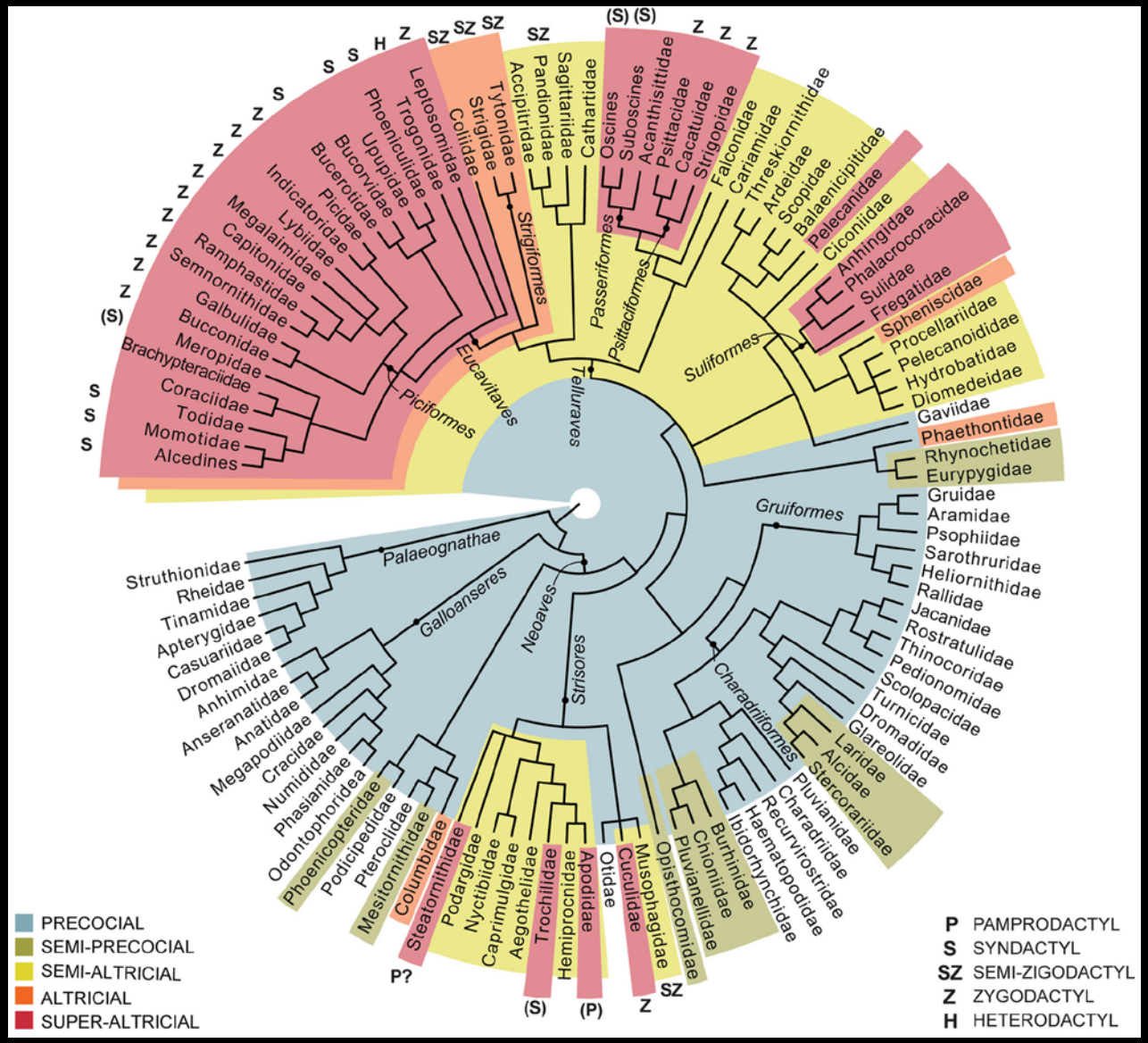

Botelho, J. F., Smith-Paredes, D., & Vargas, A. O. (2015). *Evolutionary Biology*, *42*(4), 502-510.

Las Neornithes se dividen en 2 grandes linajes sobre la base de la Configuración ósea del Paladar:

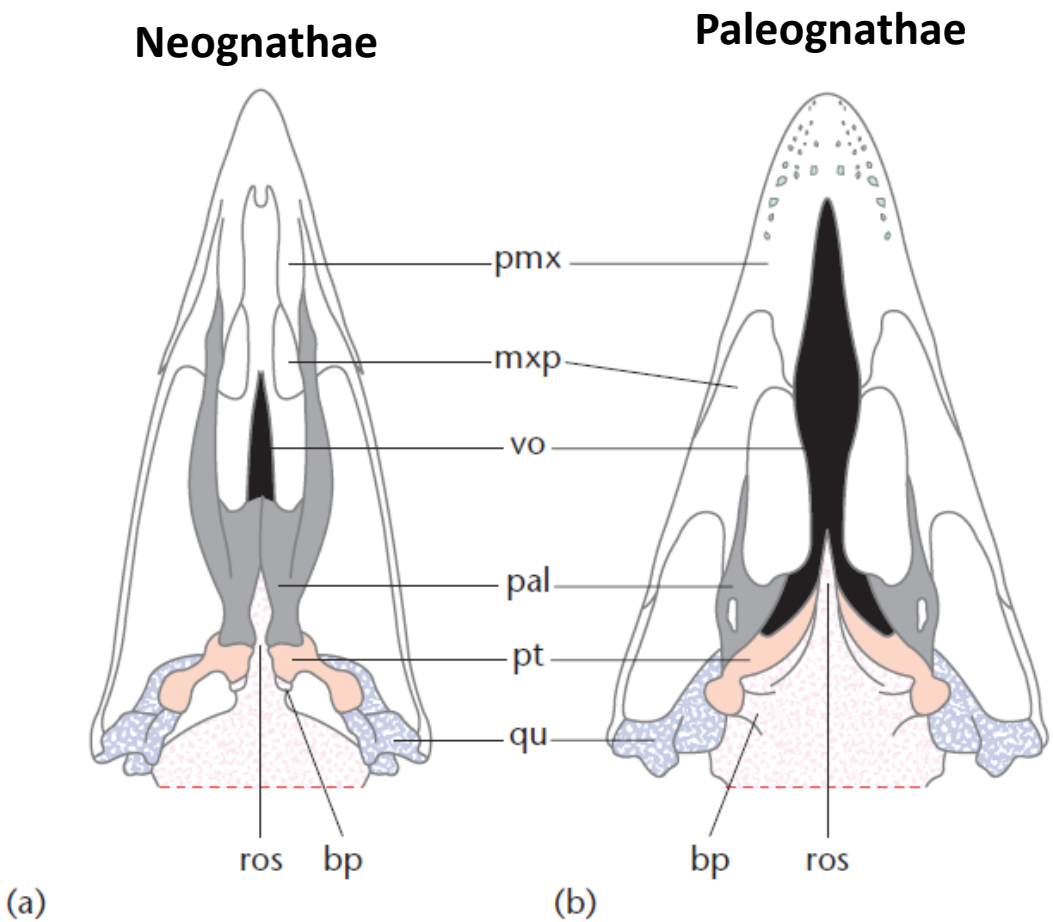

Figure 1 Palate bones, in ventral view, of (a) domestic fowl (*Gallus gallus*, Neognathae); (b) emu (*Dromaius novaehollandiae*, Palaeognathae). After Pycraft 1901b. Key: bp, basipterygoid process; mxp, maxillopalatine; pal, palatine; pmx, premaxilla; pt, pterygoid; qu, quadrate; ros, parasphenoid rostrum; vo, vomer. Note the reduced vomers (black) and juxtaposed palatines (dark grey) in Neognathae. In Palaeognathae, the palatines are separated by relatively large vomers.

Sinapomorfías:

- Ausencia de dientes
- Ausencia de sutura craneal frontoparietal en adultos*
- Presencia de puente supratendíneo en porción distal de la tibia
- Presencia de hipotarso completamente desarrollado

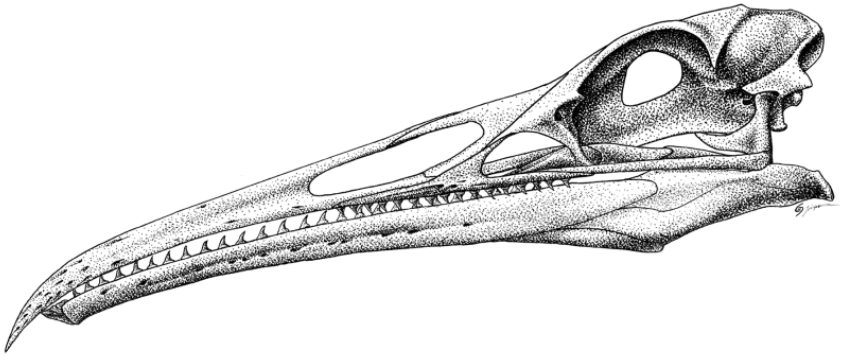

Hesperornis regalis (https://qilong.wordpress.com)

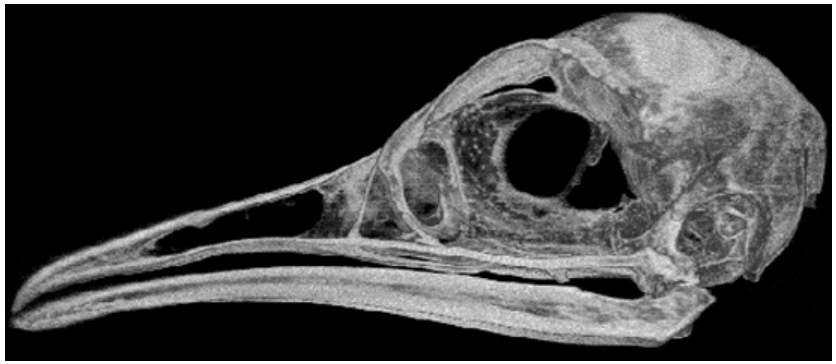

Crypturellus cinnamomeus (https://Digimorph.org)

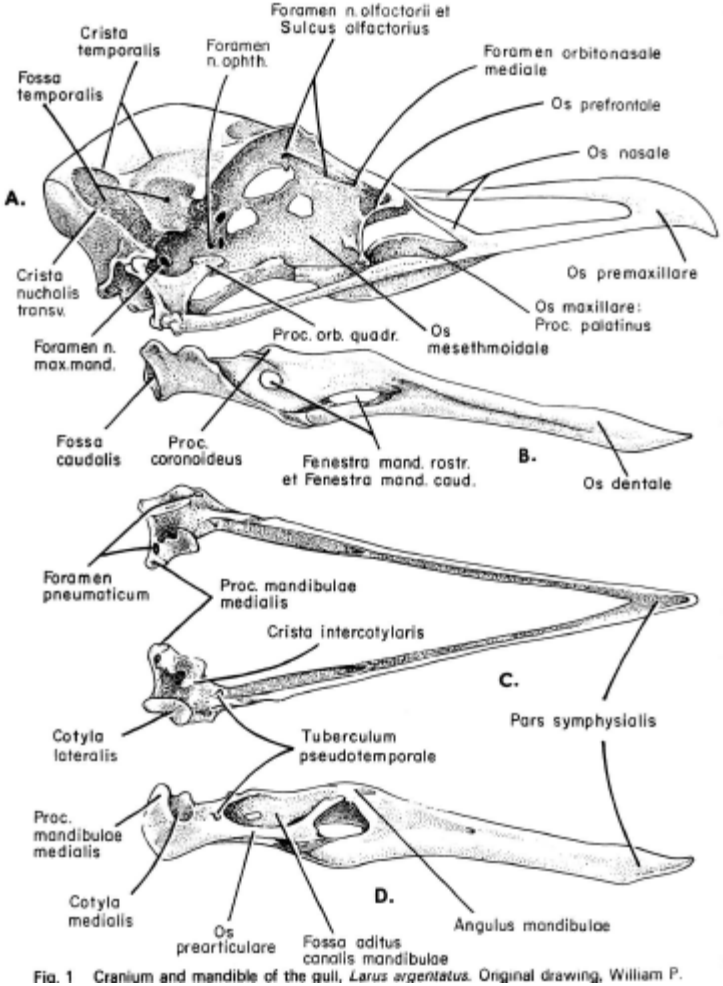

Fig. 1 Cranium and mandible of the gull, *Larus argentatus*. Original drawing, William P.

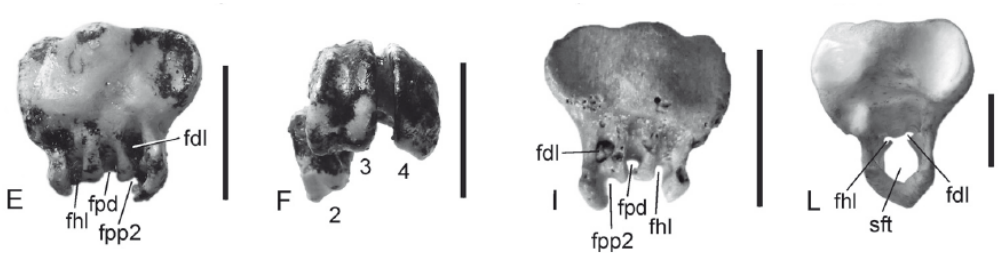

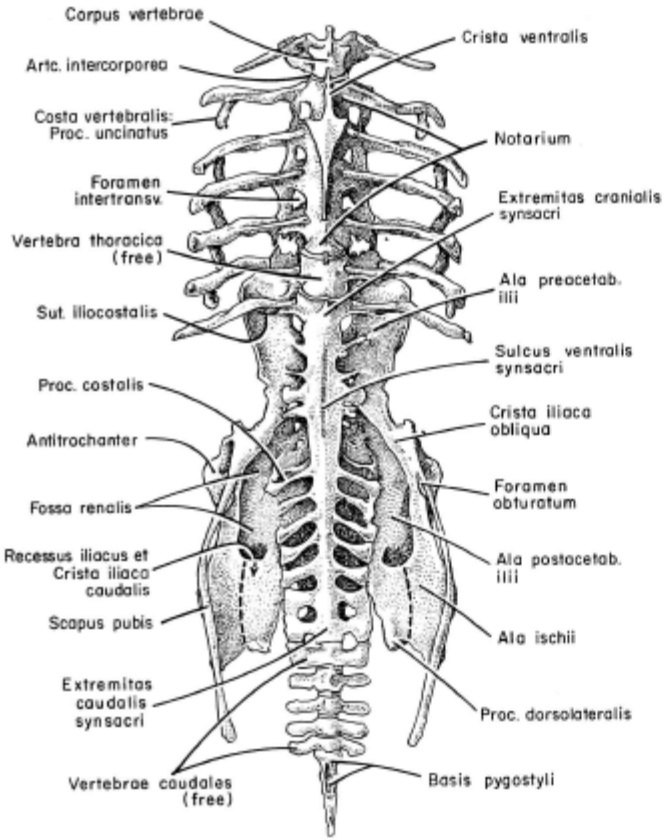

Fig. 5. Notarium, Synsacrum, and Os coxae of the turkey, *Meleagris gallapavo*; ventral view. Redrawn from Harvey, et al. (1968). The dashed lines represent the Sync. ilioischiadica (see Fig. 11). On the left side of the drawing the arrow inserted into Recessus iliacus passes dorsal to a sharp ledge of bone, the Crista iliaca caudalis.
Abbreviations: intertransv., intertransversarium; preacetabl., preacetabularis; postacetab., postacetabularis.

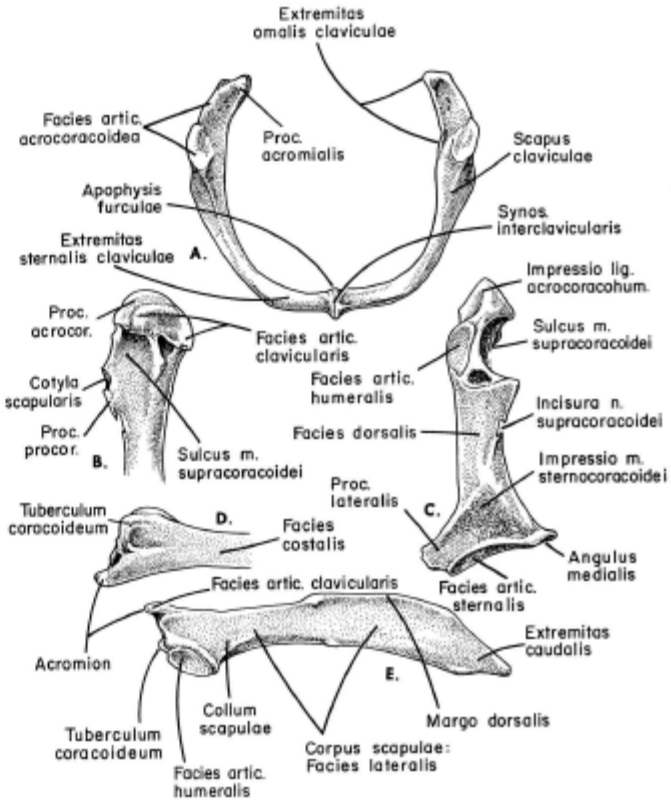

Fig. 6 Bones of the girdle of the thoracic limb of the eagle, *Aquila chrysaetos*. Redrawn from Howard (1929). A, Clavicula, caudal aspect; B, Coracoideum, left shoulder extremity, medial aspect; C, Coracoideum, left, dorsal surface; D, Scapula, left, cranial extremity, costal surfaces; E, Scapula, left, lateral surface. The ankylosed left and right clavicles form the Furcula (see Annot. 162).
Abbreviations: acrocor., acrocoracoideus; artic., articularis; procor., procoracoideus; acrocoracohum., acrocoracohumeralis.

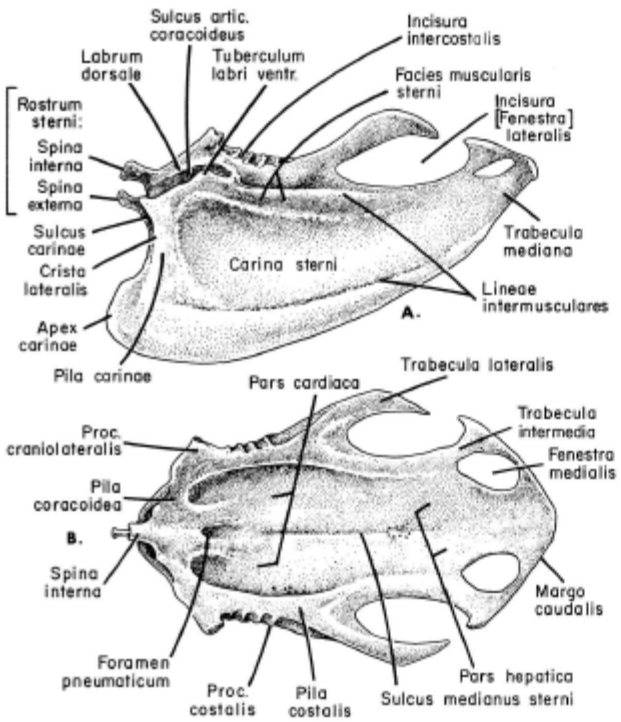

Fig. 7 Sternum of the pigeon, *Columba livia*. Adapted from original drawing of J. J. Baumel. A, left lateral aspect; B, visceral (dorsal) aspect.
Abbreviation: artic., articularis.

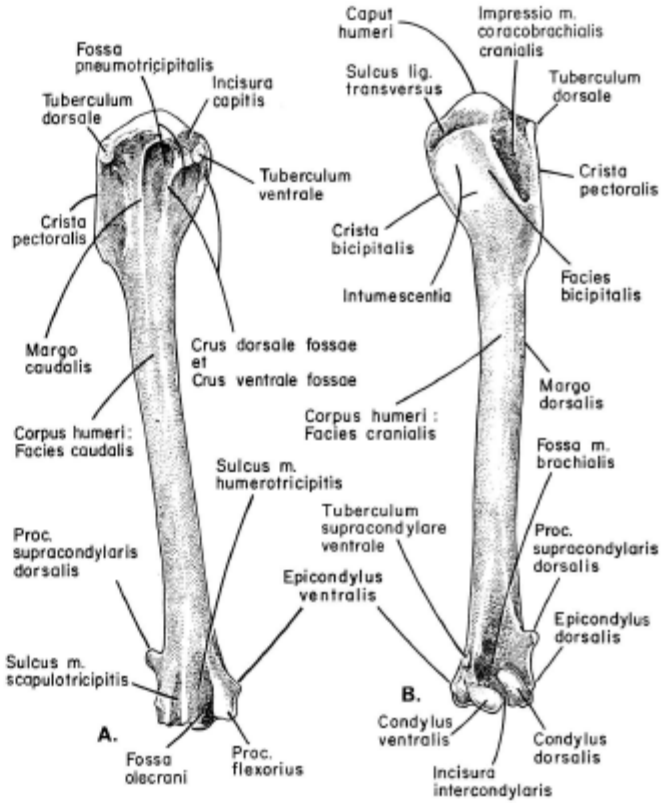

Fig. 8. Humerus of the gull, *Larus argentatus*; left side. Original drawing of Wm. P. Hamilton. A, caudal surface; B, cranial surface. In this species the pneumotricipital fossa is the dual type, not pneumatized (see Annot. 188, 189), and the impression for M. coracobrachialis cranialis is very strongly developed.

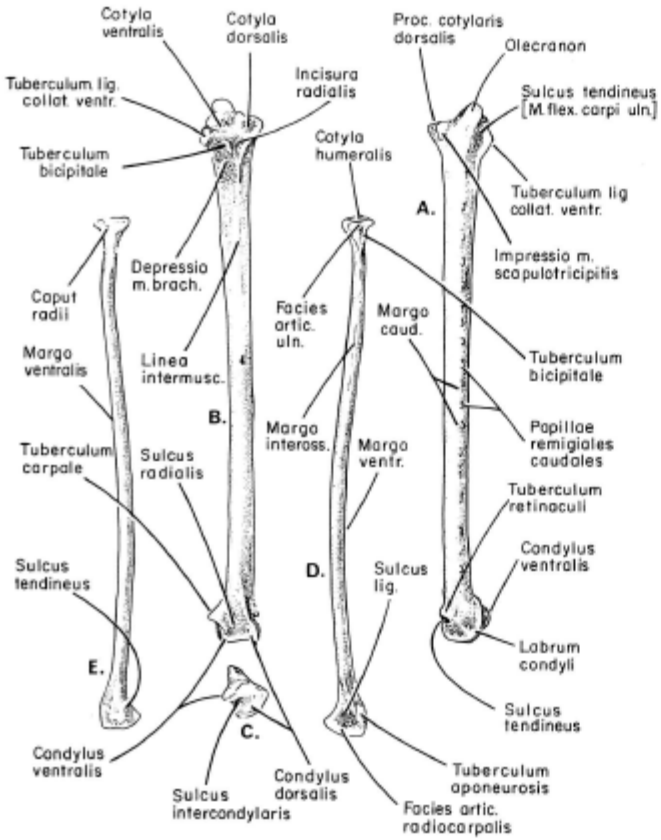

Fig. 9. Radius and Ulna of the gull, *Larus argentatus*; from the left wing. Original drawing, Wm. P. Hamilton. A, Ulna, caudal aspect; B, Ulna, cranial aspect; C, Ulna, distal end; D, Radius, caudal (interosseous) aspect; E, Radius, cranial (propatagial) aspect. Note that the terminology of these bones is based on the wing in the anatomical position (see Annot. 178 and General Intro.). In Fig. C, the Trochlea carpalis and its parts are identified; the pointed Tuberculum carpale is not labeled.
Abbreviations: artic., articularis; collat., collateralis; flex., flexor; intermusc., intermuscularis; inteross., interosseus; uln., ulnaris.

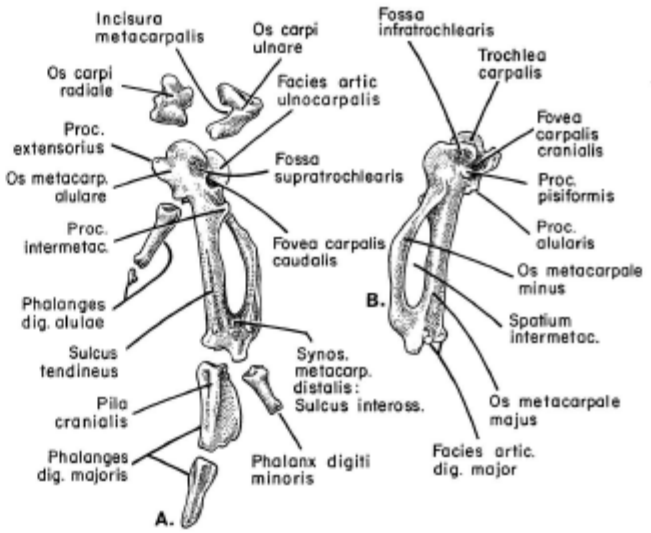

Fig. 10. Carpal and metacarpal bones, phalanges of the turkey, *Meleagris gallapavo*; bones from left wing. Redrawn from Ghetie et al. (1976). A, dorsal aspect; B, ventral aspect. Note that the alular digit of the turkey has two phalanges (see Annot. 224 and **Integ.** Annot. 70).
Abbreviations: artic., articularis; dig., digitalis or digiti; intermetac., intermetacarpale or intermetacarpalis; inteross., interosseus; metacarp., metacarpalis.

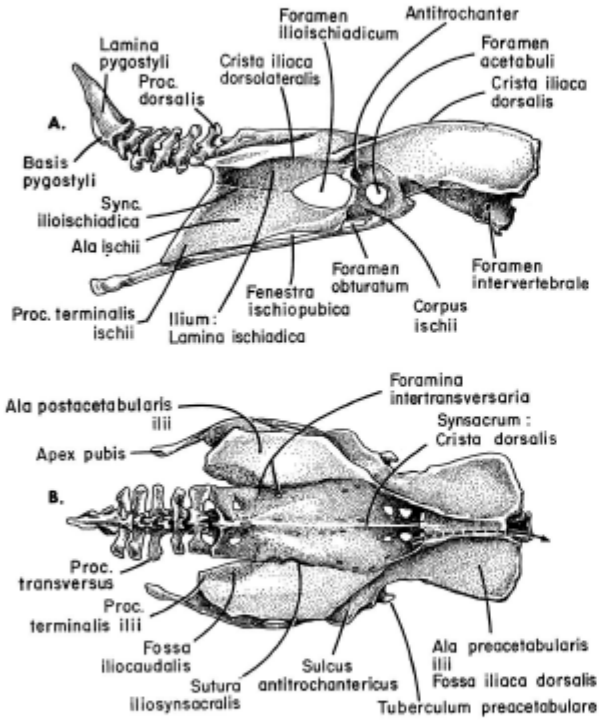

Fig. 11. Pelvis (Os coxae; Synsacrum) and tail skeleton of the turkey, *Meleagris gallapavo*. Redrawn from Harvey, et al. (1968). A, lateral aspect, right side; B, dorsal aspect. In B the arrow traverses Canalis iliosynsacralis. In A notice the dual intervertebral foramina in the synsacral part of the vertebral column (see Annot. 144).

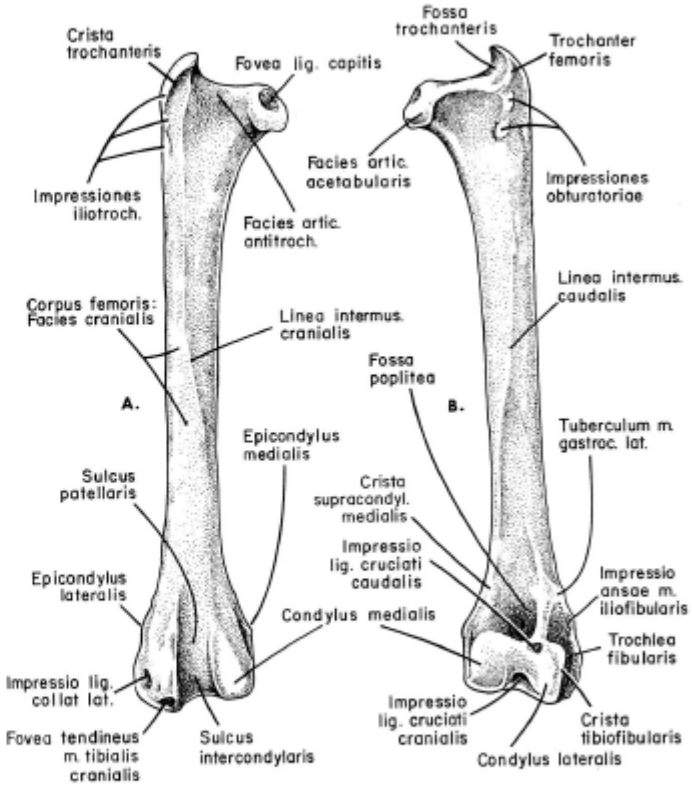

Fig. 12 Femur of the gull, *Larus argentatus*; right side. Original drawing Wm. P. Hamilton. A, cranial aspect; B, caudal aspect.
Abbreviations: antitroch., antitrochanterica; artic. articularis; gastroc., gastrocnemialis; iliotroch, iliotrochantericae; intermus., intermuscularis; supracondyl., supracondylaris.

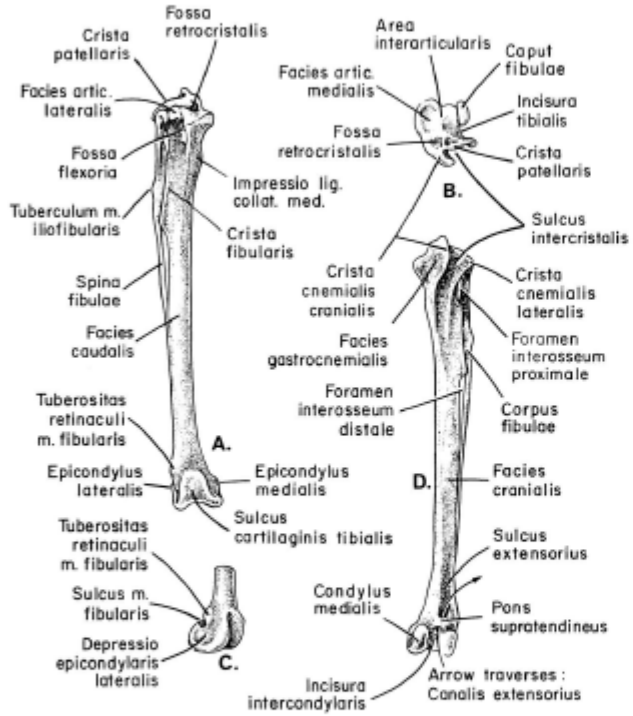

Fig. 13. Tibiotarsus and Fibula of the goose, *Branta canadensis*; left side. Original drawing Wm. P. Hamilton. A, caudal view; B, proximal articular surfaces of both bones; C, distal extremity of Tibiotarsus, lateral aspect; D, cranial view. In A Tuberositas poplitea (not labeled) is located just medial to the tip of leader on the Fossa flexoria.
Abbreviations: artic., articularis; collat., collateralis.

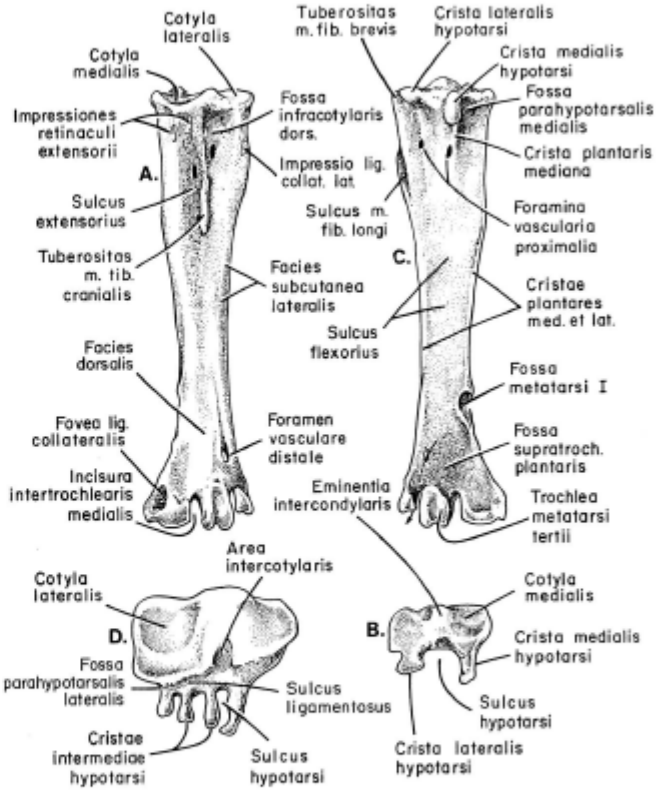

Fig. 14 Tarsometatarsus of the eagle, *Aquila chrysaetos* (A-C) and the goose, *Anser caerulescens* (*Chen hyperborea*); all bones from the left limb. Redrawn from Howard (1929). A, dorsal aspect; B, proximal end; C, plantar aspect; D, proximal end. In C the arrow traverses Canalis interosseus tendineus which conducts the tendon of M. extensor digiti IV. The Eminentia intercondylaris is a process of the proximal end of the bone that, in the articulated joint, projects between the tibiotarsal condyles and receives the distal attachment of Lig. intercondylare tibiometatarsale (see Arthr. Annot. 171).
Abbreviations: fib., fibularis; supratroch., supratrochlearis; tib., tibialis.

Neornithes: Radiación Evolutiva

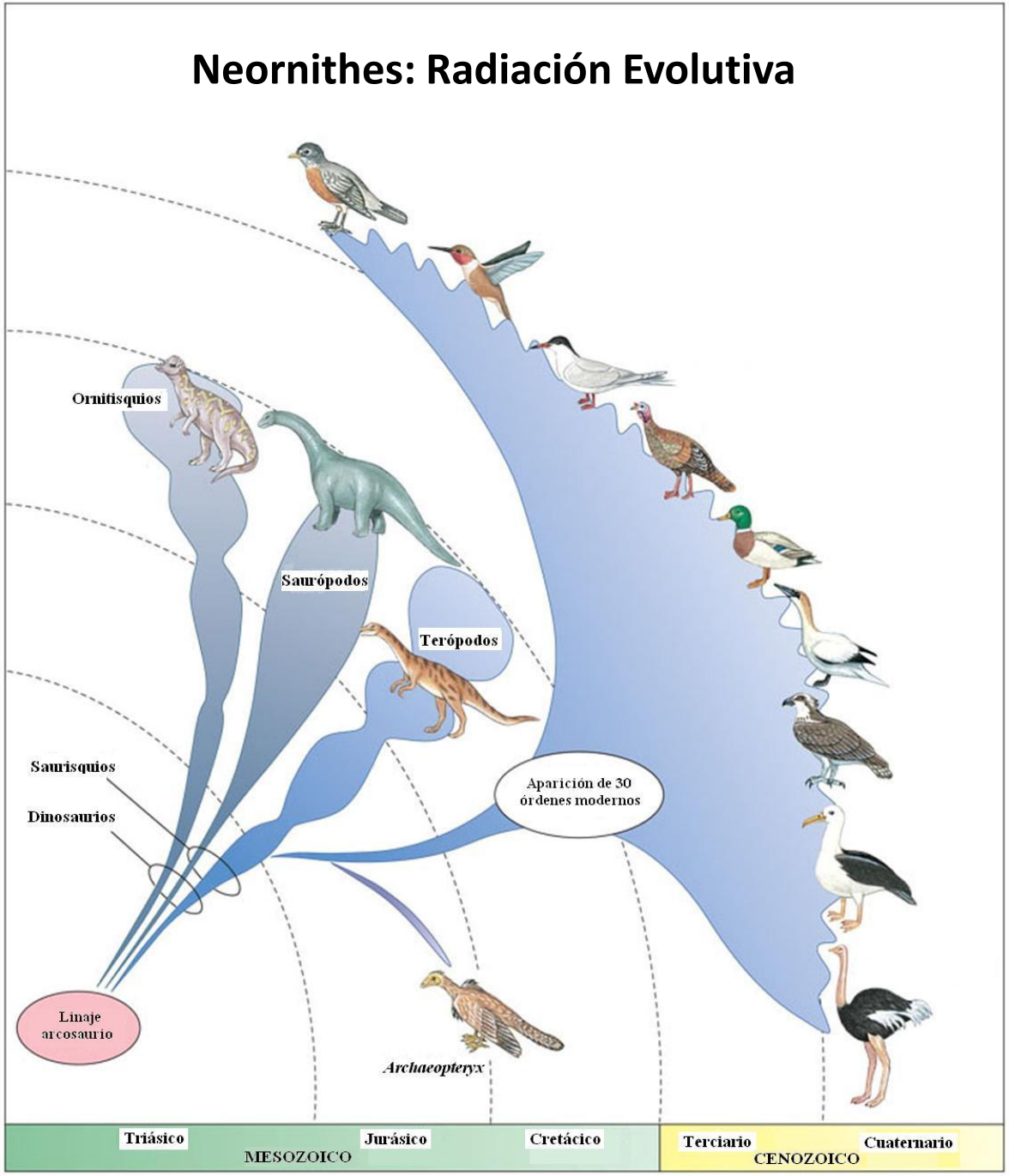

Diversificación de las Aves. Modificado de: Hickman C.P. et al. 2008. Integrates Principles of Zoology 14th Edition. The McGraw-Hill Companies, Inc.

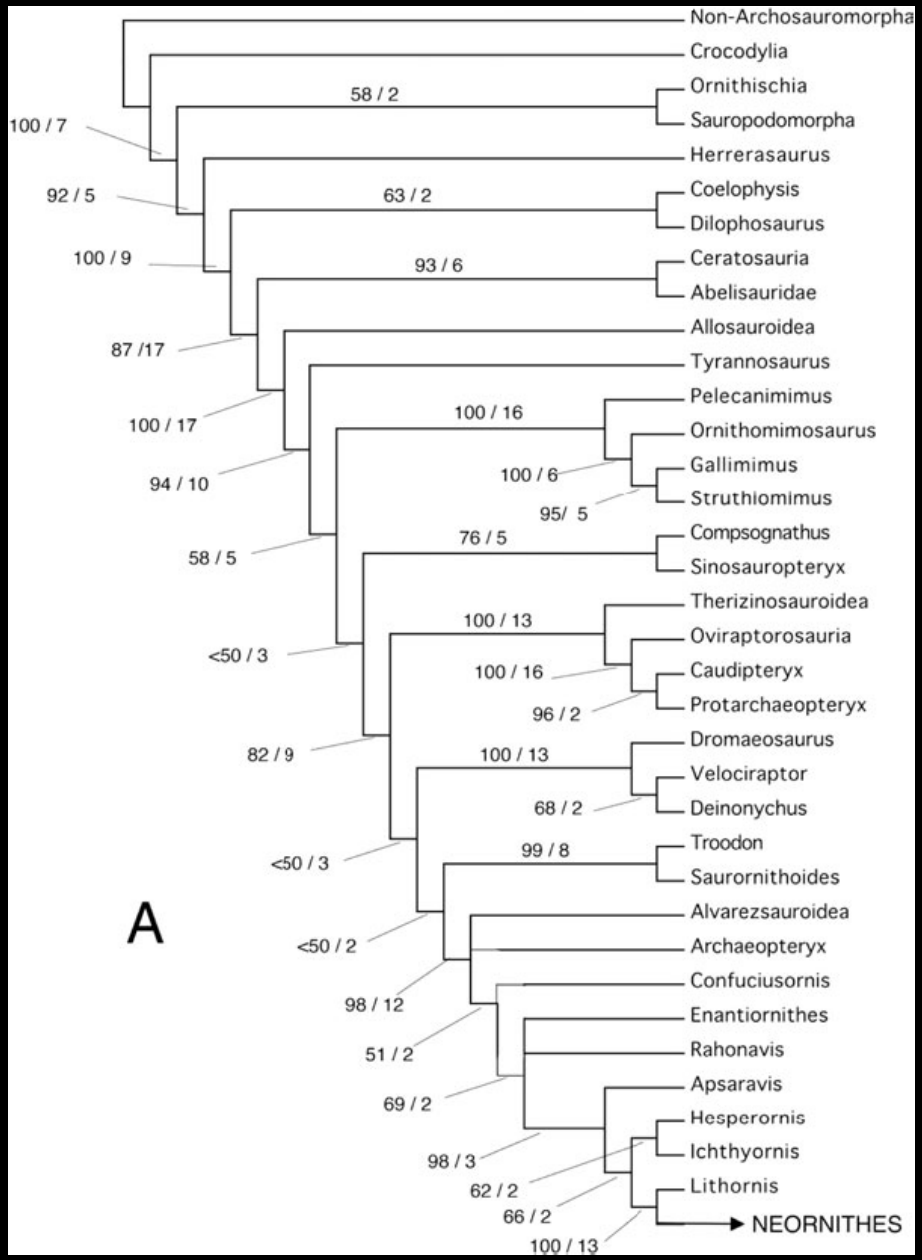

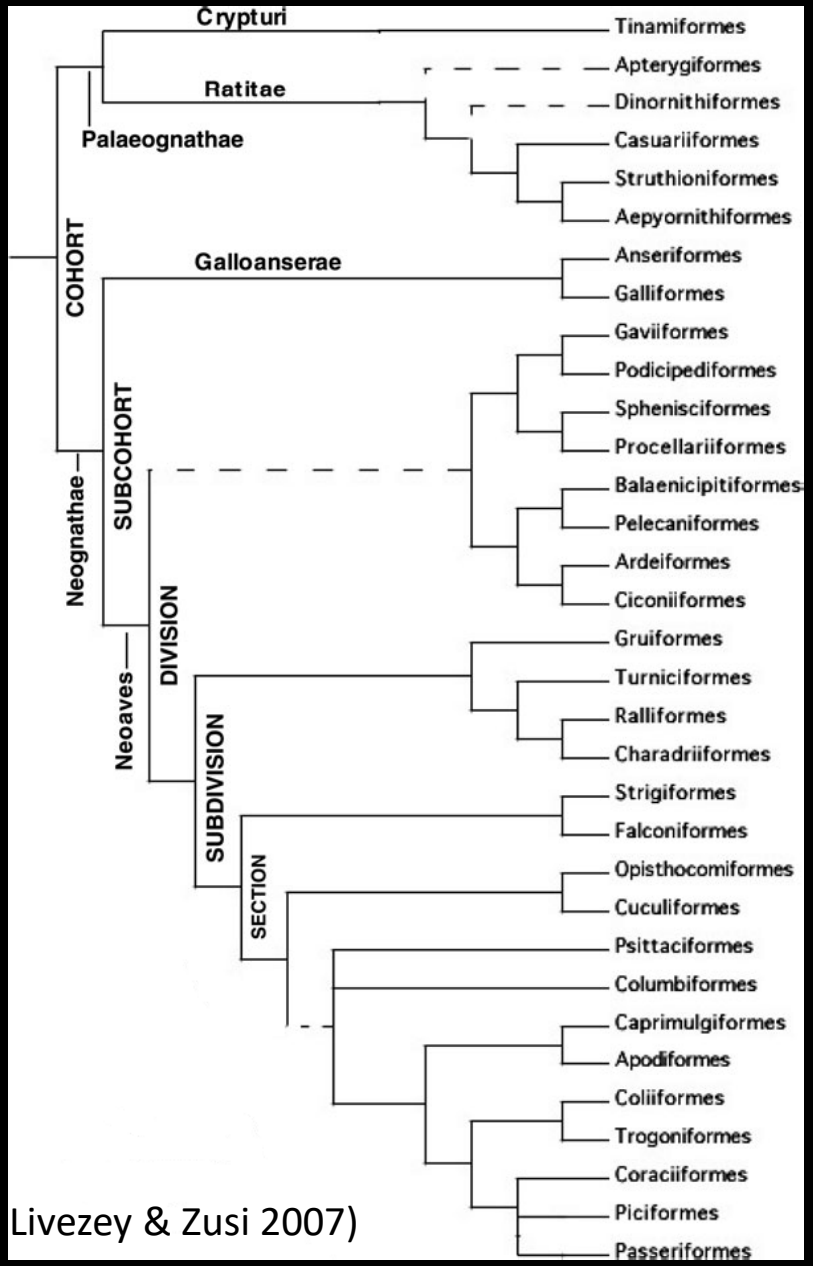

Livezey & Zusi 2007)

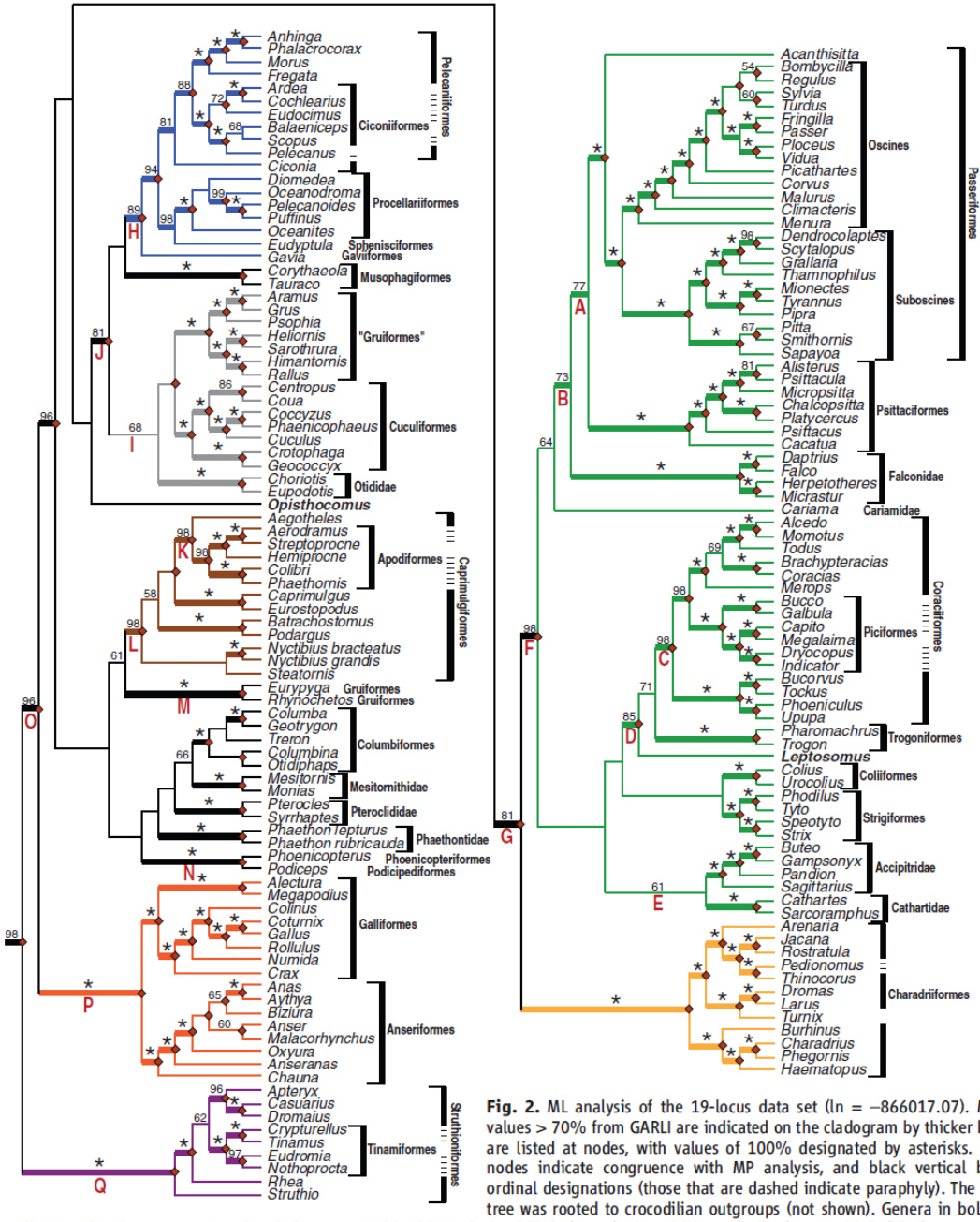

Fig. 2. ML analysis of the 19-locus data set (ln = −866017.07). ML bootstrap values > 70% from GARLI are indicated on the cladogram by thicker branches and are listed at nodes, with values of 100% designated by asterisks. Diamonds at nodes indicate congruence with MP analysis, and black vertical bars refer to ordinal designations (those that are dashed indicate paraphyly). The phylogenetic tree was rooted to crocodilian outgroups (not shown). Genera in bold are icertae sedis. Branch colors represent major clades supported in this study: land birds (green), charadriiforms (yellow), water birds (blue), core gruiforms and cuckoos (gray), apodiforms and caprimulgiforms (brown), galloanserae (orange), and paleognaths (purple). Large capital letters indicate groups discussed in the text and Fig. 1.

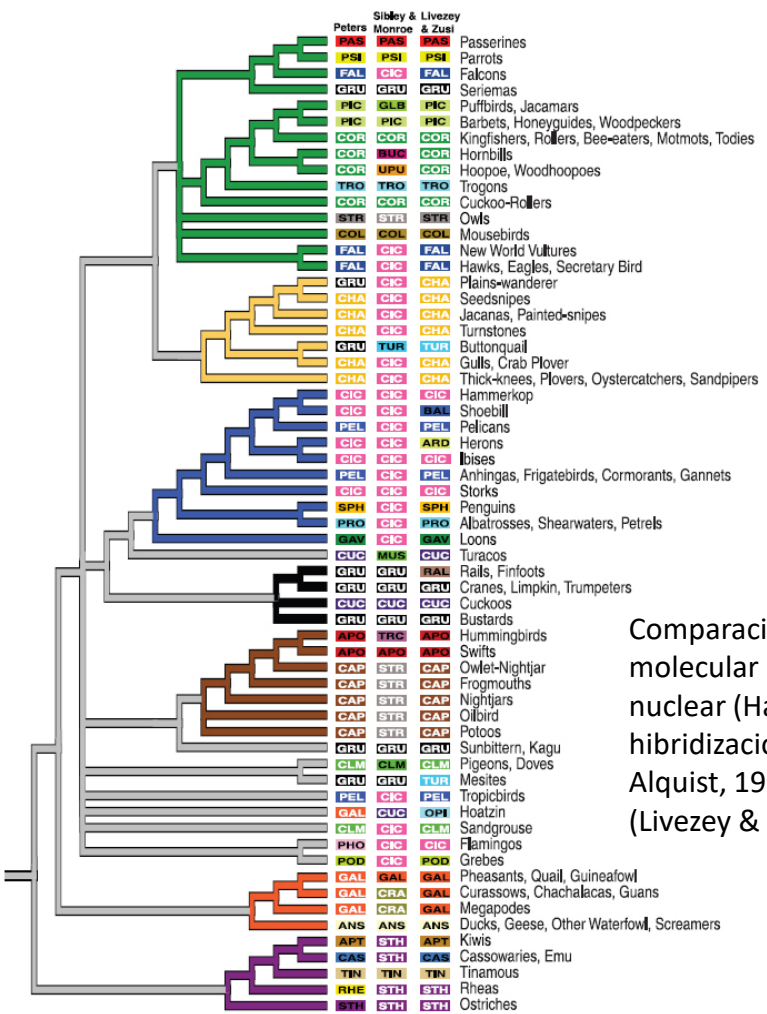

Fig. 4. Our phylogeny differs from and agrees with previous classifications. We merged well-supported (>70% bootstrap values) monophyletic clades at the tips with the same ordinal designation across all three classifications (e.g., 24 species called Passerines). Only higher relationships supported by bootstrap values >50% are shown. Colors are as in Fig. 2. Color bars to the right of the tree show membership in three different classifications: Peters' (*25*) (left), Sibley and Monroe's (*30*) (middle), and Livezey and Zusi's (*13*) (right). Black text within the bars indicates monophyletic orders in our phylogeny, whereas white text within the bars indicates nonmonophyletic orders. Ordinal name codes: ANS (Anseriformes), APO (Apodiformes), APT (Apterygiformes), ARD (Ardeiformes), BAL (Balaenicipitiformes), BUC (Bucerotiformes), CAP (Caprimulgiformes), CAS (Casuariiformes), CHA (Charadriiformes), CIC (Ciconiiformes), CLM (Columbiformes), COL (Coliiformes), COR (Coraciiformes), CRA (Craciformes), CUC (Cuculiformes), FAL (Falconiformes), GAL (Galliformes), GAV (Gaviiformes), GLB (Galbuliformes), GRU (Gruiformes), MUS (Musophagiformes), OPI (Opisthocomiformes), PAS (Passeriformes), PEL (Pelecaniformes), PIC (Piciformes), POD (Podicipediformes), PRO (Procellariiformes), PSI (Psittaciformes), RAL (Ralliformes), RHE (Rheiformes), SPH (Sphenisciformes), STH (Struthioniformes), STR (Strigiformes), TIN (Tinamiformes), TRC (Trochiliformes), TRO (Trogoniformes), TUR (Turniciformes), and UPU (Upupiformes).

ogenética de
tre 2
oleculares
l., 2006;

Comparació
molecular
nuclear (Ha
hibridizació
Alquist, 199
(Livezey & Z

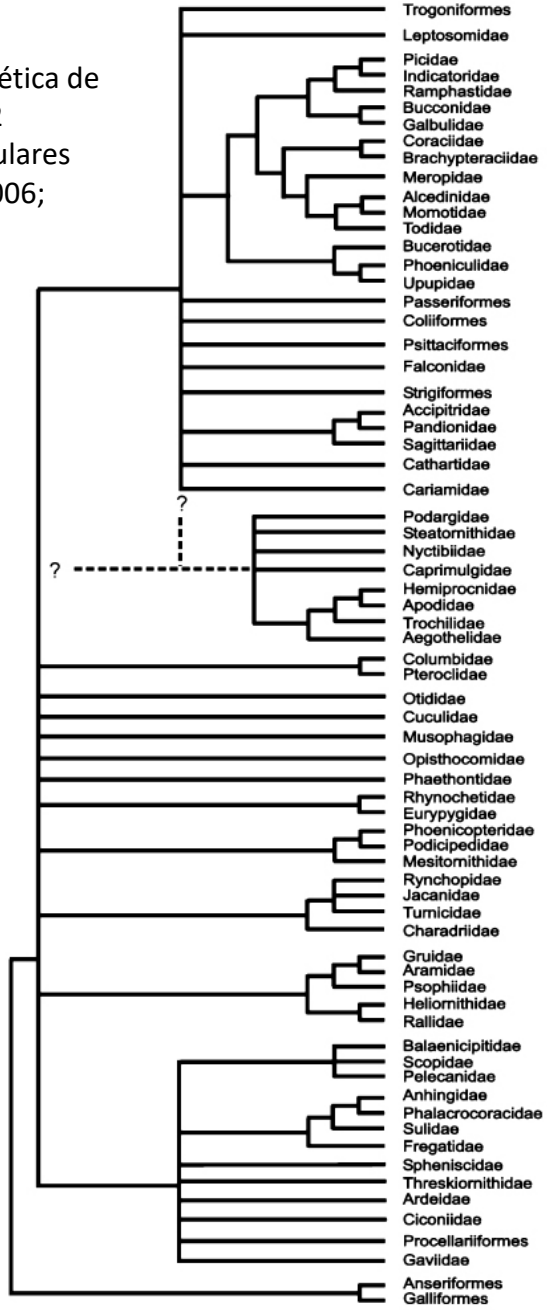

Fig. 3. Summary tree for neognathous birds with the well-supported clades discussed in the present study and those which are recovered in both gene trees in Fig. 2a and b

Neornithes: Filogenia

Mayr 2014; Palaeontology

Hackett et al., 2008; Science

Livezey & Zusi 2007; Zool J Linnean Soc

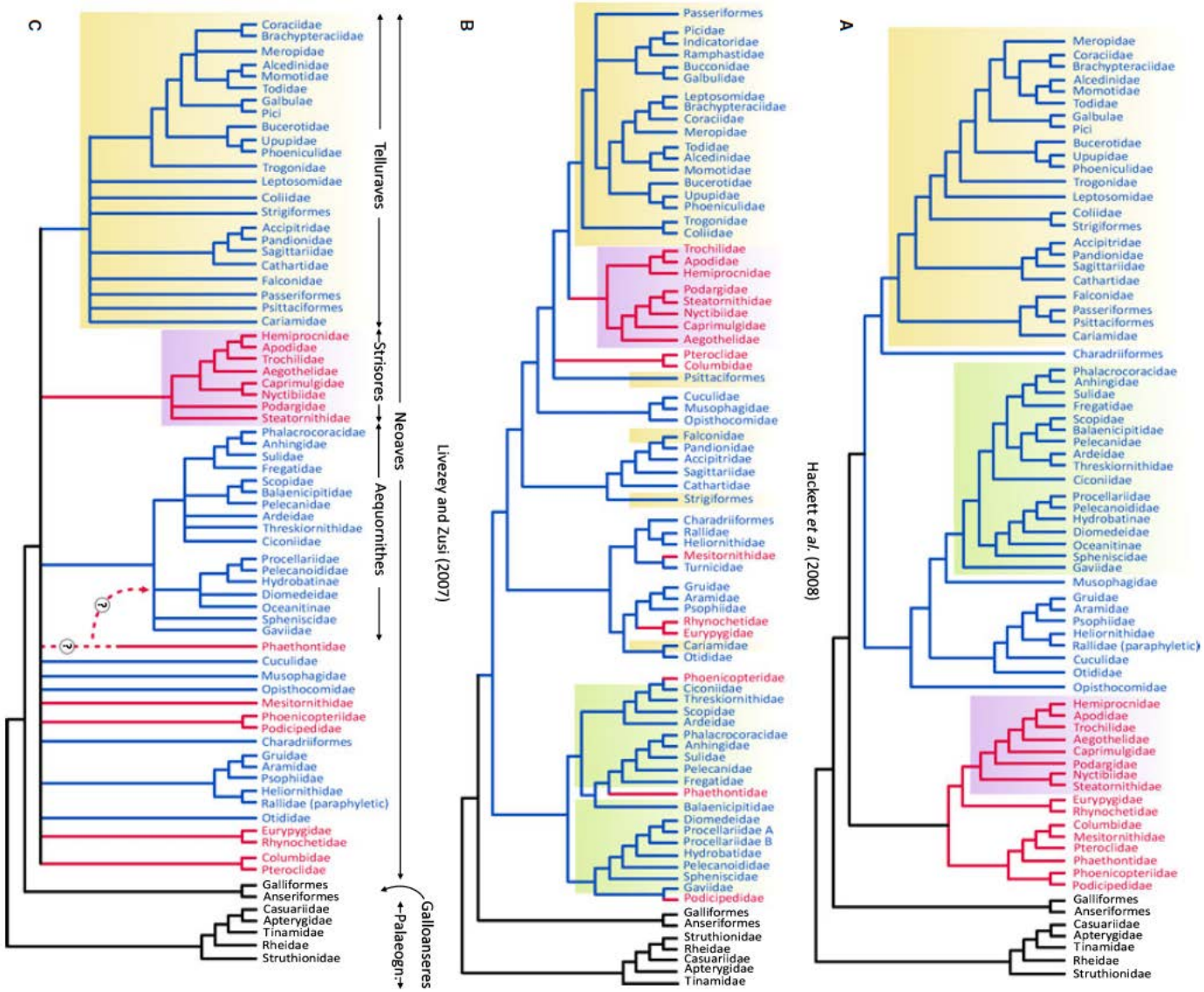

FIG. 1. Three phylogenies of neornithine birds based on molecular and morphological data. A, tree obtained from an analysis of 19 nuclear loci (Hackett *et al.* 2008). B, tree resulting from an analysis of 2954 morphological characters (Livezey and Zusi 2007). C, plausible consensus phylogeny preferred in the current study (see text and Mayr 2011*a*; Kimball *et al.* 2013; McCormack *et al.* 2013; Yuri *et al.* 2013). Taxa of the 'Metaves' clade are marked in red, the remaining Neoaves in blue; the coloured boxes highlight taxa of Telluraves (orange), Aequornithes (green) and Strisores (mauve).

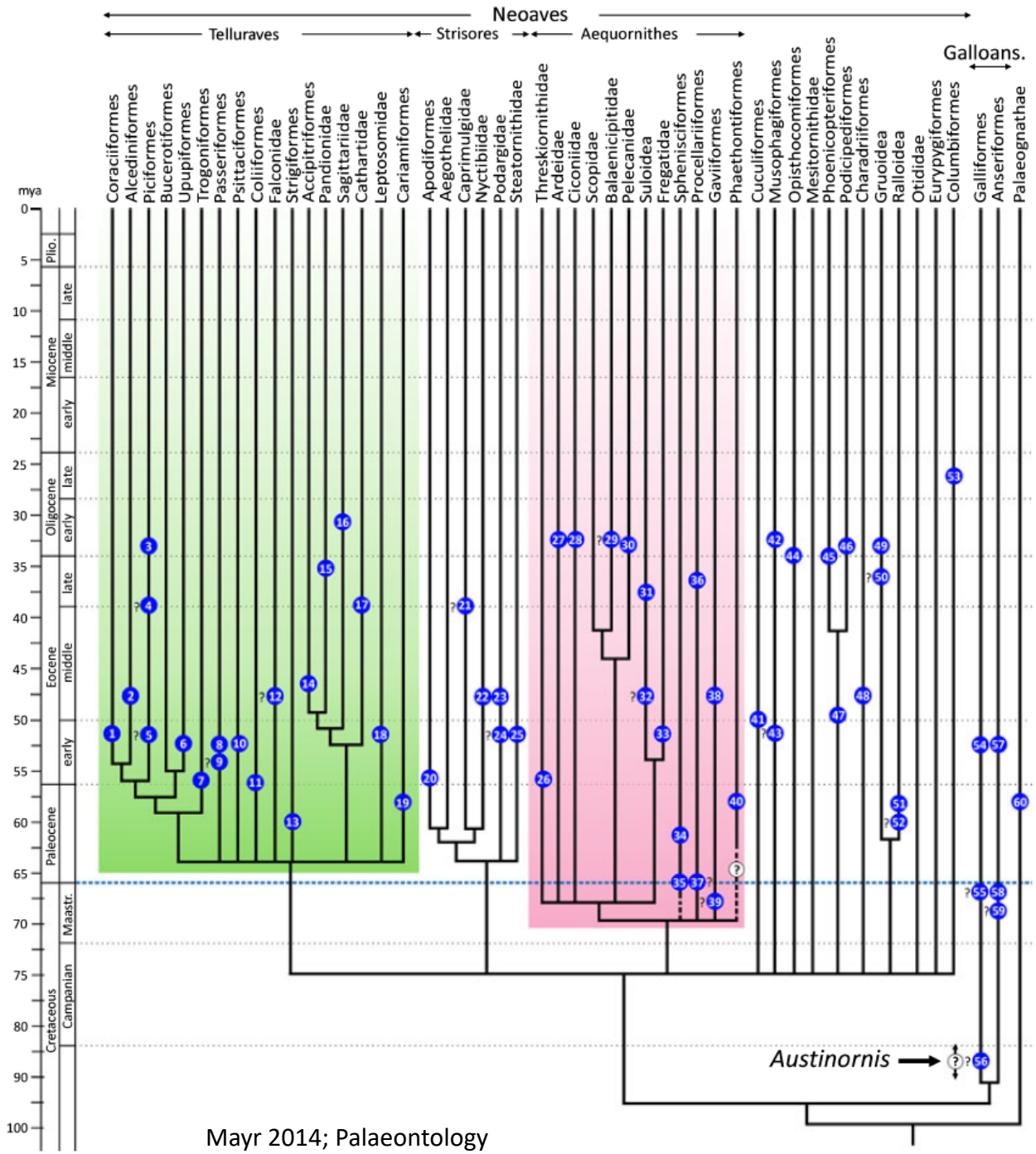

Mayr 2014; Palaeontology

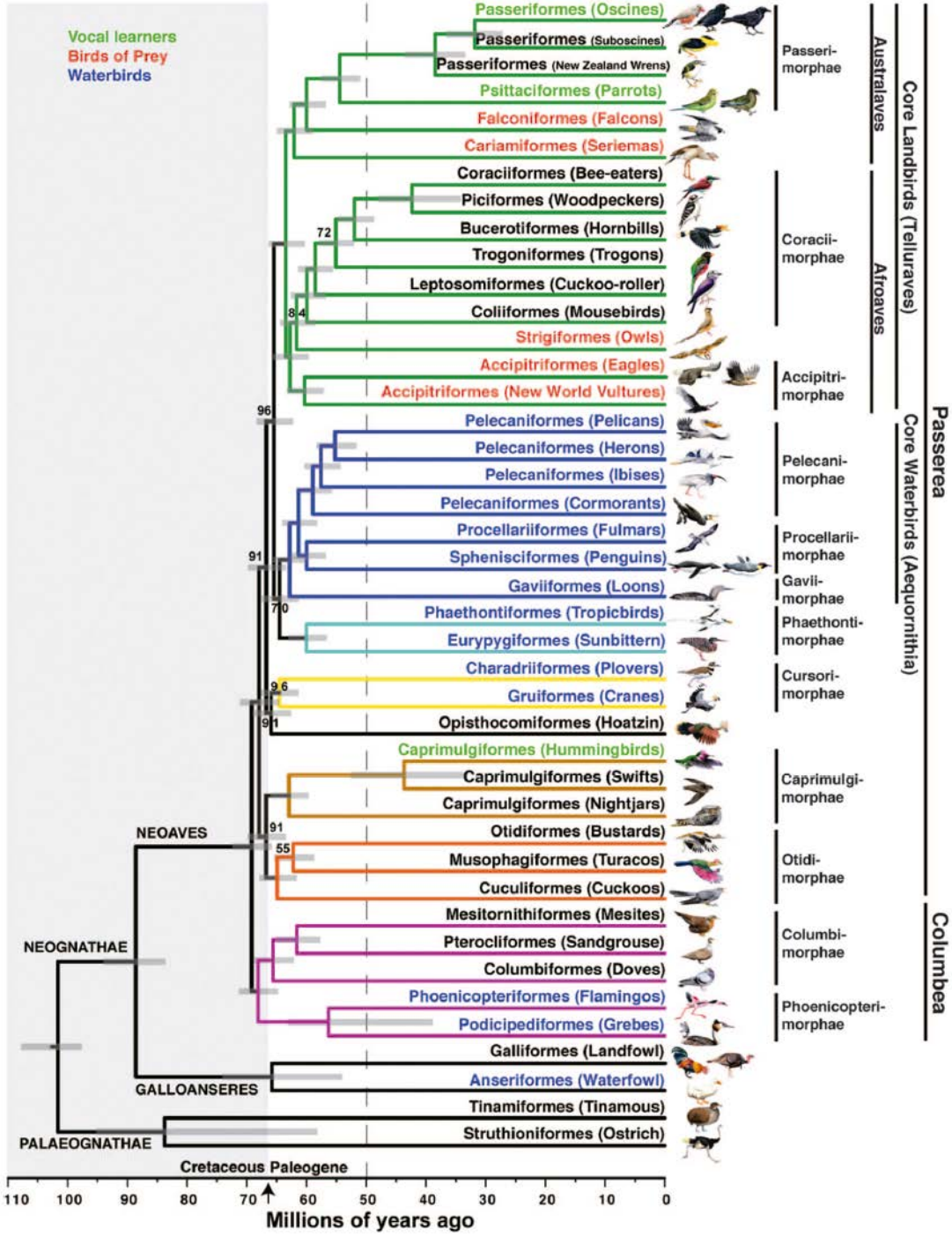
Vocal learners
Birds of Prey
Waterbirds
Passeriformes (Oscines)
Passeriformes (Suboscines)
Passeriformes (New Zealand Wrens)
Psittaciformes (Parrots)
Falconiformes (Falcons)
Cariamiformes (Seriemas)
Coraciiformes (Bee-eaters)
Piciformes (Woodpeckers)
Bucerotiformes (Hornbills)
Trogoniformes (Trogons)
Leptosomiformes (Cuckoo-roller)
Coliiformes (Mousebirds)
Strigiformes (Owls)
Accipitriformes (Eagles)
Accipitriformes (New World Vultures)
Pelecaniformes (Pelicans)
Pelecaniformes (Herons)
Pelecaniformes (Ibises)
Pelecaniformes (Cormorants)
Procellariiformes (Fulmars)
Sphenisciformes (Penguins)
Gaviiformes (Loons)
Phaethontiformes (Tropicbirds)
Eurypygiformes (Sunbittern)
Charadriiformes (Plovers)
Gruiformes (Cranes)
Opisthocomiformes (Hoatzin)
Caprimulgiformes (Hummingbirds)
Caprimulgiformes (Swifts)
Caprimulgiformes (Nightjars)
Otidiformes (Bustards)
Musophagiformes (Turacos)
Cuculiformes (Cuckoos)
Mesitornithiformes (Mesites)
Pterocliformes (Sandgrouse)
Columbiformes (Doves)
Phoenicopteriformes (Flamingos)
Podicipediformes (Grebes)
Galliformes (Landfowl)
Anseriformes (Waterfowl)
Tinamiformes (Tinamous)
Struthioniformes (Ostrich)
NEOAVES
NEOGNATHAE
GALLOANSERES
PALAEOGNATHAE
72
84
96
91
70
96
91
91
55
Passeri-morphae
Coracii-morphae
Accipitri-morphae
Pelecani-morphae
Procellarii-morphae
Gavii-morphae
Phaethonti-morphae
Cursori-morphae
Caprimulgi-morphae
Otidi-morphae
Columbi-morphae
Phoenicopteri-morphae
Australaves
Afroaves
Core Landbirds (Telluraves)
Core Waterbirds (Aequornithia)
Passerea
Columbea
Cretaceous Paleogene
110
100
90
80
70
60
50
40
30
20
10
0
Millions of years ago

Aves
70
60
50
40
30
20
10
0
Ma
Palaeognathae
Tinam.
Galloanserae
Galliformes
Anseriform.
Strisores
Apodiform.
Columbaves
Otidimorph.
Columbimorph.
Neoaves
Gruiformes
Aequorlitornithes
Struthio
Rhea
Apteryx
Casuarius
Dromaius
Eudromia
Nothoprocta
Crypturellus
Tinamus
Leipoa
Ortalis
Crax
Numida
Odontophorus
Colinus
Rollulus
Bonasa
Gallus
Chauna
Anseranas
Dendrocygna
Oxyura
Anser
Anas
Aythya
Eurostopodus
Caprimulgus
Chordeiles
Steatornis
Nyctibius
Podargus
Aegotheles
Hemiprocne
Streptoprocne
Chaetura
Topaza
Phaethornis
Archilochus
Tauraco
Corythaeola
Ardeotis
Tapera
Centropus
Cuculus
Coccyzus
Monias
Mesitornis
Syrrhaptes
Pterocles
Ptilinopus
Treron
Columbina
Leptotila
Columba
Heliornis
Sarothrura
Rallus
Micropygia
Porphyrio
Psophia
Aramus
Balearica
Grus
Phoenicopterus
Rollandia
Burhinus
Charadrius
Haematopus
Recurvirostra
Pedionomus
Jacana
Rostratula
Limosa
Arenaria
Tringa
Turnix
Glareola
Uria
Chroicocephalus
Sterna
Rynchops
Eurypyga
Phaethon
Gavia
Spheniscus
Phoebastria
Oceanites
Pelagodroma
Oceanodroma
Fulmarus
Puffinus
Pterodroma
Pelecanoides
Ciconia
Leptoptilos
Fregata
Morus
Anhinga
Phalacrocorax
Theristicus
Tigrisoma
Ardea
Ixobrychus
Scopus
Balaeniceps
Pelecanus
Upper
Palaeocene
Eocene
Oligocene
Miocene
Pli.
Ple.
Cretaceous
Palaeogene
Neogene
Q.

70
60
50
40
30
20
10
0
Ma
Neoaves continued
Accipitriformes
Coraciimorphae
Inopinaves
Australaves
Passeriformes
Opisthocomus
Cathartes
Vultur
Sagittarius
Pandion
Elanus
Buteo
Accipiter
Tyto
Strix
Colius
Urocolius
Leptosomus
Trogon
Apaloderma
Upupa
Phoeniculus
Bucorvus
Tockus
Merops
Coracias
Atelornis
Todus
Momotus
Alcedo
Chloroceryle
Galbula
Bucco
Chelidoptera
Indicator
Jynx
Picus
Megalaima
Buccanodon
Capito
Ramphastos
Cariama
Chunga
Micrastur
Falco
Ibycter
Caracara
Nestor
Probosciger
Barnardius
Psittrichas
Psittacus
Deroptyus
Acanthisitta
Pitta
Smithornis
Calyptomena
Eurylaimus
Neodrepanis
Melanopareia
Myrmornis
Thamnophilus
Terenura
Myrmothera
Sclerurus
Furnarius
Lepidocolaptes
Neopelma
Cryptopipo
Ceratopipra
Rupicola
Cotinga
Oxyruncus
Myiobius
Schiffornis
Tityra
Piprites
Rhynchocyclus
Hirundinea
Elaenia
Hymenops
Tyrannus
Menura
Climacteris
Sericulus
Ptilonorhynchus
Malurus
Lophorina
Corvus
Poecile
Calandrella
Pycnonotus
Sylvia
Regulus
Turdus
Fringilla
Spizella
Upper
Palaeocene
Eocene
Oligocene
Miocene
Pli.
Ple.
Cretaceous
Palaeogene
Neogene
Q.

Configuración ósea del Paladar

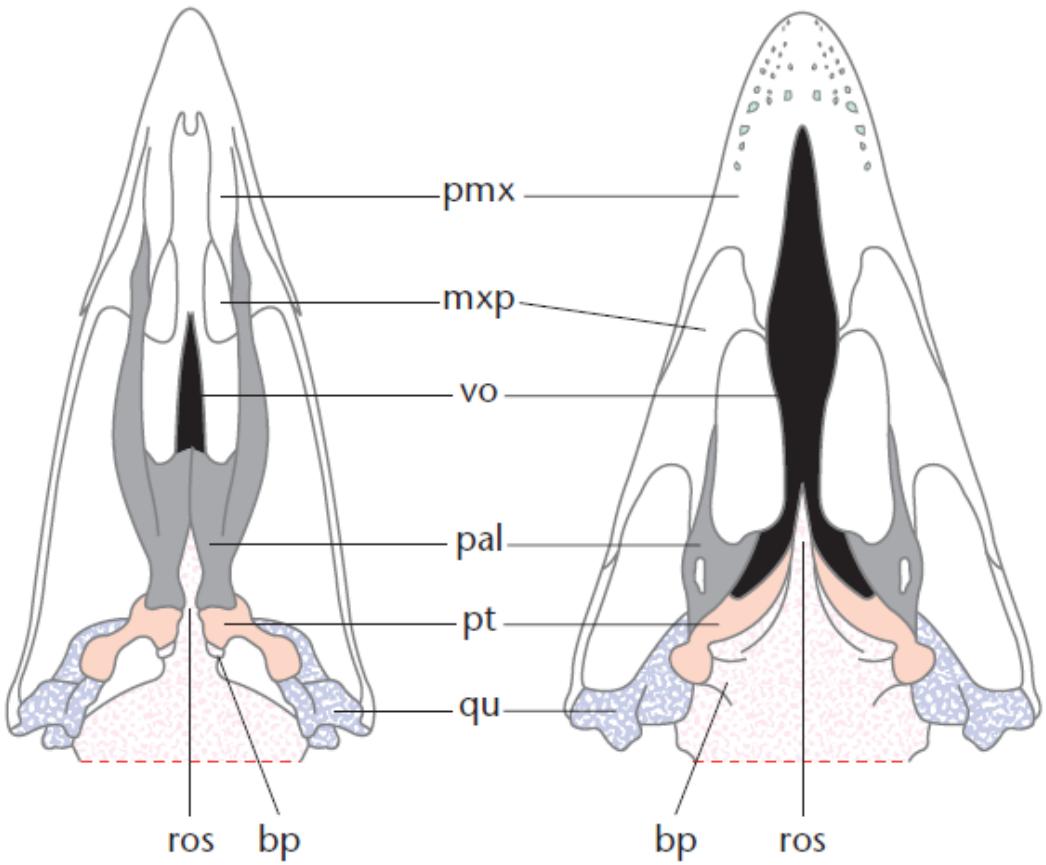

(a) **Neognathae** (b) **Paleognathae**

Figure 1 Palate bones, in ventral view, of (a) domestic fowl (*Gallus gallus*, Neognathae); (b) emu (*Dromaius novaehollandiae*, Palaeognathae). After Pycraft 1901b. Key: bp, basipterygoid process; mxp, maxillopalatine; pal, palatine; pmx, premaxilla; pt, pterygoid; qu, quadrate; ros, parasphenoid rostrum; vo, vomer. Note the reduced vomers (black) and juxtaposed palatines (dark grey) in Neognathae. In Palaeognathae, the palatines are separated by relatively large vomers.

Paleognathae

Definición: Clado más inclusivo que contiene a la perdiz chilena *Nothoprocta perdicaria* pero no al gorrión *Passer domesticus*. Tradicionalmente se ha subdividido en **Ratitae** y Tinamiformes (**Cripturi**)

- **Tinamiformes**
  - **Tinamidae**
    - (8 géneros)
- **Struthioniformes**
  - **Struthionidae**
    - *Struthio camelus*
    - *Struthio molybdophanes*
- **Rheiformes**
  - **Rheidae**
    - *Rhea americana*
    - *Rhea pennata*
- **Casuariiformes**
  - **Casuariidae**
    - *Casuarius casuarius*
    - *Casuarius bennetti*
    - *Casuarius unappendiculatus*
  - **Dromadiidae**
    - *Dromaius novaehollandiae*
- **Apterygiformes**
  - **Apterygidae**
    - *Apteryx australis*
    - *Apteryx mantelli*
    - *Apteryx rowi*
    - *Apteryx owenii*
    - *Apteryx haastii*

Filogenia: Los ratites fueron considerados durante mucho tiempo como monofiléticos, grupo hermano de perdices y con Kiwi como linaje más basal.

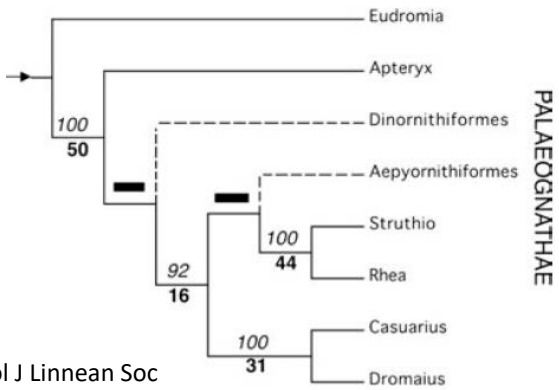

Livezey & Zusi 2007; Zool J Linnean Soc

Tinamiformes

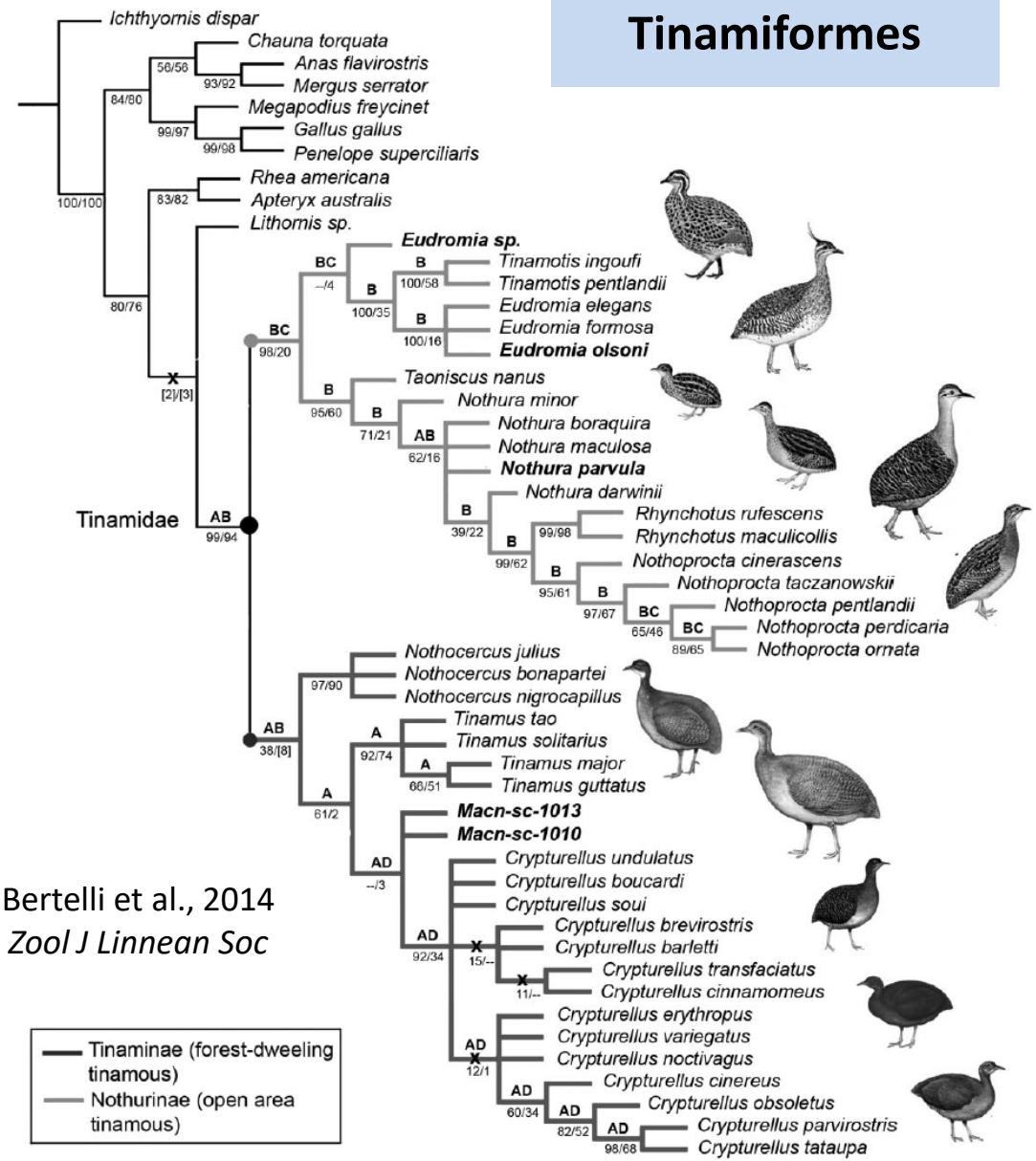

Bertelli et al., 2014
Zool J Linnean Soc

Figure 1. Reduced strict consensus of the phylogenetic analysis of fossils and living tinamous under implied weight. Differences between topologies under equal versus implied weights analyses are marked with an '×'. Alternative positions of the fossils excluded from the strict consensus a posteriori are indicated above branches (A, MACN-SC-H; B, MACN-SC-T; C, *Nothura* sp.; D, *Crypturellus reai*). Support values of the phylogenetic analysis of extant species and analysis including fossils, respectively, are below branches.

Lithornithiformes

Palaeotis weigelti

Unidad: Formación Messel (Eoceno).

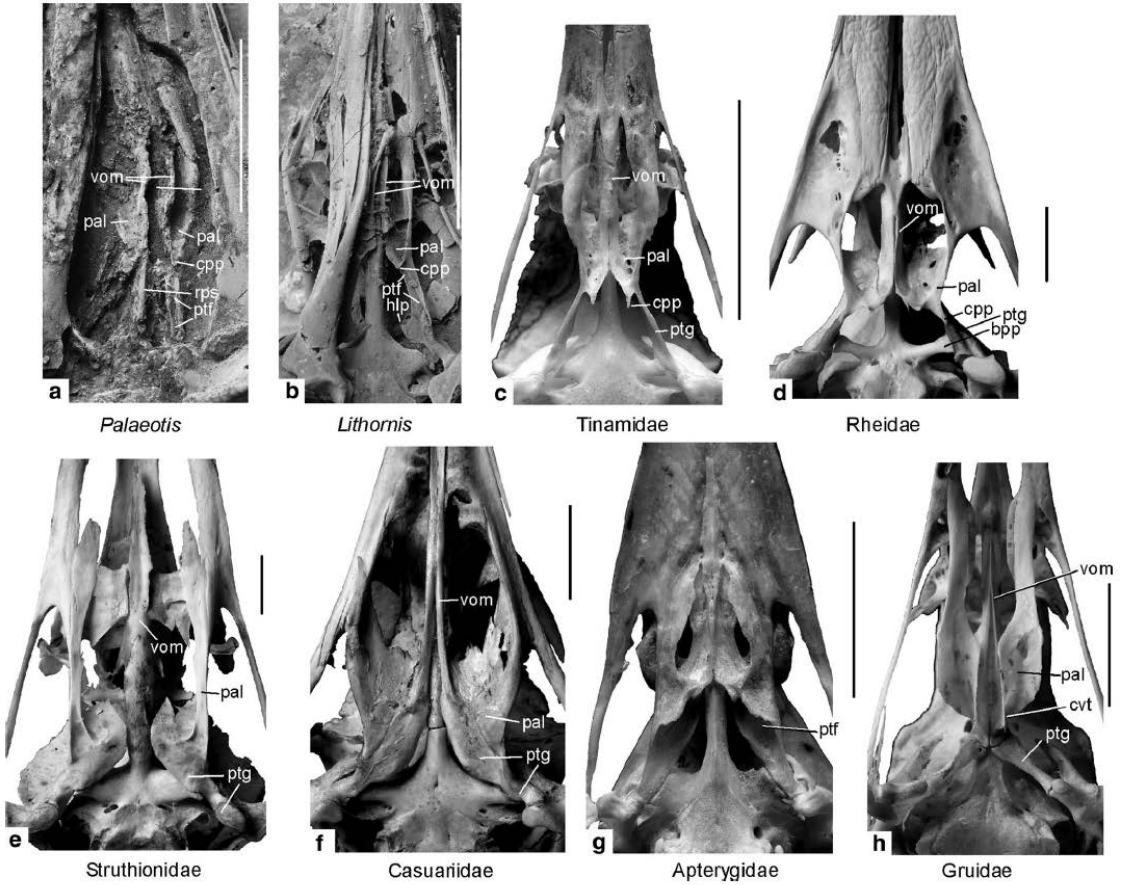

Fig. 2 **a** Detail of the bony palate of *Palaeotis weigelti* Lambrecht, 1928 from the middle Eocene of Messel (HLMD Me 771) in *ventral* view, in comparison to **b** *Lithornis* sp. from the early Eocene Fur Formation in Denmark (MGUH 26770), **c** the Yellow-legged Tinamou, *Crypturellus noctivagus* (Tinamidae), **d** the Greater Rhea, *Rhea americana* (Rheidae), **e** the Ostrich, *Struthio camelus* (Struthionidae), **f** the Southern Cassowary, *Casuarius casuarius* (Casuariidae), **g** the Southern Brown Kiwi, *Apteryx australis* (Apterygidae), and **h** the Grey Crowned Crane, *Balearica regulorum* (Gruidae). *bpp*, basipterygoid process, *cpp* caudal process of os palatinum, *cvt* crista ventralis, *hlp* hook-like medial process of pterygoid, *pal* palatinum, *ptf* fossa along pterygoid, *ptg* pterygoid, *rps* rostrum parasphenoidale, *vom* vomer. All fossils were coated with ammonium chloride to enhance the contrast of the bone structures. *Scale bars* equal 20 mm

“Ratites”

Sinapomorfías:

- Proceso zigomático elongado, 2/3 de cuadrado
- Escapulocoracoides
- Ausencia de quilla esternal
- Vertebras sinsacrales con pobre desarrollo de procesos transversos
- Ilium alto con fuerte pendiente a cada lado.
- Ausencia de puente supratendíneo en tibiotarso (ratites derivadas)

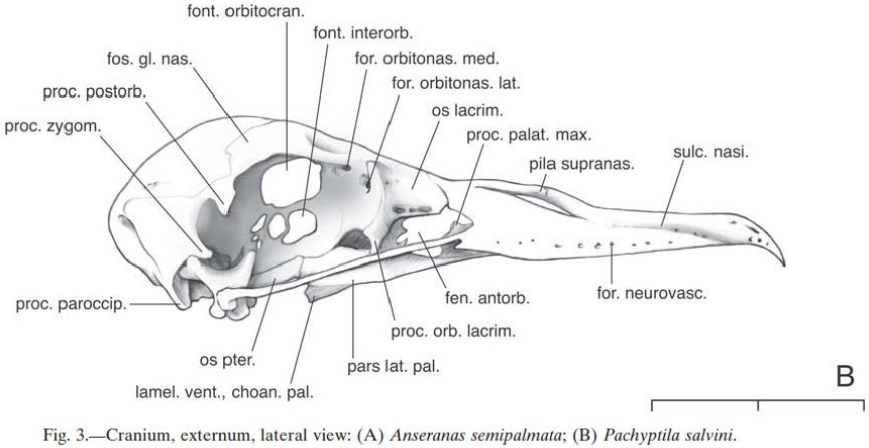

Fig. 3.—Cranium, externum, lateral view: (A) *Anseranas semipalmata*; (B) *Pachyptila salvini*.

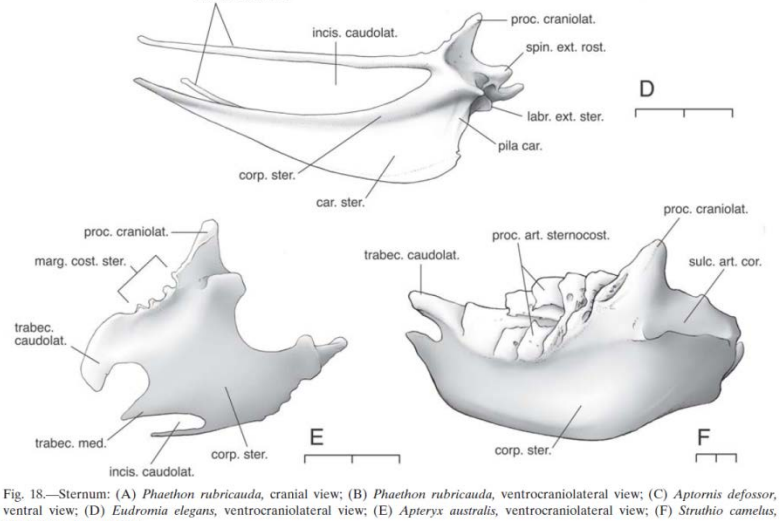

Fig. 18.—Sternum: (A) *Phaethon rubricauda*, cranial view; (B) *Phaethon rubricauda*, ventrocraniolateral view; (C) *Aptornis defossor*, ventral view; (D) *Eudromia elegans*, ventrocraniolateral view; (E) *Apteryx australis*, ventrocraniolateral view; (F) *Struthio camelus*, ventrocraniolateral view.

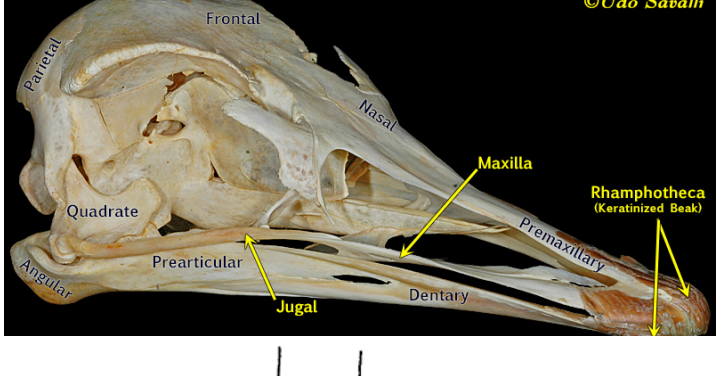

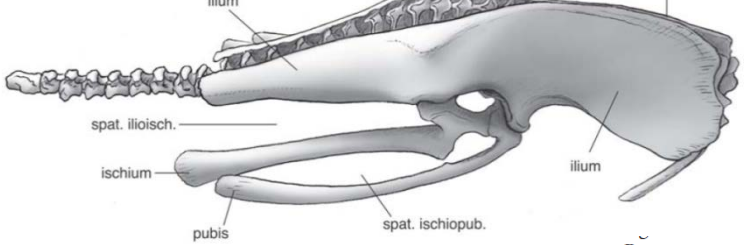

Dromaius novaehollandiae

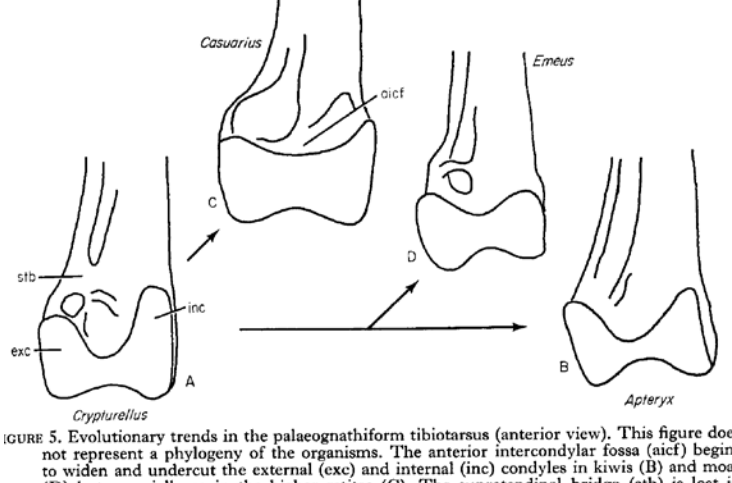

IGURE 5. Evolutionary trends in the palaeognathiform tibiotarsus (anterior view). This figure does not represent a phylogeny of the organisms. The anterior intercondylar fossa (aicf) begins to widen and undercut the external (exc) and internal (inc) condyles in kiwis (B) and moas (D) but especially so in the higher ratites (C). The supratendinal bridge (stb) is lost in higher ratites (C) and occasionally does not ossify completely in the kiwis (B).

Biogeografía de Ratites 1.0

Primeras Filogenias morfológicas

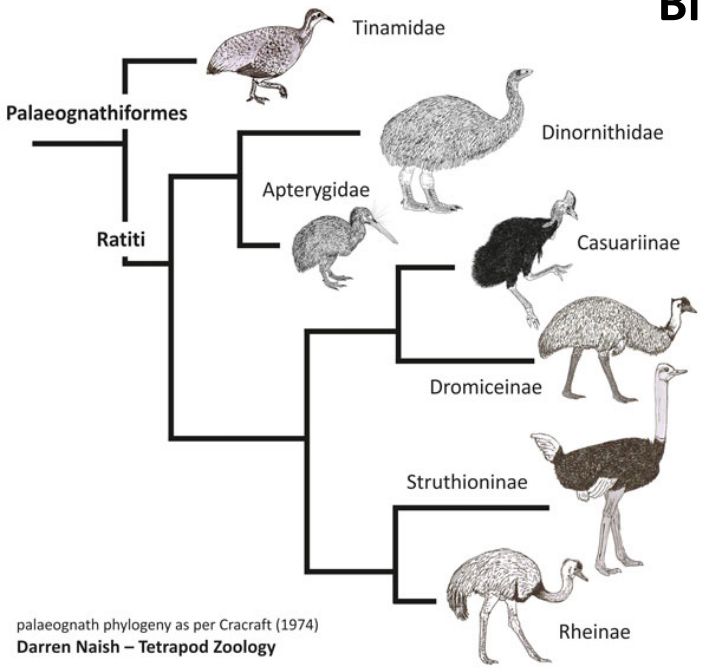

Primeras Filogenias moleculares

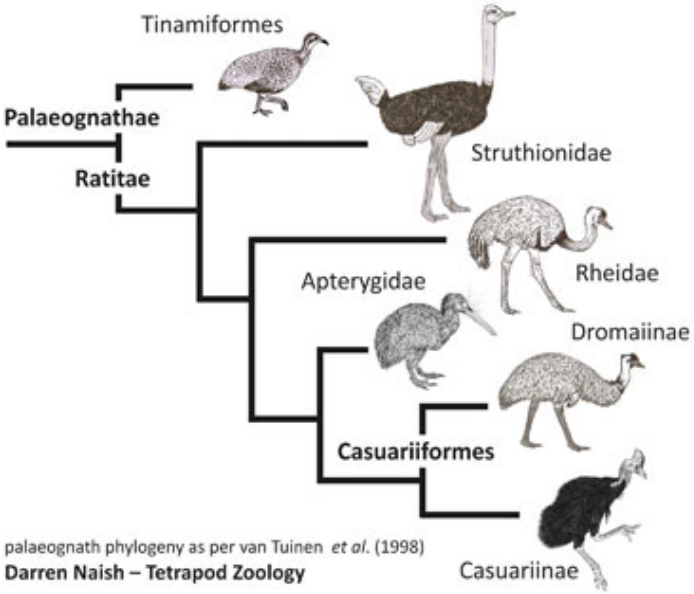

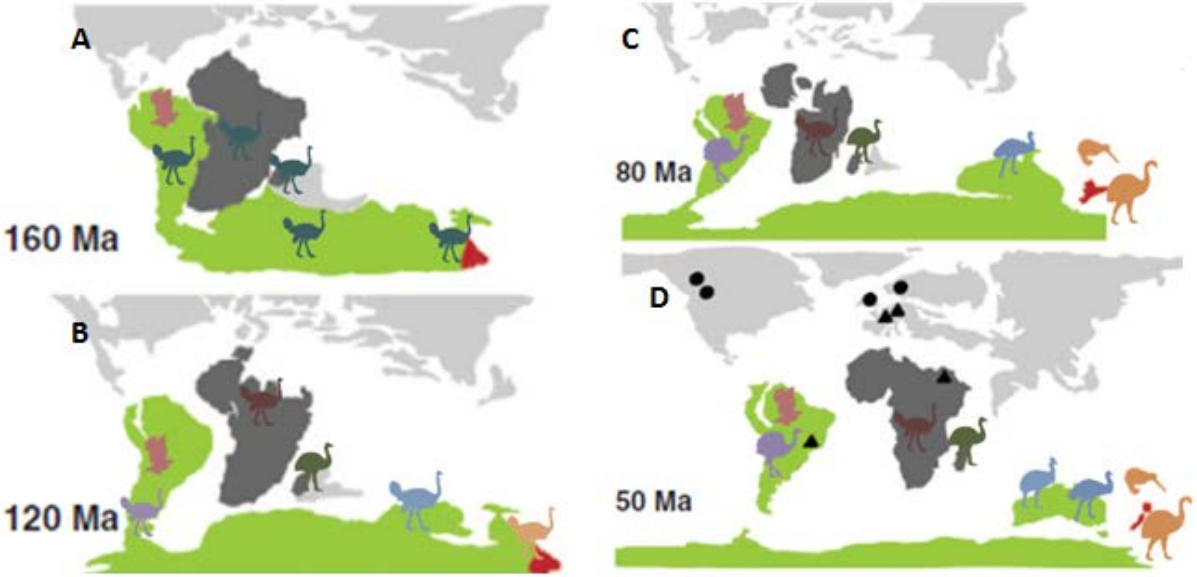

Monofilia discutida de “Ratitae”

En una reciente filogenia molecular basada en 20 genes (24 kb) nucleares se recupera a las perdices profundamente anidadas dentro de un Ratites parafilético.

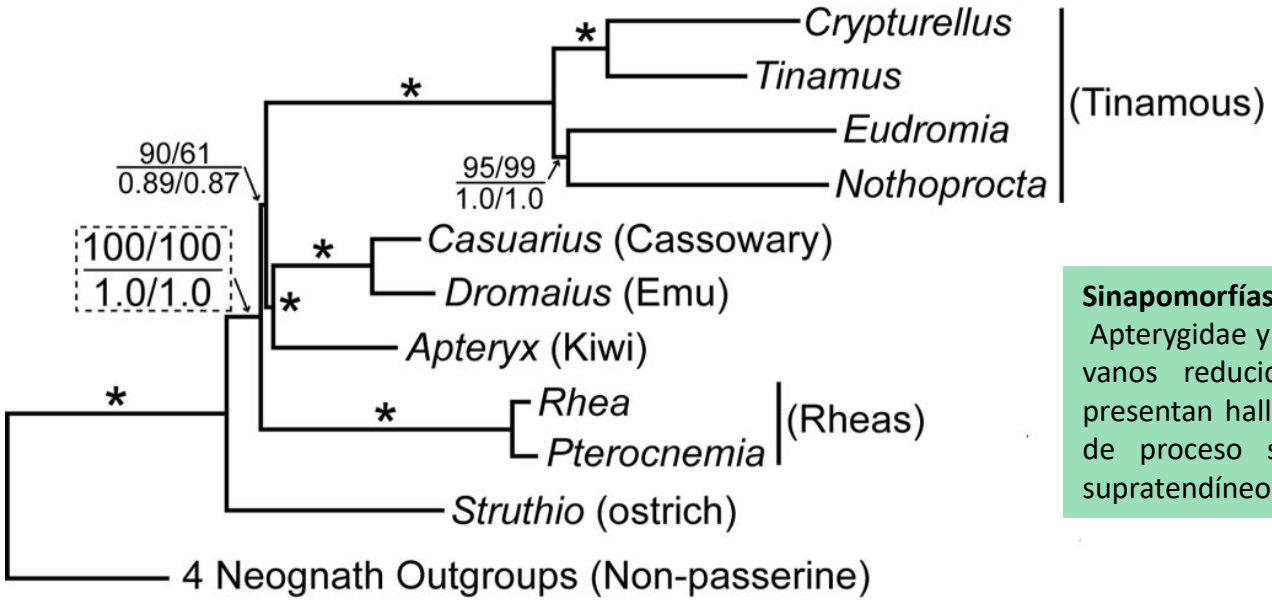

Sinapomorfías de Casuariidae+Apterygiidae:
Apterygidae y Casuariidae comparten alas cortas con vanos reducidos, y Apterygidae + Dinornithidae presentan hallux (perdido en otras ratites), ausencia de proceso supraorbital y presencia de puente supratendíneo en tibiotarso (ausente en otras ratites)

Harshmann et al., 2008

Esto implica 2 hipótesis:

- Readquisición del vuelo en Tinamiformes (más parsimoniosa?)

- Pérdida múltiple del vuelo en ratites de forma independiente (menos parsimonioso, pero más probable).

Biogeografía de Ratites 2.0

En un intento por reconciliar la evidencia molecular con la morfológica, Jhonston (2011) presenta un análisis basado en nuevos rasgos morfológicos que soporta la inclusión de Tinamiformes en Ratitae. Sin embargo la hipótesis biogeográfica de vicarianza (que intenta ser congruente con la deriva continental) es inconsistente con el registro fósil.

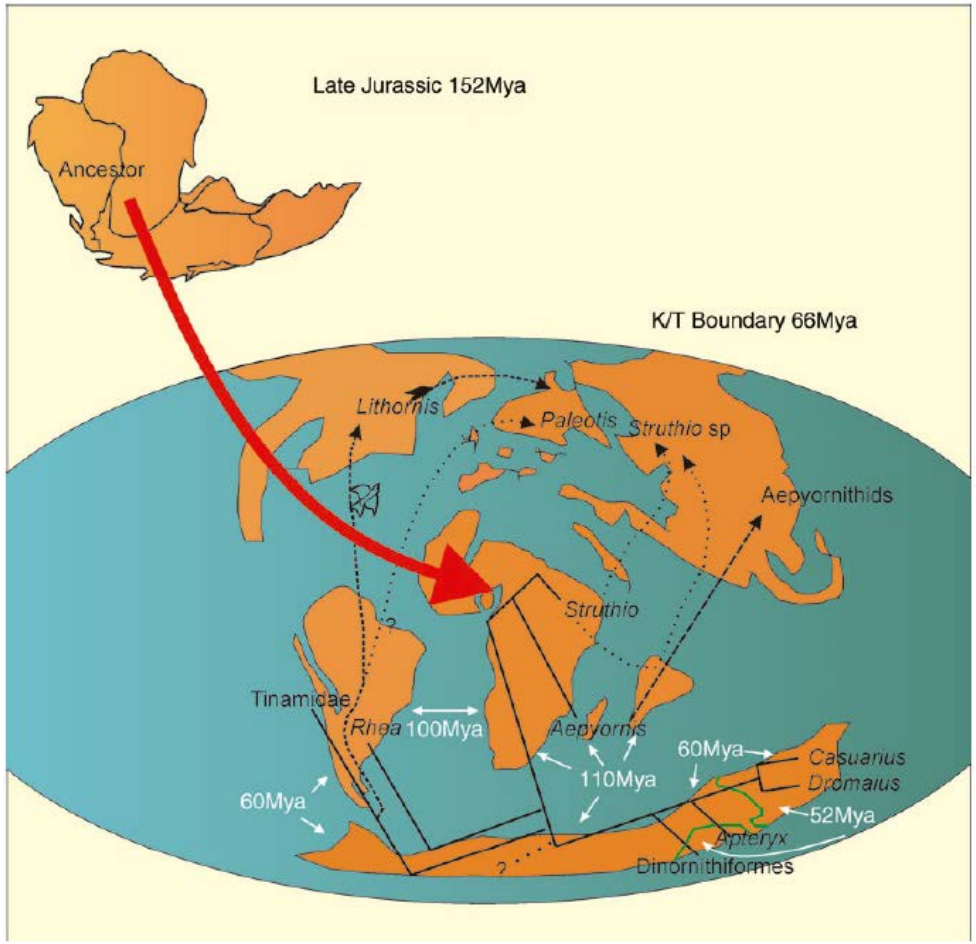

Figure 5. Schematic representation of the palaeognath ancestor in undivided Gondwana at 152 million years ago (Mya) and its distribution across divisions of the continent at 66 Mya according to the phylogeny presented here, with approximate dates of separation indicated in white type. It is assumed, based on the shape of the phylogeny, that ancestors of the South American taxa were present on the South America-Antarctica-Australasia fragment of Gondwana, rather than being the direct result of separation from Africa. Fossil palaeognath remains in Antarctica are not well enough characterized to fit into this phylogeny (Tambussi *et al.*, 1994) but are denoted with a question mark. Maps are modified from the Paleomap project (Scotese, 2001).

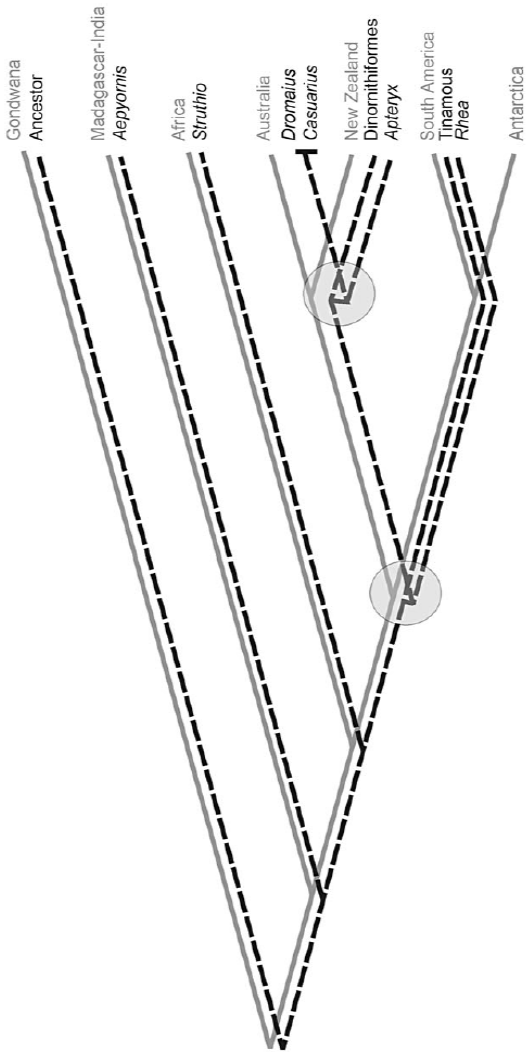

Figure 6. Gondwana area cladogram and a fully resolved palaeognath phylogeny (based on Fig. 4A) mapped together and reconciled with TREEMAP (http://taxonomy.zoology.gla.ac.uk/rod/treemap.html). Circles indicate nodes on the palaeognath tree that occur prior to geographical separations.

Johnston et al., 2011; Zool J Linnean Soc

Evidencia de un Clado Tinamiformes+Dinornithiformes

El escenario alternativo es que la pérdida de capacidad voladora haya aparecido independientemente en múltiples linajes de paleoñatas. Phillips et al. (2010), presentan un análisis basado en DNA mitocondrial, encontrando un clado conformado por Tinamiformes y Dinornithiformes. Similares resultados fueron obtenidos por Smith et al (2012) basado en evidencia molecular independiente y combinada, y Baker et al (2014) basado en 1448 loci de DNA nuclear

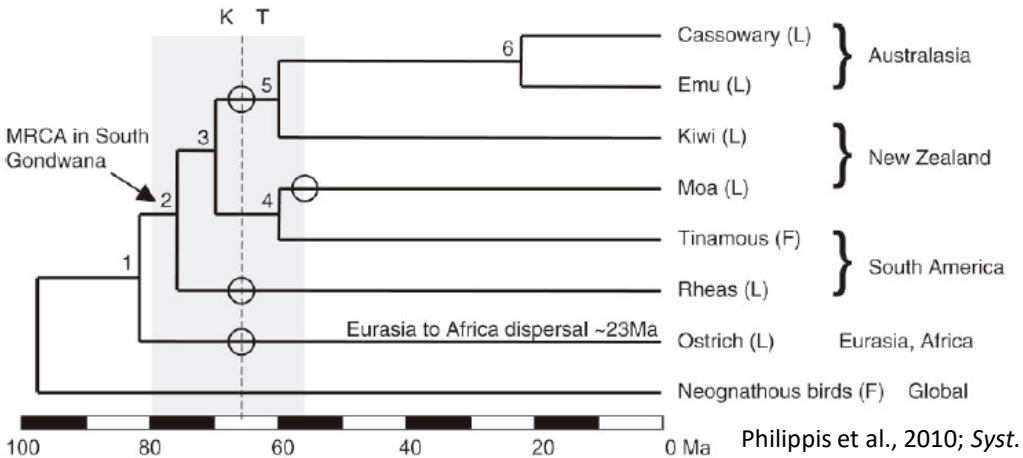

Philippis et al., 2010; *Syst. Biol.*

FIGURE 5. Timescale of palaeognath evolution with relative placements indicated for inferred losses of flight (circles), the Cretaceous-Tertiary boundary (dotted line), and the major period of fragmentation of South Gondwana (shaded). Inferred median dates from the BEAST analysis of the 24-taxon tree for palaeognath divergences at the numbered nodes in millions of years before present: (1) 83.4, (2) 76.4, (3) 70.6, (4) 60.0, (5) 59.9, (6) 20.7. 95% HPDs are shown in Table 5. Elephant birds of Madagascar have not been included due to the uncertainty of their phylogenetic placement. F and L in parentheses after taxon names denote flighted and flightless, respectively.

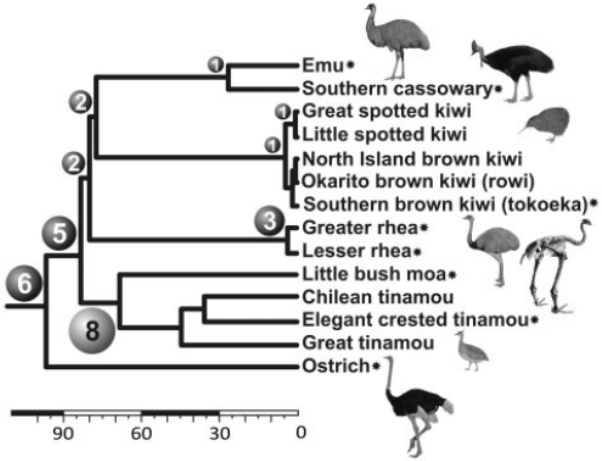

FIG. 3. Eight retroelement insertions shared by little bush moa and four tinamou species identified in the current study (light gray sphere with black numbering), mapped onto a published paleognath topology constructed from 27 nuclear genes and 21 retroelements (Haddrath and Baker 2012; published CR1 insertions are indicated by dark gray spheres with white numbering). Scale bar indicates time in millions of years. Asterisks mark species included in comparisons to morphological data. Bird drawings are modified from del Hoyo et al. (1992) with permission from Lynx Edicions, Barcelona, Spain.

Baker et al., 204; SMBE

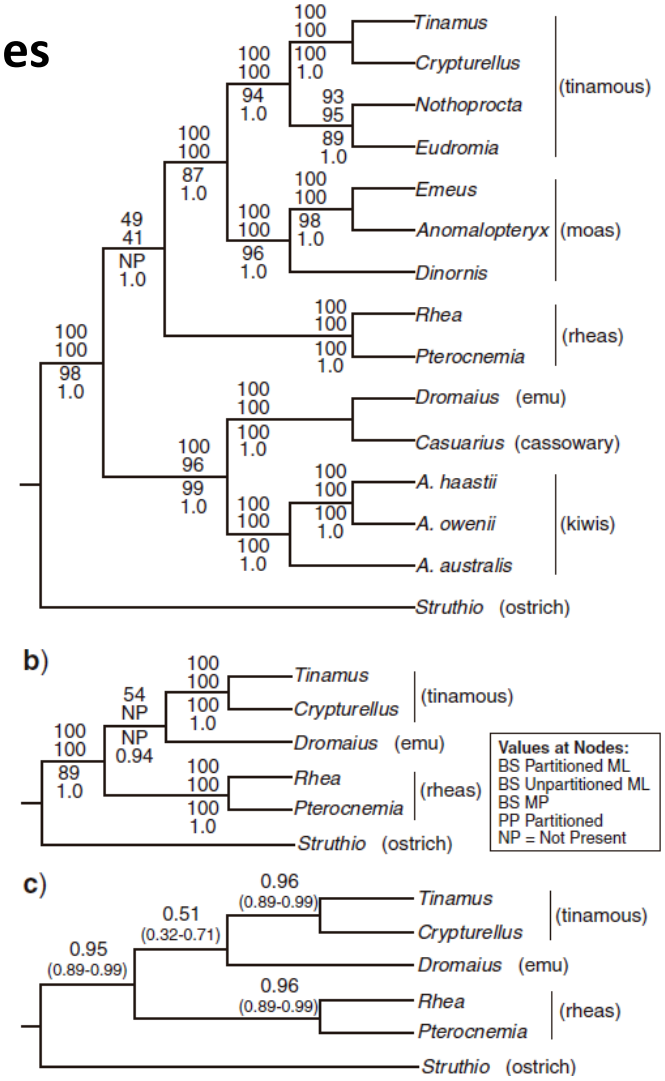

FIGURE 4. Total molecular evidence analysis, concatenating the data from this study with that of Harshman et al. (2008) and Phillips et al. (2010). Support from multiple analyses is presented (BS refers to % bootstrap support, PP refers to posterior probability values). a) ML phylogram for analyses of all paleognath taxa analyzed by Phillips et al. (2010). The Bayesian consensus tree had a different topology, uniting the kiwis, emu, cassowary, moas, and tinamous to the exclusion of the rheas (posterior probability = 0.54). b) ML phylogram for analyses of taxa used in this study. The unpartitioned ML and MP analyses united tinamous and rheas with 51% BS (unpartitioned ML) and 87% BS (MP). c) Species tree estimated using BUCKy for all 61 loci (which was topologically identical to the primary concordance tree). The top values are concordance factors (the estimated amount of the genome supporting a particular bipartition); the lower values provide the 95% credible intervals for these concordance factor estimates. The species tree estimated by BUCKy was topologically identical.

Smith et al., 2012; *Syst. Biol.*


3 cm
3 cm

Evidencia de un Clado Ave Elefante+Kiwi

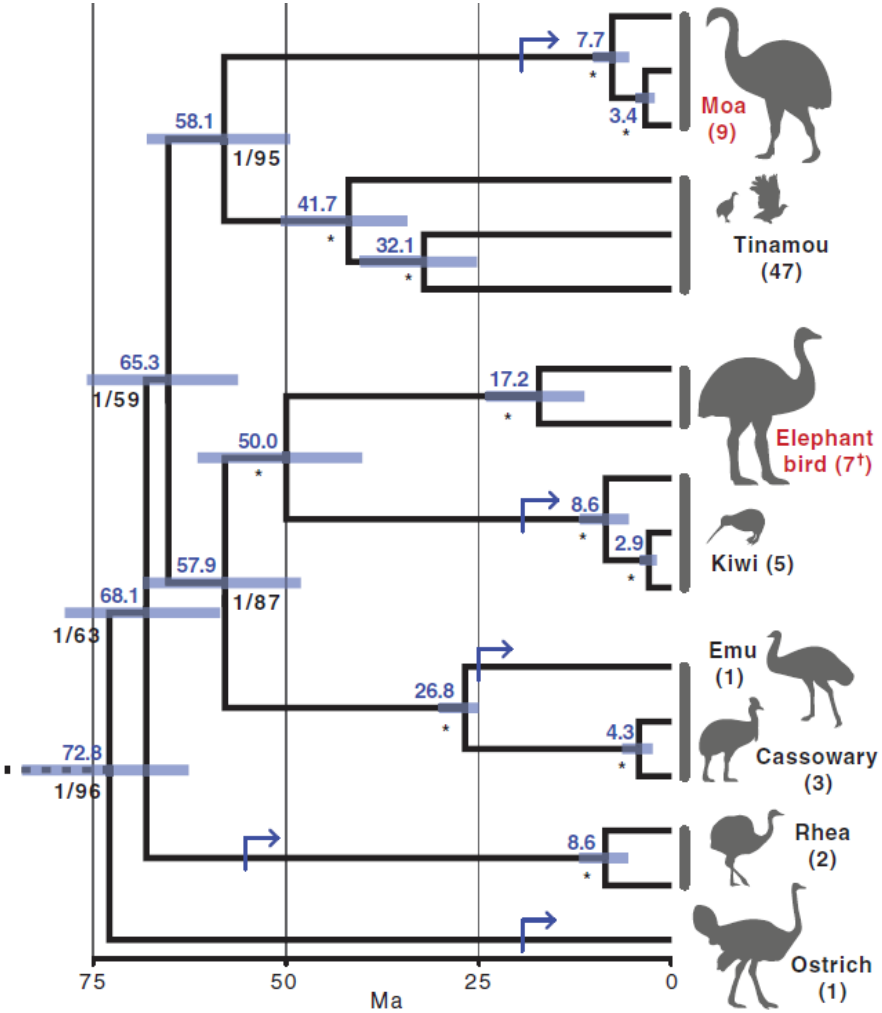

Fig. 1. Phylogenetic position of the elephant birds from mitochondrial sequence data. Bayesian posterior probabilities and maximum likelihood bootstrap are presented in black below each branch; asterisks denote branches that received maximum possible support (bootstrap = 100%, Bayesian posterior probability = 1.0). Divergence dates [blue numbers above branches; blue bars represent 95% highest posterior density (HPD) intervals] were inferred with six well-supported node age constraints (table S5). Blue arrows mark the minimum date for the evolution of flightlessness in lineages for which fossil evidence is available (*21*, *22*). The scale is given in millions of years before the present. Silhouettes indicate the relative size of representative taxa. Species diversity for each major clade is presented in parentheses, with extinct groups shown in red. The dagger symbol (†) indicates that the number of elephant bird species is uncertain.

Mitchell et al.,2014; Science

Ancient DNA reveals elephant birds and kiwi are sister taxa and clarifies ratite bird evolution

Kieren J. Mitchell,[1] Bastien Llamas,[1] Julien Soubrier,[1] Nicolas J. Rawlence,[1*] Trevor H. Worthy,[2] Jamie Wood,[3] Michael S. Y. Lee,[1,4] Alan Cooper[1†]

- Confirma una vez más que Ratitae es parafilético
- Soporta un clado Aepyornithiformes+Apterygiformes
- Implica que gigantismo y pérdida del vuelo evolucionan paralelamente en Paleognathae.
- Origen es consistente con divergencia molecular calibraada con fósiles.
- Distribución de paleognatas actuales no es explicada por vicarianza.
- Distribución es congruente con una dispersión posterior al quiebre de Gondwana.

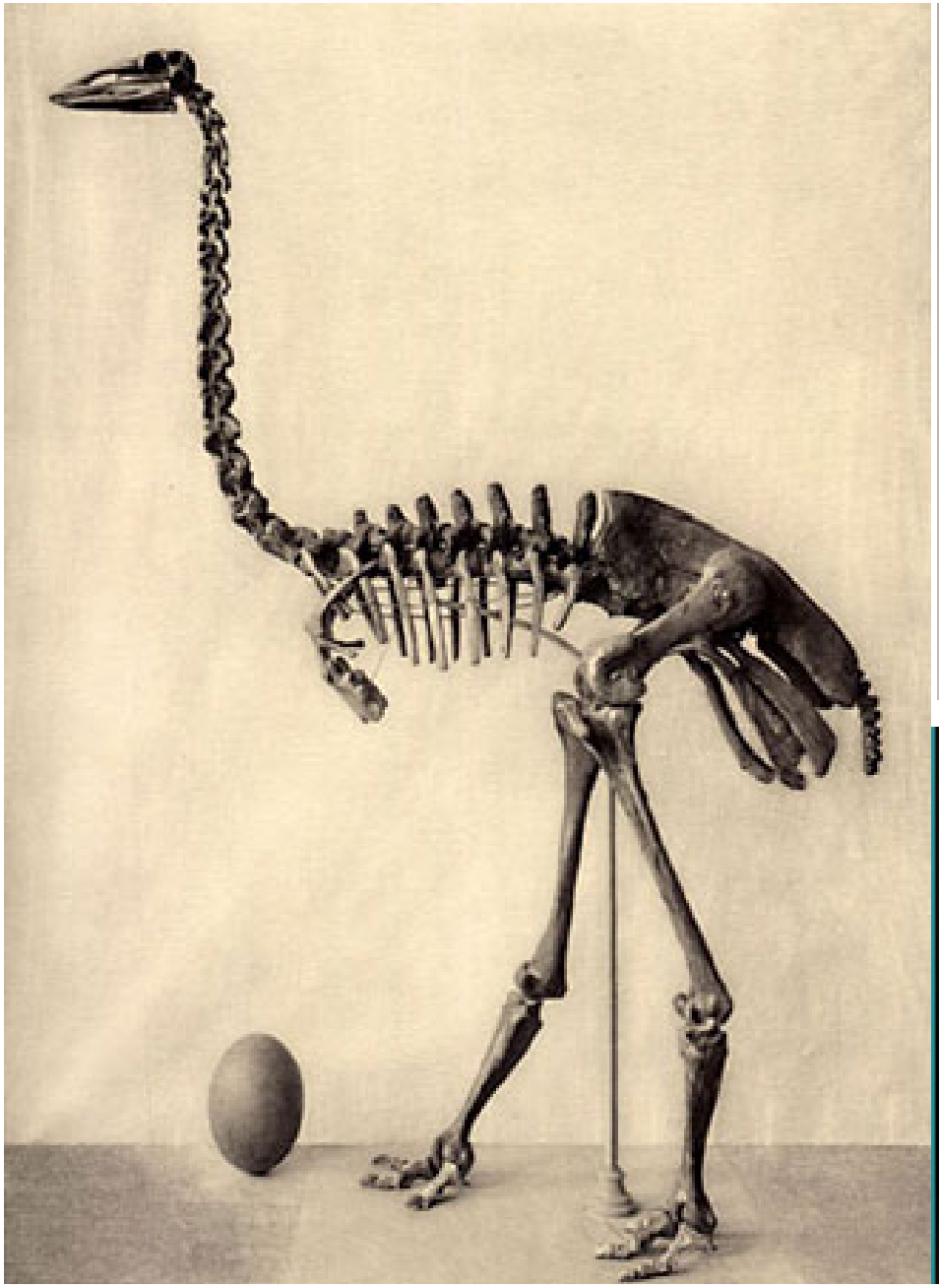

Biogeografía de Ratites 3.0

Fig. 3. Conflict between inferred palaeognath phylogeny and the topology predicted by continental vicariance. (**A**) Relative position of continents during the Late Cretaceous and Tertiary. Continental landmasses are colored according to order of severance from the remaining Gondwanan landmass: Africa and Madagascar first (dark gray; 100 to 130 Ma), followed by New Zealand (red; 60 to 80 Ma), then finally Australia, Antarctica, and South America (green; 30 to 50 Ma). Palaeognath-bearing fossil localities from the late Palaeocene and Eocene (*21*, *22*) are represented by circles (flighted taxa) and triangles (flightless taxa). (**B**) Predicted phylogeny of ratites under a model of speciation governed solely by continental vicariance. (**C**) Palaeognath phylogeny as inferred in the present study (see Fig. 1).

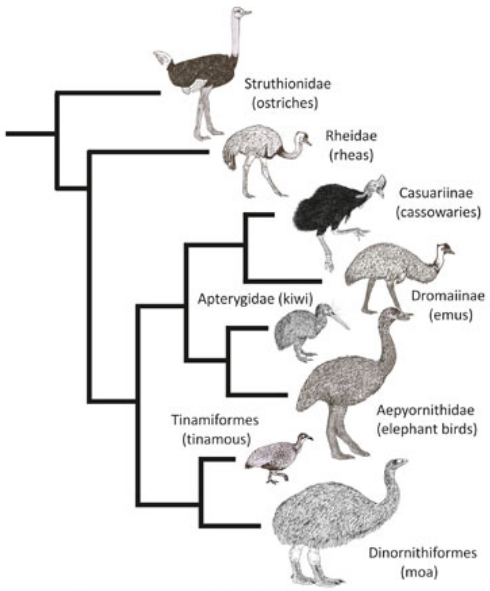

palaeognath phylogeny as per Mitchell *et al.* (2014)
Darren Naish – Tetrapod Zoology

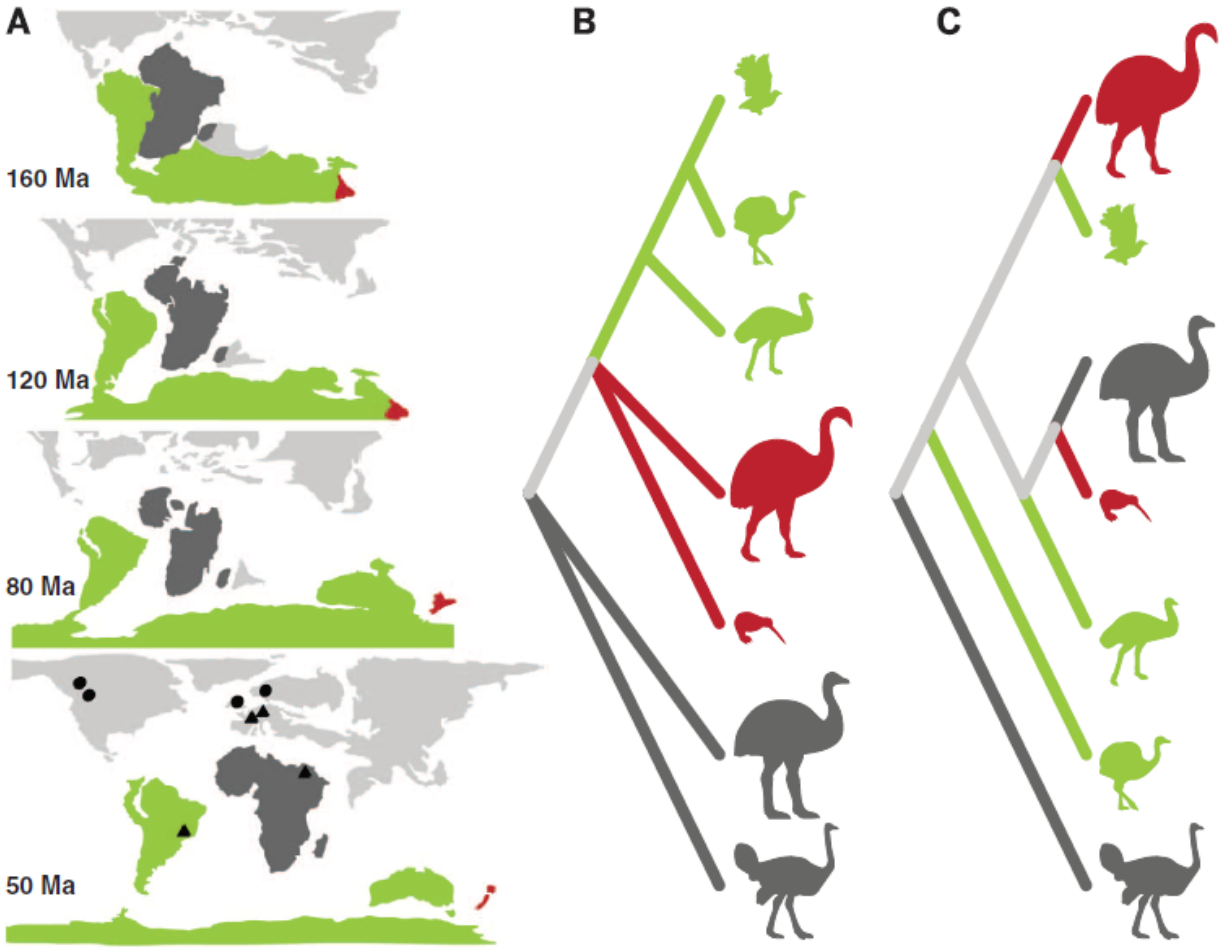

Mitchell et al.,2014; Science

Neognathae

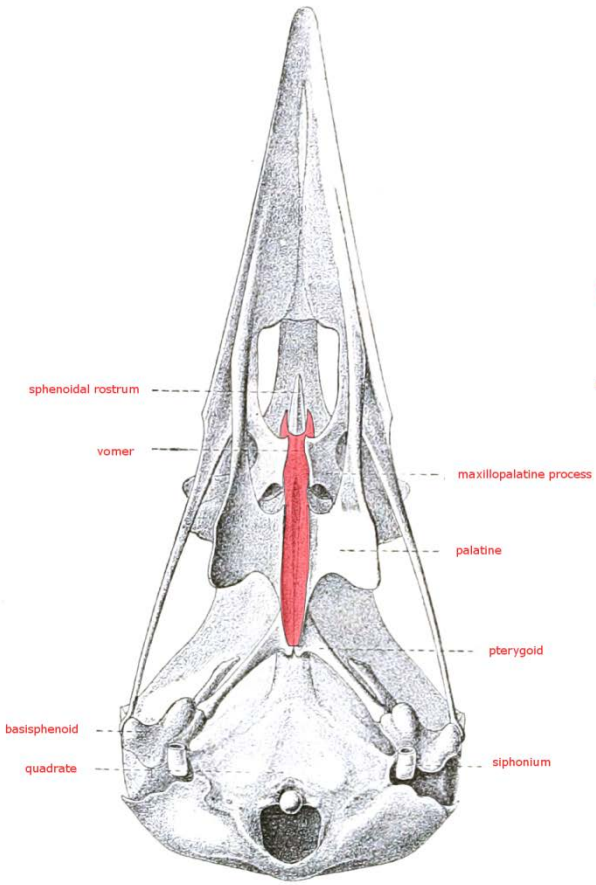

Skull of Corvus frugilegus

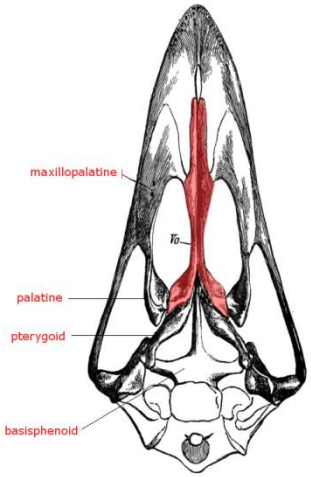

Skull of an Emu

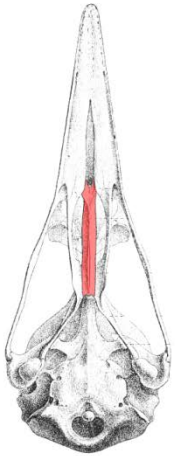

Skull of a Tinamou
Rhynchotus rufescens

Galloanseres

Clado menos inclusivo que contiene a pollos (Galliformes) y patos (Anseriformes).

Soportado por evidencia morfológica:

- Proceso Basipterigoides inmóvil.
- Proceso retroarticular largo y en forma de hoja.
- Morfología “derivada” del cuadrado.

También soportado por evidencia molecular: Hibridización DNA-DNA, secuencias de genes nucleares, mitocondriales.

Está compuesto por los grupos corona Galliformes y Anseriformes, más varios grupos extintos.

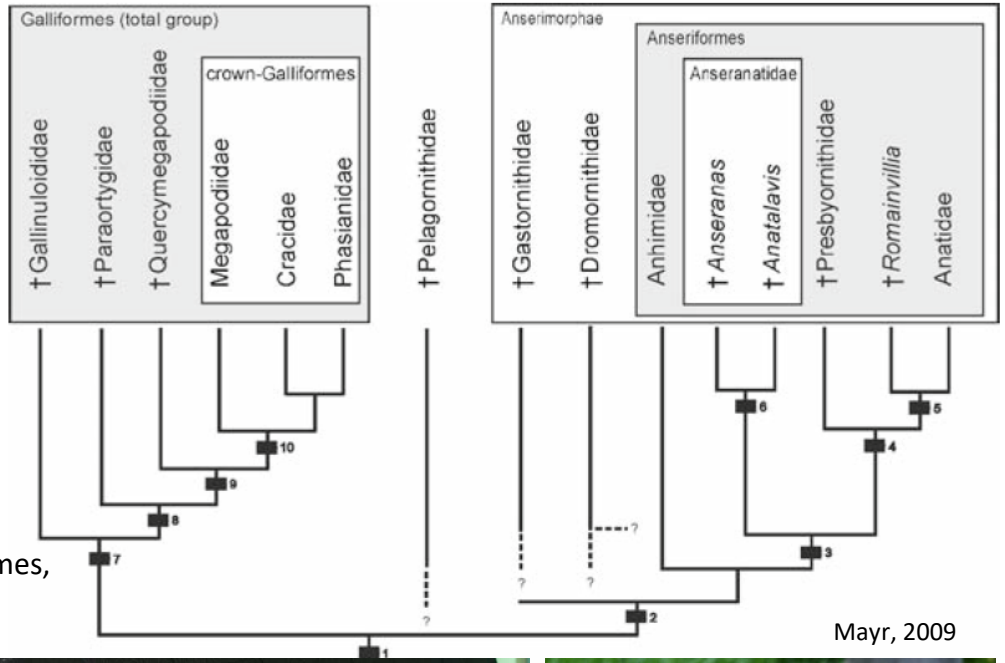

Mayr, 2009

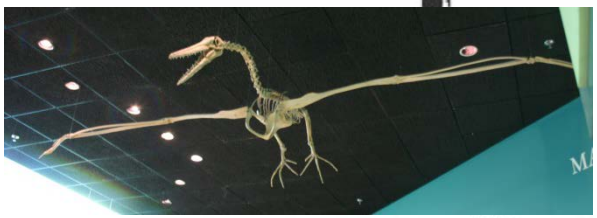

Vegavis iaai

Unidad: Formación López de Bertodano (Maastrichtiano).

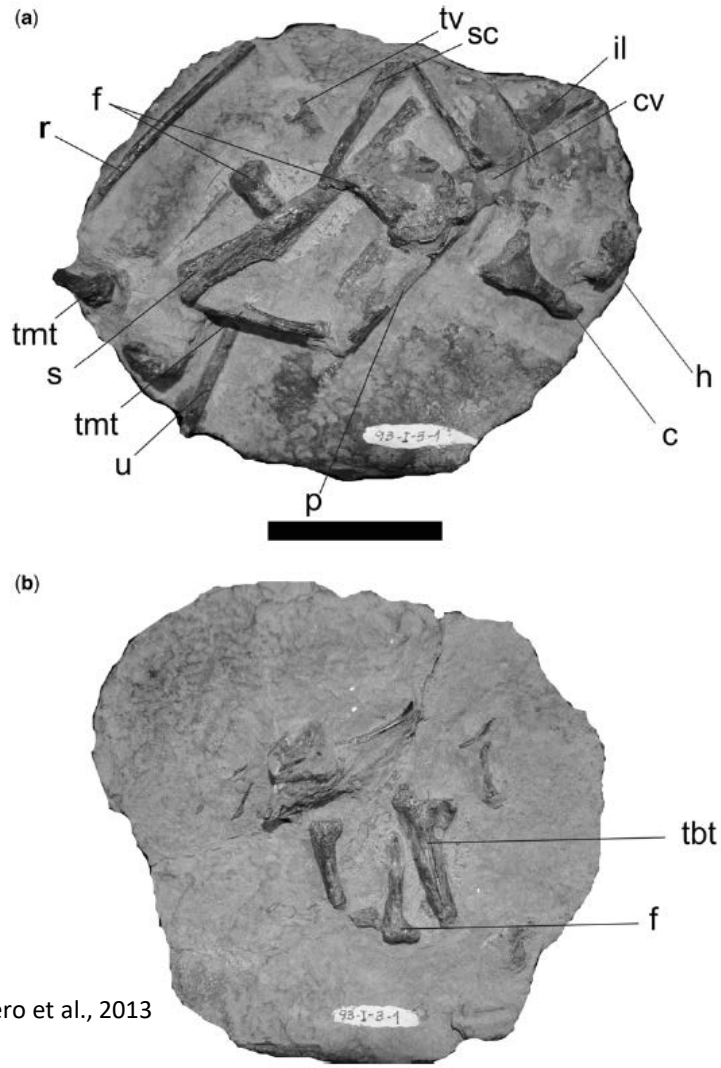

Reguero et al., 2013

Fig. 8. *Vegavis iaai* (Clarke *et al.* 2005), MLP 93-I-3-1, holotype. (**a**) The half of the concretion preserving most of the skeleton of the holotype; (**b**) the other half of the concretion with few bones. *Abbreviations*: c, coracoids; cv, cervical vertebra; f, femora; h, humerus; il, ilium; p, pubis; r, radius; tmt, tarsometatarsus; tv, thoracic vertebrae; s, sacrum; sc, scapula; u, ulna (scale bar 50 mm).

Sinapomorfías compartidas con Neornithes:

- Cresta deltopectoral del húmero desviada anteriormente.
- Al menos 15 vértebras sacrales ankilosadas.
- Puente supratenineo osificado en el tibiotarso.

Sinapomorfías compartidas con Anseriformes:

- Fenestra isquiádica cerrada.
- Surco humeral para m. escápulotricipatlis.

Sinapomorfías compartidas con Anseriformes:

- Proceso pectíneo diminuto en pelvis
- Hipotarso con cristas y sulci bien desarrolladas.

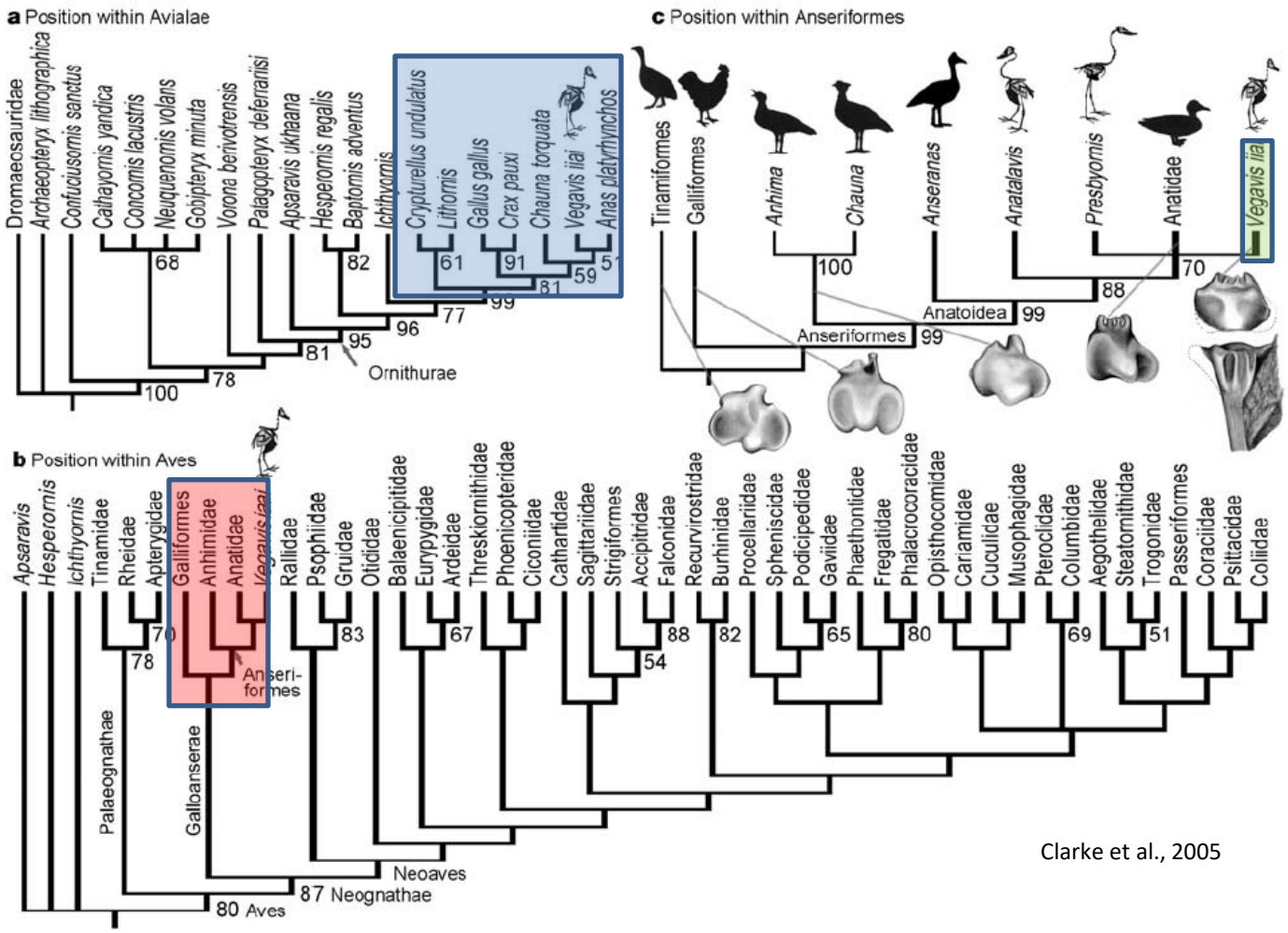

Clarke et al., 2005

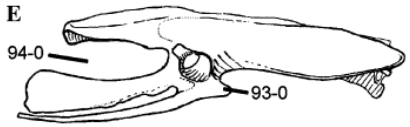

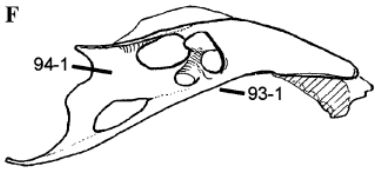

Figure 3 Phylogenetic placement of *Vegavis* in three successive cladistic analyses progressing from Avialae to Anseriformes (see Methods). **a**, Placement within Avialae in the strict consensus cladogram of two most parsimonious trees (MPTs): length, 385; consistency index (CI), 0.67; retention index (RI), 0.81; rescaled consistency index (RC), 0.54. **b**, Placement within Aves in the strict consensus of three MPTs: length, 822; CI, 0.33; RI, 0.48; RC, 0.16. **c**, Placement in Anseriformes in one MPT: length, 148; CI, 0.91; RI, 0.88; RC, 0.81. Bootstrap support values >50% from 2,000 replicates (10 random addition sequences/replicate; random start trees; tree bisection reconnection) are reported below and to the right of corresponding nodes. Insets in **c** compare the right hypotarsus (see also character 90:0, ref. 16) of exemplars for Tinamiformes (*Eudromia elegans*), Galliformes (*Ortalis canicollis*), Anhimidae (*Chauna torquata*) and Anatidae (*Anas platalea*). All analyses used PAUP* 4.0b10 (ref. 28) and branches were collapsed if minimum length was 0. Character scoring of *Vegavis* in all data sets is given in the Supplementary Information.

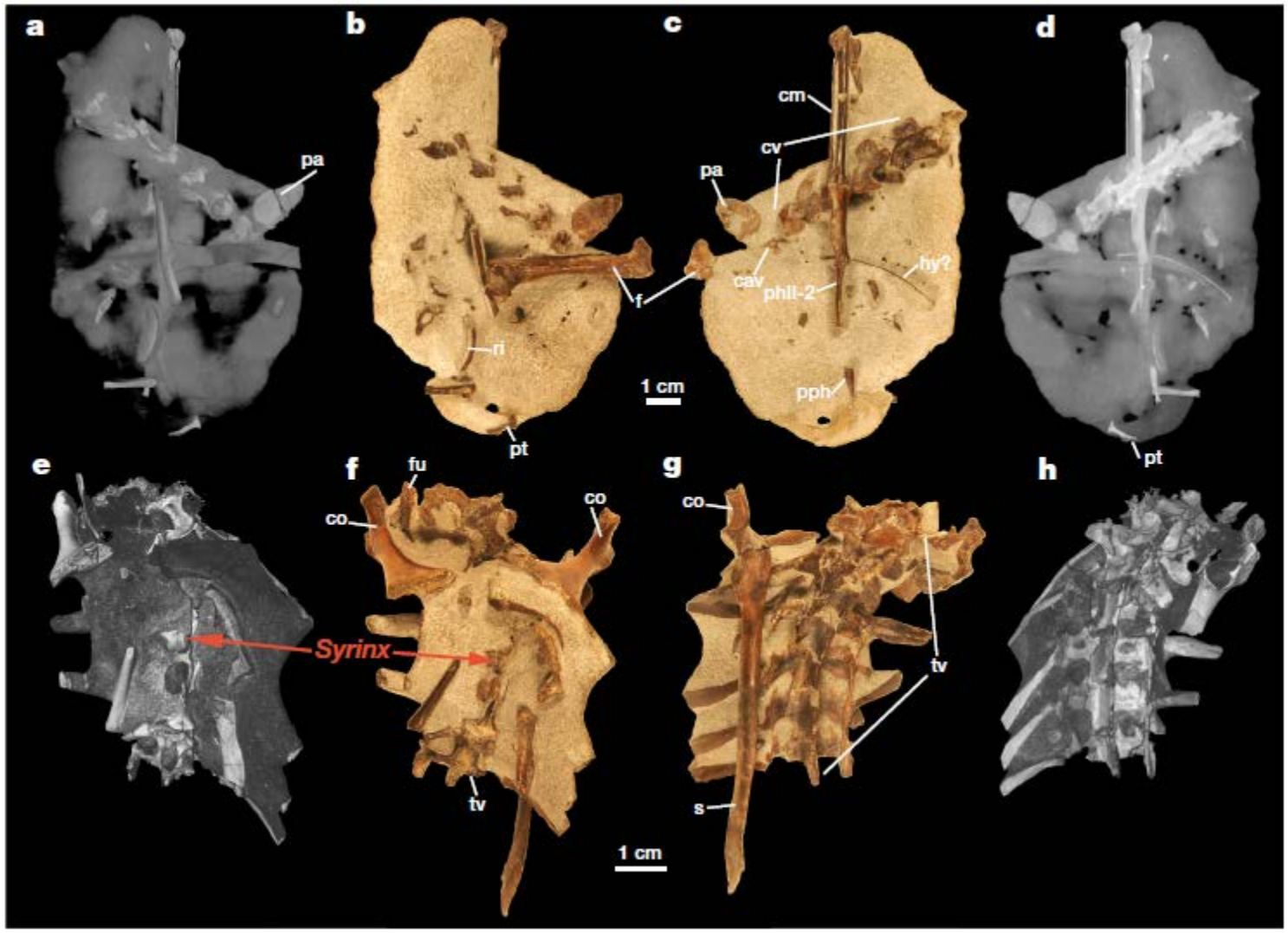

Clarke et al., 2016

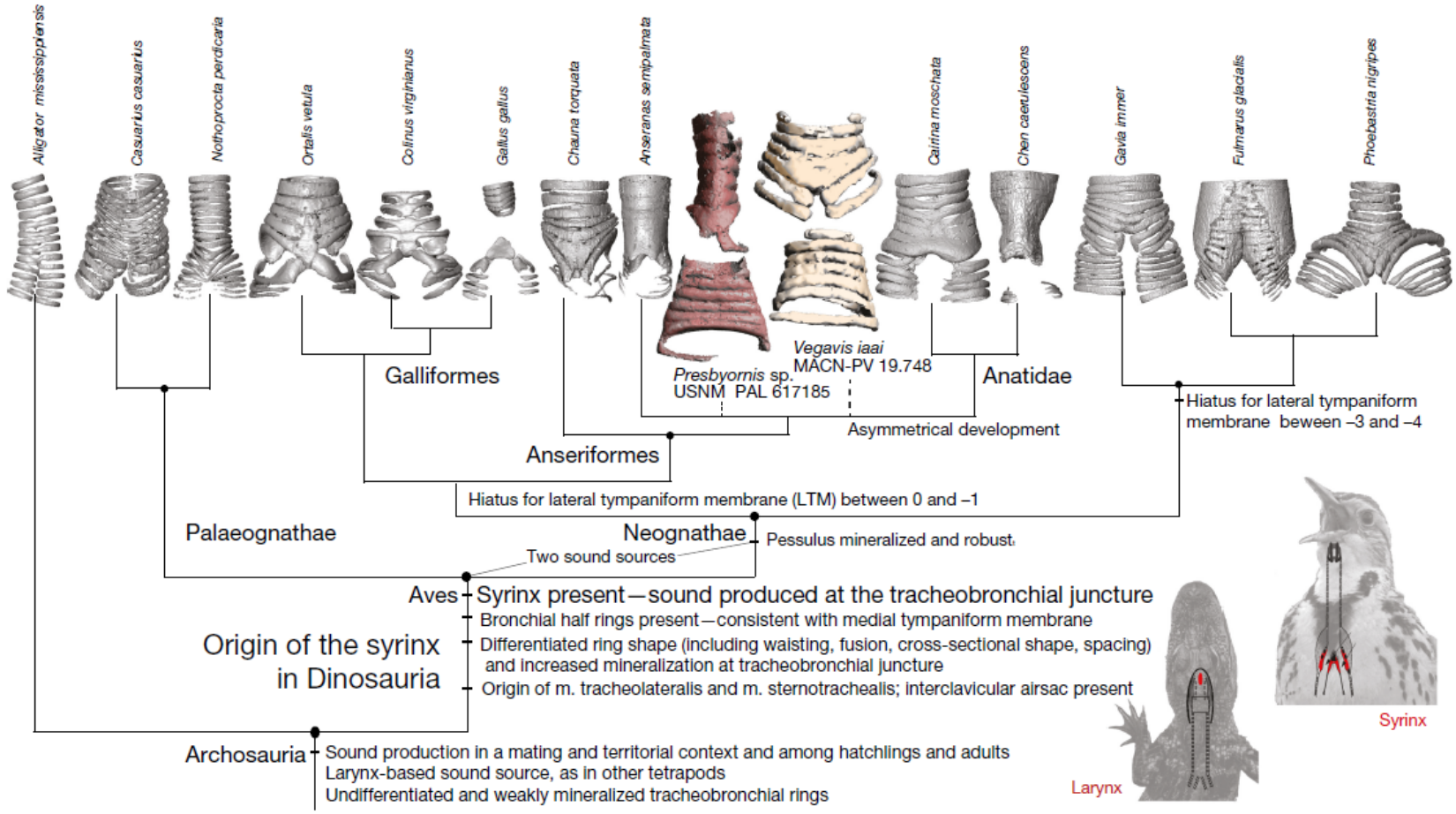

Figure 3 | Comparison of the Cretaceous *Vegavis* and Eocene *Presbyornis* syrinxes to extant avian exemplars showing the optimization of major traits present in the fossil and arising during the origin of living birds. The transition from the larynx-based sound source seen in outgroups to a syrinx, located at the tracheobronchial junction, (inset) occurred within Dinosauria, before or at the origin of Aves; unlike surveyed outgroup taxa, all extant birds (Aves) have some bronchial half-rings and a medial tympaniform membrane, the origin of which may represent a key first step in syrinx evolution. Many basally divergent Aves lack a pessulus, thought by some to be key to anchoring larger vocal membranes or labia[5]. A well mineralized pessulus, present in both fossils is here found to be ancestral to Neognathae with several subsequent losses of this trait (for example in Columbiformes and some Passeri). Although mineralized structures of the syrinx in *Vegavis* and many parts of extant Anatidae (for example, ducks) show asymmetry, *Presbyornis*, *Chauna* and Galliformes lack this asymmetry. Of the taxa surveyed here and in the literature, loons, penguins and other waterbirds show a caudad shift of the lateral tympaniform membrane (LTM) not seen in *Vegavis*. The origin of two sound sources is ambiguously optimized as ancestral to Aves or Neognathae. Syrinxes not to scale. Three-dimensional PDFs of the fossils and detailed data on extant exemplars are provided as Supplementary Figs 1 and 2, as well as in Extended Data Fig. 8. For detailed images of referenced features of the extant and fossil specimens see http://www.jsg.utexas.edu/syrinx-evolution/ and http://dx.doi.org/10.5061/dryad.50n8j.

Clarke et al., 2016

Stem-Galloanseres?: Pelagornithidae

Tradicionalmente considerados "Pelecaniformes", recientemente se han incluido como crown Galloanseres (Bourdon, 2005) o stem Galloanseres (Mayr, 2011).

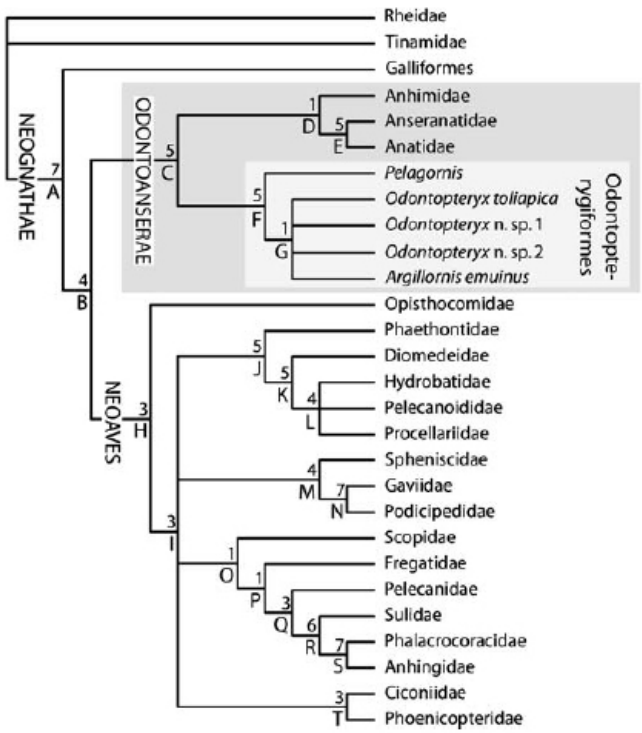

Fig. 2 Phylogenetic position of the Odontopterygiformes within Neognathae in the single most parsimonious tree. Length (L), 212; consistency index (CI), 0.7; retention index (RI), 0.85. The parsimony analysis was performed using PAUP 4b10 [63], with the branch-and-bound search option. Node support (*numbers* above branches) was assessed using Bremer-support indices [8], calculated with AutoDecay 5.0 [23]. Constrained tree with a sister group relationship of Galliformes and Odontoanserae: L, 219; CI, 0.68; RI, 0.83. Constrained tree with a sister group relationship of Odontopterygiformes and Galloanserae: L, 231; CI, 0.64; RI, 0.8

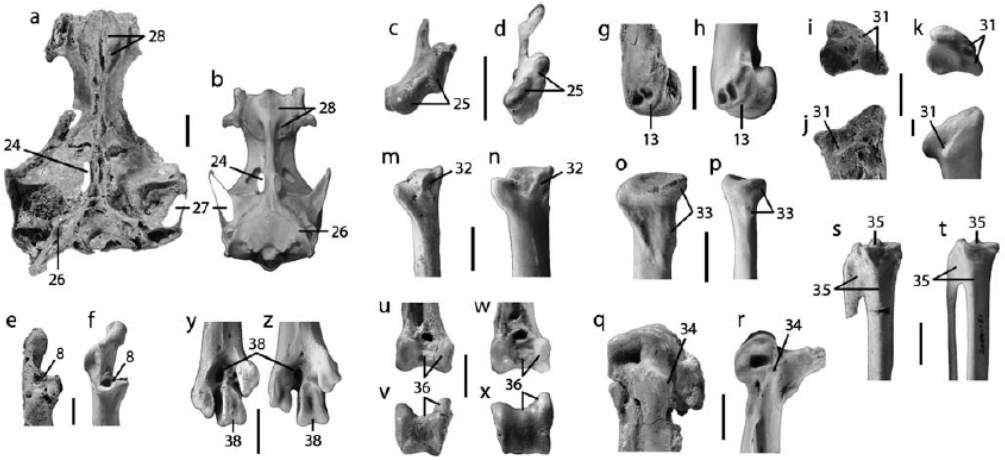

Fig. 3 Crania in ventral view: **a** *Odontopteryx* n. sp. 1 (OCP); **b** *Anser anser* (MNHN-LAC 1933-94). Right ossa quadrati in ventral view: **c** *O. toliapica* (BMNH 44096); **d** *Anseranas semipalmata* (MNHN-LAC 2004-151). Omal ends of left ossa coracoidei in dorsal view: **e** *Odontopteryx* n. sp. 1; **f** *Anser cygnoides* (MNHN-LAC 1985-23). Distal ends of right humeri in dorsal view: **g** *Odontopteryx* n. sp. 1; **h** *A. cygnoides*. *O. toliapica* (BMNH A224), proximal end of left ulna: **i** proximal view; **j** caudodorsal view. *A. semipalmata*, proximal end of left ulna: **k** proximal view; **l** caudodorsal view. Distal ends of right ulnae in cranial view: **m** *Odontopteryx* n. sp. 1; **n** *A. cygnoides*. Proximal ends of left radii in caudal view: **o** *Odontopteryx* n. sp. 2 (OCP); **p** *A. cygnoides*. Proximal ends of left carpometacarpi in ventral view: **q** *Odontopteryx* n. sp. 1; **r** *Chloephaga* sp. (MNHN-LAC 1884-848). Distal parts of right carpometacarpi in ventral view: **s** *Odontopteryx* n. sp. 1; **t** *A. semipalmata*. *Odontopteryx* n. sp. 1, distal end of right tibiotarsus: **u** cranial view; **v** distal view. *Chloephaga* sp., distal end of right tibiotarsus: **w** cranial view; **x** distal view. Distal ends of left tarsometatarsi in plantar view: **y** *Odontopteryx* n. sp. 1; **z** *A. cygnoides*. *Numbers* refer to the apomorphy list for the Odontoanserae. Scale bars equal 10 mm

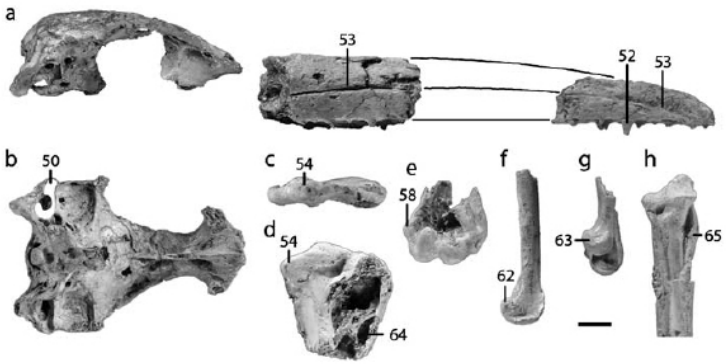

Fig. 1 *Odontopteryx* n. sp. 1 (collections of the OCP and the Rhinopolis Association). **a** Cranium and reconstructed maxilla in lateral view. **b** Cranium in ventral view. **c** Proximal end of left humerus in proximal view **d** Proximal end of left humerus in caudal view **e** Distal end of right humerus in cranial view. **f** Distal part of right tibia in medial view. **g** Distal end of left tarsometatarsus in medial view. **h** Proximal part of right ulna in cranial view. Apomorphies of the Odontopterygiformes include: *52* pseudo-teeth; *53* deep groove on maxilla; *50* cotylae quadratica rostrally continuous; *54* caput humeri with distinct dorsal prominence on facies cranialis and tuberculum dorsale continuing far distally as a smooth convexity; *58* prominent epicondylus dorsalis on humerus; *62* condylus medialis of tibiotarsus strongly protruding cranially; *63* tarsometatarsus, trochlea metatarsi II extending far less distally than trochlea metatarsi IV and showing smooth semicircular external part continuous with proximally pointed process. Apomorphies of the clade that comprises *Odontopteryx* and *A. emuinus* include: *64* elongated foramen pneumaticum on humerus; *65* elongated tuberculum ligamenti collateralis ventralis on ulna. *Numbers* refer to the character list of the "Electronic supplementary material". Scale bars equal 10 mm

Bourdon 2005; Naturwissenschaften

Pelagornis sandersi

Unidad: Formación Chandler Bridge (Oligoceno superior).

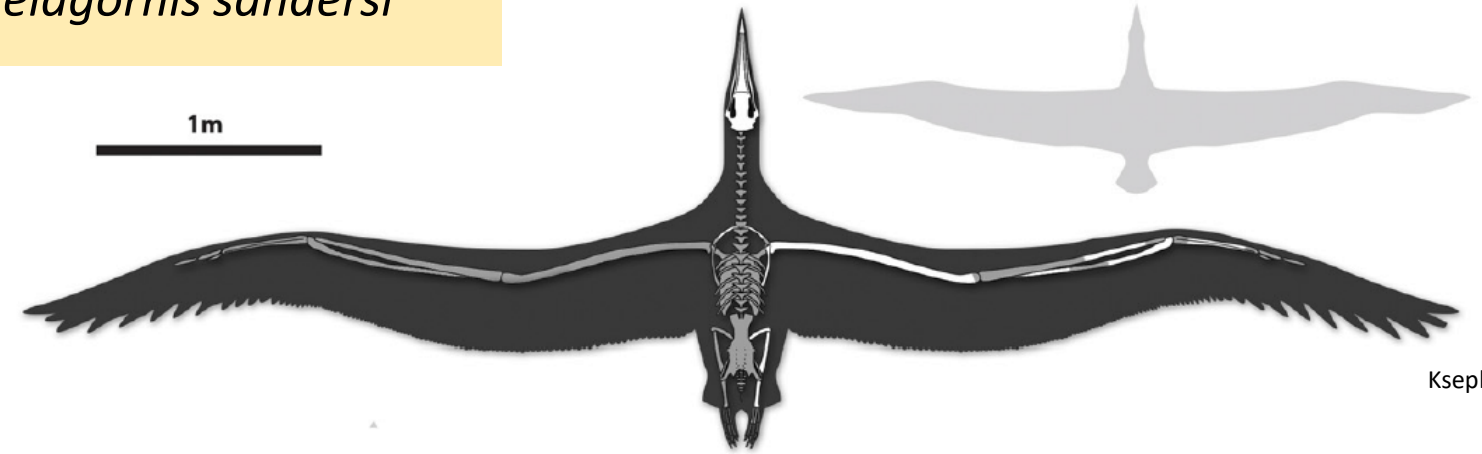

Ksepka, 2014; PNAS

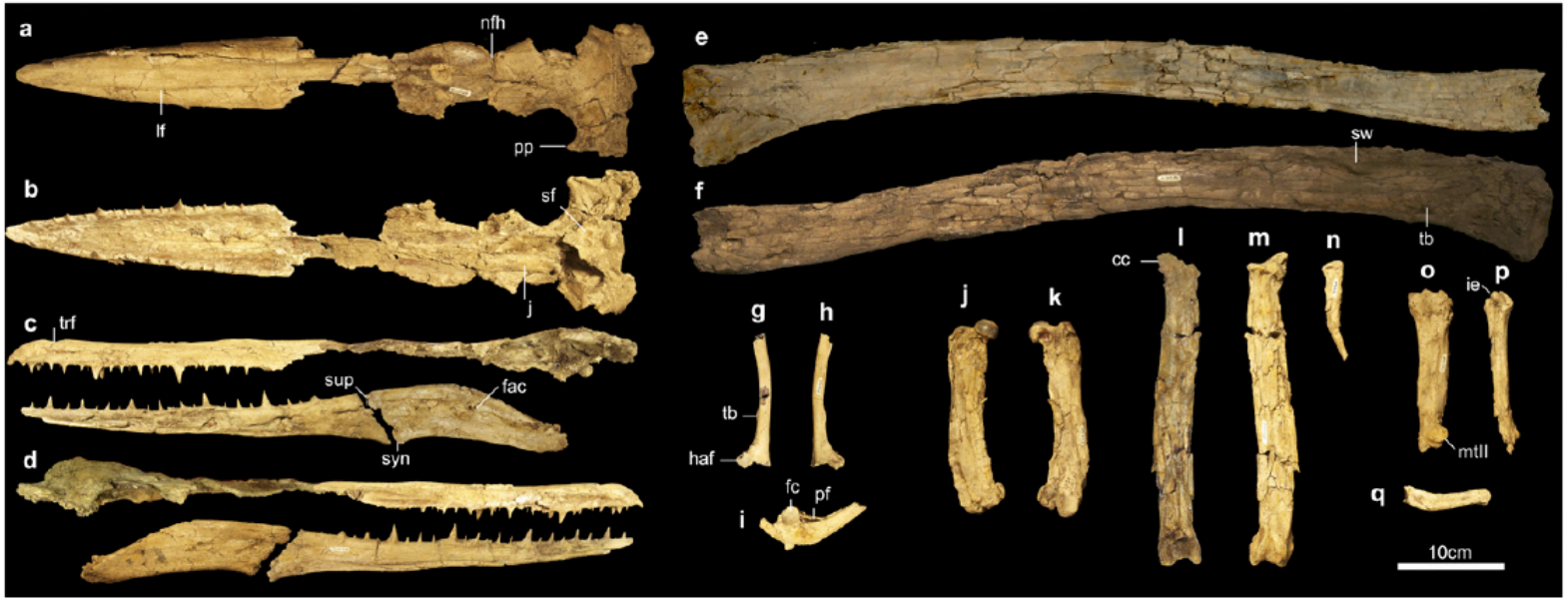

Fig. 1. (*Upper*) Reconstruction of *P. sandersi* (elements preserved in the holotype are shown in white) with *D. exulans* (Royal Albatross; 3-m average wingspan) for scale. (*Lower*) *P. sandersi* holotype (ChM PV4768) skull in (a) dorsal, (b) ventral, (c) left lateral (mandible in medial view), and (d) right lateral views (mandible in lateral view). Right humerus in (e) caudal and (f) cranial views. Scapula in (g) lateral and (h) medial views. (i) Partial furcula femur in (j) cranial and (k) caudal views. Tibiotarsus in (l) cranial and (m) caudal views. Fibula in (n) lateral view. Tarsometatarsus in (o) dorsal view (distal portion exposed in the medial view because of deformation) and (p) rotated to show the distal portion in dorsal view. (q) Pedal phalanx. cc, Lateral cnemial crest; fac, fossa aditus canalis neurovascularis; fc, facet; haf, humeral articular facet; ie, intercotylar eminence; j, jugal; lf, lateral furrow; mtII, metatarsal trochlea II; nfh, nasofrontal hinge; pf, pneumatic foramen; pp, paroccipital process; sf, subcondylar fossa; sup, supra-angulare; sw, swelling on crista deltopectoralis; syn, synovial joint; tb, tubercle; trf, transverse furrow.

Pelagornithidae carecen de cresta ventral en el palatino (presente en Neoaves). Además presentan un surco nasal prolongado, similar al de Pelecaniformes, pero no es homólogo (**ver más adelante**)

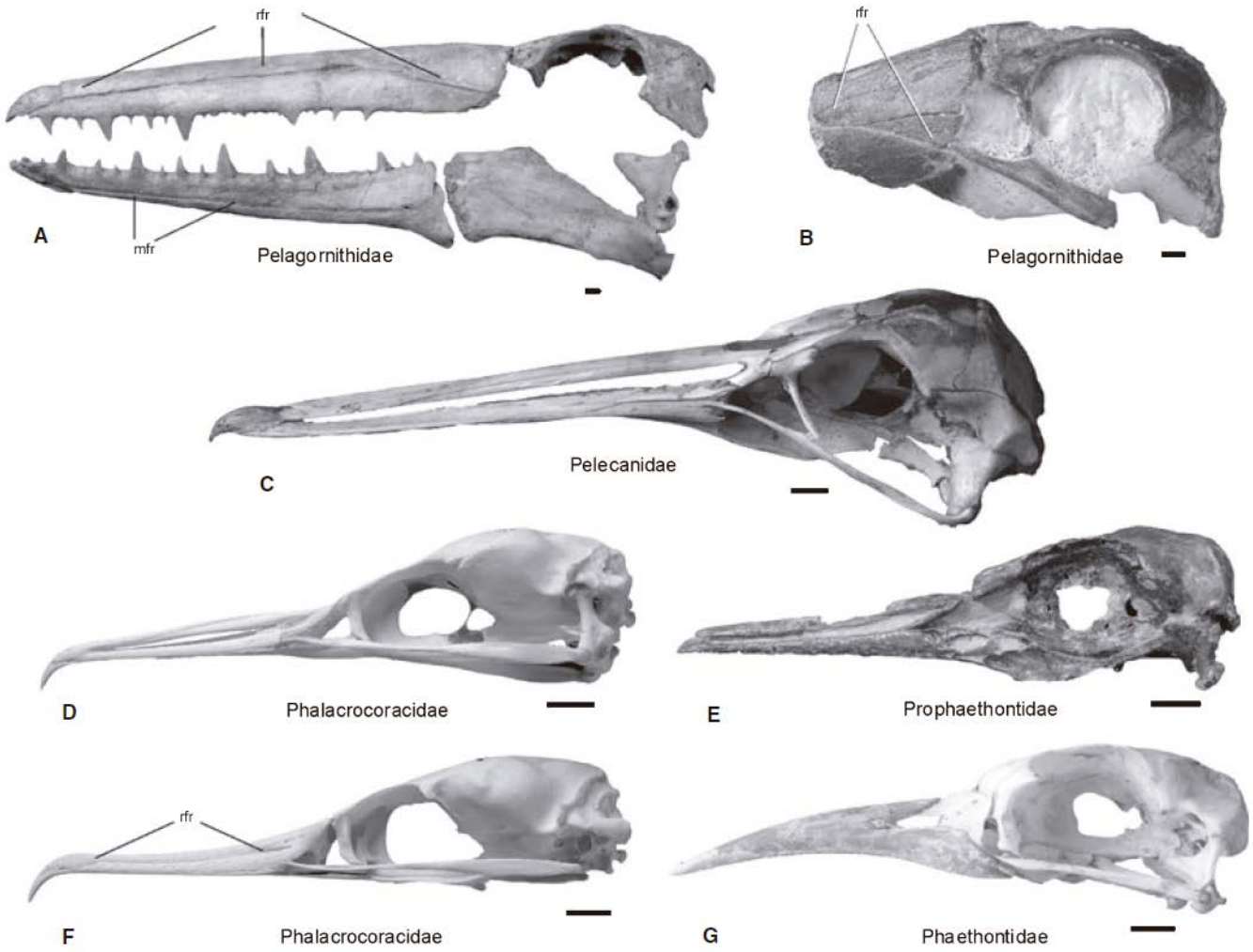

Fig. 5 Skulls in comparison. —A. *Pelagornis chilensis* from the Miocene of Chile (Pelagornithidae; MNHN SGO.PV 1061). —B. *Dasornis emuinus* from the early Eocene London Clay in England (Pelagornithidae; SMNK-PAL 4017). —C. Juvenile *Pelecanus occidentalis* ('Pelecaniformes', Pelecanidae) with long nostrils. —D. Juvenile *Phalacrocorax carbo* ('Pelecaniformes', Phalacrocoracidae) with long nostrils. —E. *Prophaethon shrubsolei* from the early Eocene London Clay in England (Prophaethontidae; BMNH A 683) with long nostrils. —F. Adult *P. carbo*. —G. *Phaethon aethereus* ('Pelecaniformes', Phaethontidae). mfr, mandibular furrow; rfr, rostral furrow (nasolabial groove). The scale bars equal 10 mm.

Posición de Pelagornithidae en Neognathae

En un nuevo análisis cladístico, Mayr (2011) recuperó al grupo como hermano de Galloanseres, soportado por los siguientes rasgos:
(6) Skull, distinct nasofrontal hinge, i.e., caudal part of beak markedly set off by a furrow against rostral part of cranium. The character optimization implies a reversal into the primitive state in crown-group Galloanseres (see Discussion).
(102) Impressio musculi adductoris mandibulae externus, pars coronoidea in medial position.

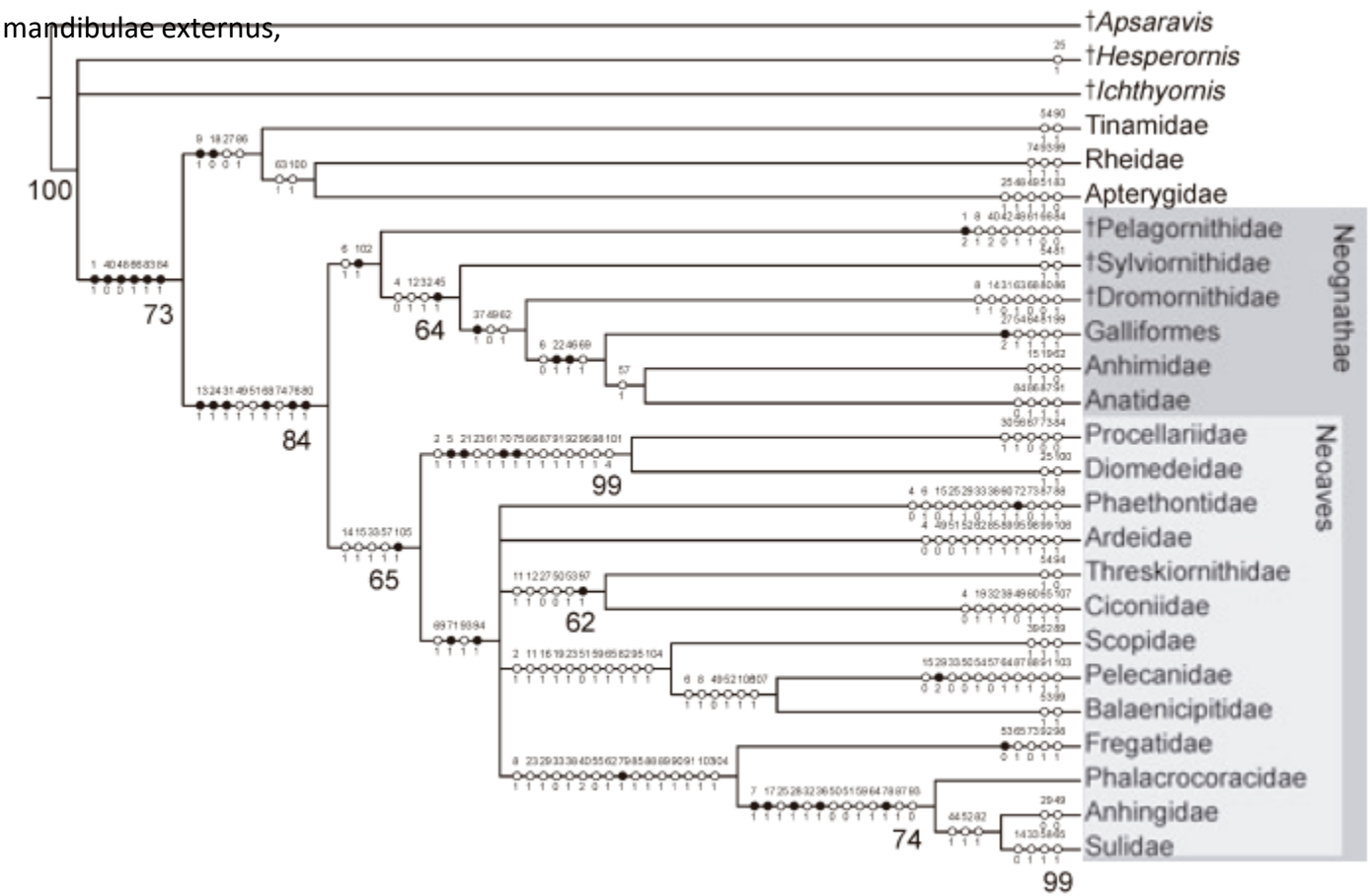

matrix. Apomorphies and character states are listed on the internodes (numbers refer to the character list in Appendix 1); filled circles represent strict apomorphies, open circles homoplastic ones. Bootstrap support values are indicated below the internodes. Extinct taxa are marked with a dagger.

Mayr 2011; Zoologica Scripta

Pelagornis chilensis

Unidad: Formación Bahía Inglesa
(Mioceno medio – Plioceno superior).

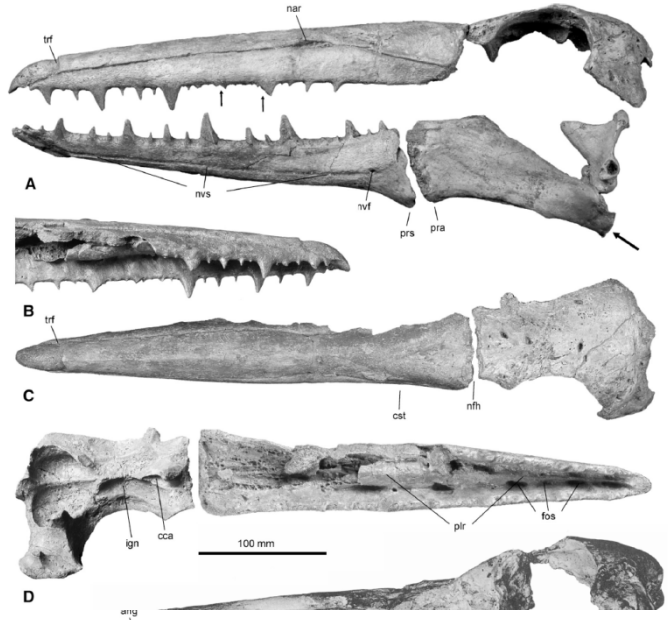

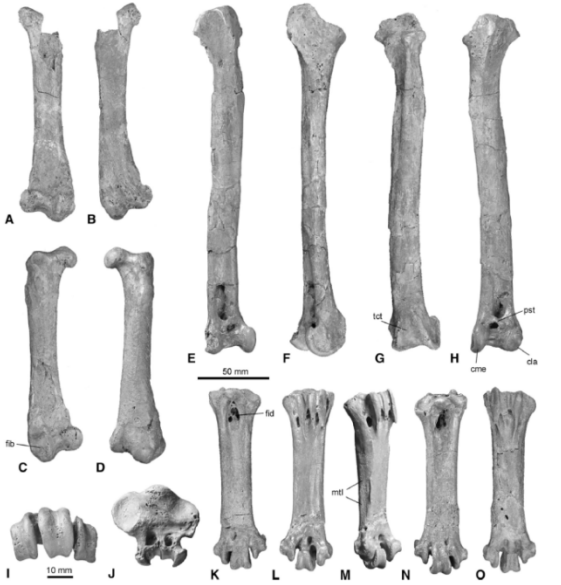

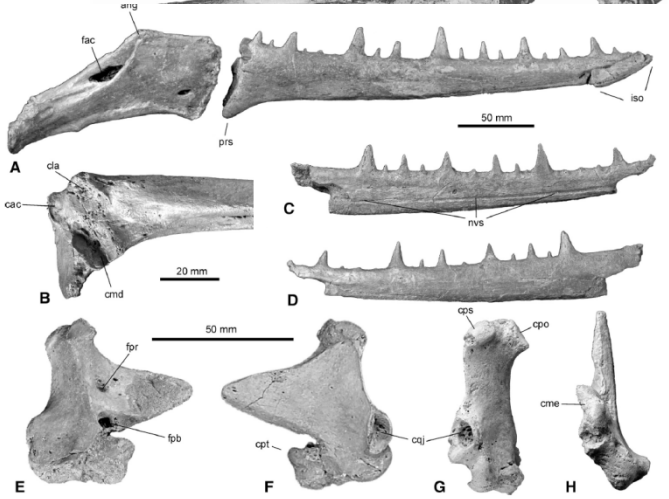

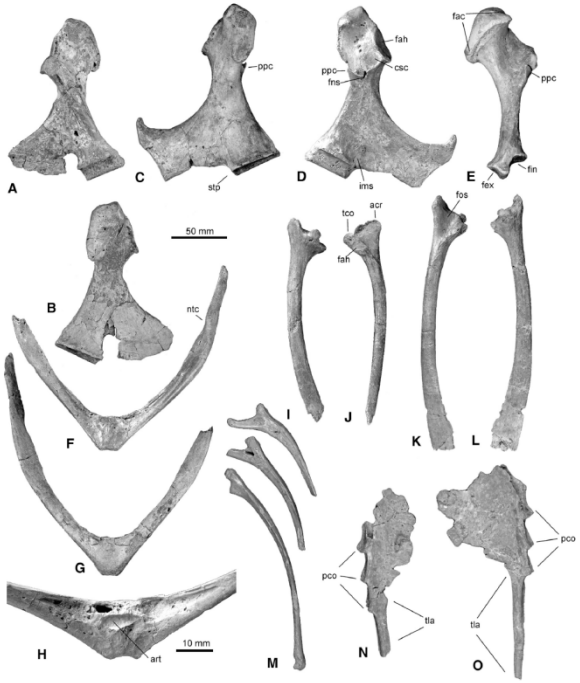

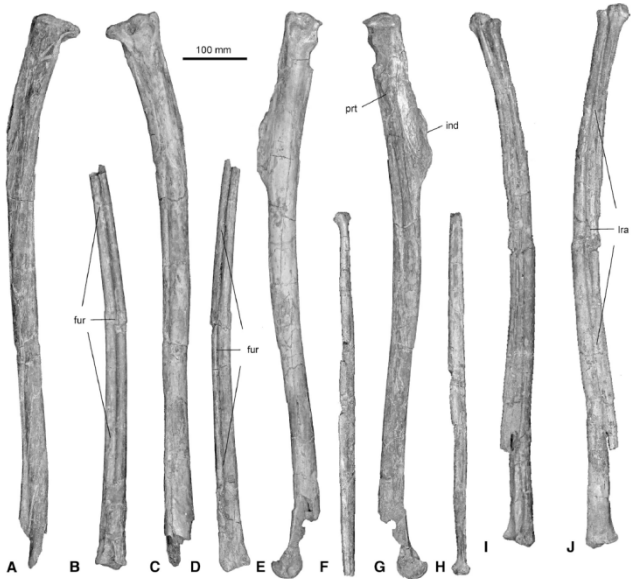

Mayr & Rubilar-Rogers, 2010; JVP

Pelagornis chilensis

Unidad: Formación Bahía Inglesa
(Mioceno medio – Plioceno superior).

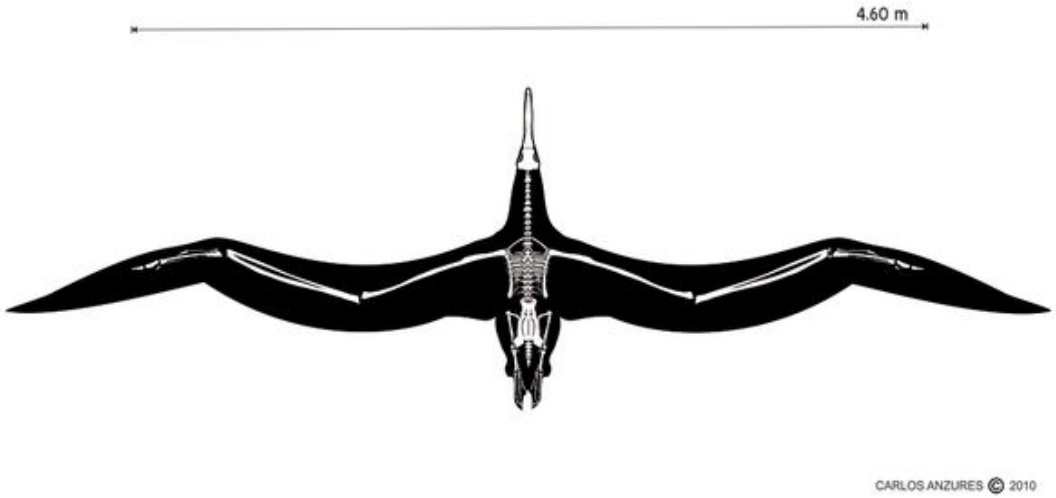

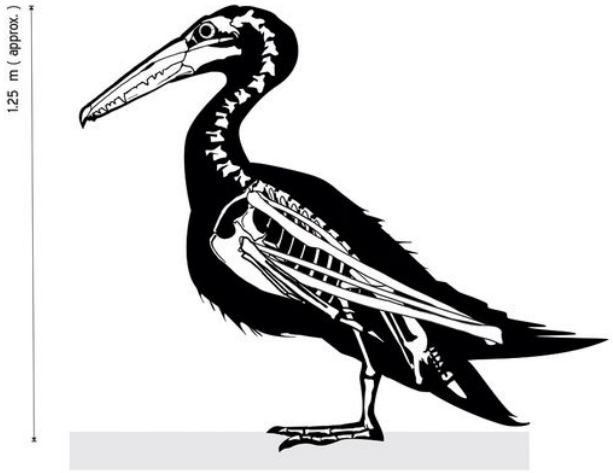

Stem-Galloanseres: Dromornithidae

Rango temporal: Registro fósil Cenozoico de Australia.

- Aves graviportales, no voladoras y de hábitos probablemente herbívoros.
- Presencia de facetas articular del prceso basipterigoides bien desarrolladas (Galloanseres).
- Presencia de marcada cresta vetral del palatino.
- Ausencia de hallux.
- Dígito 4 con 4 falanges.
- Ausencia de procesos uncinados.

Anseriformes: Gastornithidae

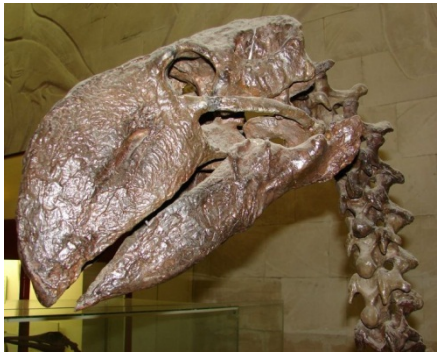

Rango temporal: Registro fósil Paleoceno-Eoceno de Europa.

- Aves graviportales y no voladoras.
- Presencia de pico enorme lateralmente comprimido, con culmen convexo y sin punta curvada.
- Presencia de fenestra temporal superior.
- Alas muy reducidas.
- Esternón sin quilla.
- Escapulocoracoides.

- Carece de procesos uncinados.
- Paladar neognato.
- Foramen ilioisquiádico cerrado.
- Hallux corto.

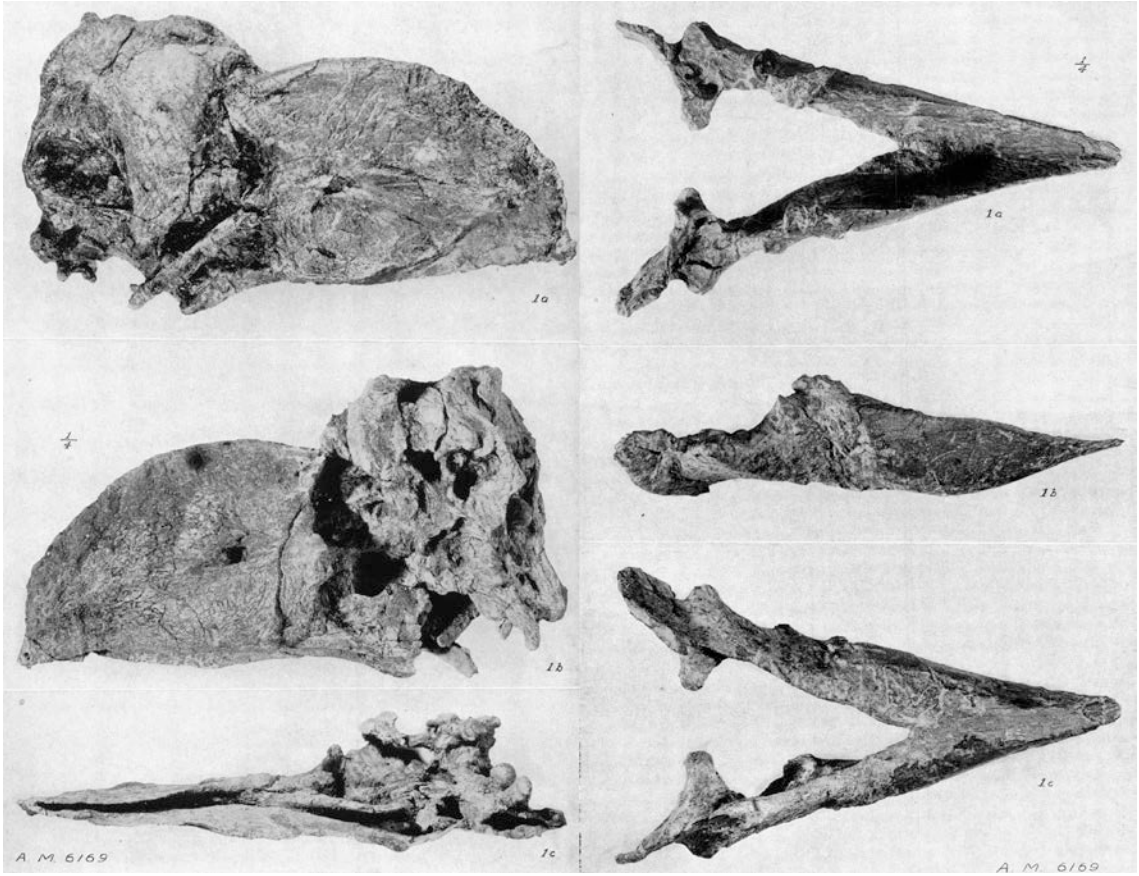

Isotopic and anatomical evidence of an herbivorous diet in the Early Tertiary giant bird *Gastornis*. Implications for the structure of Paleocene terrestrial ecosystems

D. Angst · C. Lécuyer · R. Amiot · E. Buffetaut · F. Fourel · F. Martineau · S. Legendre · A. Abourachid · A. Herrel

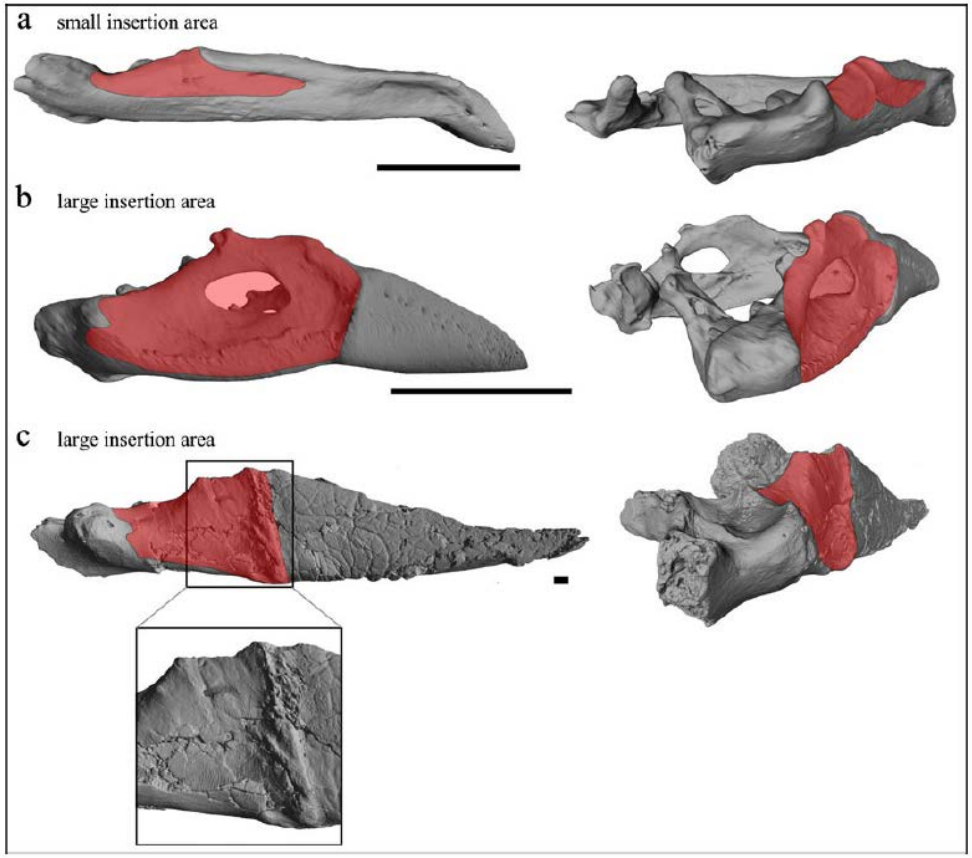

Fig. 4 Comparisons between the insertion area of the musculus adductor mandibulae externus superficialis (MAMES) (*red area*) on the mandible of modern birds and *Gastornis* in lateral view (*left part*) and in oblique posterior view. **a** Carnivorous modern bird (*Buteo platypterus*), **b** seed-crushing passeriform (*Geospiza magnirostris*), and **c** *Gastornis* mandible and photo of the insertion area. *Scale bar* 1 cm

Table 4 Results of the Kruskal–Wallis statistical test performed for calculated $\delta^{13}C$ of diets between either a hypothetical carnivorous *Gastornis* or a hypothetical herbivorous *Gastornis* and the associated contemporaneous herbivorous mammals for each studied site

Mont-de-Berru		
P-value=7.704×10^{-5}	*Gastornis* carnivorous	*Gastornis* herbivorous
Gastornis herbivorous	1.075×10^{-4}	–
Mammals herbivorous	6.334×10^{-5}	0.9176
Cernay-les-Reims		
P-value=0.04298	*Gastornis* carnivorous	*Gastornis* herbivorous
Gastornis herbivorous	0.03887	–
Mammals herbivorous	0.01391	1
Saint-Papoul		
P-value=0.0001229	*Gastornis* carnivorous	*Gastornis* herbivorous
Gastornis herbivorous	3.097×10^{-5}	–
Mammals herbivorous	0.03389	0.8997
Monthelon		
P-value=NA	*Gastornis* carnivorous	*Gastornis* herbivorous
Gastornis herbivorous	–	–
Mammals herbivorous	–	0.6434

Angst et al., 2014; Naturwissenschaften

Neoaves

Definición Clado más inclusivo que contiene al gorrión *Passer domesticus* pero no al pollo *Gallus gallus.*

Rango: Origen en el Cretácico superior.

Soportado ampliamente por evidencia molecular y morfológica.

Sinapomorfías:

- Presencia de crista ventralis en el palatino, con pars lateralis bien desarrollada.
- Pérdida del phallus (pene).
- Cóndilo medialis del cuadrado con una rostralmente o lateralmente marcada superficie articular cóncava.

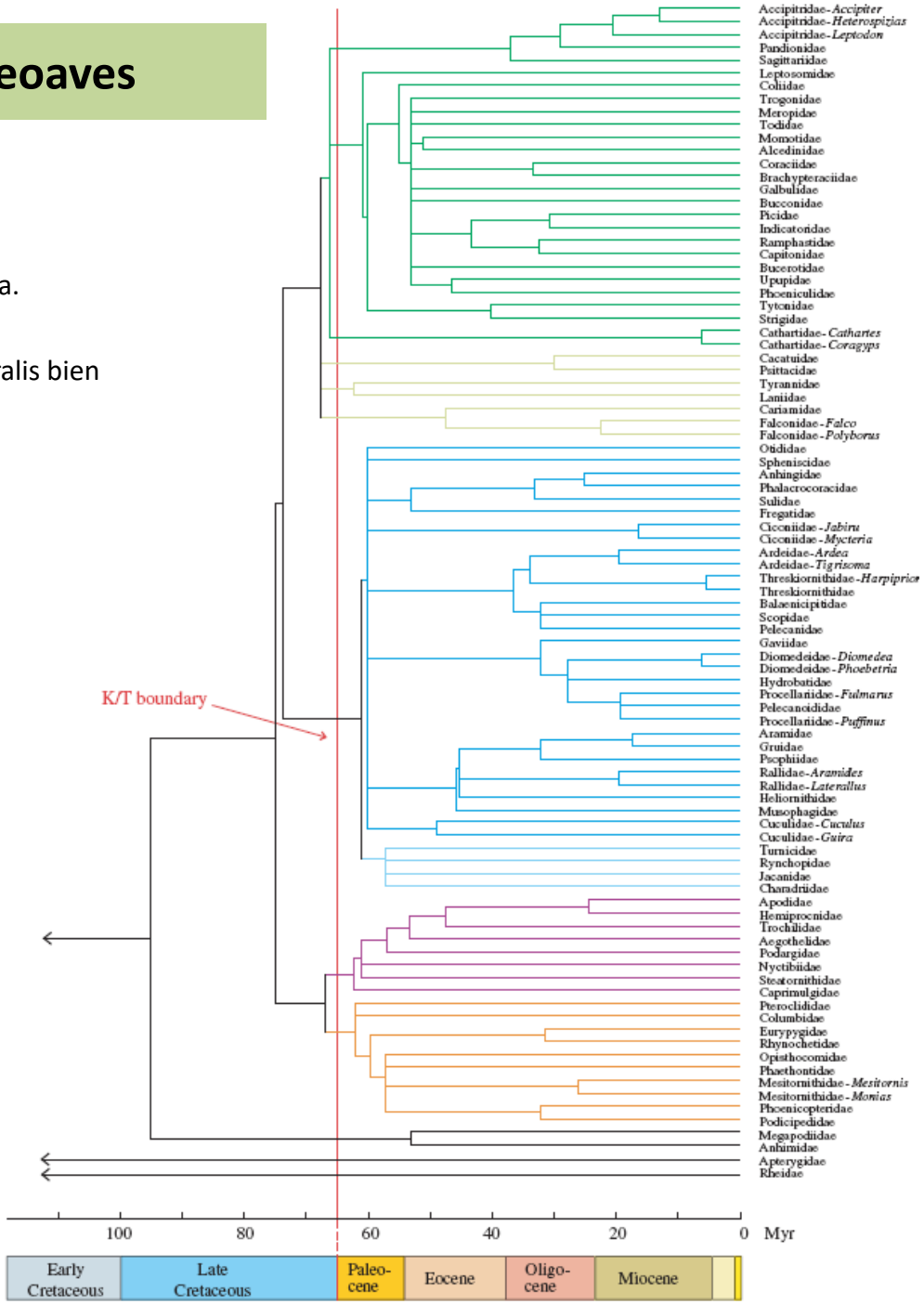

Neoaves Basales

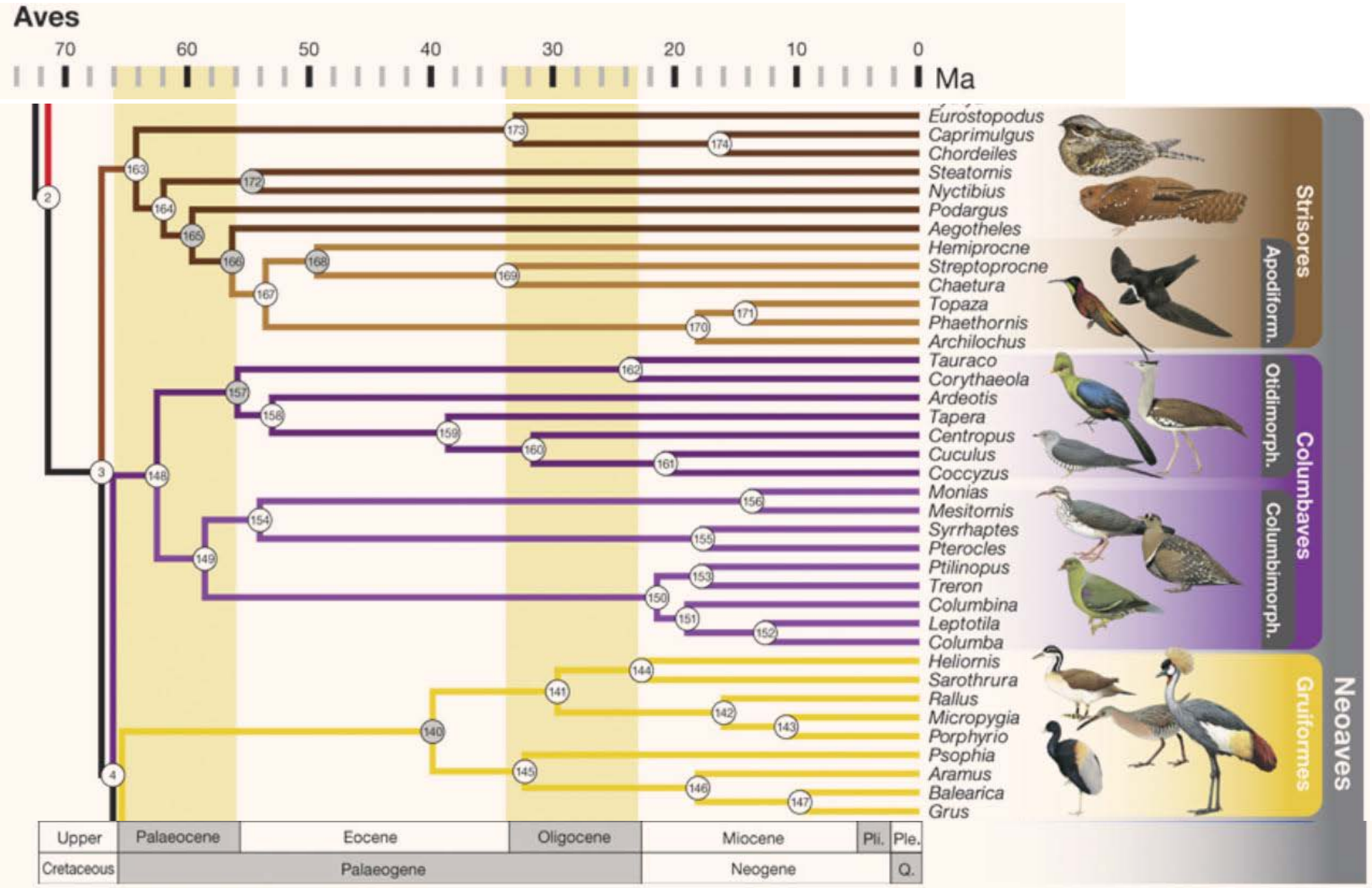

Strisores

Definición: Clado que incluye a “Caprimulgiformes” y Apoddiformes (Mayr, 2010). Está bien soportado por evidencia molecular independiente en varios trabajos recientes (Erickson et al., 2006; Mayr, 2008; Mayr, 2010; Hackett et al., 2008; Prum et al., 2015). Estos análisis revelaron que “Caprimulgiformes” es parafilético respecto a Apodiformes.

Sinapomorfías: Elongado crus longum del carpal ulnar (pisiforme).

Implicancias en historia evolutiva del grupo: ¿Reaparición de actividad diurna en Apodiformes o nocturnidad múltiple en “Caprimulgiformes”?.

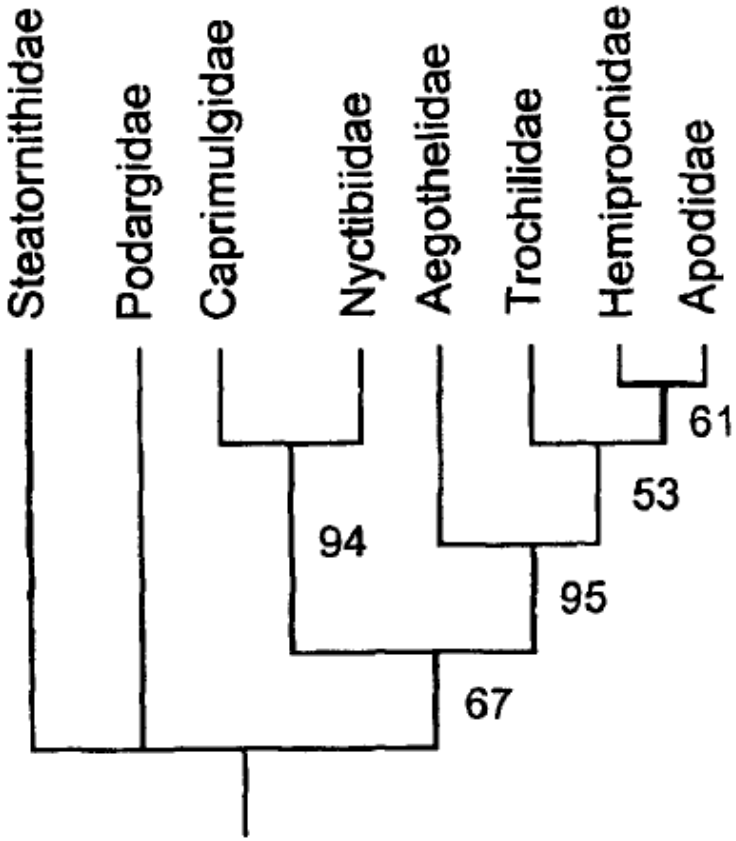

Escenarios Evolutivos de Nocturnidad en Strisores

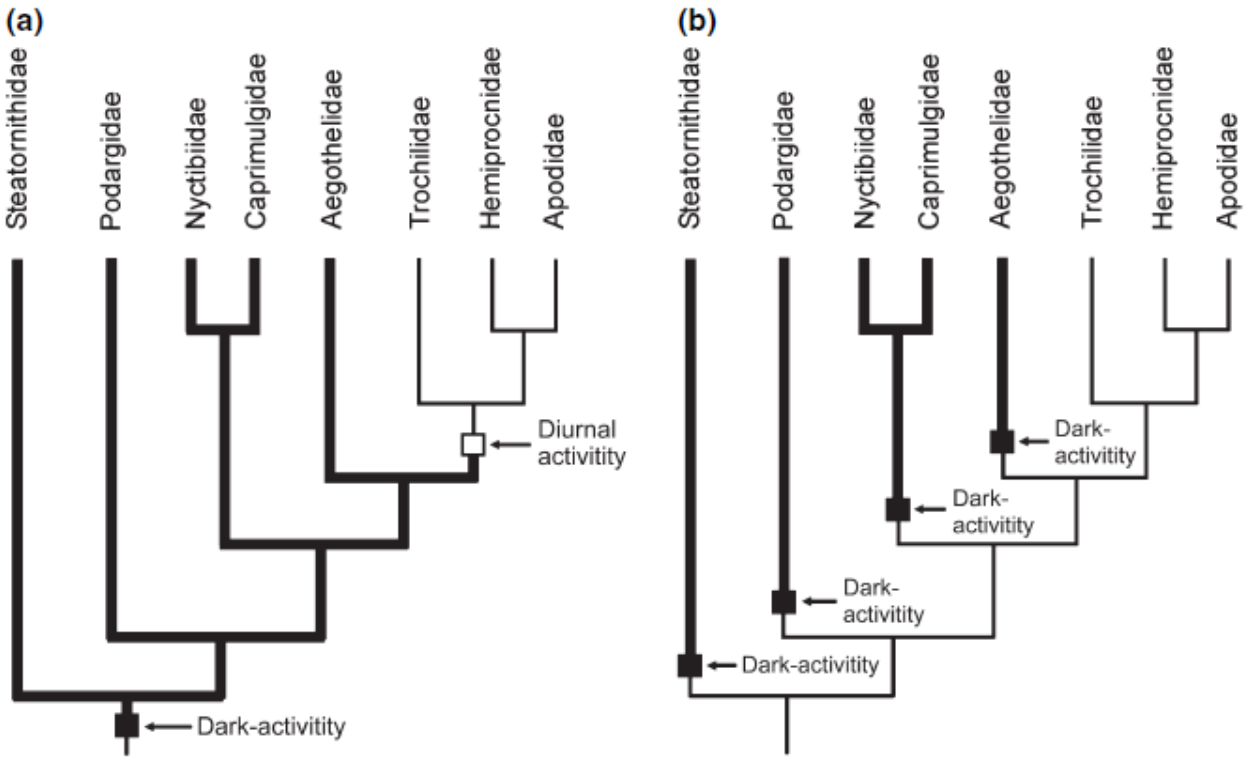

Fig. 9. Two hypotheses on the origin of dark-activity (thick lines) in Strisores. (a) Single origin in the stem lineage of the taxon and reversal into diurnal activity in the stem lineage of the Apodiformes. (b) Fourfold origin in the stem lineages of Steatornithidae, Podargidae, Caprimulgi and Aegothelidae

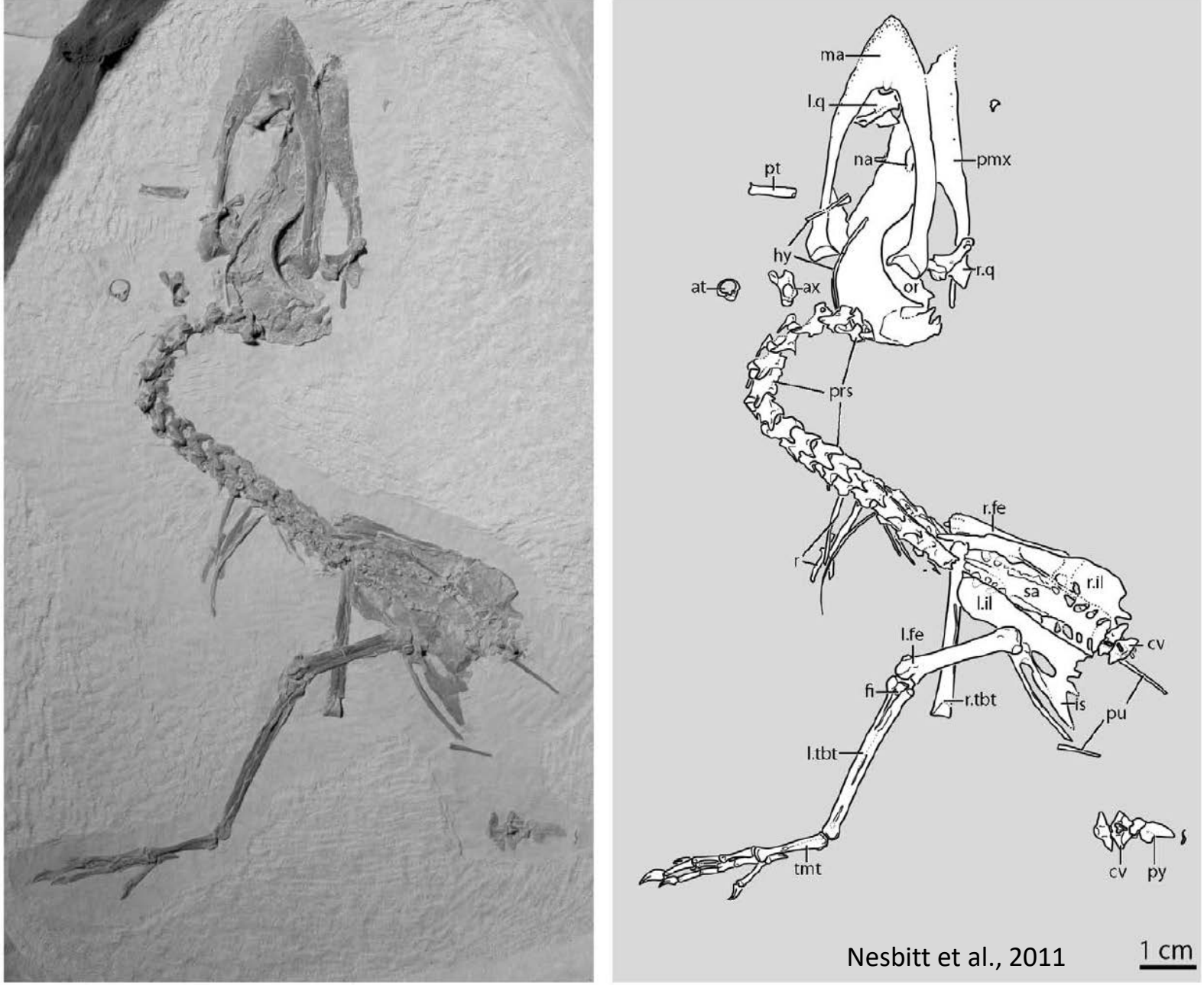

Figure 3. The main slab of the second specimen of *Fluvioviridavis platyrhamphus* (FMNH PA 607) from the Eocene Green River Formation. Abbreviations: at, atlas; ax, axis; cv, caudal vertebra; fe, femur; fi, fibula; hy, hyoid; il, ilium; is, ischium; l., left; ma, mandible; na, naris; or, orbit; pmx, premaxilla; prs, presacral vertebrae; pt, pterygoid; pu, pubis; py, pygostyle; q, quadrate; r., right; r, rib; sa, sacrum; tbt, tibiotarsus; tmt, tarsometatarsus.

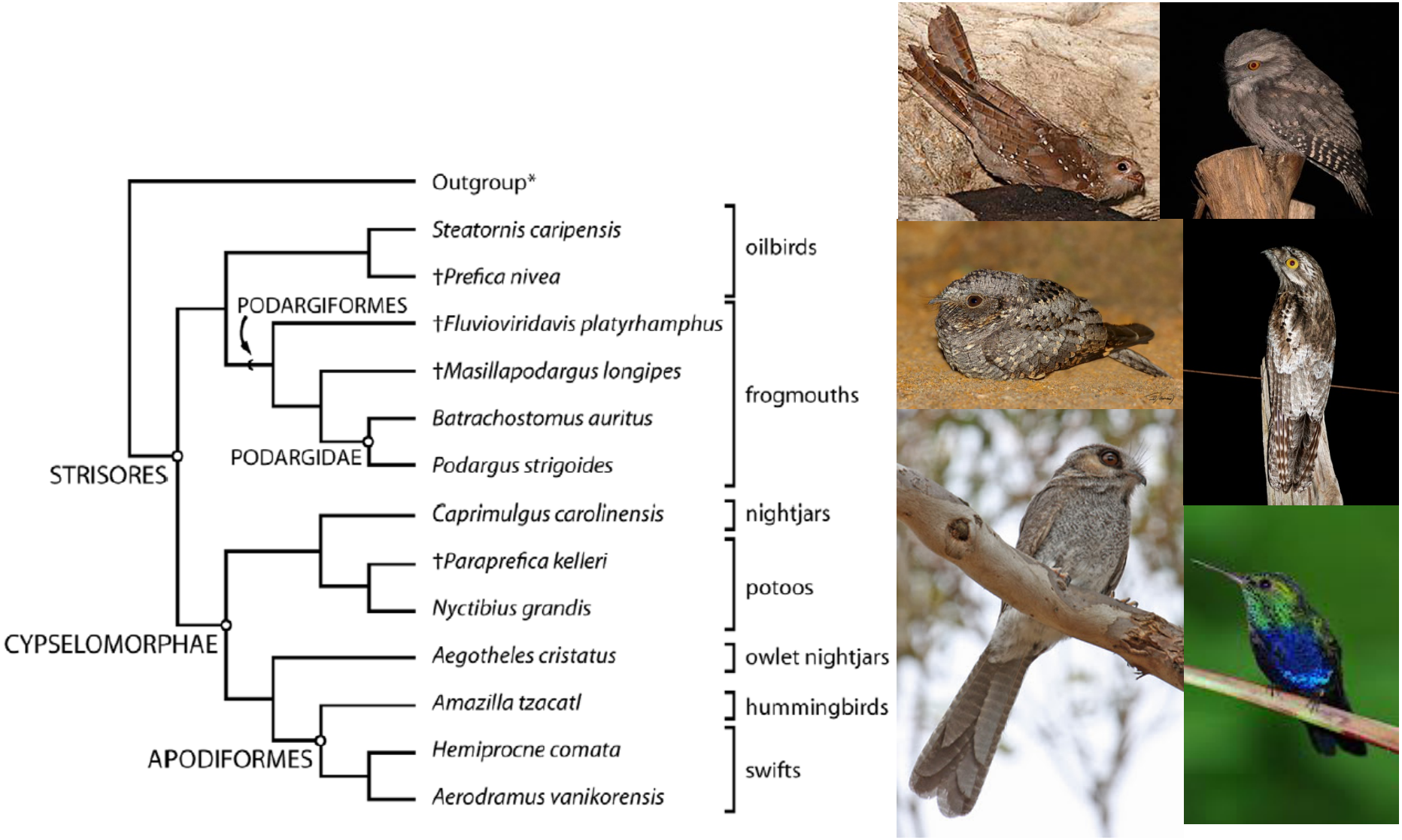

Figure 7. The relationship of *Fluvioviridavis platyrhamphus* to that of other Strisores using a combined dataset (TL = 2119, CI = 0.713, RI = 0.439) and a morphology-only dataset (TL = 175, CI = 0.600, RI = 0.700). See text for outgroup selection(s). Circles = nodes, chevrons = stem-groups.

Eocypselus rowei

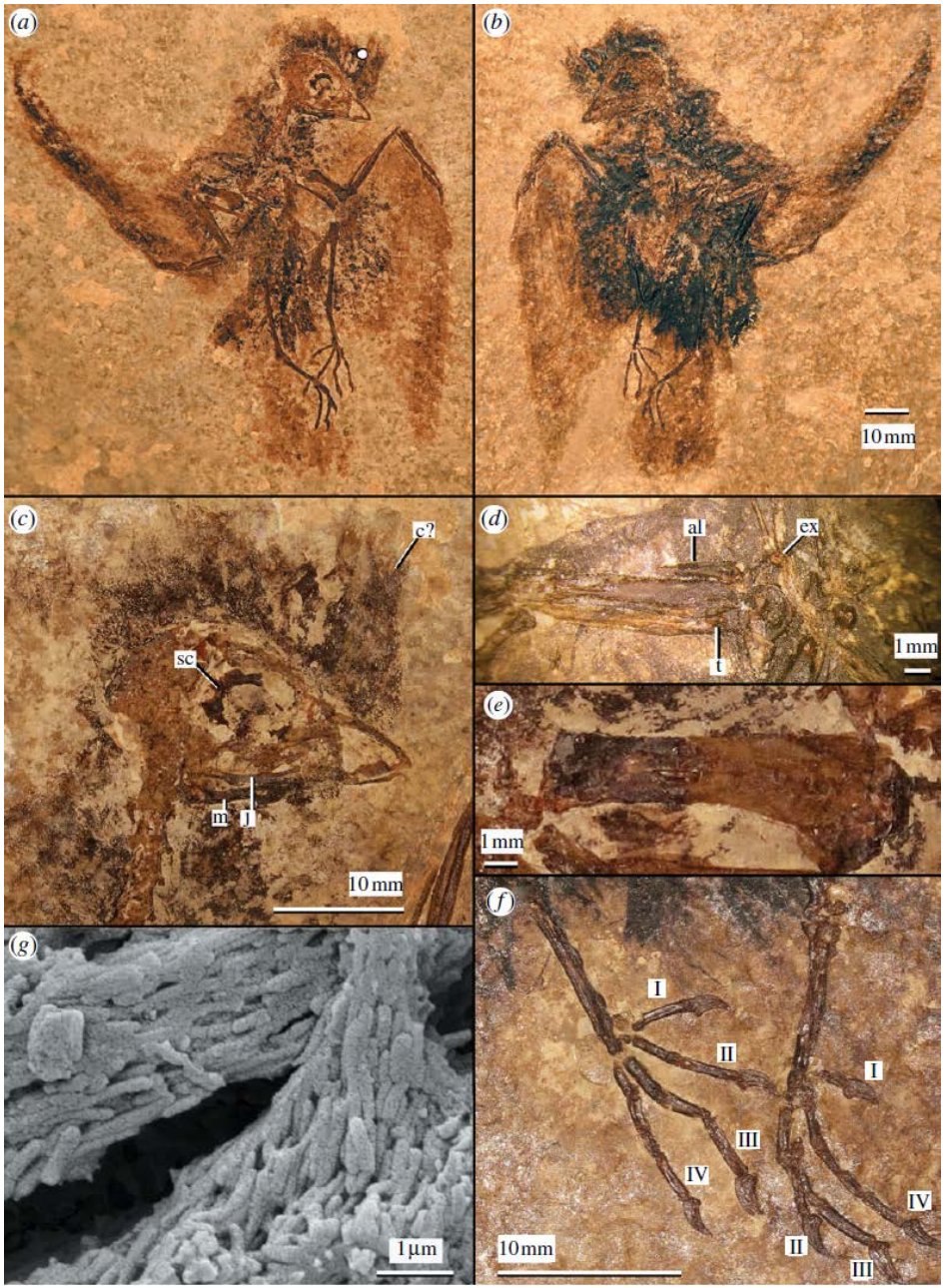

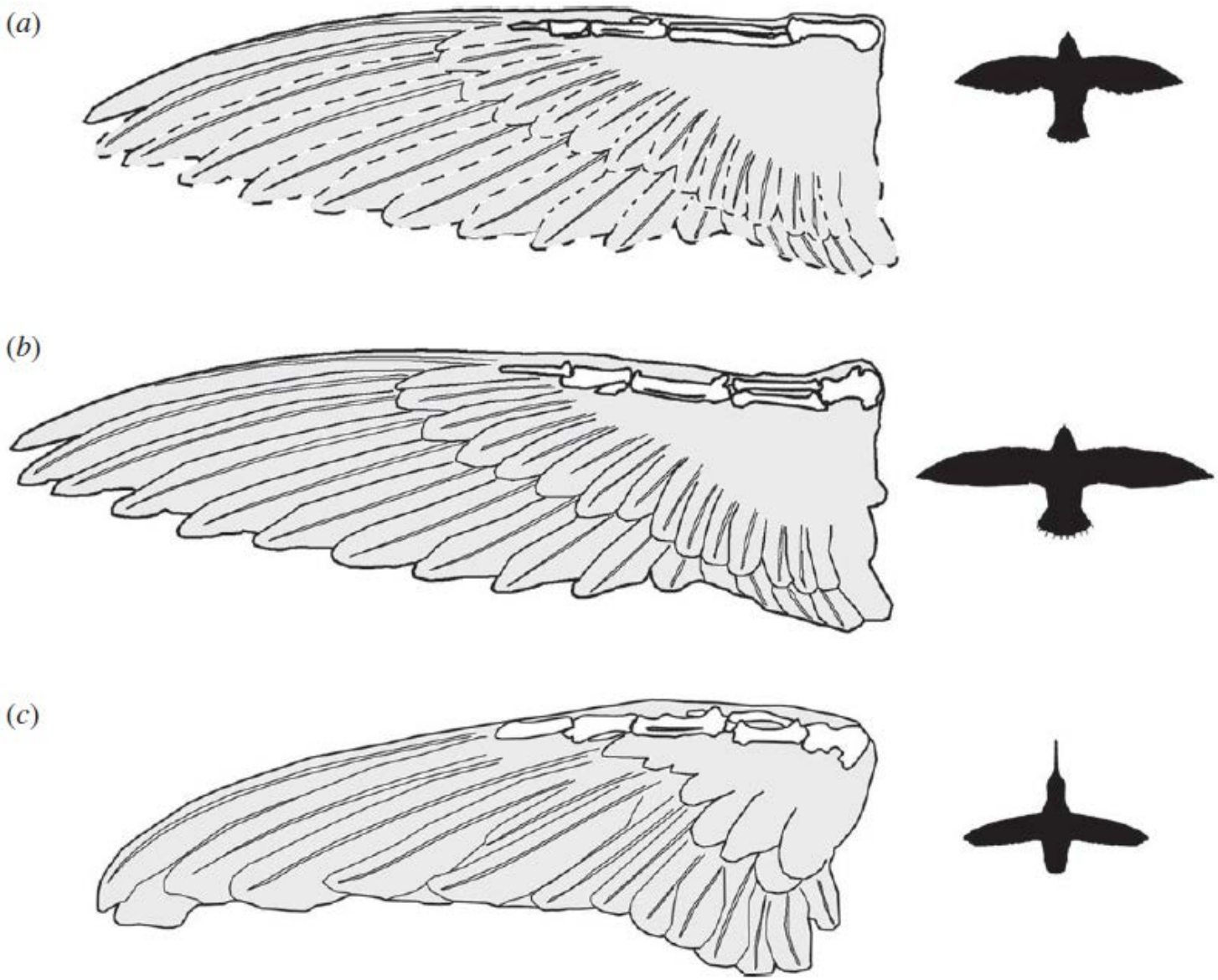

Figure 3. Comparison of wing structure in (*a*) *Eocypselus rowei* (WDC-CGR-109), (*b*) an extant swift (Apodidae: *Hirundapus caudacutus*: University of Washington Burke Museum, UWBM 47230) and (*c*) an extant hummingbird (Trochilidae: *Archilochus colubris*: UWBM 49825), with overall body outlines at right. Skeletal elements (right side) and spread wings (left side) from the same specimen were outlined and traced, with wings mirrored to create images for extant taxa. For the fossil taxon wing length was reconstructed from the leading primary, and dotted lines indicate the uncertain breadth of the wing. For comparison, wings were scaled to the same skeletal wing length and body outlines to the same head-to-tail length (excluding the long beak of the hummingbird).

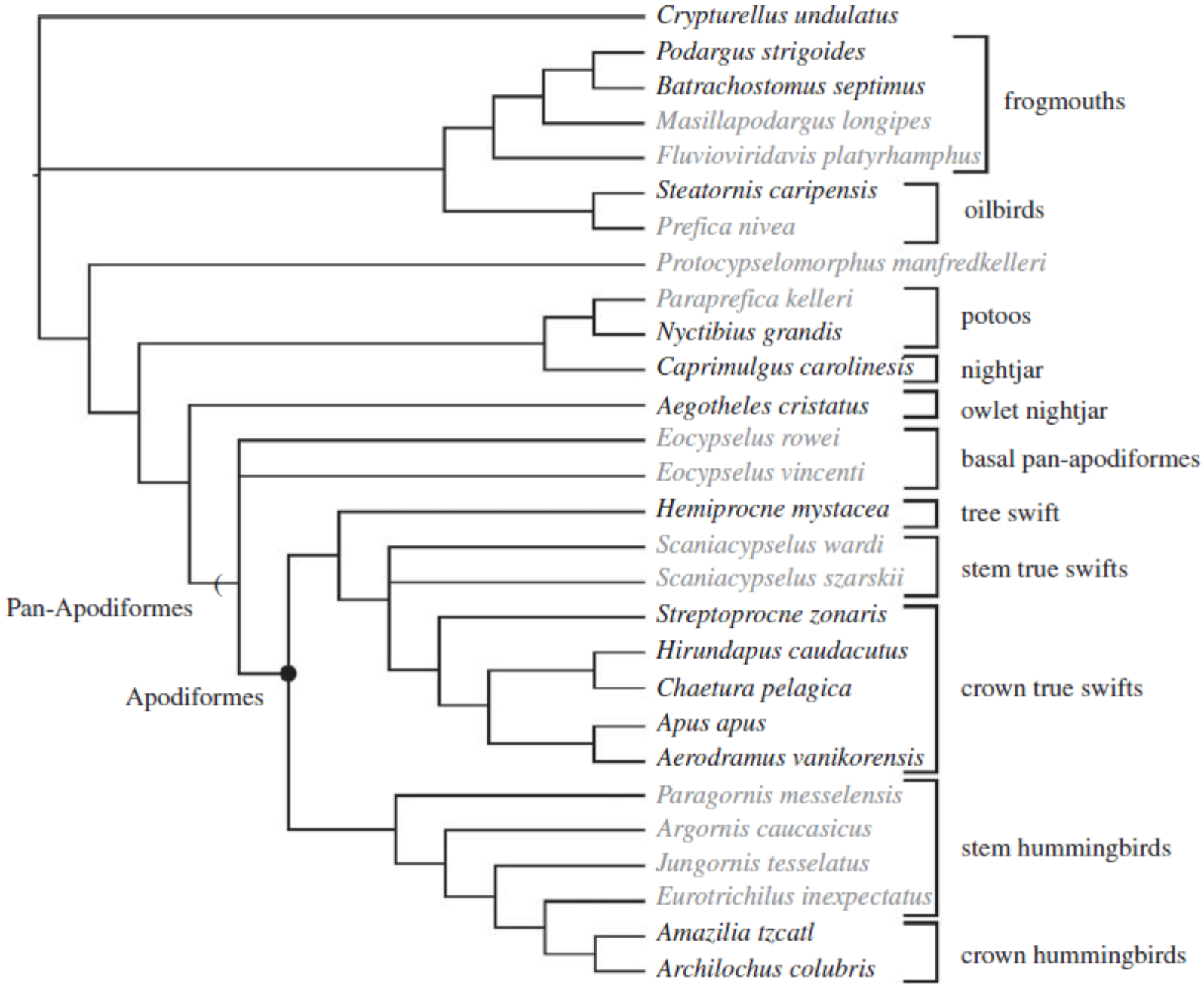
Crypturellus undulatus
Podargus strigoides
Batrachostomus septimus
Masillapodargus longipes
Fluvioviridavis platyrhamphus
frogmouths
Steatornis caripensis
Prefica nivea
oilbirds
Protocypselomorphus manfredkelleri
Paraprefica kelleri
Nyctibius grandis
potoos
Caprimulgus carolinesis
nightjar
Aegotheles cristatus
owlet nightjar
Eocypselus rowei
Eocypselus vincenti
basal pan-apodiformes
Hemiprocne mystacea
tree swift
Scaniacypselus wardi
Scaniacypselus szarskii
stem true swifts
Pan-Apodiformes
Streptoprocne zonaris
Hirundapus caudacutus
Chaetura pelagica
Apus apus
Aerodramus vanikorensis
crown true swifts
Apodiformes
Paragornis messelensis
Argornis caucasicus
Jungornis tesselatus
Eurotrichilus inexpectatus
stem hummingbirds
Amazilia tzcatl
Archilochus colubris
crown hummingbirds

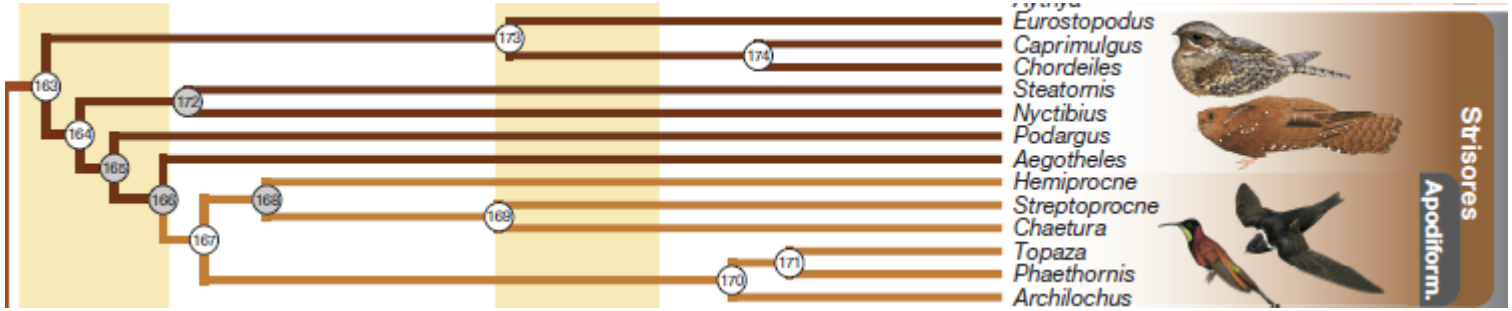

Taxonomía

Strisores Baird, 1858.
1 Steatornithiformes, new taxon
1.1 Steatornithidae Bonaparte, 1842
2 Podargocypseli, new taxon
2.1 Podargiformes Mathews, 1918
2.1.1 Podargidae Bonaparte, 1838
2.2 Cypselomorphae Huxley, 1867
2.2.1 Caprimulgi Ridgway, 1881
2.2.1.1 Caprimulgidae Vigors, 1825
2.2.1.2 Nyctibiidae Chenu and des Murs, 1851
2.2.2 Apodimorphae Sibley et al., 1988
2.2.2.1 Aegotheliformes Worthy et al., 2007
2.2.2.1.1 Aegothelidae Bonaparte, 1853
2.2.2.2 Apodiformes Peters, 1940
2.2.2.2.1 Apodi Peters, 1940
2.2.2.2.1.1 Apodidae Olphe-Galliard, 1887
2.2.2.2.1.2 Hemiprocnidae Oberholser, 1906
2.2.2.2.2 Trochilidae Vigors, 1825

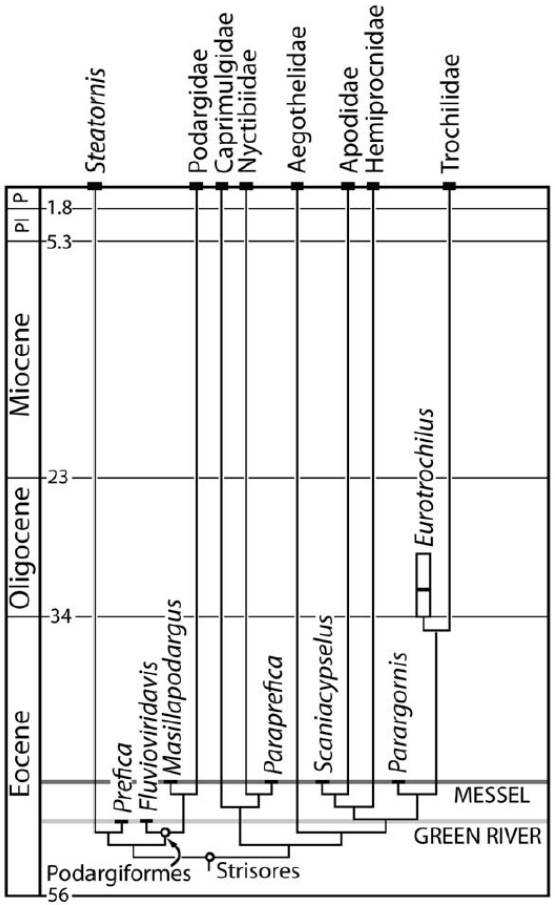

Figure 8. Time calibrated phylogeny of Strisores showing the early diversification by the middle Eocene. The relationships of the Apodiformes were based on Mayr [5,71]. Time scale based on Gradstein et al. [72] and the ages of Messel and Fossil Butte Member were based on Mertz and Renne [70] and Smith et al. [32], respectively.

Columbaves: Columbimorphae + Otidimorphae

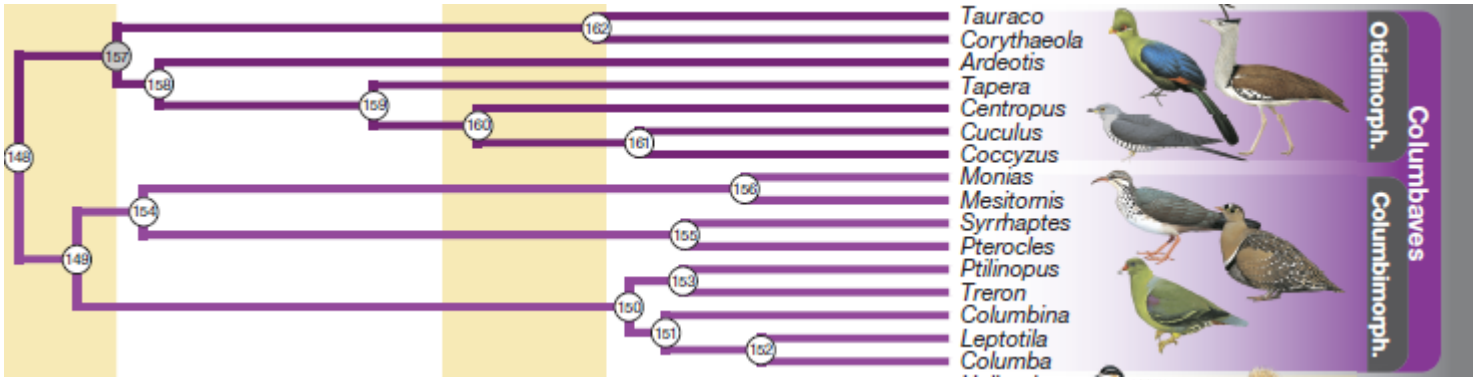

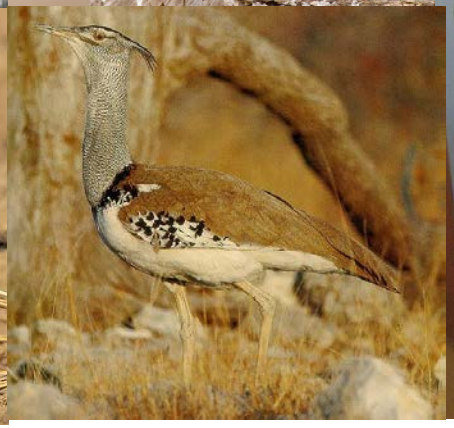

Gruiformes

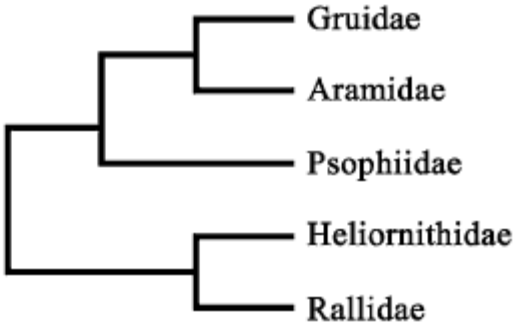

Fig. 4 Phylogenetic relationship of core Gruiformes

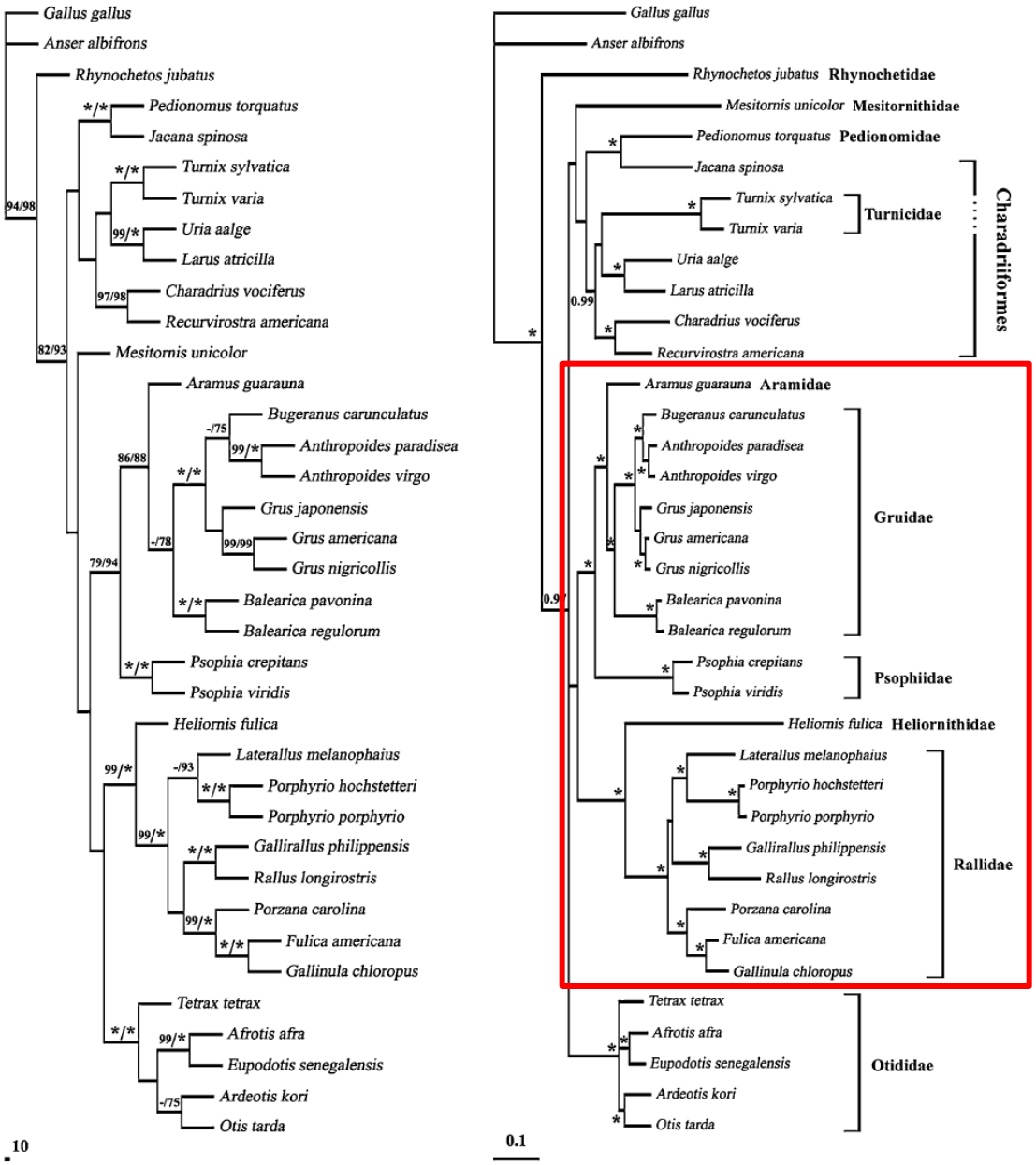

Fig. 3 Phylogenetic relationships of Gruiformes based on mitochondrial 12S, 16S and Val sequences. (*Left*) Trees obtained with maximum parsimony (CI = 0.3638, RI = 0.5126) and maximum likelihood (−LnL = 35142.11765) analysis. *Numbers* represent bootstrap values (MP/ML) and only those >70% are shown. *Asterisks* indicate bootstrap values of 100%. (*Right*) Tree obtained with Bayesian analysis (−LnL = 30320.417, Pinvar = 0.369941). *Numbers* represent posterior probabilities and only those >95% are shown. *Asterisks* indicate posterior probabilities of 100%

Gruiformes

Sarothruridae
Sarothrura spp

Heliornithidae
Podica senegalensis
Heliopais personatus
Heliornis fulica

Rallidae
(37 géneros)

Psophiidae
Psophia crepitans
Psophia leucoptera
Psophia viridis

Gruidae
Balearica spp
Grus spp

Aramidae
Aramus guarauna

Recordatorio:
No son Gruiformes!

Otidiformes (Columbaves)
Otididae
(11 géneros)

Mesitornithiformes (Columbaves)
Mesitornithidae
Mesitornis variegatus
Mesitornis unicolor
Monias benschi

Eurypygiformes (Aequorlithornithes)
Rhynochetidae
Rhynochetos jubatus
Eurypygidae
Eurypyga helias

Turnicidae y **Pedionomidae (Charadriiformes)**

Cariamiformes (Inopinaves)
Cariamidae
Cariama cristata
Chunga burmeisteri

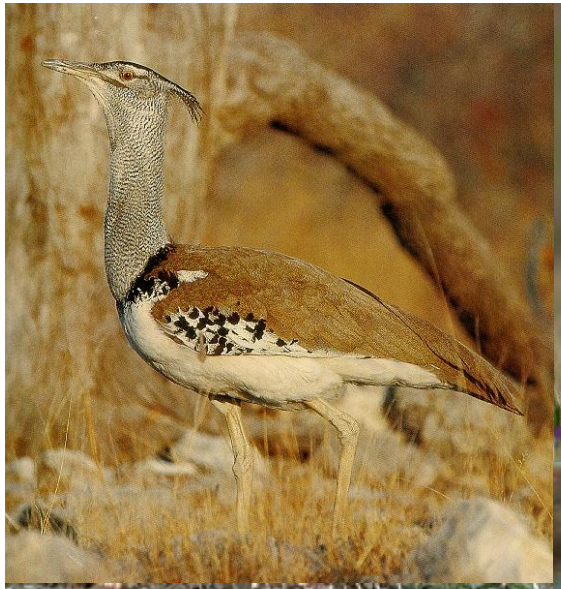



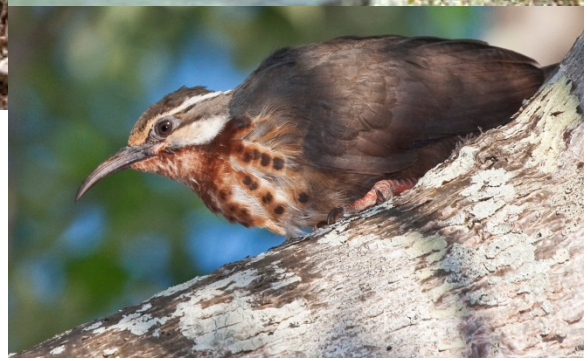

Aequorlithornithes

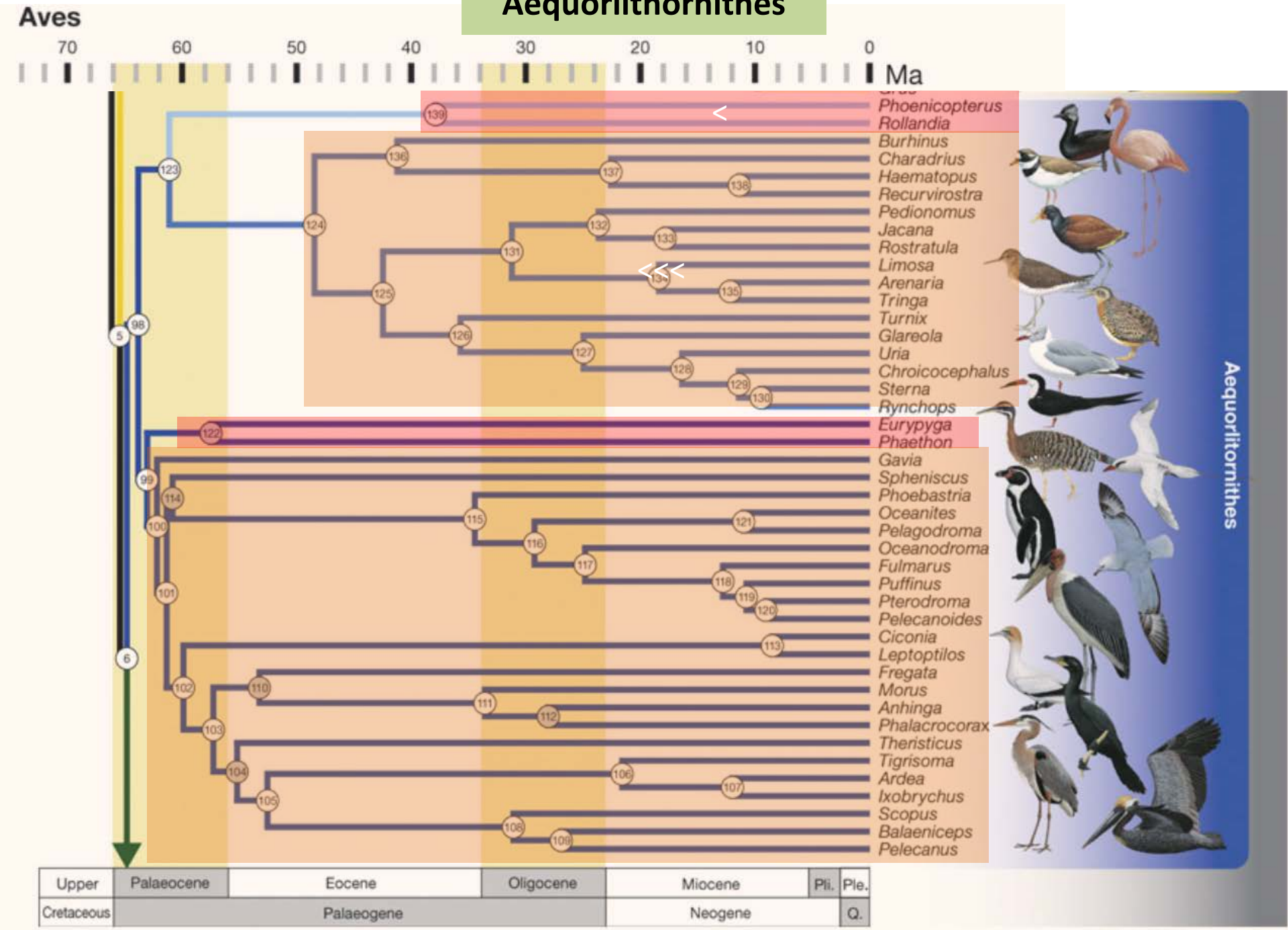

Mirandornithes: Phoenicopteriformes+Podicipediformes

Livezey & Zusi, 2007

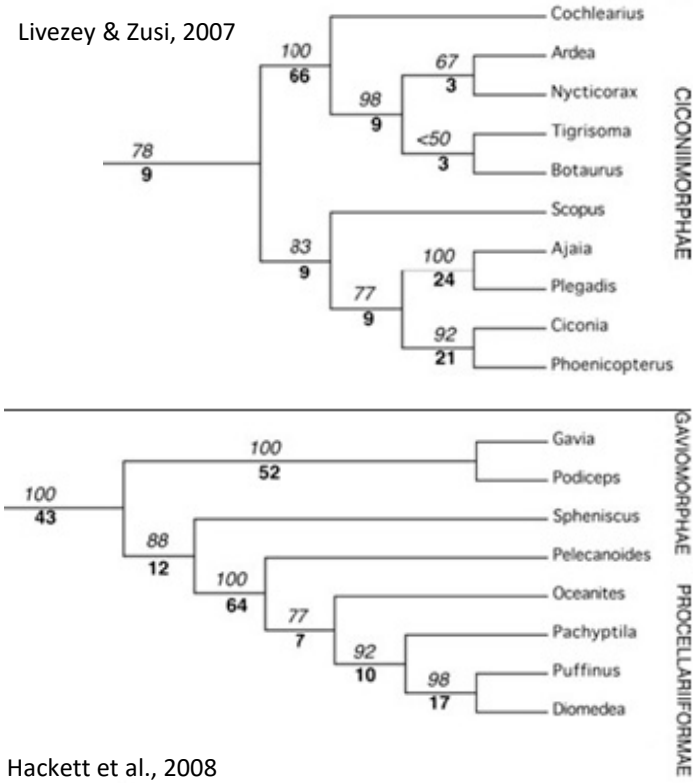

Hackett et al., 2008

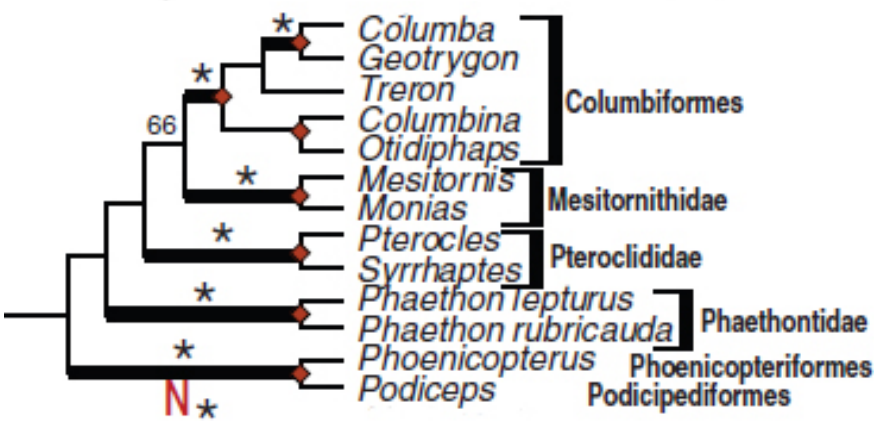

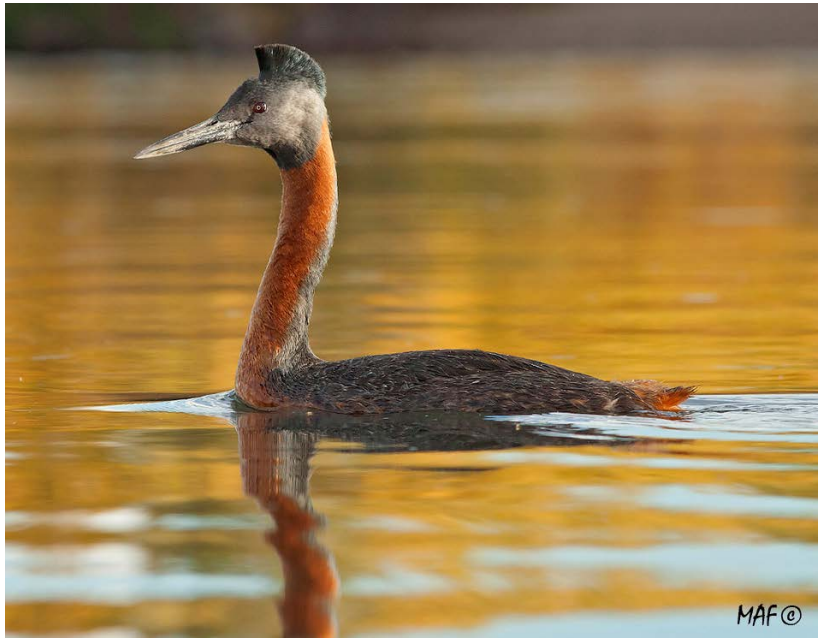

Evidencia morfológica

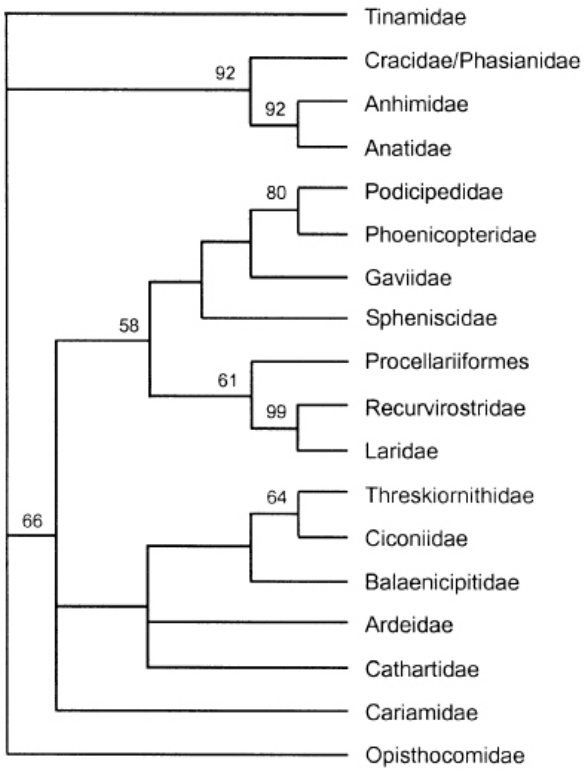

Figure 1. Strict consensus tree of three most parsimonious trees resulting from a cladistic analysis of the character matrix in Appendix 2 (Length = 197, CI = 0.39, RI = 0.56, RC = 0.21). Bootstrap values of more than 50% are indicated above the internodes.

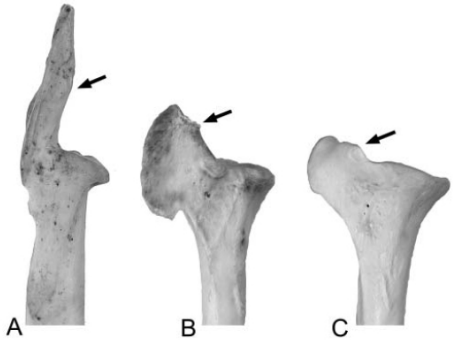

Figure 3. Right tibiotarsus, proximal end in comparison. (A) *Podiceps cristatus* (Podicipedidae); (B) *Phoenicopterus ruber* (Phoenicopteridae); (C) *Ciconia ciconia* (Ciconiidae). The arrows indicate the cnemial crest (character 55). Not to scale.

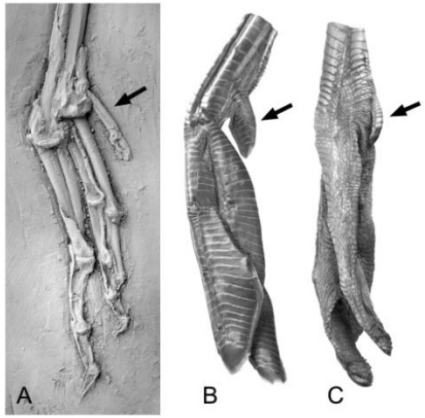

Figure 4. Right foot in comparison. (A) *Juncitarsus merkeli* (cast of holotype in SMF, coated with ammonium chloride); (B) *Podiceps cristatus* (Podicipedidae); (C) *Phoenicopterus ruber* (Phoenicopteridae, figure reversed to facilitate comparison). The arrows point to the hallux (character 59); note the comparatively well-developed hindtoe in *Juncitarsus*. Not to scale.

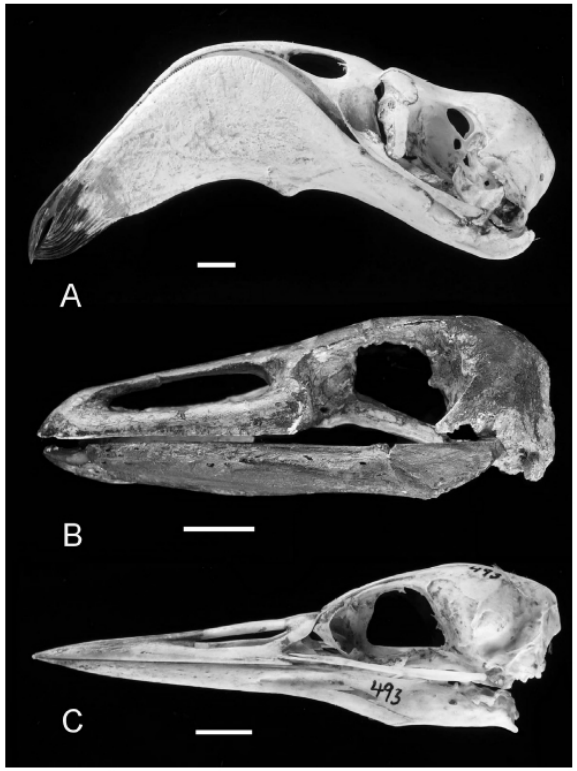

Figure 2 - Skulls in comparison. A: Lesser flamingo (*Phoenicoparias minor*, Phoenicopteridae); B: *Palaelodus* sp. (Palaelodidae; uncatalogued specimen from Alliers in France in the collection of the Forschungsinstitut Senckenberg); C: Great crested grebe (*Podiceps cristatus*, Podicipedidae). Note that the upper beak and part of the cranium in B are reconstructed; an actual specimen is figured by Cheneval & Escuillié (1992) and slightly differs in proportions. Scale bars equal 10 mm.

Apomorphies of the clade (Phoenicopteriformes + Podicipediformes) include the presence of a notarium (fused thoracic vertebrae), an unusually high number of cervical vertebrae, 11 primaries (except for storks, all other birds have 9 or 10 primaries), a layer of calcium phosphate that covers the eggshell and that is found otherwise only in the galliform Megapodiidae, and nail-like ungual phalanges (Mayr, 2004a, Manegold, 2006).

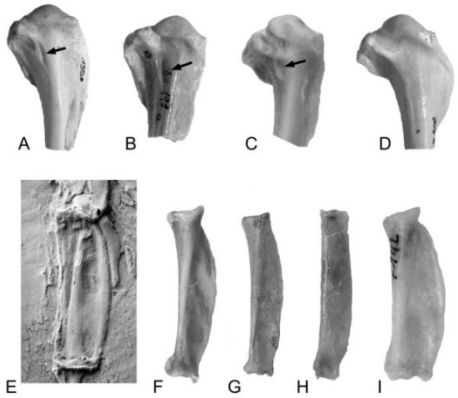

Figure 2. Proximal end of right humerus (A–D) and proximal phalanx of major digit (E–I) in comparison. (A) *Phoenicopterus chilensis* (Phoenicopteridae); (B) *Palaelodus* sp. (Palaelodidae, SMF Av 191a); (C) *Tachyhaptus ruficollis* (Podicipedidae); (D) *Eudocimus ruber* (Threskiornithidae); (E) *Juncitarsus merkeli* (cast of holotype in SMF, coated with ammonium chloride); (F) *Phoenicopterus ruber* (Phoenicopteridae); (G) *Palaelodus* sp. (Palaelodidae, SMF Av 274g); (H) *Aechmophorus occidentalis* (Podicipedidae); (I) *Eudocimus ruber* (Threskiornithidae). The arrows indicate the marked depression at the attachment site of musculus scapulohumeralis cranialis (character 41). Not to scale.

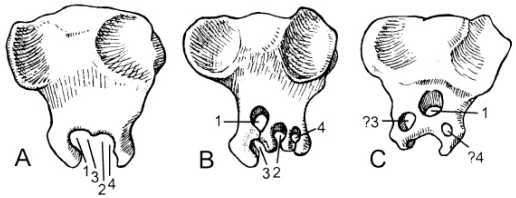

Figure 5. Hypotarsus in comparison. (A) *Phoenicopterus chilensis* (Phoenicopteridae); (B) *Palaelodus* sp. (Palaelodidae, SMF Av182c); (C) *Aechmophorus occidentalis* (Podicipedidae). Not to scale. The numerals indicate the furrows/canals for the tendons of: 1, musculus flexor digitorum longus; 2, musculus flexor perforatus digiti II; 3, musculus flexor perforans et perforatus digiti II; 4, musculus flexor hallucis longus. Homology of tendineal furrows/canals was verified against spirit specimens for Phoenicopteridae (J. Bosch, pers. comm.) and deduced from position of bony canals for the other taxa. Note that identification of tendineal furrows/canals departs from Strauch (1978: fig. 29). Not to scale.

Mayr in press; *Zoologischer Anzeiger*

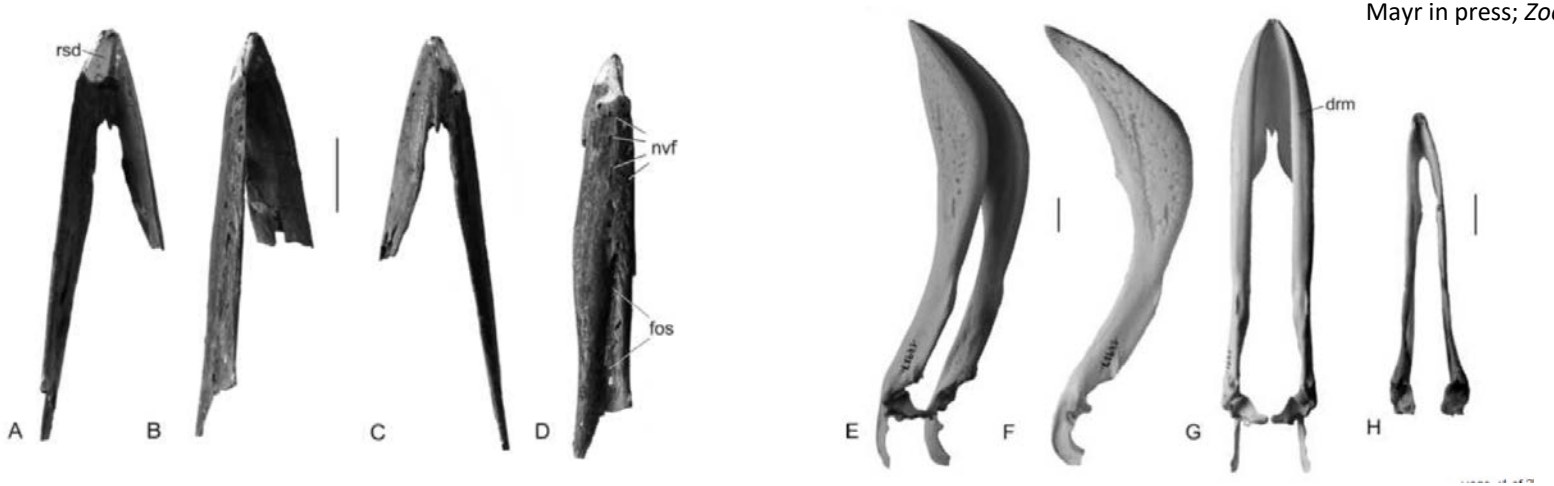

Fig. 3. (A-D) Mandible of *Palaelodus ambiguus* (SMF Av 604; Palaelodidae) in dorsal (A), dorsolateral (B), ventral (C) and lateral (D) view. (E-G) Mandible of an adult Chilean Flamingo, *Phoenicopterus chilensis* (Phoenicopteridae), in dorsolateral (E), lateral (F) and dorsal (G) view. (H) Mandible of a juvenile of *Phoenicopterus* sp. (*P. chilensis* or *P. ruber*) in dorsal view. Abbreviations: drm, wide dorsal rim of ramus mandibulae; fos, fossa in caudal section of mandible; nvf, neurovascular foramina; rsd, restored part of symphysis (white plaster). Scale bars equal 10 mm.

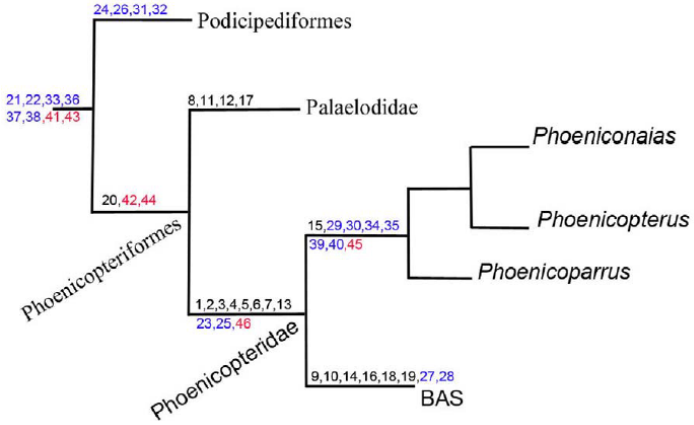

Figure 7. Osteological, oological, nesting strategy, and ecological characters mapped onto a phylogenetic tree modified from Mayr [23] by the insertion of the BAS specimen to show hypothesised character transitions on the flamingo lineage. Characters come directly from the text. Black, blue, and red numbers illustrate osteological, oological/nest, and environmental characters, respectively. OSTEOLOGICAL CHARACTERS (black numbers): Tibiotarsus: 1: distinct notches on the distal rim of *condylus lateralis* and *medialis*; 2: a wide *sulcus extensorius*; 3: a medially located *sulcus extensorius*; 4: a longer supratendinal bridge (in comparison with Palaelodidae); 5: a distinct projection of the lateral and medial condyles from the shaft; 6: a distinct and conspicuous sulcus proximal to the medial condyle; 7: lack of a medial ridge in the *trochlea cartilaginis tibialis*; 8: a rounded and prominent tuberosity for the lateral attachment of the *Retinaculum Extensorium Tibiotarsi* (RET). *Retinaculum Extensorium Tibiotarsi* separated from the articular facet of the intercotylar eminence by: 9: conspicuous sulcus; 10: deep sulcus; 11: narrow *sulcus extensorius*; 12: lateral attachment of RET laterally to the *sulcus extensorius*; 13: deep intercondylar incision; 14: intercondylar incision extends over lateral condyle to the diaphysis; 15: ridge in the medio-distal portion of *sulcus extensorius*; 16: tuberosity for the RET medial attachment; 17: shallow sulcus cranial to the *trochlea cartilaginis tibialis*; 18: deep sulcus surrounded by crests. Tarsometatarsus: 19: a conspicuous crest in *trochlea metatarsi* III, in plantar view. Skull: 20: presence of salt glands. EGGS AND NESTS (blue numbers): 21: trilaminated eggshell structure; 22: thin outer granulose calcium phosphate layer; 23: eggshell thickness of or approximately 466 µm; 24: eggshell thickness of or approximately 258 µm; 25: Layer 3 of or approximately 63 µm; 26: Layer 3 of or approximately 30 µm; 27: thin columns in L2; 28: Pronounced spherulitic crystals in L1; 29: Wide columns in L2; 30: moderately pronounced spherulitic crystals in L1; 31: Large cylindrical columns in L2; 32: Bulky spherulitic crystals in L1; 33: 45×30 mm eggs; 34: 90×53 mm eggs; 35: Single egg per clutch; 36: Two to seven eggs per clutch; 37: Floating nest; 38: Twig-nest; 39: Ground nest; 40: Mud, volcano-shaped nest. NESTING ENVIRONMENTS (red numbers): 41: Nesting in lacustrine environment; 42: Nesting in endorheic lacustrine environment; 43: Nesting in normal-oligohaline lacustrine environment; 44: Nesting in oligohaline to mesohaline lacustrine environment; 45: Nesting in mesohaline to hyperhaline lacustrine environment; 46: Nesting in shallow to extremely shallow lacustrine environment.
doi:10.1371/journal.pone.0046972.g007

Grellet-Tinner et al 2012; PlosONE

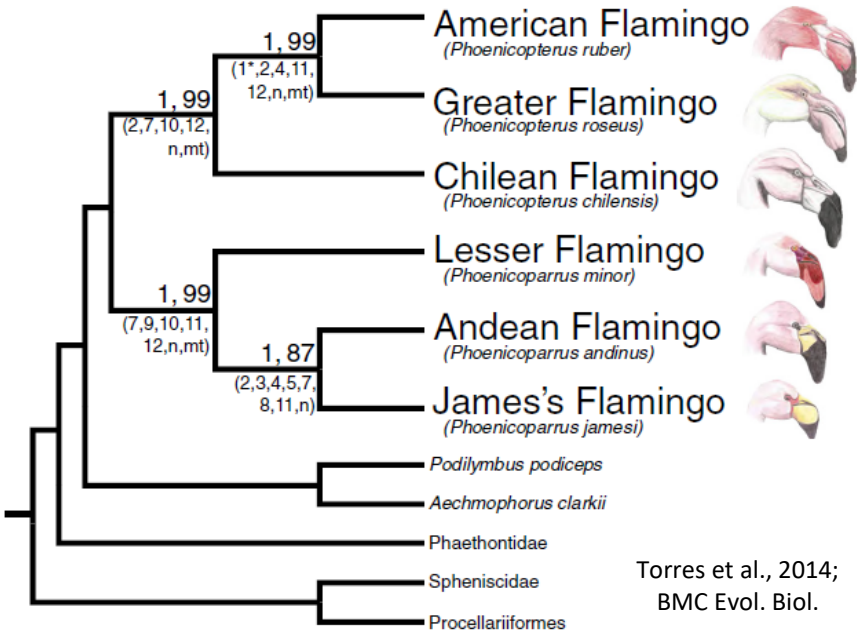

Torres et al., 2014; BMC Evol. Biol.

Figure 1 Relationships and ages of the flamingos. Cladogram showing the relationships of the living flamingos. The flamingos fall out in two sub-clades with high support, congruent with the topology recovered by Sibley and Ahlquist [15]. Genus *Phoenicoparrus* has been expanded to include all members of the deep-keeled clade (see Discussion). Posterior probabilities (Bayesian inference) and bootstrap support values (maximum likelihood) are shown above each node. Numbers and letters to the right of each node indicate individual genes and data subsets which recover that monophyletic clade. Key: 1, RHEB1; 2, TIMM17A; 3, TCF3; 4, RPS24; 5, SLC29A4; 6, NFKBIZ; 7, G3PDH; 8, myoglobin; 9, ZENK; 10, ZENK 3'UTR; 11, COI; 12, cyt b; n, nDNA subset; mt, mtDNA subset. RHEB1 failed to recover sister status between the American and Greater Flamingos in a maximum likelihood framework with high support, denoted by '1*'.

Charadriiformes

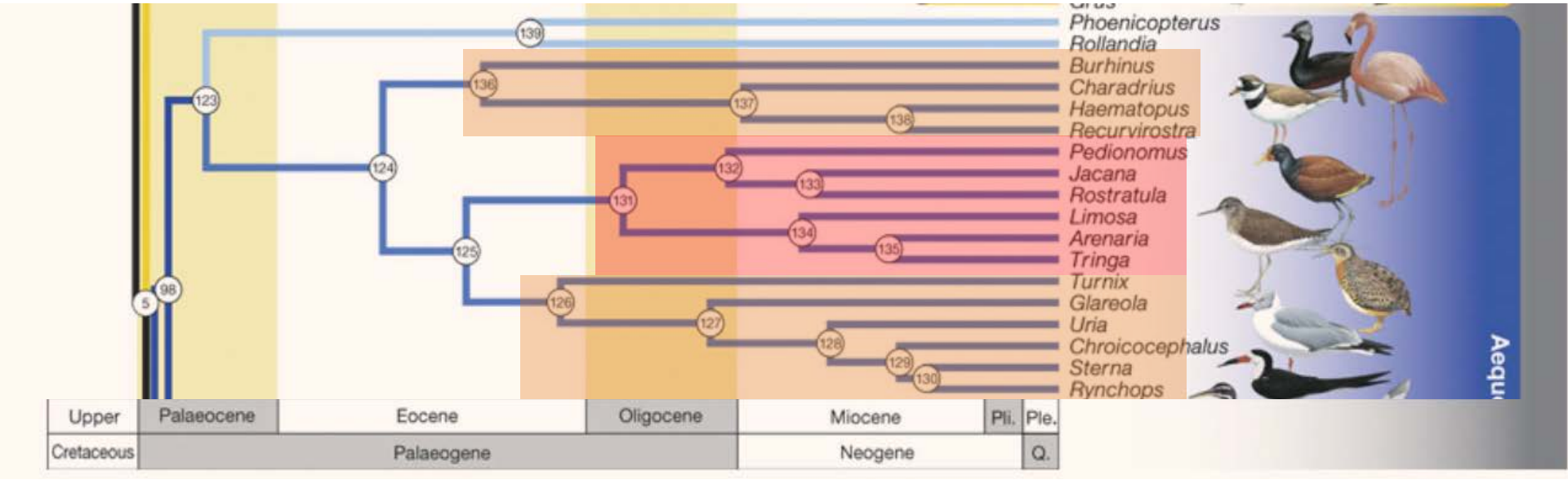

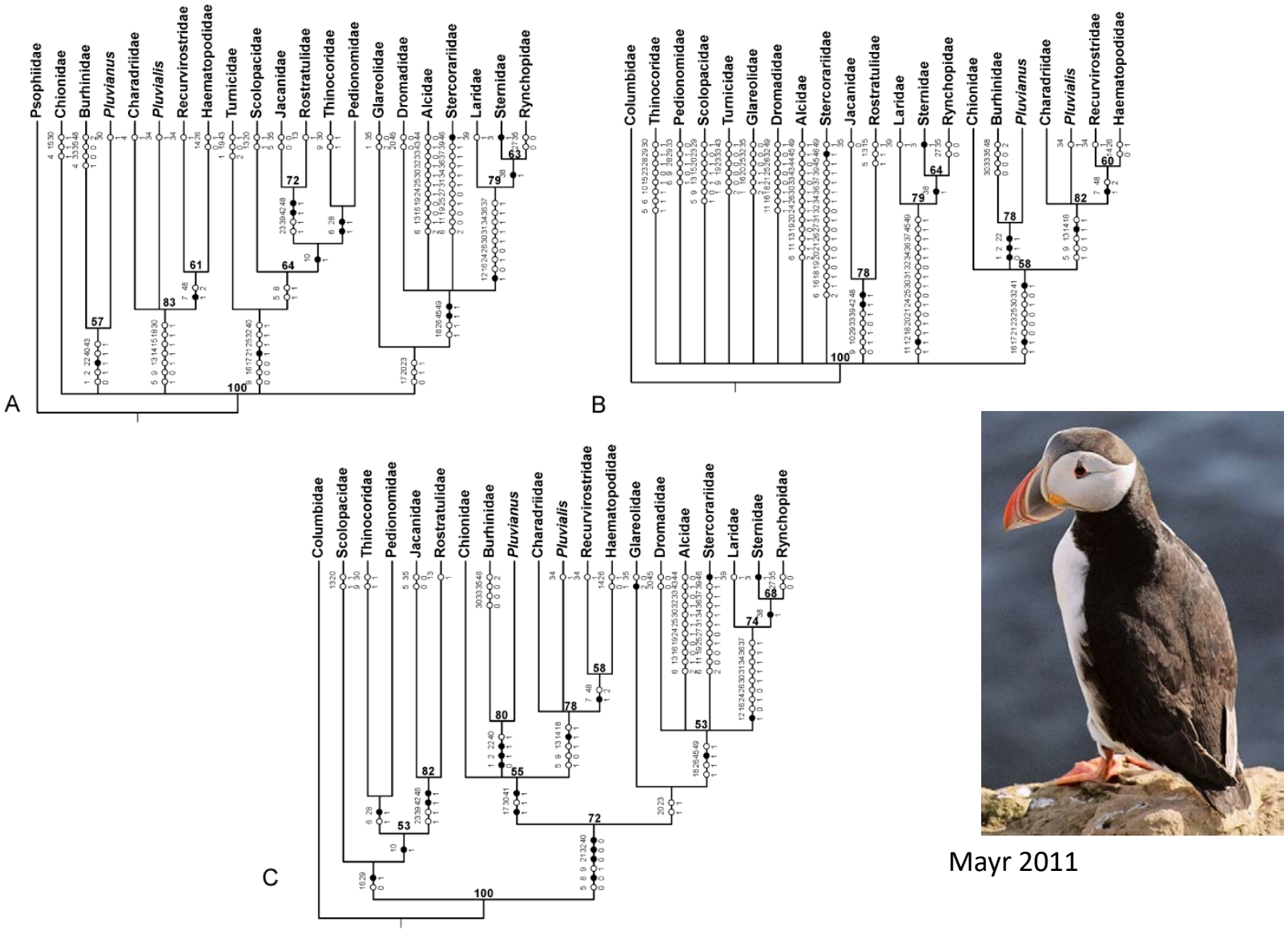

Mayr 2011

Figure 3. Trees resulting from analyses of the character matrix in Appendix 2 with NONA 2.0 with different settings. A, Psophiidae as outgroup taxon, consensus of 12 most parsimonious trees [length = 118, consistency index (CI) = 0.44, retention index (RI) = 0.67]. B, Columbidae as outgroup taxon, consensus of 19 most parsimonious trees (length = 115, CI = 0.45, RI = 0.68). C, Columbidae as outgroup taxon and Turnicidae removed from analysis, consensus of six most parsimonious trees (length = 110, CI = 0.47, RI = 0.69). Bootstrap support values are listed above the nodes, characters and characters states next to the internodes (numbers refer to the character list in Appendix 1). Filled circles represent strict apomorphies, open circles homoplastic ones.

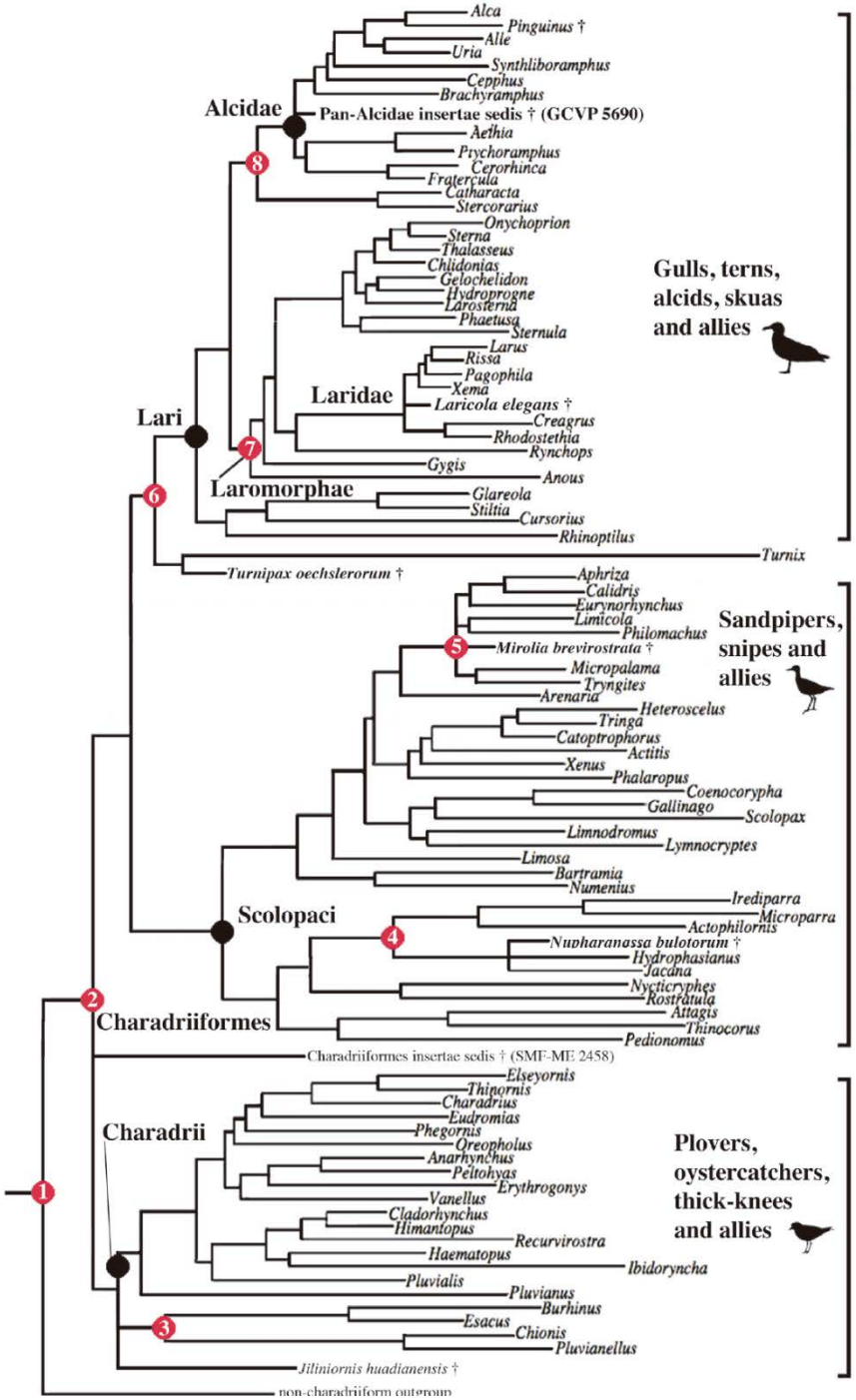

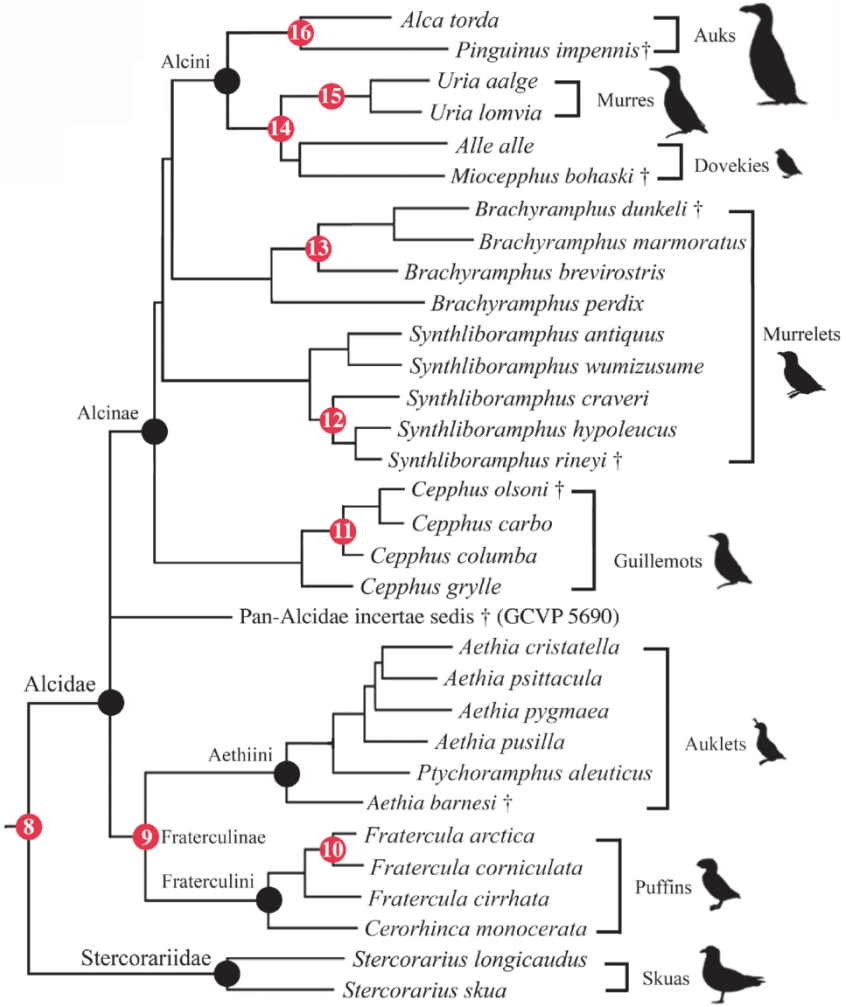

FIGURE 1. Phylogram of charadriiform relationships showing calibrated nodes 1-7 (modified from Baker et al., 2007, figure 1). Numbered nodes in red correspond to the following calibrations: (1) divergence of Charadriiformes from its nearest outgroup; (2) divergence of Charadrii from other Charadriiformes; (3) divergence of Burhinidae from *Chionis* and *Pluvianellus*; (4) divergence of Jacanidae from other Scolopaci; (5) basal divergence among Calidridinae; (6) divergence of Turnicidae from Lari; (7) basal divergence of Laromorphae; (8) divergence of Alcidae from Stercorariidae.

FIGURE 2. Phylogram of alcid relationships showing calibrated nodes 7-15 (modified from Smith, 2011a, figure 1.26). Numbered nodes in red correspond to the following calibrations: (8) divergence of Alcidae from Stercorariidae; (9) divergence of Aethiini from Fraterculini; (10) divergence of *Fratercula arctica* from *Fratercula corniculata;* (11) divergence of *Cepphus carbo* from *Cepphus columba;* (12) divergence of *Synthliboramphus hypoleucus* from Synliboramphus craveri;divergence of Synthliboramphus hypoleucus from *Synthliboramphus craveri;* (13) divergence of *Brachyramphus marmoratus* from *Brachyramphus brevirostris;* (14) divergence of *Alle alle* from *Uria;* (15) divergence of *Uria lomvia* from *Uria aalge;* (16) divergence of *Alca torda* from *Pinguinus impennis.*

Eurypigiformes+Phaetontiformes

Clado de Neoaves marinas soportado por evidencia molecular. Integra a aves del trópico (*Phaeton*), ave sol (*Rhynochetos*) y kagú (*Eurypiga*).

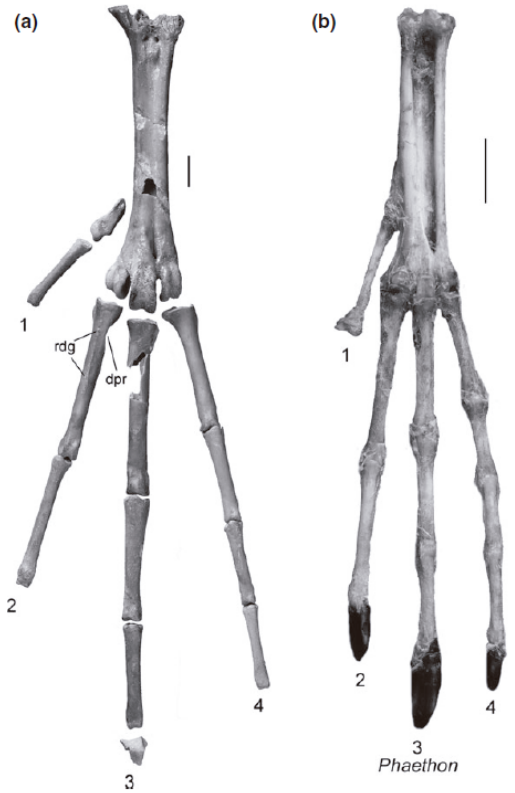

Figure 7. (a) Assembled left foot of *Prophaethon shrubsolei* Andrews, 1899 from the early Eocene London Clay of Walton-on-the-Naze, Essex, UK (SMF Av 602); position of the single fragmentary ungual phalanx is arbitrary. (b) Articulated, partially macerated foot of the White-tailed Tropicbird *Phaethon lepturus* (right side, reversed to ease comparisons). dpr, pathological depression in first phalanx of second toe; rdg, pathological ridge along phalanx of second toe. The toes are numbered. Scale bars: 5 mm.

Aequornithes

Clado de Neoaves (“waterbirds assemblage”) bien soportado por evidencia molecular (Erickson et al., 2006; Hackett et al., 2008; Prum et al., 2015). Integra aves marinas.

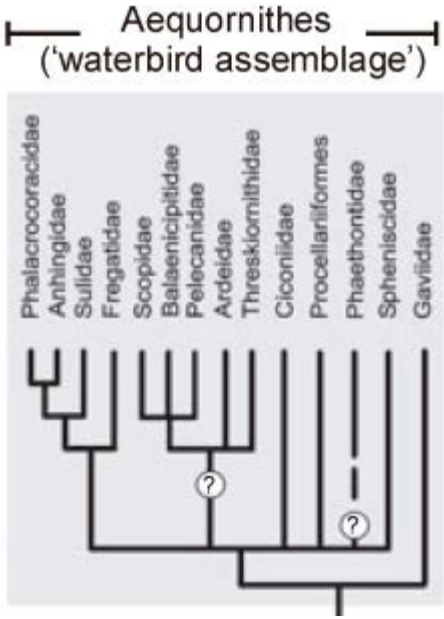

Evidencia morfológica

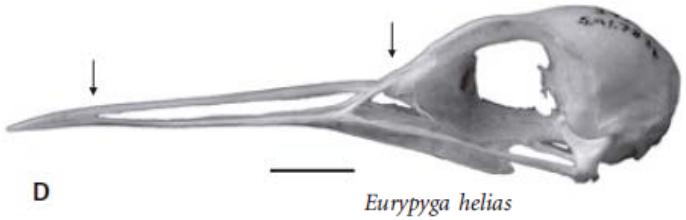

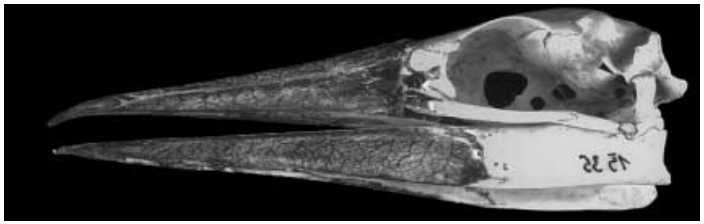

Morus

Scopus

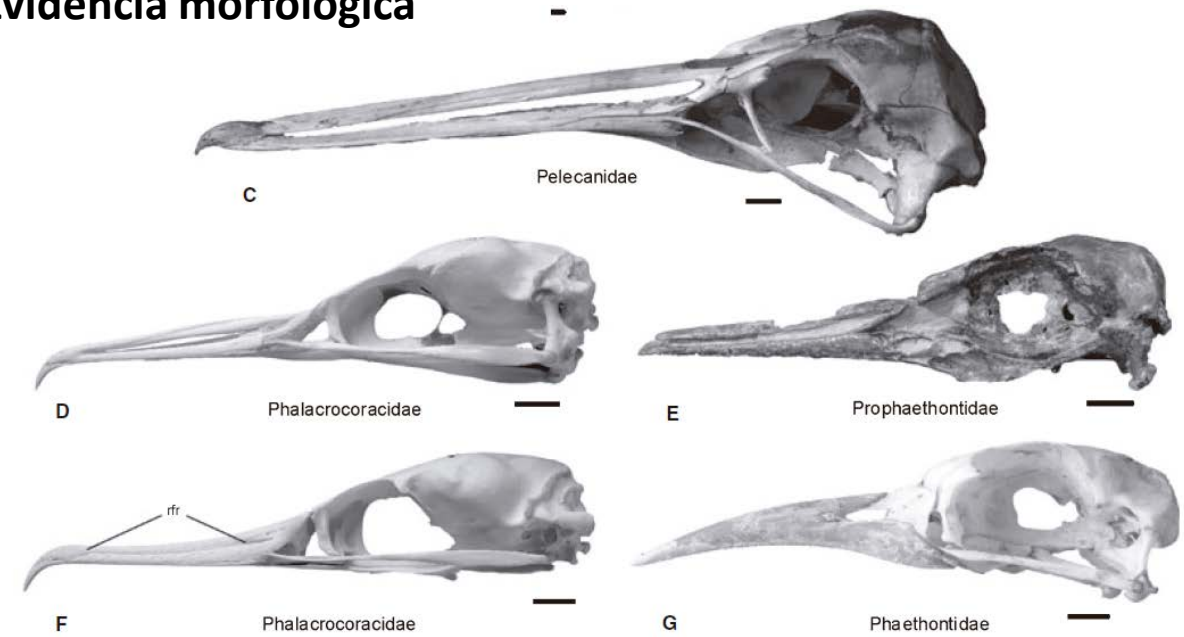

Fig. 5 Skulls in comparison. —A. *Pelagornis chilensis* from the Miocene of Chile (Pelagornithidae; MNHN SGO.PV 1061). —B. *Dasornis emuinus* from the early Eocene London Clay in England (Pelagornithidae; SMNK-PAL 4017). —C. Juvenile *Pelecanus occidentalis* ('Pelecaniformes', Pelecanidae) with long nostrils. —D. Juvenile *Phalacrocorax carbo* ('Pelecaniformes', Phalacrocoracidae) with long nostrils. —E. *Prophaethon shrubsolei* from the early Eocene London Clay in England (Prophaethontidae; BMNH A 683) with long nostrils. —F. Adult *P. carbo*. —G. *Phaethon aethereus* ('Pelecaniformes', Phaethontidae). mfr, mandibular furrow; rfr, rostral furrow (nasolabial

Una posible sinapormorfía de Aequornithes es la presencia de un surco a lo largo del pico (nasolabial groove). Éste está ausente sólo en Ciconidae (cigueñas), Phaetontidae (aves del trópico) y poco desarrollado en Ardeidae (garzas). Este surco produce cornificaciones separadas en la ramfoteca. En juveniles hay narinas alargadas y desarrolladas a lo largo de una hendidura en esta zona.

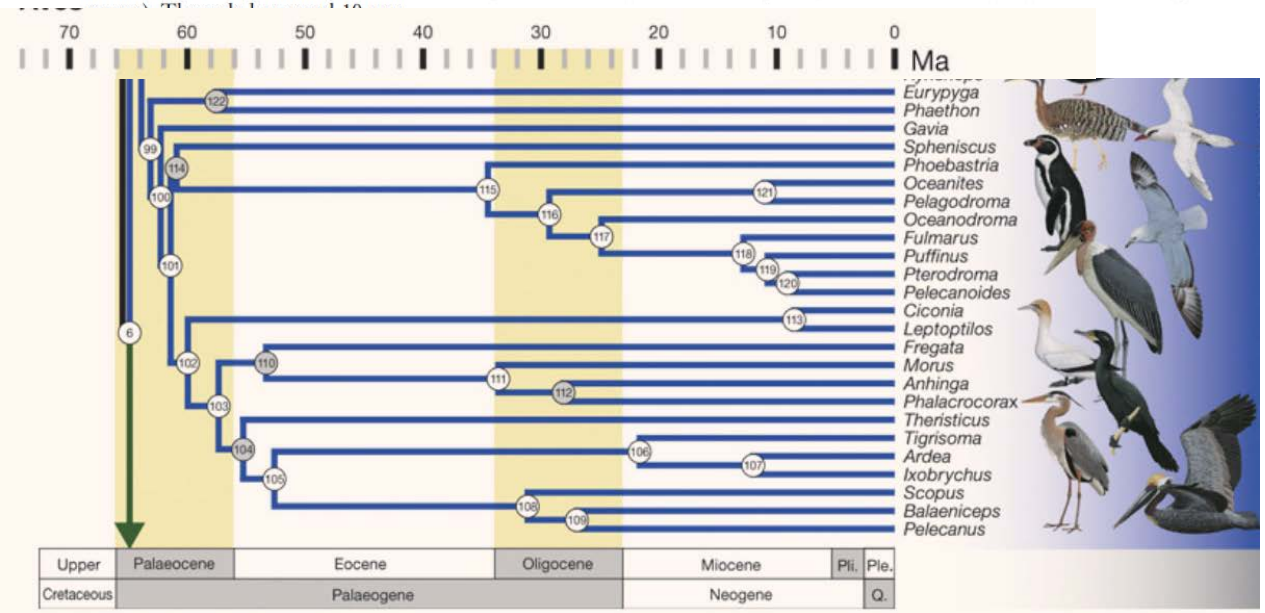

Gaviiformes

Orden de aves buceadoras cuya distribución actual es Holártica, pero cuyo registro fósil revela una distribución más amplia en el pasado. Existen registros del Cretácico superior de Chile (*Neogaeornis wetzelii*) y Antártica (*Polarornis gregorii*), pero la afinidad de estos taxa es incierta debido a la naturaleza fragmentaria del material fósil.

Gaviiformes derivados comparten un hipotarso desarrollado, en donde las crestas hipotarsales se alargan y contactan, encerrando un gran canal para tendones flexores.

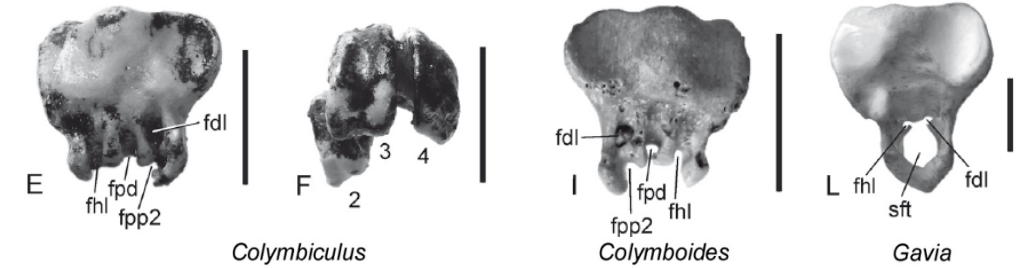

Registro de Gaviidae en Chile

Neogaeornis wetzelii . Formación Quiriquina (Masstrichtiano)

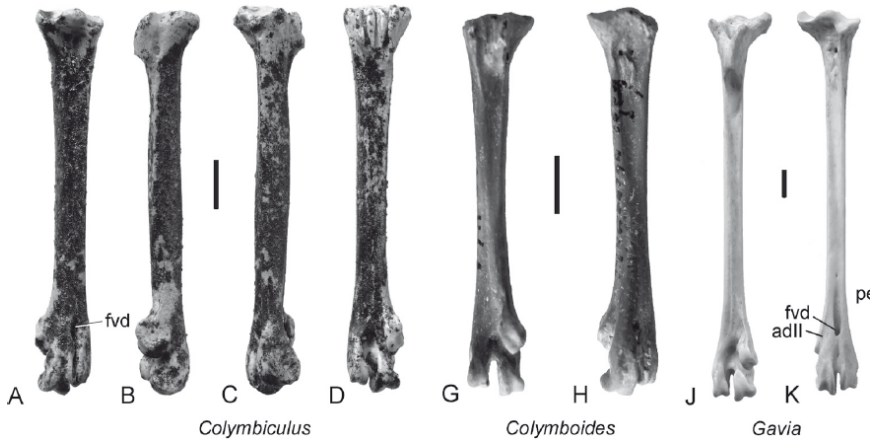

FIGURE 1. Tarsometatarsus of **A–F**, *Colymbiculus udovichenkoi* from the Middle Eocene of Ukraine in comparison with **G–I**, the Early Miocene *Colymboides minutus* and **J–L**, the extant *Gavia stellata*. **A–F**, left tarsometatarsus (SMF Av 592) in dorsal (**A**), medial (**B**), lateral (**C**), plantar (**D**), proximal (**E**), and distal (**F**) view. **G**, **H**, left tarsometatarsus (NMB MA. 2668) in plantar (**G**) and dorsal (**H**) view. **I**, right tarsometatarsus (NMB S.G. 20829) in proximal view. **J–L**, left tarsometatarsus in plantar (**J**), dorsal (**K**), and proximal (**L**) view. **M**, left carpometacarpus (SMF Av 593, ventral view) of an unidentified small bird from the Middle Eocene of the Ikovo sand quarry. Abbreviations: adII, sulcus for tendon of musculus abductor digiti II; fdl, canal for tendon of musculus flexor digitorum longus; fhl, canal for tendon of musculus flexor hallucis longus; fpd, canal for tendon of musculus flexor perforatus digiti II; fpp2, canal for tendon of musculus flexor perforans et perforatus digiti II; fvd, foramen vasculare distale; pex, base of broken processus extensorius; sft, canal for superficial flexor tendons. In (**F**) the trochleae are numbered. Scale bars equal 5 mm.

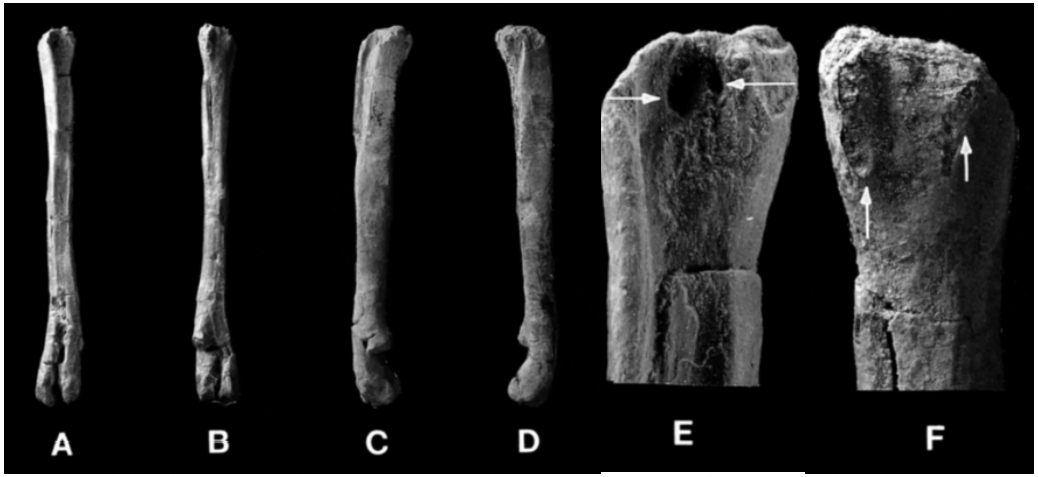

FIGURE 1. *Neogaeornis wetzeli,* holotype (GMPK 123), right tarsometatarsus: **A**, anterior; **B**, posterior; **C**, medial; **D**, lateral; **E**, anterior view of proximal end showing the proximal foramina (arrows); **F**, posterior view of proximal end showing the remains of calcaneal ridges of the hypotarsus (arrows). **A–D**, natural size; **E–F**, 5×.

Originalmente *Neogaeornis* fue clasificado junto con otras aves buceadoras mesozoicas (Hesperornithiformes). Sin embargo hay presencia de hipotarso, lo que indica que el ejemplar es un Neornithes Olson, 1992.

Suliformes

Evidencia molecular y fósil excluye a Pelecanidae y Phaetontidae del grupo (desarmando el Pelecaniformes tradicional), rescatando a Fregatidae+Suloidea [Sulidae+(Phalacrocoracidae+Anhingidae)] en un nuevo clado: Suliformes

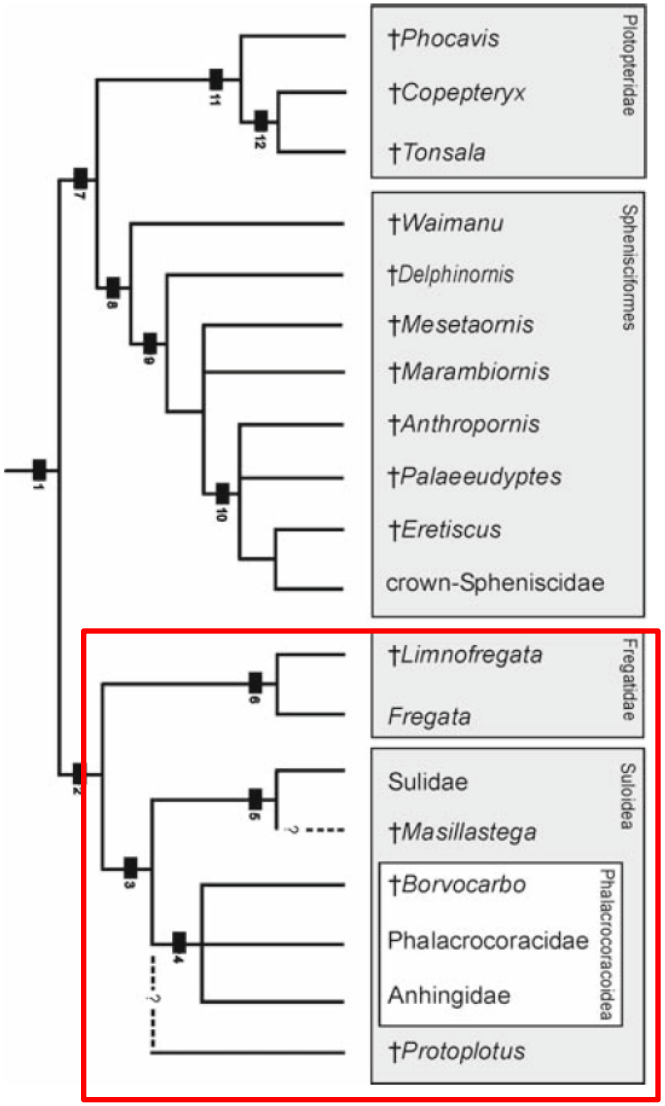

Hipótesis de relaciones filogenéticas propuesta por Mayr (2008). Integra datos morfológicos, moleculares y paleontológicos.

Plotopteridae

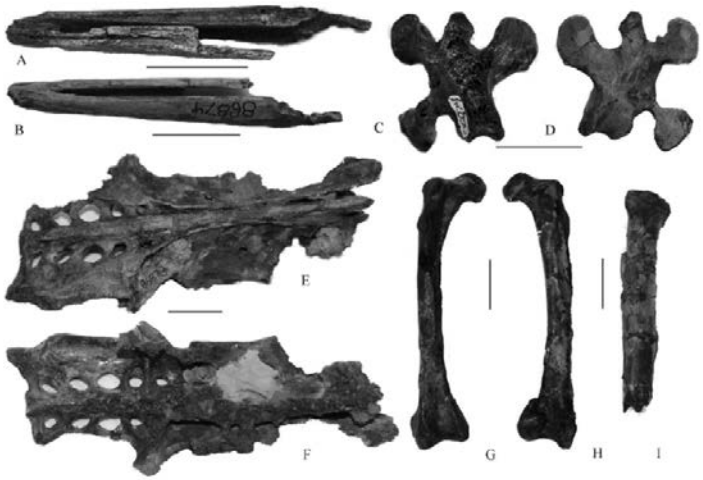

Figure 1. Fossil material referred to *Tonsala hildegardae*. A–D, dentary in dorsal (A) and ventral (B) views, UWBM 86874. C–D, cervical vertebrate in dorsal (C) and ventral (D) view, UWBM 86874. E–F, pelvis in dorsal (E) and ventral (F) view, UWBM 86873. G–H, right femur in cranial (G) and caudal (H) view, UWBM 86873. I, right tibiotarsus in caudal view, UWBM 86873. Scale bar is 2 cm.
doi:10.1371/journal.pone.0025672.g001

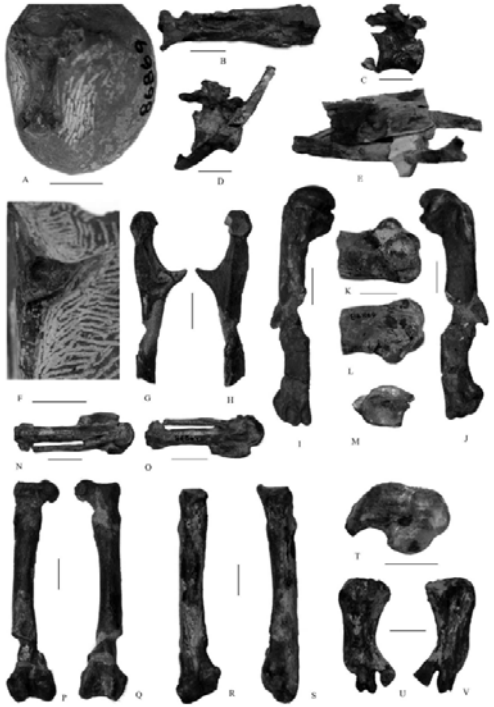

Fregattidae

FIGURE 6. *Limnofregata hasegawai*, new species, paratype, FMNH PA 719, skull and mandible. Scale = 2 cm. Inset: right and left lacrimal bones showing pneumatic foramina in the corpus.

Stem-Suloidea

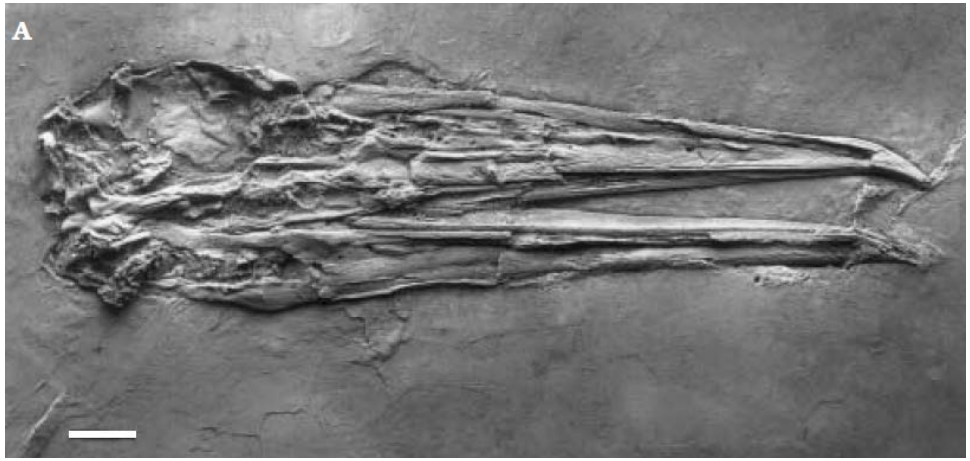

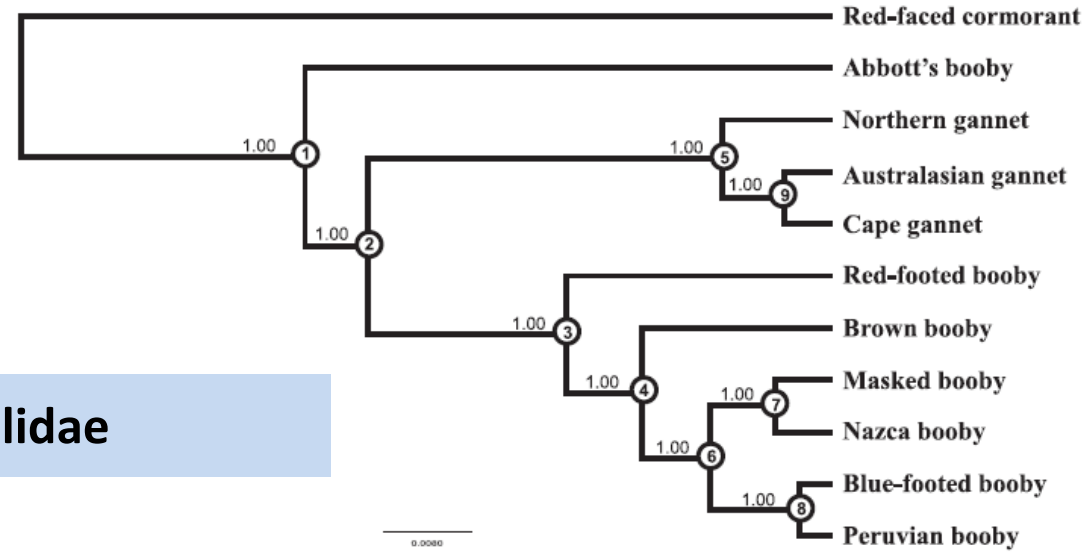

Sulidae

Fig. 3. Concatenation and BEST species trees. Estimates of the sulid species tree from the (a) concatenation and (b) BEST analyses. Nodal support is indicated with Bayesian posterior probabilities. Numbers in open circles refer to node numbers that are used in Table 3.

Registro de Sulidae en Chile

Sula aff. *variegata*, *Sula* spp. *Morus* sp. Formación Bahía Inglesa (Mioceno medio-Plioceno)

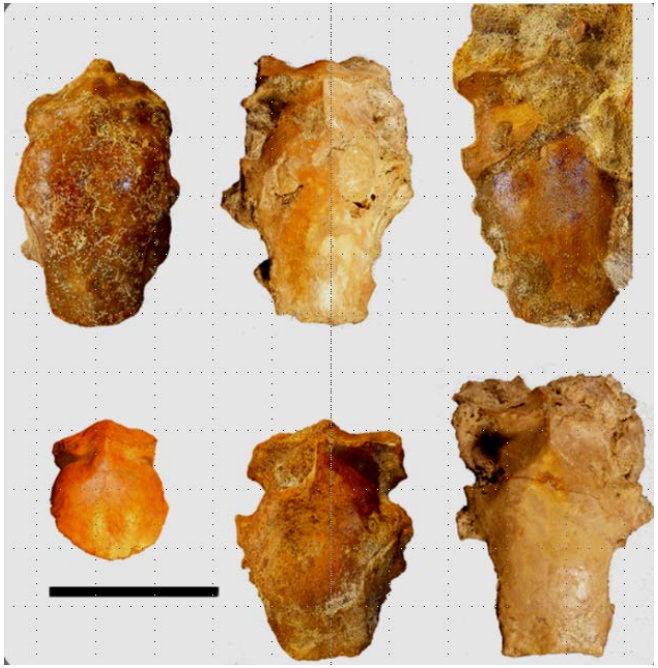

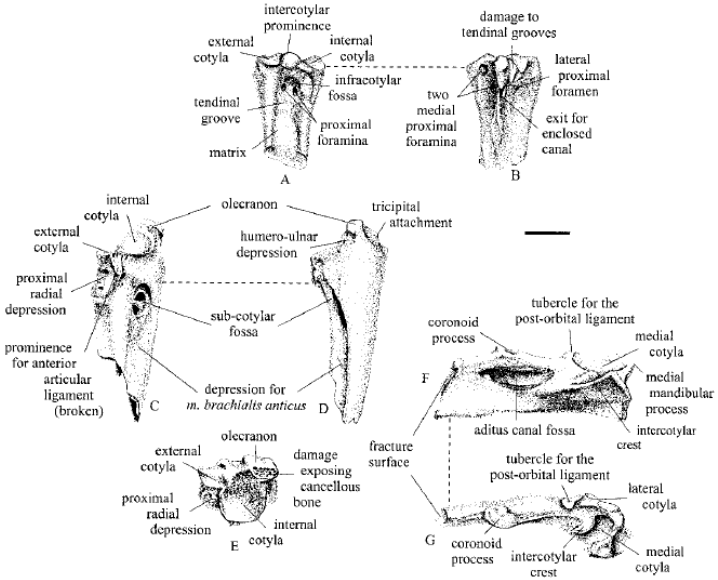

FIGURE 3. *Sula* sp. tarsometatarsus (UOP/01/74) in **A**, anterior and **B**, posterior aspects; left ulna (UOP/01/76) in **C**, medial, **D**, medio-anconal, and **E**, proximal aspects; and right mandible (UOP/01/91) in **F**, medial, and **G**, dorsal aspects. Scale bar equals 10 mm.

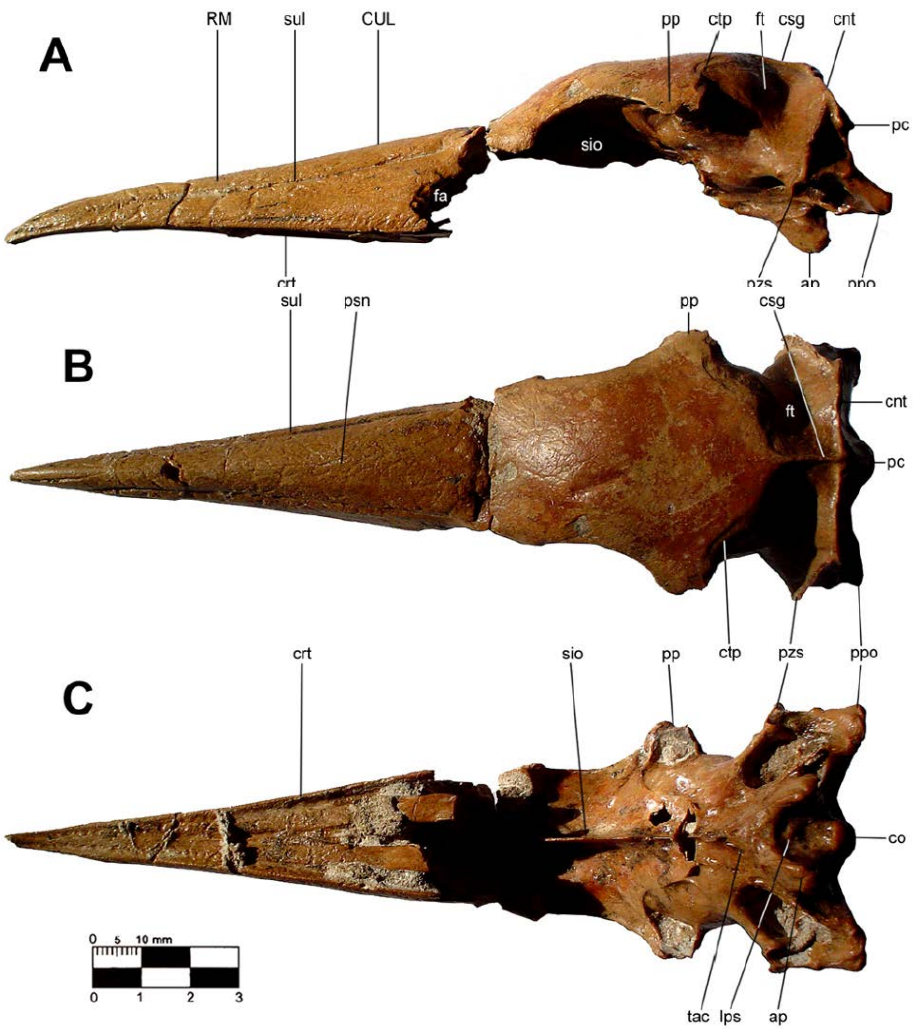

Figura 21. Cráneo de *Sula?* nov. sp. ACH 02 de la FBI: **A**. vista lateral, **B**. vista dorsal, **C**. vista ventral. Escala: 30 mm.

Anhigidae

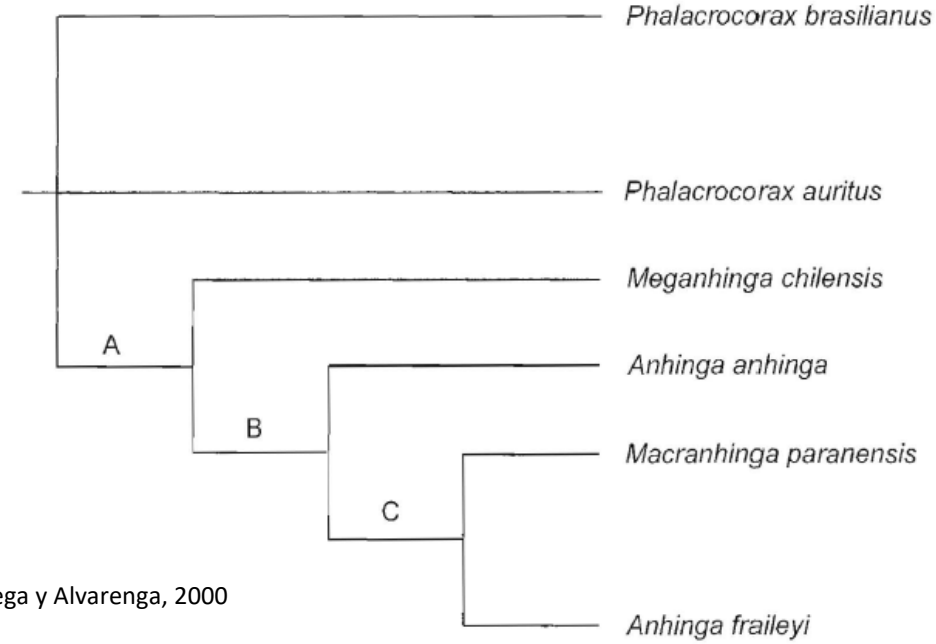

Noriega y Alvarenga, 2000

FIGURE 4. Cladogram with the non-ambiguous synapomorphies supporting each node; Character state indicated as super-index. Node A: 1^1, 8^1, 13^1; Node B: 1^2, 2^1, 14^1; Node C: 5^1, 7^1, 9^1, 12^1.

FIGURE 2. Dorsal (left) and ventral (right) view of the femora of: **A**, *Macranhinga ranzii* (holotype UFAC-3640). **B**, *Anhinga anhinga* (MHNT-924). **C**, *M. ranzii* (paratype UFAC-4034). A and B are left side; C is right side.

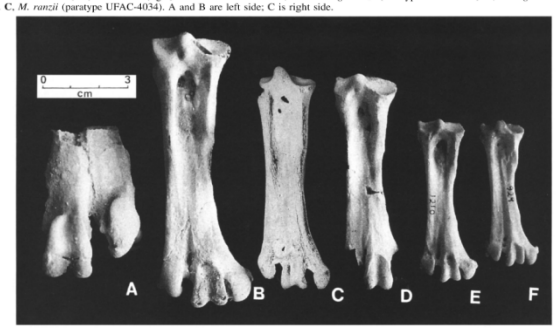

FIGURE 3. A comparison of the tarsometatarsus, in dorsal view, of some Anhingidae: **A**, *Macranhinga ranzii* (paratype UFAC-3523). **B**, *Macranhinga paranensis* (cast of holotype). **C**, *Anhinga fraileyi* (holotype LACM-135356). **D**, *Meganhinga chilensis* (holotype). **E**, *Anhinga novaehollandiae* (MHNT-1210). **F**, *Anhinga anhinga* (MHNT-924). Note: A, B and D are coated with ammonium chloride.

Alvarenga y Guilherme, 2003

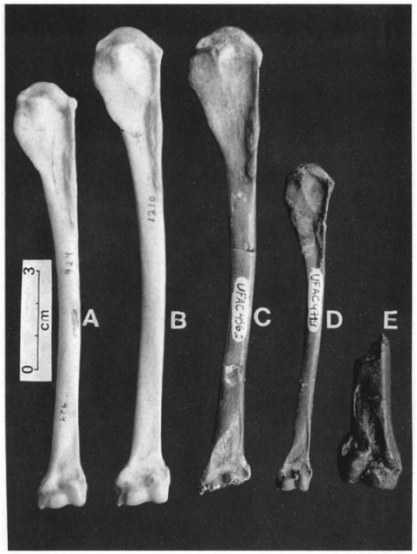

FIGURE 9. Comparison of the humeri of some Anhingidae in ventral view: **A**, *Anhinga anhinga* (MHNT-924). **B**, *Anhinga novaehollandiae* (MHNT-1210). **C**, *Anhinga* cf. *fraileyi* (UFAC-4562). **D**, *Anhinga minuta* (paratype UFAC-4719). **E**, *Anhinga* cf. *grandis* (UFAC-4721).

FIGURE 7. The left tibiotarsus in ventral (left) and lateral (right) views of **A**, *Anhinga minuta*, sp. nov. (holotype UFAC-4720), **B**, *A. anhinga* (MHNT-924), and **C**, *A. novaehollandiae* (MHNT-1210).

Registro de Anhingidae en Chile

Meganhinga chilensis. Formación Cura-Mallín (Mioceno inferior)

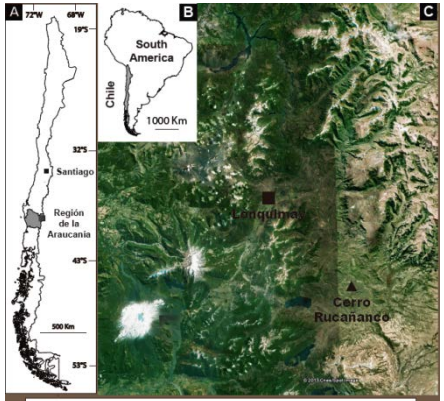

Figura 1: Mapa con la localidad de procedencia del material estudiado. **A**, Mapa de Chile. **B**, Mapa de Sudaméra. **C**, Mapa del sector de Lonquimay, mostrando la ubicación del sitio del hallazgo respecto de la ciudad de Lonquimay.

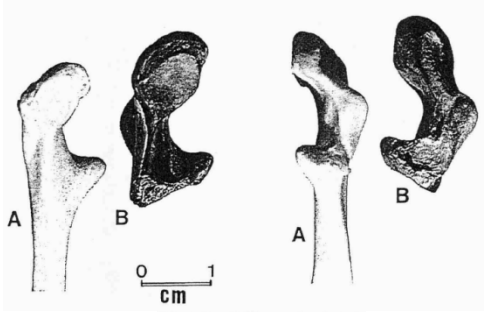

Ventral (left) and dorsal (right) views of the humeral portion of the right coracoid of *Anhinga anhinga* (A) and *Meganhinga chilensis* n.g. n.sp., SGO-PV 4001-J, (B).

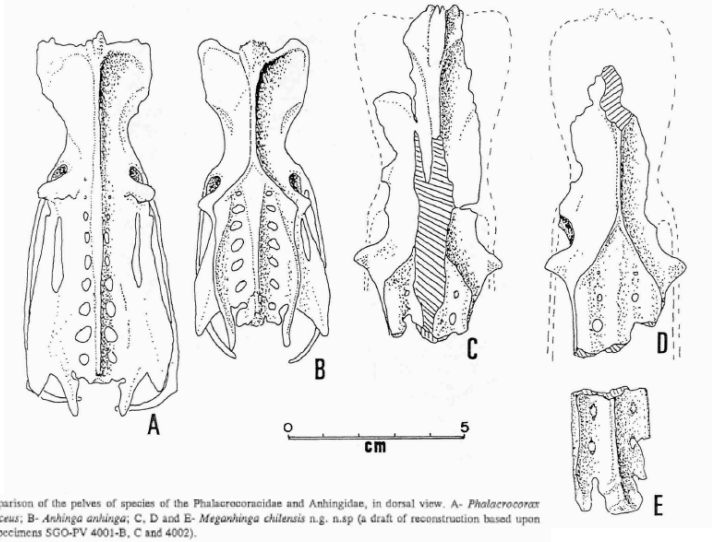

Comparison of the pelves of species of the Phalacrocoracidae and Anhingidae, in dorsal view. A- *Phalacrocorax olivaceus*; B- *Anhinga anhinga*; C, D and E- *Meganhinga chilensis* n.g. n.sp (a draft of reconstruction based upon the specimens SGO-PV 4001-B, C and 4002).

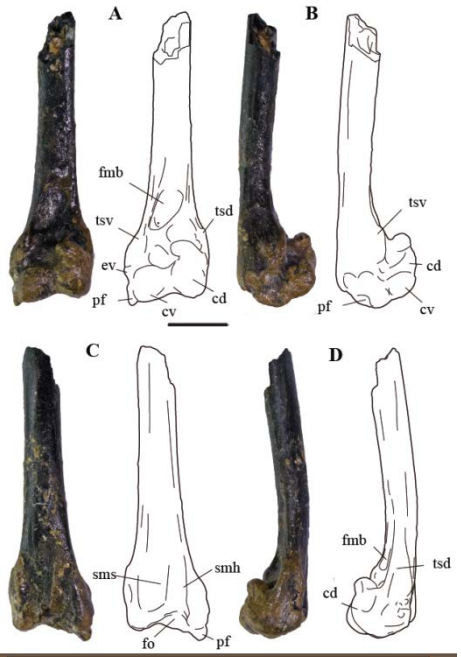

Figura 3: Fotografías y esquemas del húmero izquierdo SGO.PV.22212b. **A**, vista craneal. **B**, vista ventral. **C**, vista caudal. **D**, vista lateral. Barra de escala = 10 mm.

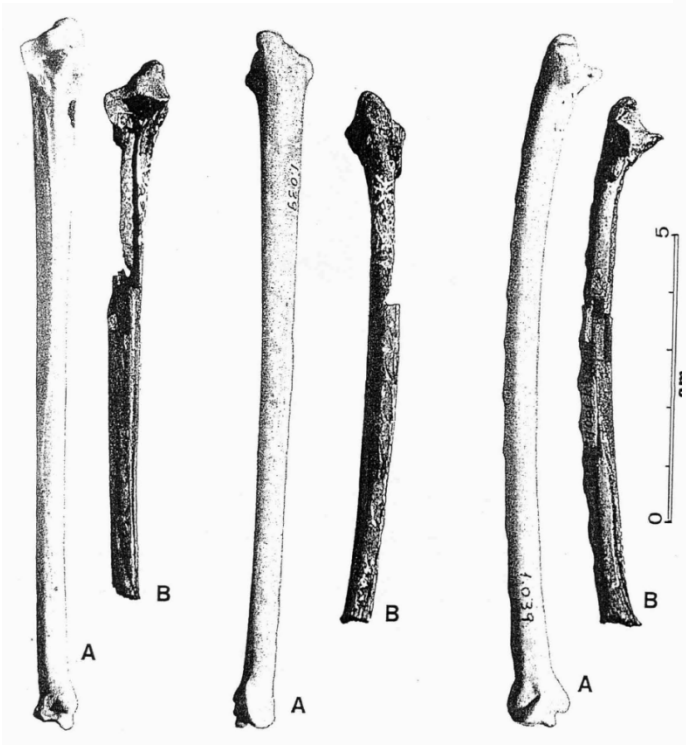

Right ulna of *Anhinga anhinga* (A), in comparison with *Meganhinga chilensis* n.g. n.sp.. SGO-PV 4001-K, (B), in palmar (left), anconal (center) and lateral (right) views.

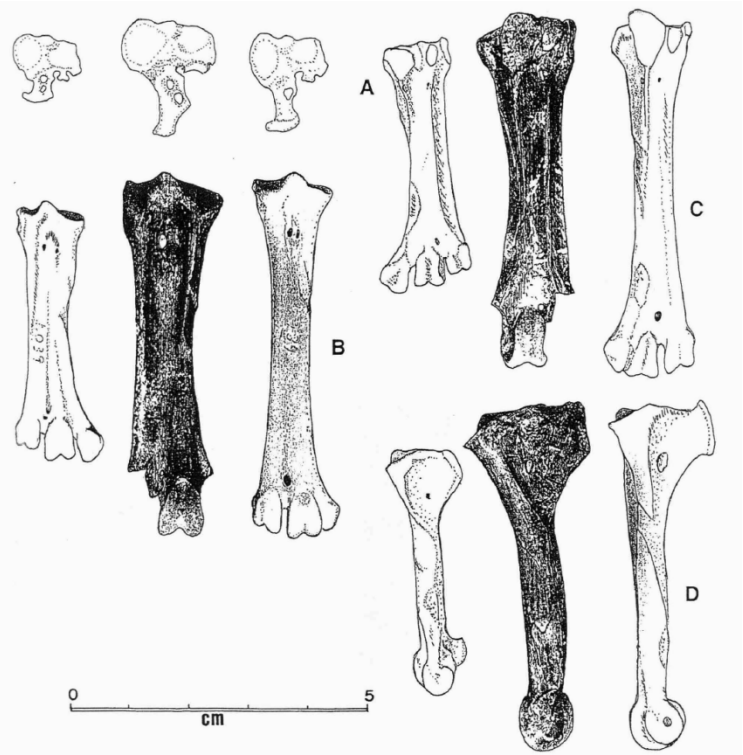

Comparison of right tarsometatarsi of species of Anhingidae and Phalacrocoracidae: *Anhinga anhinga* (left), *Meganhinga chilensis* n.g. n.sp. (middle) and *Phalacrocorax carbo* (right), in cranial (A); anterior (B); posterior (C); and medial (D) views.

Phalacrocoracidae

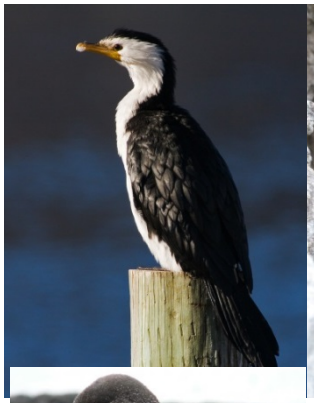

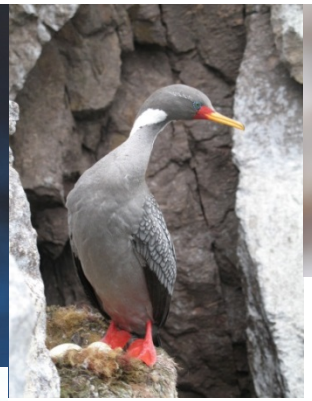

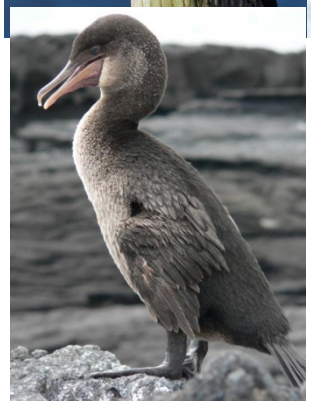

bransfieldensis[c]
bransfieldensis
melanogenis
nivalis
purpurascens
verrucosus
atriceps[b]
georgianus
albiventer[a]
campbelli
colensoi
chalconotus
onslowi
carunculatus
ranfurlyi
bougainvillii
magellanicus
auritus
brasilianus
harrisi
aristotelis
carbo carbo
carbo novaehollandiae
capillatus
carbo lucidus
carbo sinensis
capensis
fuscescens
varius
sulcirostris
featherstoni
punctatus
nigrogularis
neglectus
pelagicus
urile
penicillatus
gaimardi
melanoleucos
pygmaeus

Leucocarbo
Nannopterum
Gulosus
Phalacrocorax
Urile
Poikilocarbo
Microcarbo

0.02 substitutions/site

Fig. 1. The Bayesian phylogram for the combined dataset (outgroups not shown, for the phylogram including the outgroups see Fig. S1). The numbers associated with the branches represent posterior probabilities from Bayesian MCMC searches, ML bootstrap values (bold), and equally weighted MP bootstrap values. Bootstrap values ⩾50% are shown. Branch and number color represent the Bayesisan posterior probability on a gradient of red (very high) to blue (low) as applied in FigTree 1.3.1 (tree.bio.ed.ac.uk/software/figtree/). Black branches are terminal. The asterisks indicate strong support from all of these measures, i.e., a Bayesian posterior probability of 0.95 and above and bootstrap values of 90% and above. Our classification is shown. [a–c]As in Table 2. (For interpretation of the references to color in this figure legend, the reader is referred to the web version of this article.)

Registro de Phalacrocoracidae en Chile

Phalacrocorax sp. Formación Bahía Inglesa
(Mioceno medio-Plioceno)

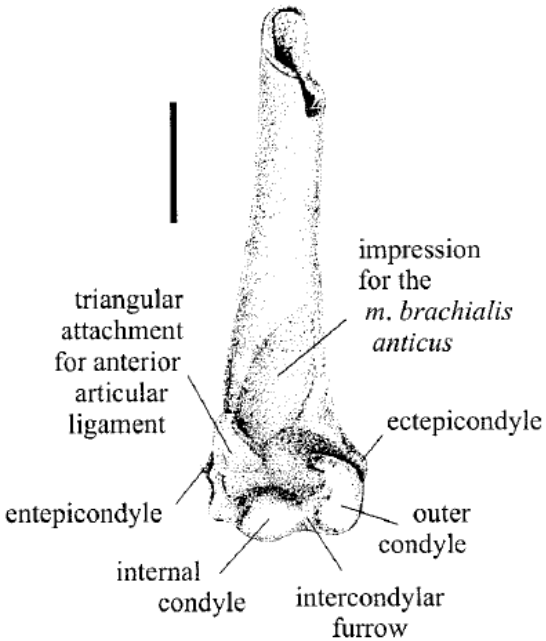

FIGURE 4. *Phalacrocorax* sp. distal left humerus (UOP/01/01) in palmer aspect. Scale bar equals 10 mm.

Phalacrocorax sp. Formación Horcón
(Plioceno)

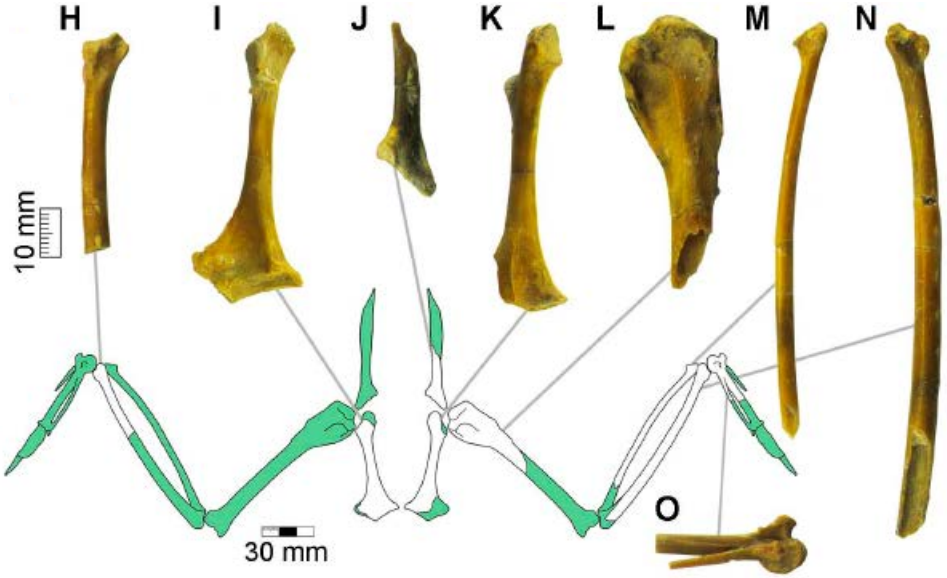

Figure 4. Fossil shearwater and cormorant from the Horcon Formation. Proximal fragment of a fossil left tarsometatarsus assigned as *Puffinus* cf. *griseus* (SGO-PV 21490) in (**A**) dorsal, (**C**) plantar and (**E**) proximal views; and (**F**) sketch showing the details of the proximal surface. Proximal section of the same element in the extant great shearwater (*Puffinus gravis*) in (**B**) dorsal, (**D**) plantar and (**G**) proximal views. Partial wings and pectoral girdle of the small cormorant *Phalacrocorax* sp. (SGO-PV 21443): (**H**) fragment of right ulna in dorsal view; (**I**) right coracoid in dorsal view; (**J**) proximal fragment of left scapula in medial; (**K**) left coracoid in ventral view; (**L**) proximal fragment of left humerus in caudal view; (**M**) left radius lacking of proximal end in ventral view; (**N**) left ulna lacking of proximal end in ventral view; and (**O**) proximal fragment of left carpometacarpus in ventral view.

Pelecaniformes

El nuevo orden Pelecaniformes integra a *Pelecanus*, *Balaeniceps*, *Scopus*, Threskiornithidae y Ardeidae.

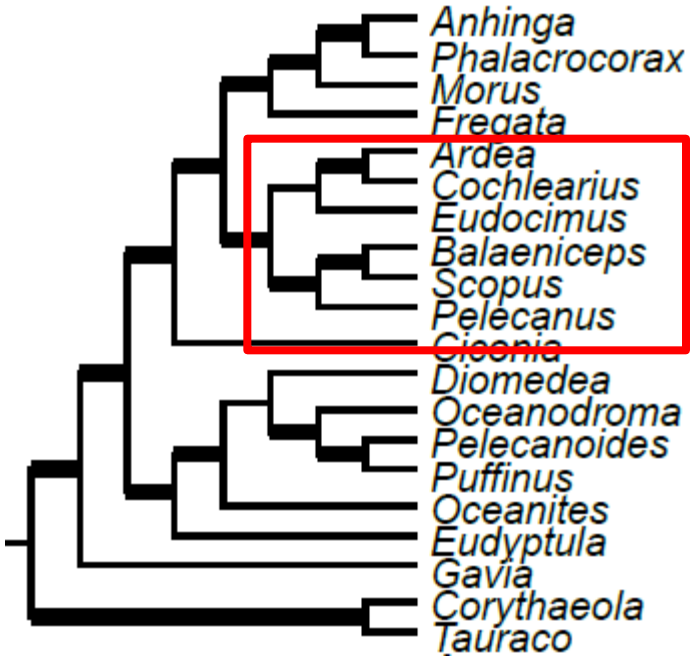

Pelecaniformes

Threskiornithidae
(13 géneros)

Ardeidae
(18 géneros)

Scopidae
Scopus umbretta

Balaenicipitidae
Balaeniceps rex

Pelecanidae
Pelecanus spp.

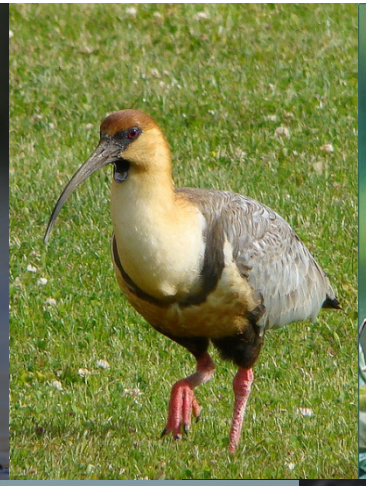

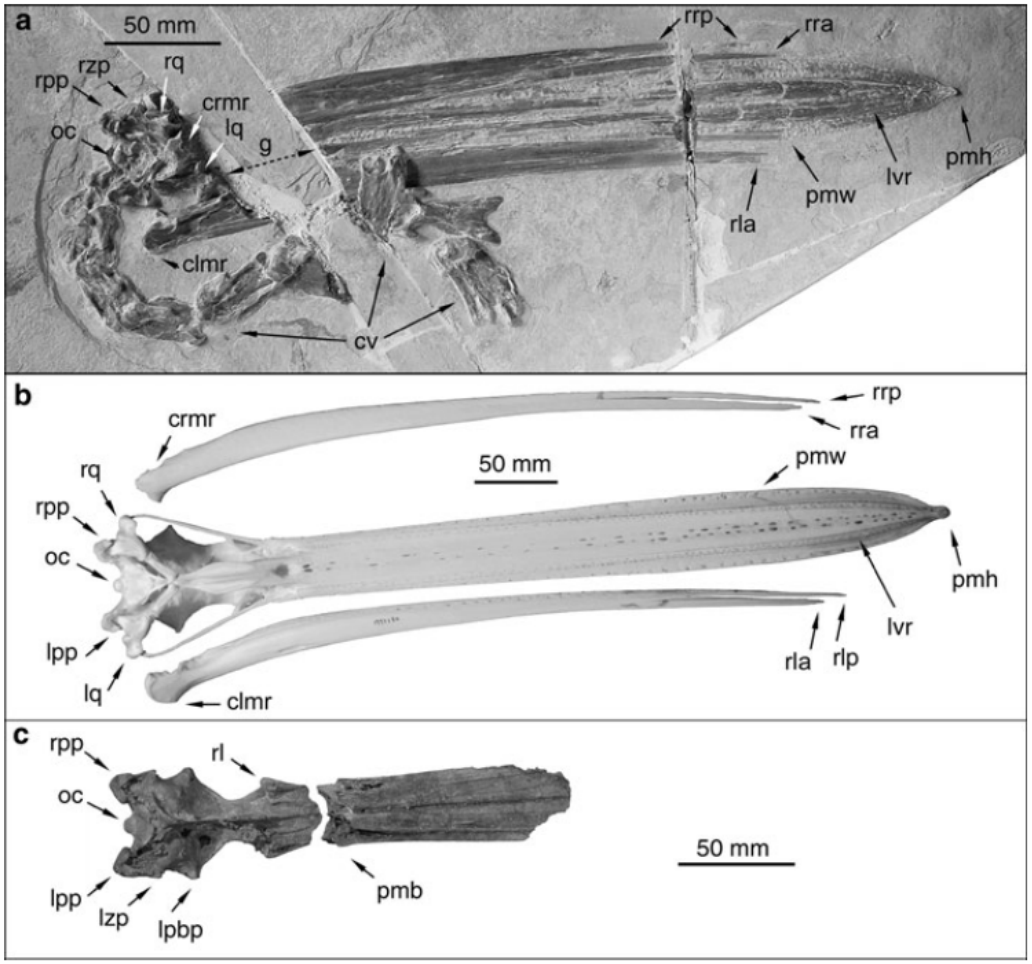

Fig. 1 Early Oligocene fossil pelican from the Luberon (France) compared to modern and early Miocene specimen. **a** Fossil *Pelecanus* sp. NT-LBR-039, on slab, **b** extant *P. onocrotalus* (LAC.1997.186, Muséum National d'Histoire Naturelle, Paris), **c** fossil *Miopelecanus gracilis* (ML.StG.1438 and ML.StG.3556, C.C.E.C.—Centre de Conservation et d'Etude des Collections—du Musée des Confluences de Lyon, France). In all specimens, skull and rostrum are in ventral view, left hemimandible in medial view, and right one in lateral view. In (**a**), the fossil quadrates and hemimandibles show post-mortem displacement, the latter partly overlying skull and rostrum; **g** reconstituted gap between the preserved fossil parts of NT-LBR-039. In (**c**), the distance between the two fossil parts of *M. gracilis* is estimated. The symphysial part of the mandible (dentaries and splenials) is dissociated from the angulars and prearticulars, and it is not preserved on the slab with the rest of the fossil (**a**) and not shown here for the modern specimen (**b**). *clmr* and *crmr* caudal extremities of left and right mandibular rami; *cv* 10–11 cervical vertebrae; *rl* right lacrymal; *oc* occipital condyle; *lpbp* left postorbital process; *pmb* premaxillary base; *pmh* premaxillary hook; *pmw* level of premaxillary maximal width measured; *lpp* and *rpp* left and right paroccipital processes; *lq* and *rq* left and right quadrates; *lvr* left ventral ridge of premaxillary; *lzp* and *rzp* zygomatic process of left and right squamosals; *rla* and *rra* rostral extremities of left and right angulars; *rlp* and *rrp* rostral extremities of left and right prearticulars

Registro de Ardeidae en Chile

Journal of Paleontology, 84(6), 2010, p. 1061–1070

0022-3360/10/0084-1061$03.00

EOCENE BIRDS FROM THE WESTERN MARGIN OF SOUTHERNMOST SOUTH AMERICA

MICHEL A. SALLABERRY,[1] ROBERTO E. YURY-YÁÑEZ,[1] RODRIGO A. OTERO,[1,2] SERGIO SOTO-ACUÑA,[1] AND TERESA TORRES G.[3]

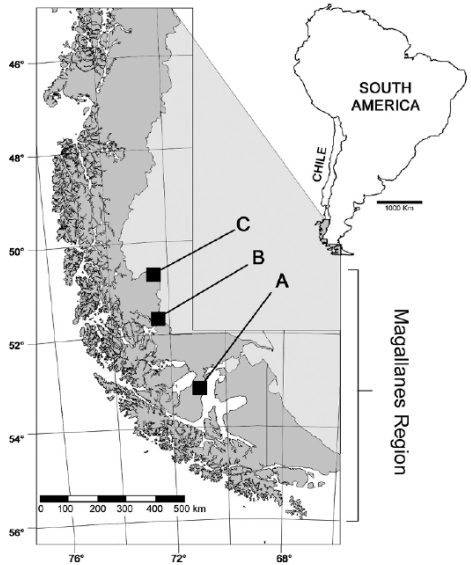

FIGURE 1—Map of the studied localities in the Magallanes Region of southernmost Chile, where fossil birds were recovered A) Rio de Las Minas. B) Sierra Dorotea. C) Sierra Baguales.

Fragmento proximal de tibiotarso conferido a Ardeidae indet. (garzas) Destaca por su gran tamaño.

FIGURE 7—Differences in the tibiotarsi from some aquatic birds. *1*, Humboldt Penguin, *Spheniscus humboldti* (Spheniscidae, Sphenisciformes); *2*, Great Grebe, *Podiceps major* (Podicipedae, Podicipediformes); *3*, Peruvian Booby, *Sula variegata* (Sulidae, Pelecaniformes); *4*, Sooty Shearwater, *Puffinus griseus* (Procellariidae, Procellariiformes); *5*, Red-fronted Coot, *Fulica rufifrons* (Rallidae, Gruiformes); *6*, Crested Duck, *Lophonetta specularoides* (Anatidae, Anseriformes); *7*, Franklin's Gull, *Larus pipixcan* (Laridae, Charadriiformes). Scale bar = 1 cm.

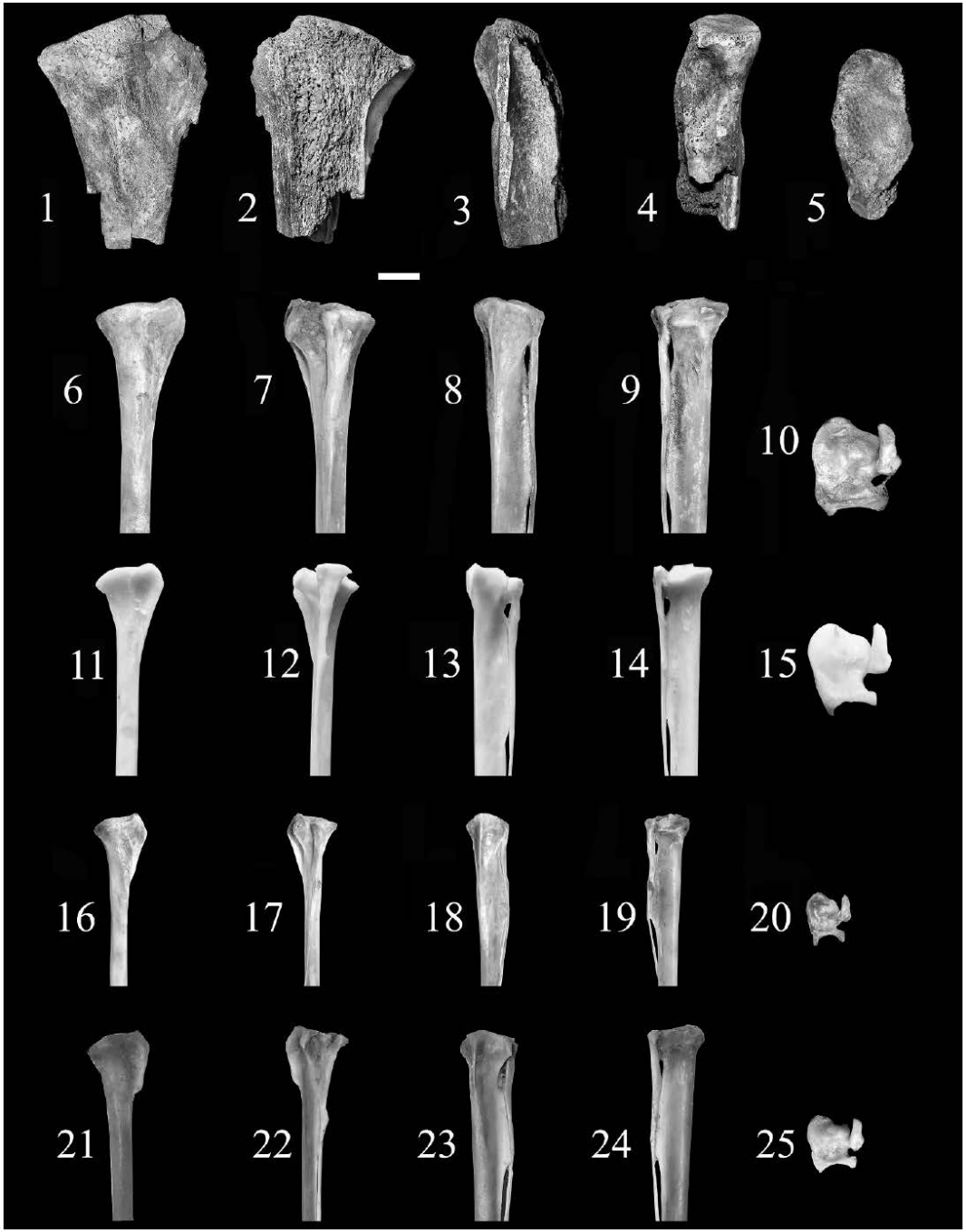

FIGURE 6—Comparison between fossil Egret from Sierra Dorotea and the extant egrets and herons present in Chile. Ardeidae gen. et sp. indet. Proximal portion of left tibiotarsus (SGO.PV.6584); *1*, lateral internal view; *2*, lateral external view; *3*, cranial view; *4*, caudal view; *5*, proximal view; left

Ciconiformes

Incluye solamente a **Ciconidae** (cigueñas y marabúes)

Sphenisciformes y Procellariiformes

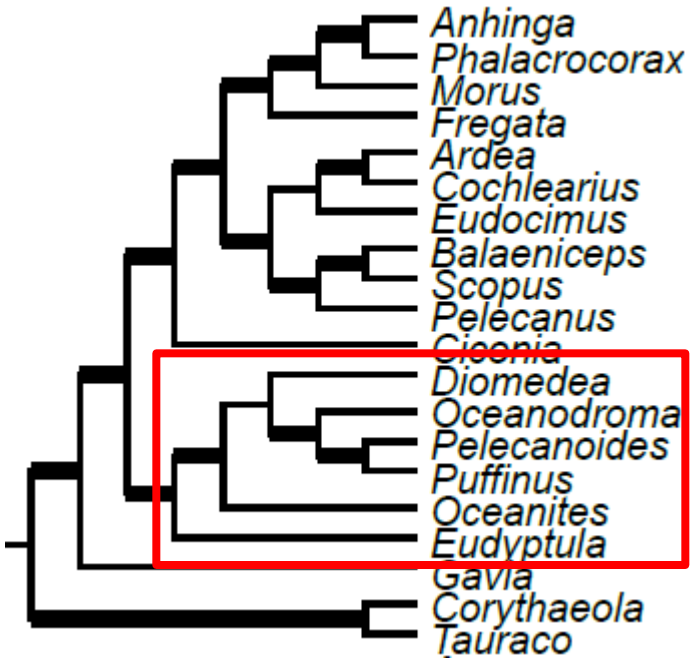

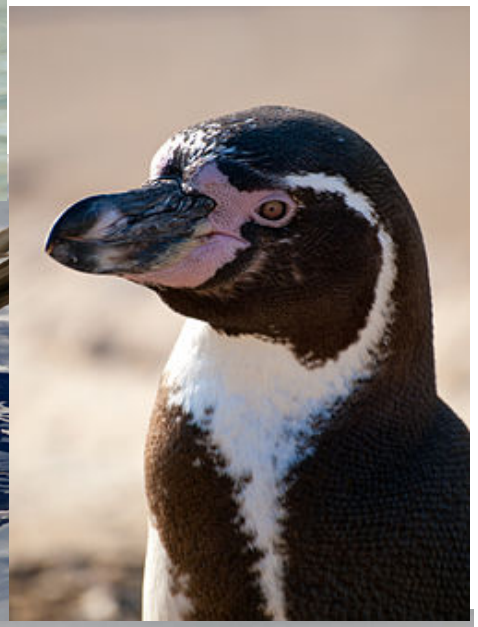

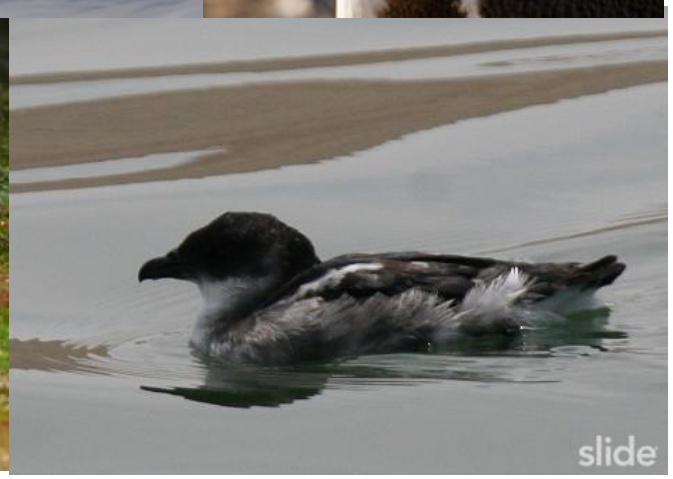

Sphenisciformes

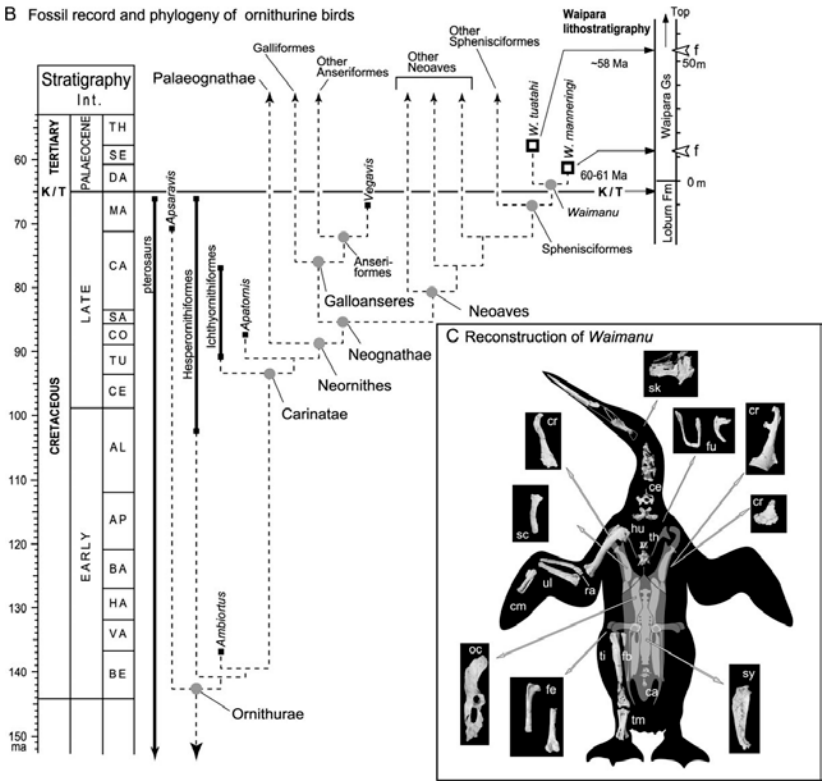

Waimanu, pingüino fósil más antiguo
(Paleoceno, Nueva zelanda)(Ksepka et al., 2006)

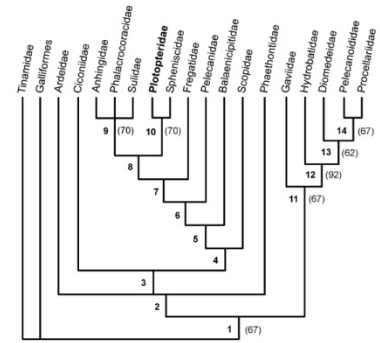

Fig. 1. Strict consensus tree of six most parsimonious trees (length = 176, CI = 0.44, RC = 0.29) resulting from an analysis of the character matrix in Appendix 2. The nodes are characterized by the following synapomorphies that were found in all most parsimonious trees (if not indicated otherwise, character transformation is 0 → 1; asterisked characters have CI = 1.0; superscript letters indicate character that were only found in either the ACCTRAN or DELTRAN transformation mode): **1** – 13, 19^{A}, 29^{A}, 31 (1 → 0); **2** – 6, 38, 51^{A}, 53; **3** – 7, 8, 9, 34, 61; **4** – 1, 5^{D}, 10, 27, 47, 62*; **5** – 3, 4 (0 → 2)*, 25^{A}, 28 (0 → 2), 35^{A}, 39 (0 → 2/1 → 2); **6** – 16^{A}, 19 (1 → 0)^{A}, 26^{A} *, 31^{A}, 33^{A}, 45^{A}, 52, 54 (1 → 2)^{A}, 56 (0 → 2), 57, 59, 63, 64; **7** – 8 (1 → 0), 9 (1 → 0), 16^{D}, 25 (1 → 0)^{A}, 26^{D}*, 29 (1 → 0)^{A}, 35^{D}, 46^{A}, 47 (1 → 0), 49, 51 (1 → 0); **8** – 7 (1 → 0)^{A}, 15^{A}, 19^{A}, 21^{A}*, 28 (2 → 1), 33^{D}, 34 (1 → 0)^{A}, 43*, 45^{D}; **9** – 11*, 12, 14, 20*, 21^{D}*, 22^{A}, 25^{A}, 31^{D}, 46 (1 → 0)^{A}, 65, 66*, 67*, 68^{A}; **10** – 3 (1 → 0)^{A}, 6 (1 → 0)^{A}, 10 (1 → 0)^{A}, 32*, 36*, 37*, 41*, 42*, 46^{D}, 48*, 50*, 53 (1 → 0)^{A}, 56 (2 → 0)^{A}, 58^{A}, 63 (1 → 0)^{A}; **11** – 18, 29^{D}, 44*, 52, 54 (1 → 4), 57^{D}; **12** – 1, 4*, 5, 30*, 40*, 58 (0 → 2/1 → 2); **13** – 24, 39^{A}; **14** – 13 (1 → 0), 17. Bootstrap values above 50% are indicated in parentheses to the right of the internodes

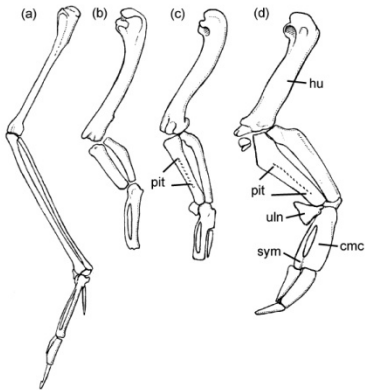

Fig. 2. Right wing in comparison: (a) *Phalacrocorax carbo* (Phalacrocoracidae); (b) *Mancalla cedrosensis* (Mancallinae, Charadriiformes, after Howard 1971); (c) *Copepteryx hexeris* (Plotopteridae, after Olson and Hasegawa 1979, 1996; Goedert and Cornish 2002 [carpometacarpus]); (d) *Eudyptula minor* (recent, Spheniscidae). Abbreviations: cmc, carpometacarpus; hu, humerus; pit, row of pits on ulna for attachment of feather quills; sym, symphysis metacarpalis distalis; uln, os carpi ulnare. Not to scale and slightly schematic; in (b) and (c) the distal phalanges are not shown

in modern penguins, ulna and radius of plotopterids strongly resemble the corresponding elements of a late Paleocene/early Eocene penguin figured by Fordyce and Jones (1986, 1990).

A highly characteristic derived peculiarity of the ulna of plotopterids is the presence of a row of marked pits for the attachment of feather quills (Olson 1980, Fig. 3; Olson and

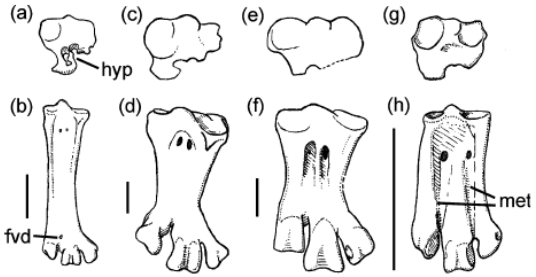

Plotopteridae (Eoceno-Mioceno)
Mayr (2004)

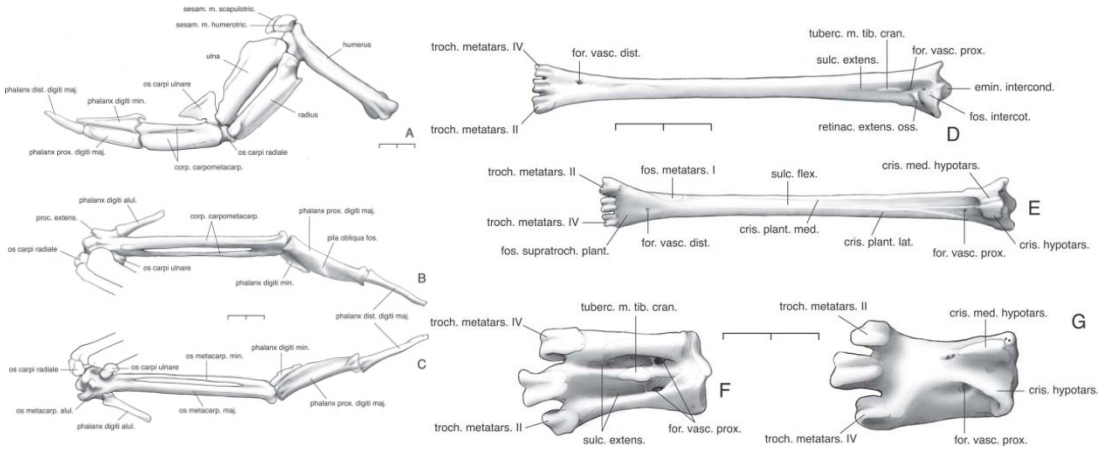

Registro de Spheniscidae en Chile

Journal of Paleontology, 84(6), 2010, p. 1061–1070

0022-3360/10/0084-1061$03.00

EOCENE BIRDS FROM THE WESTERN MARGIN OF SOUTHERNMOST SOUTH AMERICA

MICHEL A. SALLABERRY,[1] ROBERTO E. YURY-YÁÑEZ,[1] RODRIGO A. OTERO,[1,2] SERGIO SOTO-ACUÑA,[1] AND TERESA TORRES G.[3]

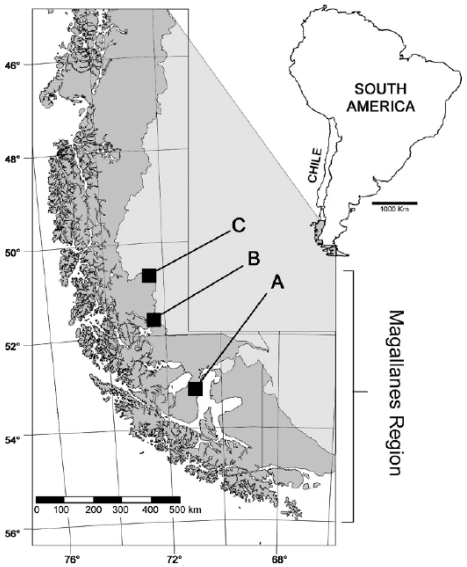

FIGURE 1—Map of the studied localities in the Magallanes Region of southernmost Chile, where fossil birds were recovered A) Río de Las Minas. B) Sierra Dorotea. C) Sierra Baguales.

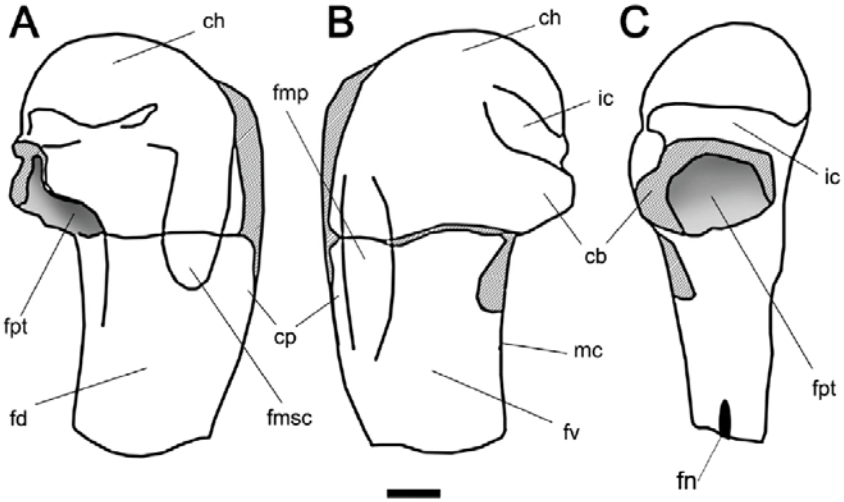

FIGURE 4—Anatomical nomenclature of penguin humerus. cb: crista bicipitalis. ch: caput humeri. cp: crista pectoralis. f: foramen. fd: facies dorsalis. fmsc: facies musculi supracoracoideus. fn: foramen nutricium fpt: fossa pneumotricipitalis. ic: incisura capitis. mc: margo caudalis.

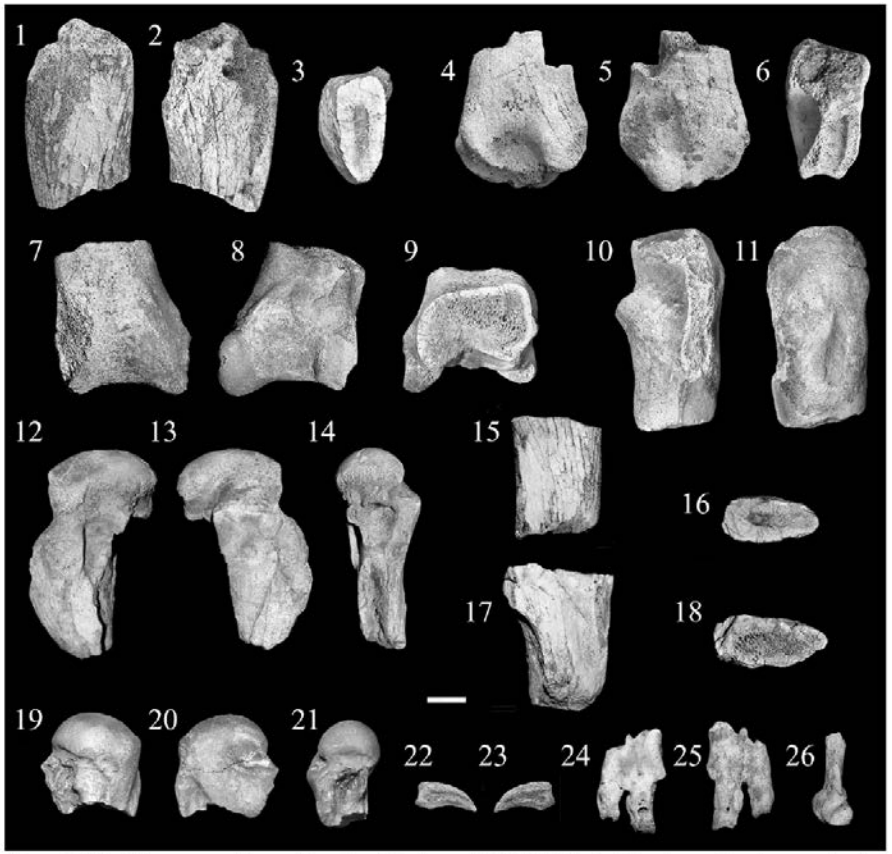

FIGURE 2—Spheniscidae gen., et sp. indet., medial portion of right humerus (SGO.PV.6588). *1*, dorsal view; *2*, ventral view; *3*, cross section, distal portion of left humerus (SGO.PV.6587); *4*, dorsal view; *5*, ventral view; *6*, cross section, distal portion of left tibiotarsus (SGO.PV.6590); *7*, posterior view; *8*, anterior view; *9*, cross section, proximal portion of left femur (SGO.PV.6589); *10*, anterior view; *11*, lateral left view, proximal portion of left humerus with part of the diaphysis (SGO.PV.6650); *12*, dorsal view; *13*, ventral view; *14*, cranial view, two fragments of humerus, preserving only the diaphysis (SGO.PV.6655); *15*, lateral view; *16*, cross section; *17*, lateral view; *18*, cross section, proximal portion of right humerus (SGO.PV.6649); *19*, dorsal view; *20*, ventral view; *21*, cranial view, isolated ungual phalanx (SGO.PV.6652); *22*, *23*, incomplete left tarsometatarsus (SGO.PV.6653); *24*, plantar view; *25*, dorsal view; *26*, lateral view. Scale bar = 1 cm.

FIGURE 3—*Palaeeudyptes* sp. Right humerus (SGO.PV.6585): *1*, caudal view; *2*, cranial view; *3*, side view; *4*, proximal view of the articular head; *5*, cross section view of the diaphysis. Sierra Dorotea, southernmost Chile. Río Turbio Formation, middle to late Eocene. Scale bar = 1 cm.

Registro de Spheniscidae en Chile

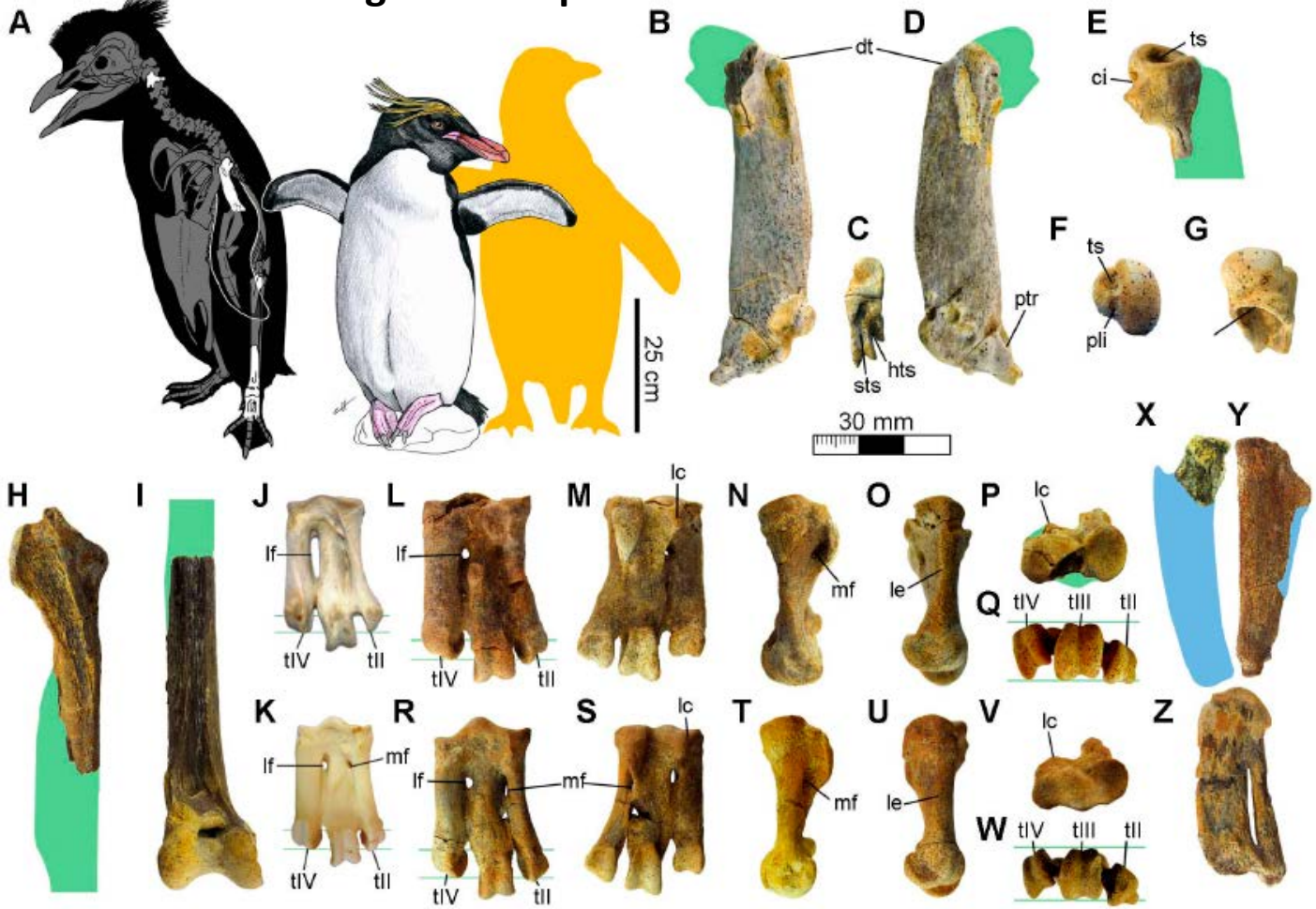

Figure 1. Fossil penguins from the Horcon Formation. A. Skeletal reconstruction of *Eudyptes calauina* sp. nov. showing the identified elements; and size comparison with the Macaroni penguin *E. chrysolophus* and the Yellow-eyed penguin *Megadyptes antipodes* (yellow silhouette). Referred specimens: left humerus (SGO-PV 21451) in (**B**) cranial, (**C**) distal and (**D**) caudal views; proximal fragment of left humerus (SGO-PV 21449) in (**E**) cranial, (**F**) proximal and (**G**) ventral views; (**H**) proximal fragment of right tibiotarsus (SGO-PV 21447) in cranial view; and (**I**) distal portion of right tibiotarsus (SGO-PV 21488) in cranial view. Tarsometatarsus of Humboldt penguin *Spheniscus humboldti* (**J**) and Northern Rockhopper penguin *E. moseleyi* (**K**). Holotype: right tarsometatarsus attributed to an adult (SGO-PV 21487) in (**L**) dorsal, (**M**) plantar, (**N**) medial, (**O**) lateral, (**P**) proximal and (**Q**) distal views. Paratype: right tarsometatarsus attributed to a subadult (SGO-PV 21444) in (**R**) dorsal, (**S**) plantar, (**T**) medial, (**U**) lateral, (**V**) proximal and (**W**) distal views. Spheniscidae indet.: (**X**) proximal fragment of right radius (SGO-PV 21450) in ventral view; (**Y**) right ulna (SGO-PV 21455) in ventral view; and (**Z**) right carpometacarpus (SGO-PV 21454) in ventral view. Silhouettes (green for *E. calauina*, blue for Spheniscidae indet.) based on complementary specimens attributed to the same species or living relatives. **Abbreviations:** ci, capital incisure; dt, dorsal tubercle; hts, humerotricipital sulcus; lc, lateral hypotarsal crest; le, lateral edge of the metatarsi IV; lf, lateral proximal vascular foramen; mf, medial proximal vascular foramen; pli, pit for ligament insertion; ptr, posterior trochlear ridge; sts, scapulotricipital sulcus; tf, tricipital fossa; tII, trochlea metatarsi II; tIII, trochlea metatarsi III; tIV, trochlea metatarsi IV; ts, transverse sulcus.

Registro de Procellariiformes en Chile

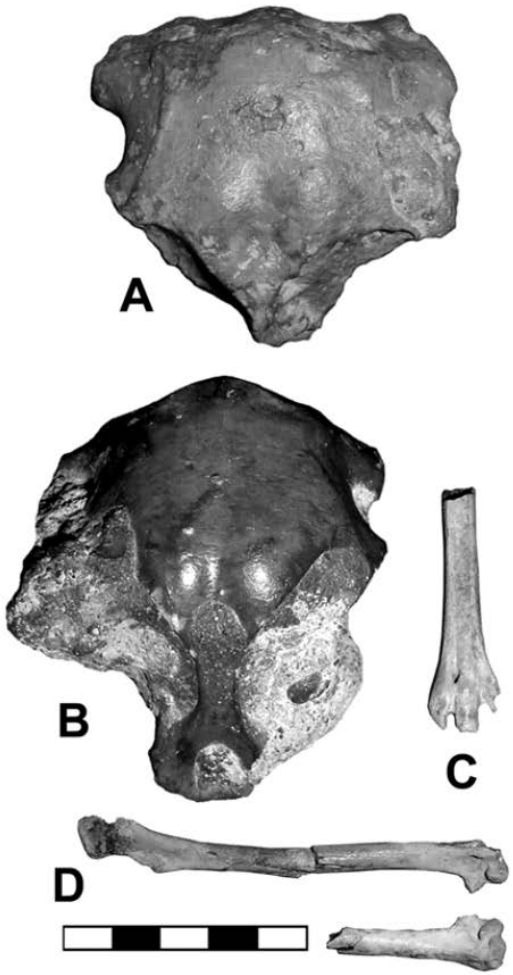

Fig.4- Procellariiformes. Diomedeidae: (A) cf. *Diomedea*; partial skull (MPC1011) and (B) aff. *Thalassarche*?; partial skull (MPC1012); both from Bahía Inglesa Formation (Late Miocene). (C) Diomedeidae indet.; distal portion of right tarsometatarsus (MPC1018) from Coquimbo Formation (Late Miocene). Procellariidae: (D) Right humerus (MPC1013) and left distal extreme of humerus (MPC1014) from Bahía Inglesa Formation (Late Miocene). Scale bar = 5cm.

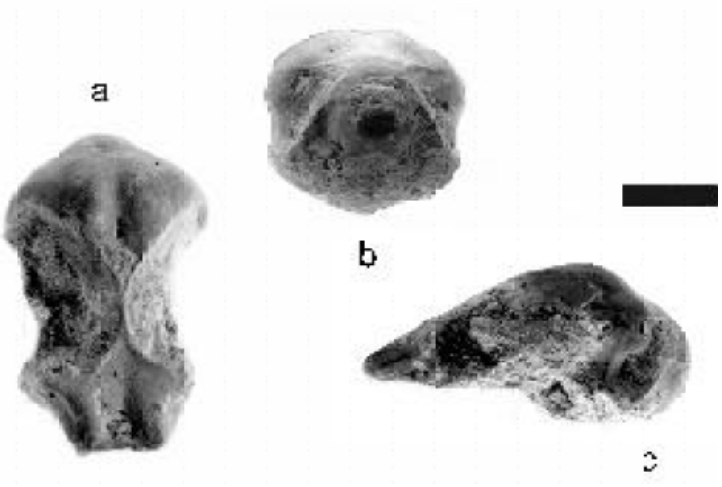

Pachyptila sp. MPC-601, Late Miocene (Tortonian), Bahía Inglesa Formation, Caldera. a) Dorsal view; b) Posterior view; and c) Left lateral view. Scale bar = 1 cm

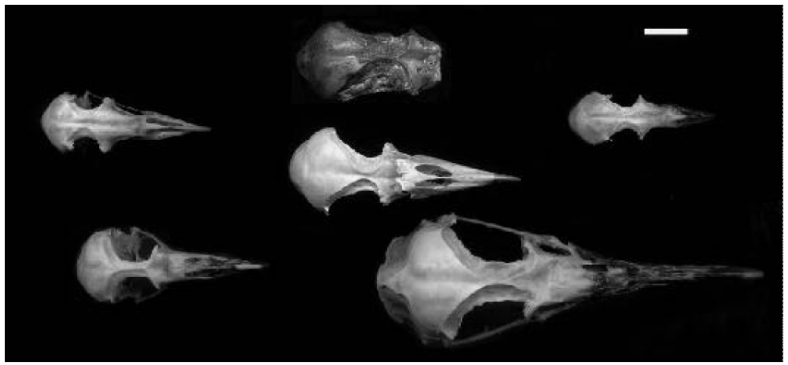

Lower left	*Pelecanoides garnotii* (Lesson)
Upper center	*Pachyptila* sp. (Gmelin) (MPC-601)
Middle center	*Pachyptila belcheri* (Mathews)
Upper left	*Oceanites oceanicus* (Kuhl)
Upper left	*Fregetta* tropica (Gould)
Lower left	*Puffinus griseus* (Gmelin)

Figure 4. Fossil shearwater and cormorant from the Horcon Formation. Proximal fragment of a fossil left tarsometatarsus assigned as *Puffinus* cf. *griseus* (SGO-PV 21490) in (**A**) dorsal, (**C**) plantar and (**E**) proximal views; and (**F**) sketch showing the details of the proximal surface. Proximal section of the same element in the extant great shearwater (*Puffinus gravis*) in (**B**) dorsal, (**D**) plantar and (**G**) proximal views. Partial wings

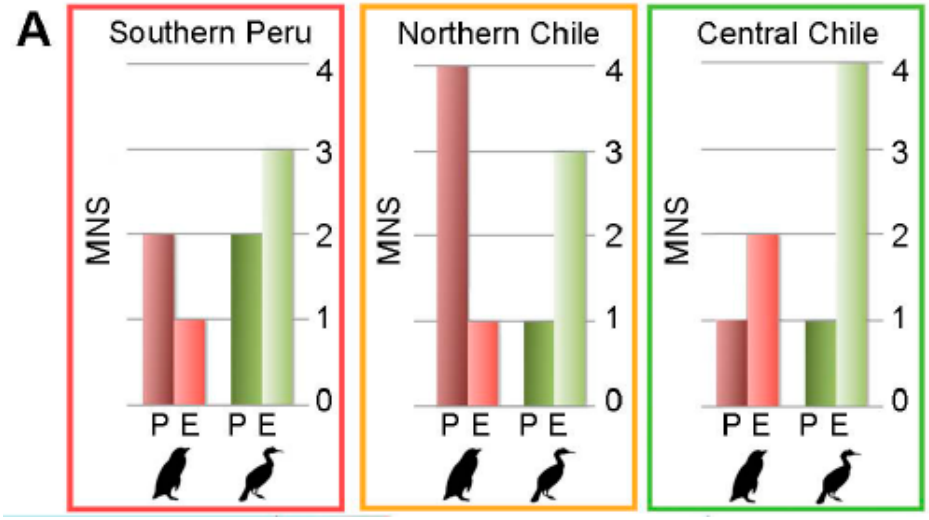

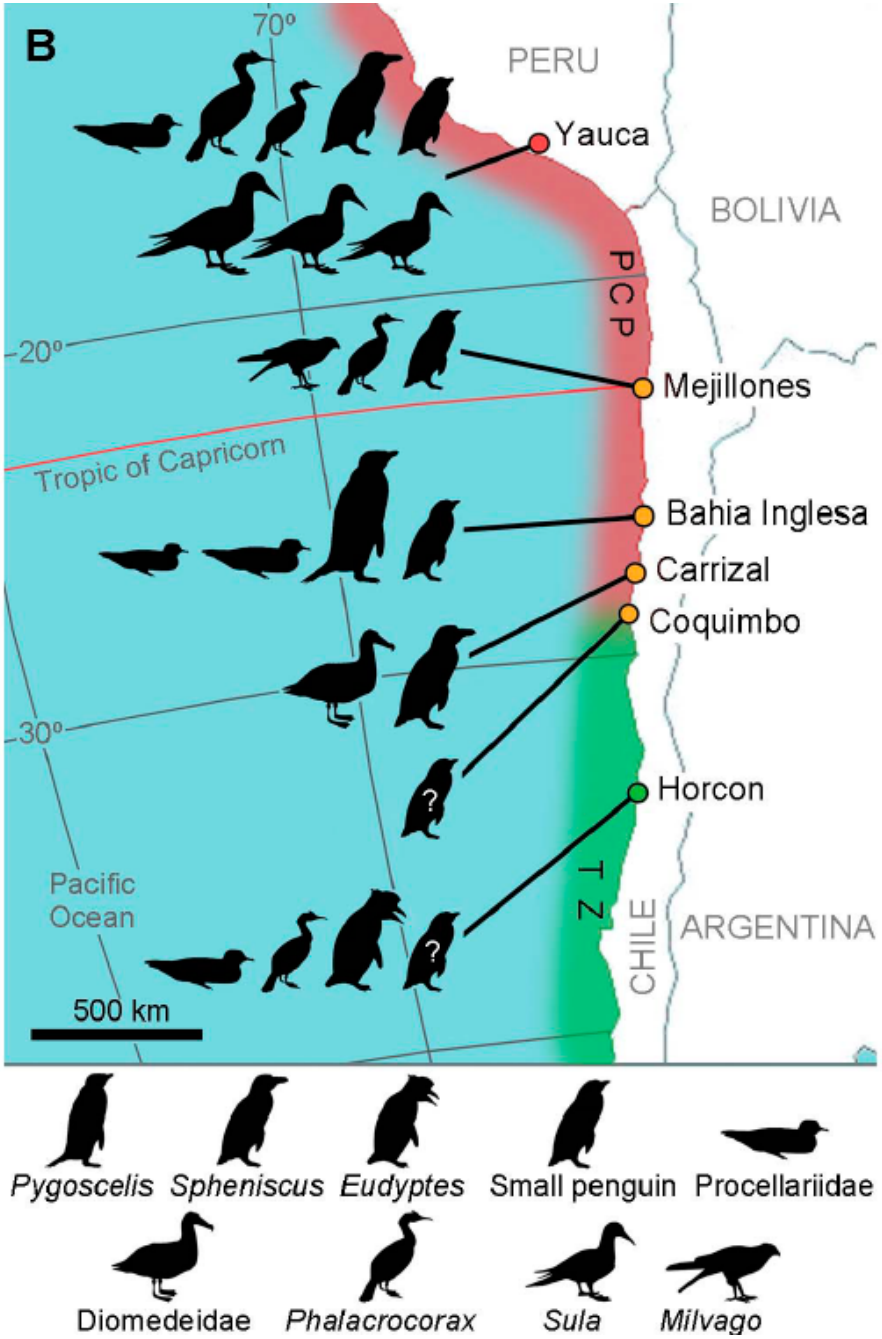

Figure 5. The Pliocene record of birds in the Southeast Pacific. **A.** Comparison between the Pliocene (P) and extant (E) richness of penguins and cormorants for each major area represented as minimum number of species (MNS); **B.** Map showing the main fossiliferous localities, the zoogeographical regions (PCP, Peruvian–Chilean Province; TZ, Transition Zone) and the species recorded.

doi:10.1371/journal.pone.0090043.g005

Inopinaves

Clado de Neoaves sustentado por evidencia molecular (a través de un análisis genómico con un amplio muestreo filogenético, ver Prum et al., 2015) e incluye a Opisthocomiformes (Hoatzin) y Telluraves (grupo exclusivo de aves continentales).

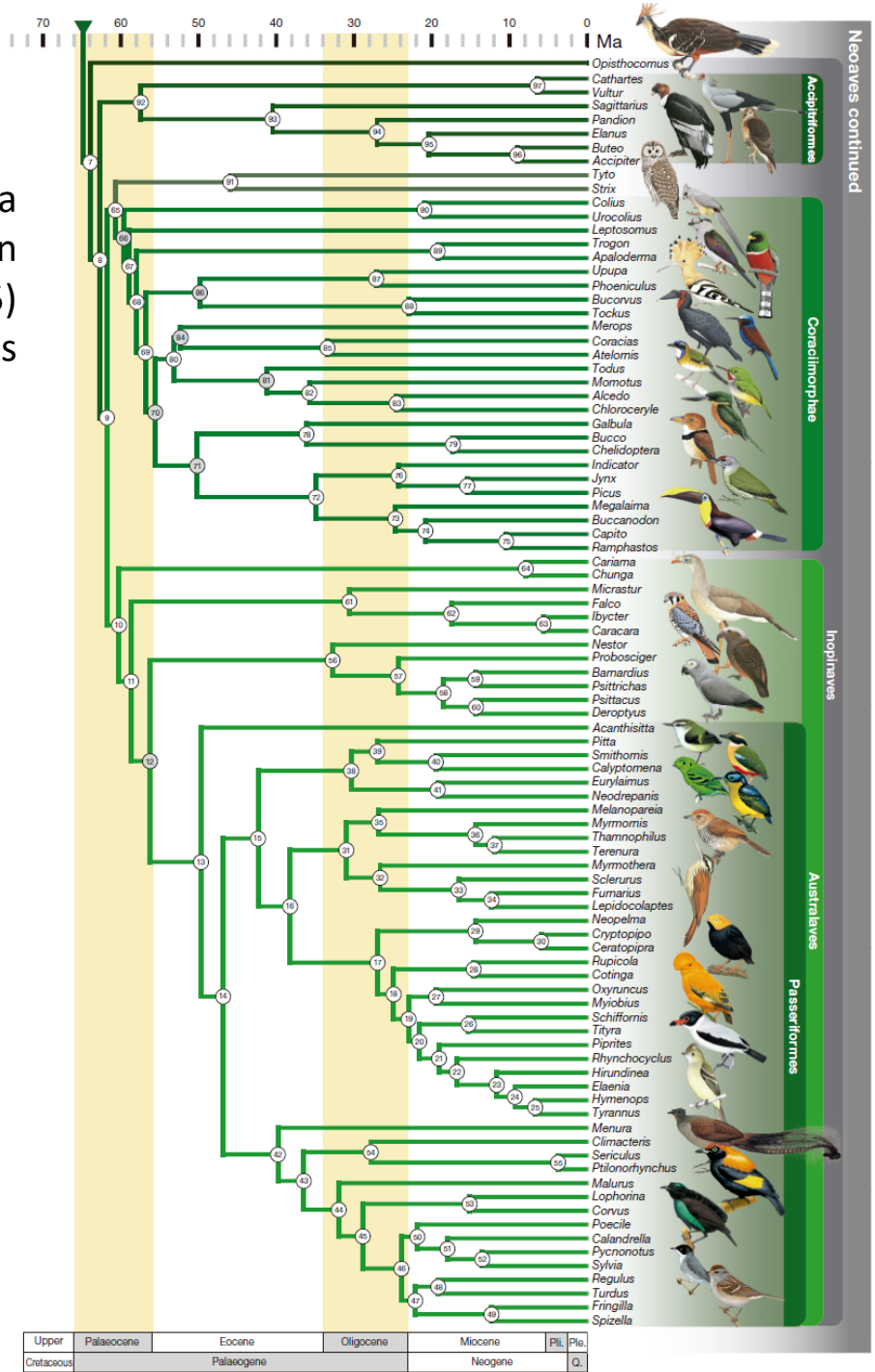

Opisthocomiformes

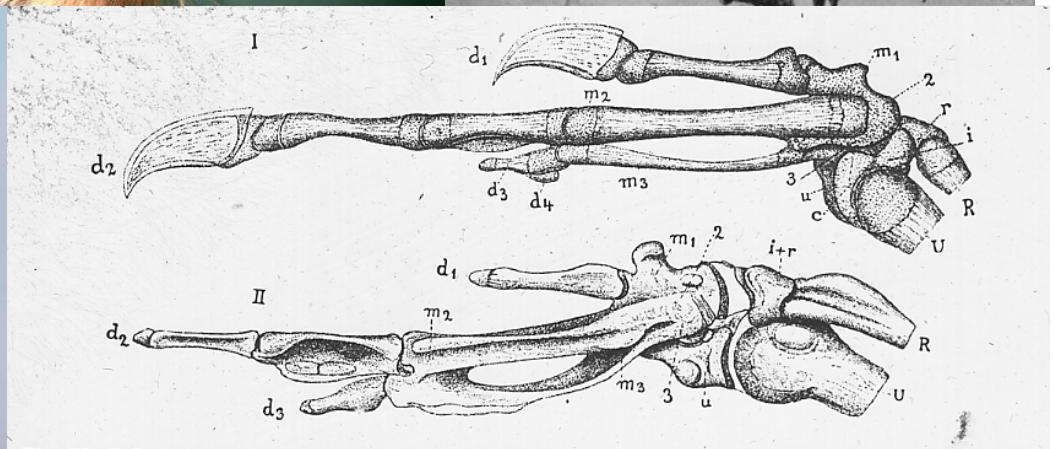

Fig. 72. I Left hand of Hoatzin-embryo, II left hand of adult Hoatzin after Parker; c centrale, d1—d4 first to fourth fingers, i intermedium, m1, m2, m3 the three metacarpals, R radius, r radiale, U ulna, u ulnare, 2, 3 distal carpals. I c. 4/1 nat. size, II nat. size.

Telluraves

Clado conocido previamente como “land birds” o “core landbirds”, sustentado por evidencia molecular a través de análisis genómicos de gran escala. Incluye Australaves (Paserios, loros, rapaces falconiformes y seriemas) y Afroaves (rapaces accipitriformes, búhos, carpinteros, trogones, martín pescador).

En la base de ambas ramas (Australaves y Afroaves) se ubican algunos linajes de aves depredadoras. Esto sugiere un ancestro común depredador para todas las Telluraves.

Afroaves

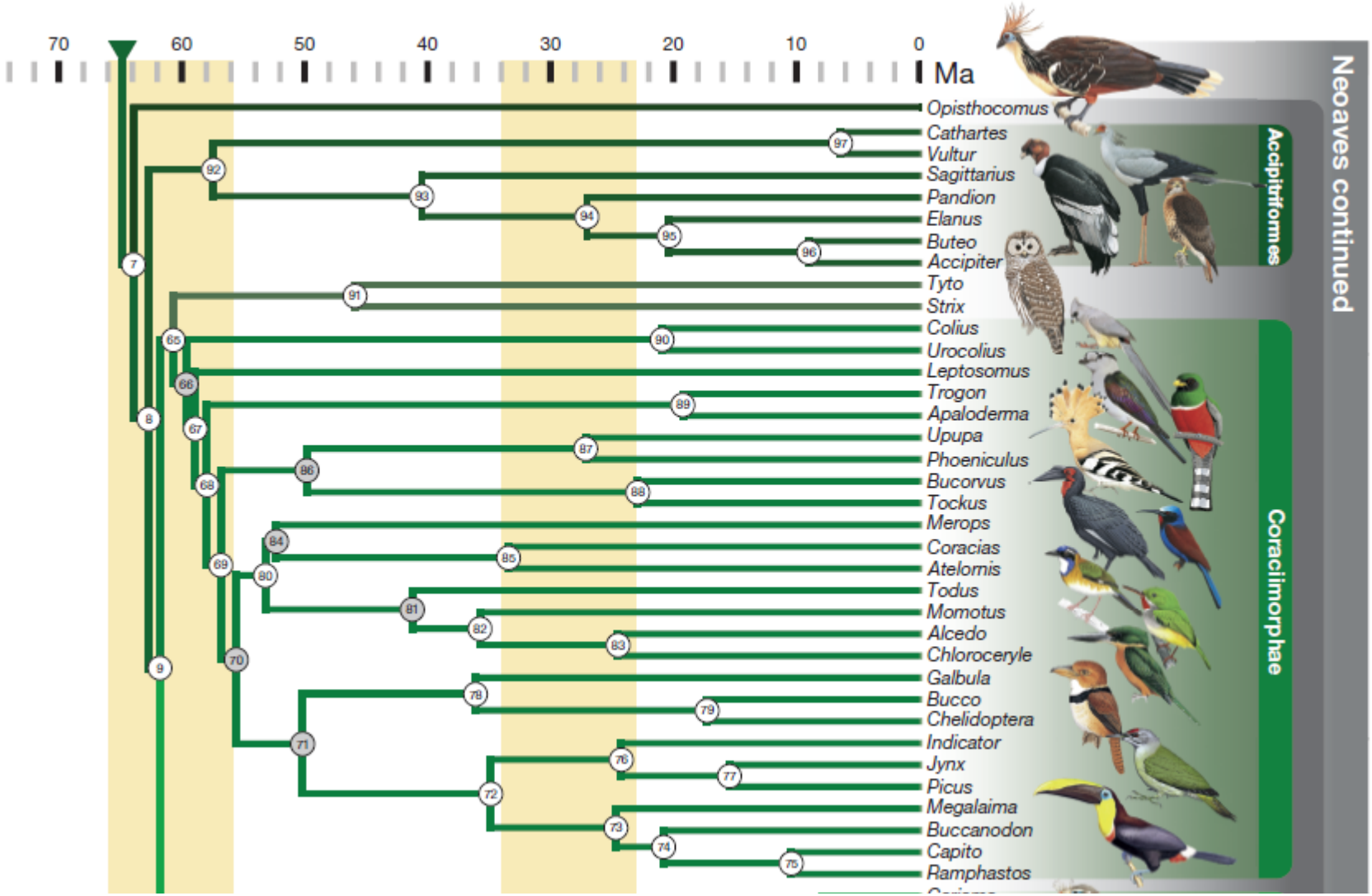
70
60
50
40
30
20
10
0
Ma
Neoaves continued
Accipitriformes
Coracimorphae
Opisthocomus
Cathartes
Vultur
Sagittarius
Pandion
Elanus
Buteo
Accipiter
Tyto
Strix
Colius
Urocolius
Leptosomus
Trogon
Apaloderma
Upupa
Phoeniculus
Bucorvus
Tockus
Merops
Coracias
Atelornis
Todus
Momotus
Alcedo
Chloroceryle
Galbula
Bucco
Chelidoptera
Indicator
Jynx
Picus
Megalaima
Buccanodon
Capito
Ramphastos

Coraciimorphae

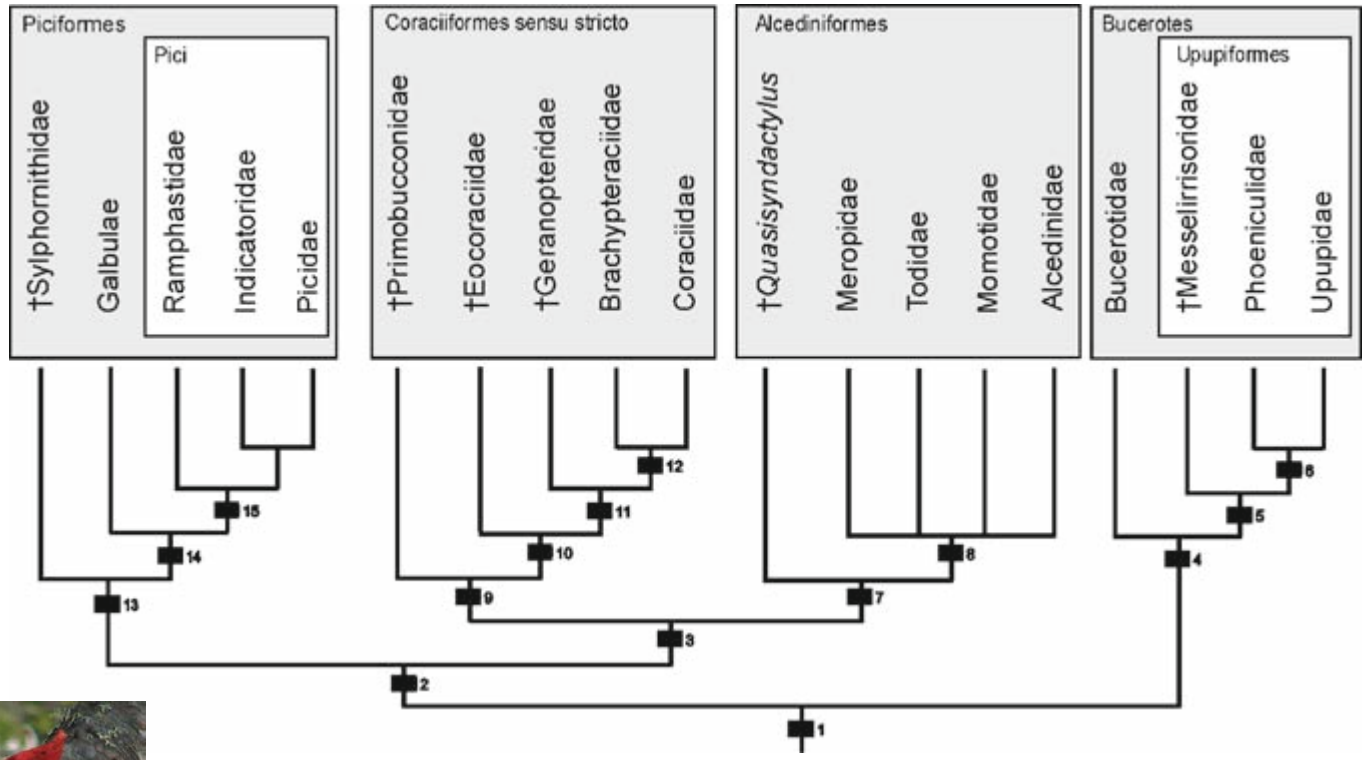

Australaves

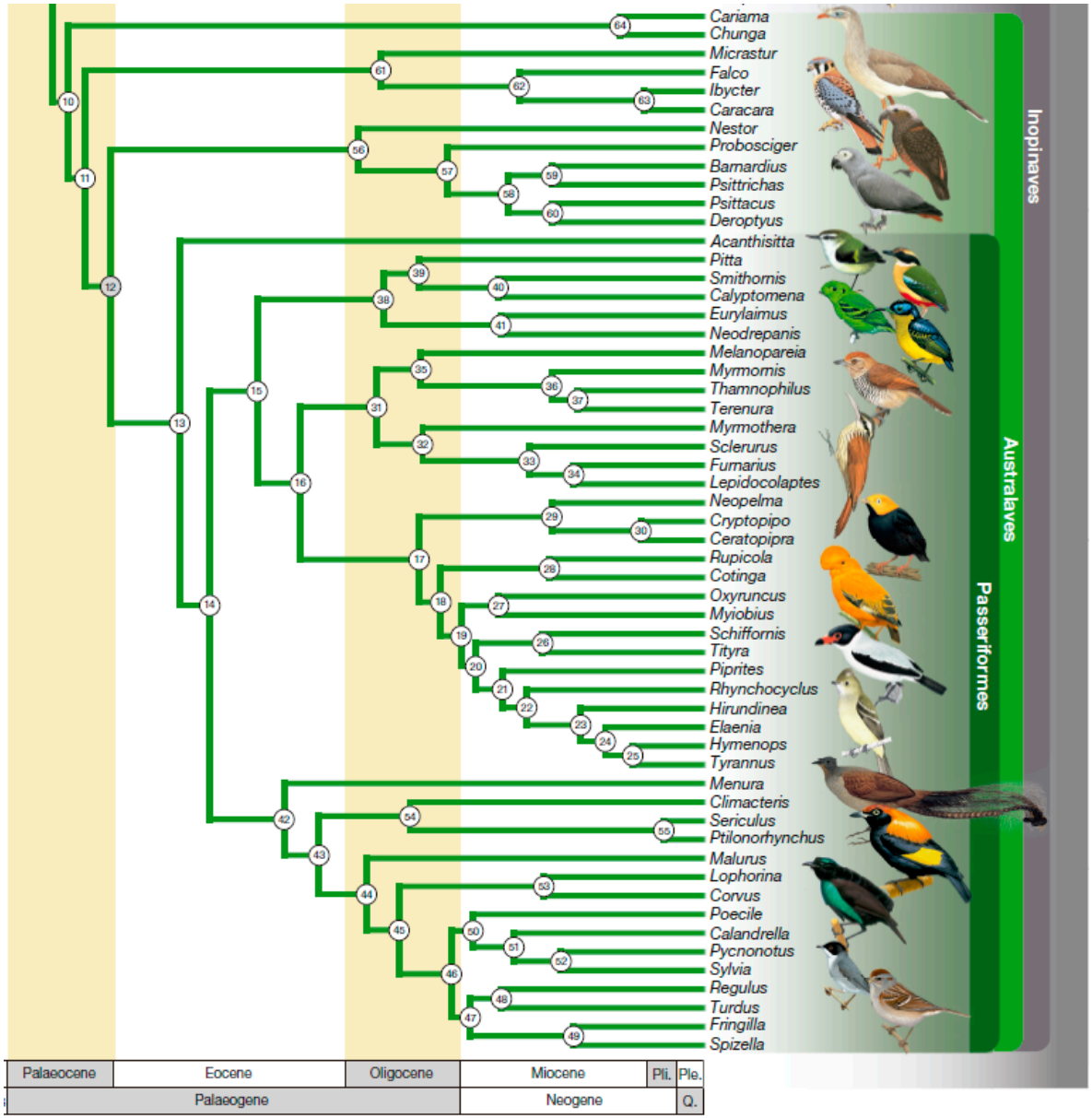

Cariamiformes:
Cariamidae (Seriemas)

Según la filogenia molecular se ubicarían basales a Falcónidos (halcones y caranchos), Psittaciformes (loros) y Passeriformes (aves canoras). Antiguamente eran clasificados como “Gruiformes”, hoy grupo polifilético.

Cariamiformes: Phorusrhacidae

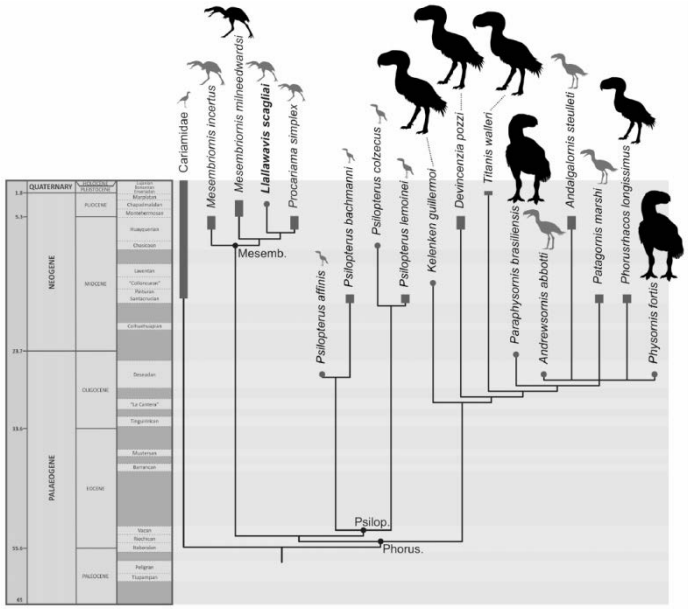

FIGURE 10. Phylogenetic relationships of *L. scagliai* among phorusrhacids. Silhouettes indicate body size according to Degrange (2012). Black silhouettes indicate birds of more than ~70 kg. Different phorusrhacids seem to have attained gigantic body size independently in the early Miocene and Pliocene. **Abbreviations**: **Mesemb.**, Mesembriornithinae; **Phorus.**, Phorusrhacidae; **Psilop.**, Psilopterinae.

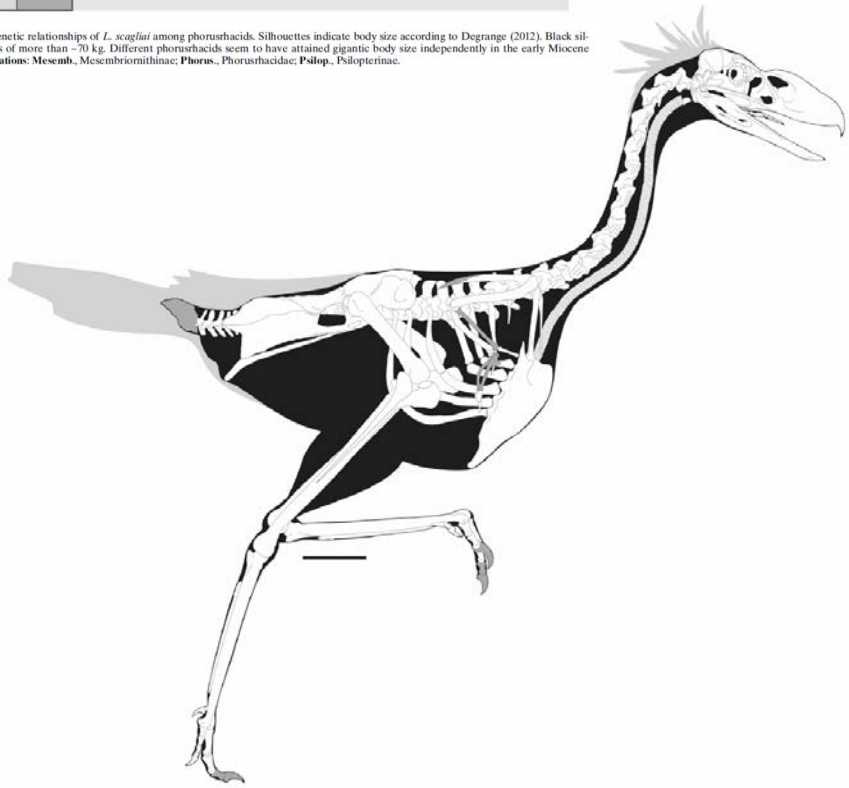

FIGURE 2. Skeletal anatomy of *Llallawavis scagliai*, gen. et sp. nov. MMP 5050. Bones colored in gray are missing. Scale bar equals 0.10 m.

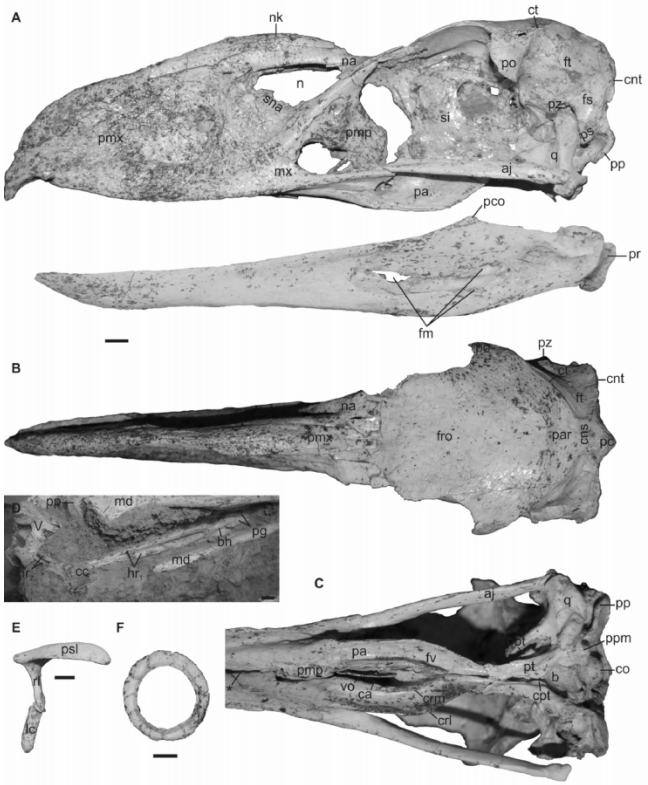

←FIGURE 3. The skull of *Llallawavis scagliai*, gen. et sp. nov. Autapomorphies are noted by an asterisk. **A**, **B**, skull and mandible in **A**, lateral view and **B**, dorsal view; **C**, detail of the palate (ventral view); **D**, hyoid apparatus (during preparation); **E**, os lacrimale and os lacrimale communicans; **F**, scleral ring of the left eye. Note that the beak is high and narrow, as in all phorusrhacids, although it is proportionally longer. **Abbreviations**: **aj**, arcus jugalis; **b**, lamina basitemporalis (= lamina parasphenoidalis); **bh**, basihyale; **ca**, choanes; **cc**, cricoid cartilage; **cns**, crista nuchalis sagittalis; **cnt**, crista nuchalis transversa; **co**, condylus occipitalis; **crl**, crista lateralis (os palatinum); **crm**, crista medialis (os palatinum); **cpt**, pterygoid process; **ct**, crista temporalis; **fm**, mandible fenestra; **fro**, os frontale; **fs**, fossa subtemporalis; **ft**, fossa temporalis; **fv**, fossa ventralis (os palatinum); **hr**, hyoid ramus; **lc**, os lacrimale communicans; **md**, mandible; **mx**, os maxillare; **n**, nares; **na**, os nasale; **nk**, narial knob; **pa**, os palatinum; **par**, os parietale; **pbt**, processus basipterygoideus; **pc**, prominentia cerebellaris; **pco**, processus coronoideus; **pg**, paraglossum; **pmp**, processus maxillopalatinus; **pmx**, os premaxillare; **po**, processus postorbitalis; **pp**, processus paraoccipitalis; **ppm**, processus medialis parasphenoidalis; **pr**, processus retroarticularis; **ps**, processus suprameaticus; **psl**, processus supraorbitalis (os lacrimale); **pt**, os pterygoideus; **pz**, processus zygomaticus; **q**, os quadratum; **rl**, processus orbitalis (os lacrimale); **si**, septum interorbitale; **sna**, septum nasi osseum; **V_2**, second cervical vertebra (axis); **vo**, vomer. Scale bars equal 1 cm.

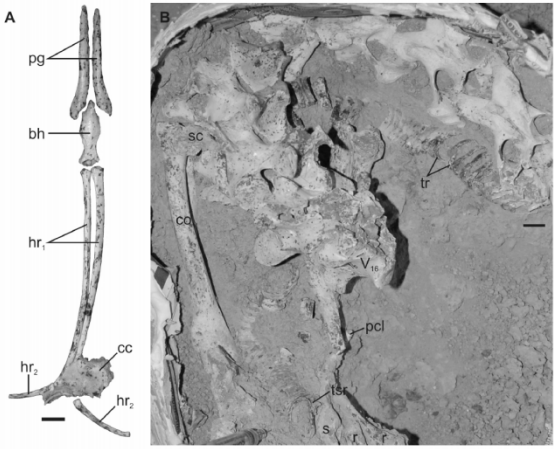

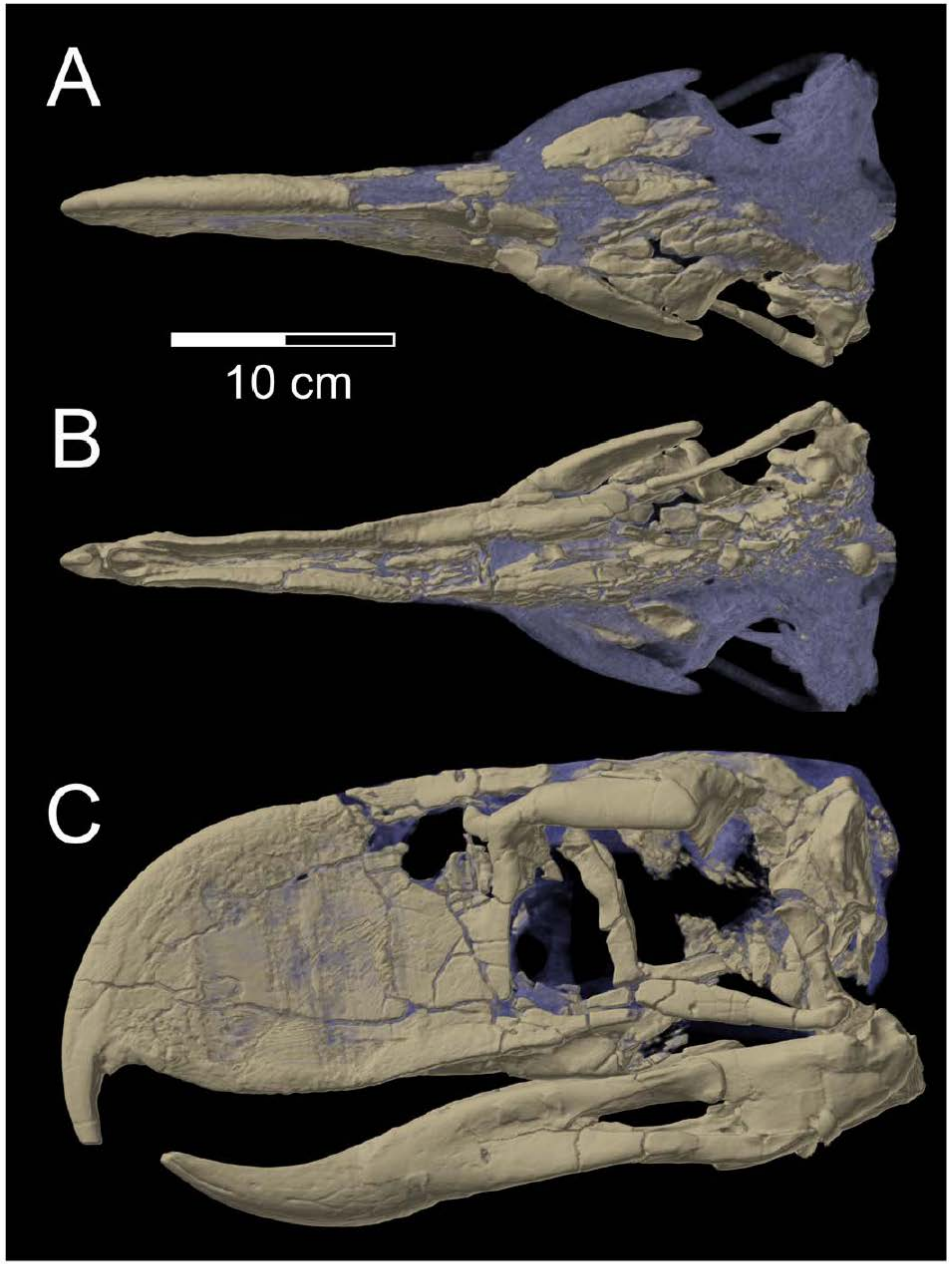

Figure 1. Skull of *Andalgalornis steulleti* (FMNH P1435). A, dorsal view, B, ventral view, and C, left lateral view scan data. Fossil bone is shown in light brown, and rock matrix and plaster restoration are shown in grey.
doi:10.1371/journal.pone.0011856.g001

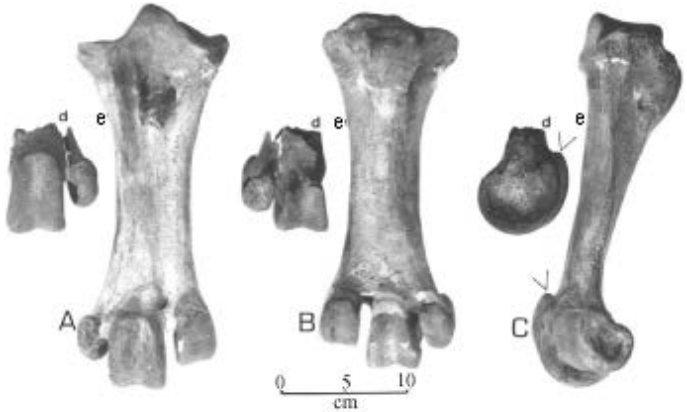

FIGURE 8. *Brontornis burmeisteri* (FM-P13259), left complete tarsometatarsus (l) and distal end of the right one (r), in dorsal view (A), plantar view (B), and lateral view (C). This specimen, around 25% smaller than the lectotype (MLP-91), represents an important variation in size in these birds. The arrow in "C" indicates the dorsoproximal spreading of the edge of the articular surface of the middle trochlea, a characteristic of the Brontornithinae.

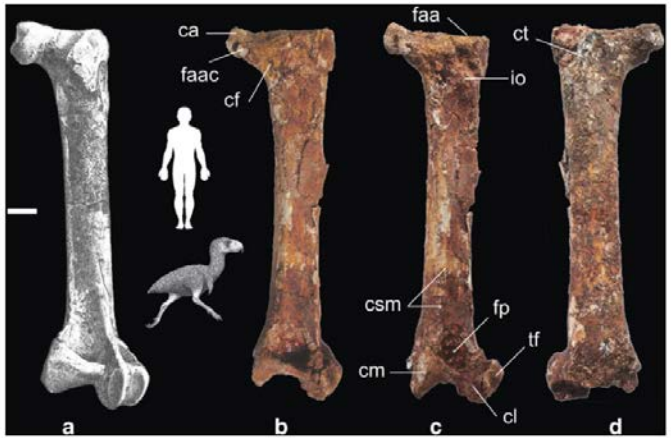

Fig. 2 Femur of *Lavocatavis africana* gen. et sp. nov. in comparison to that of *Patagornis marshi* Moreno and Mercerat 1891, early to middle Miocene of Argentina. *Patagornis marshi*, left femur, reversed, a caudal view, after Andrews (1899, pl. XVII, figure 8) and reconstruction of the Patagornithine *Andalgalornis steulleti* (Patterson and Kraglievich 1960) scaled for comparison to a human (Alvarenga and Höfling 2003); femur measurements (Table 1) indicate that *P. marshi* and *L. africana* were of similar body size. *L. africana*, right femur, holotype, UM HGL 51–55. **b** Caudal view. **c** Caudal view slightly mediocaudally oriented. **d** Cranial view. Abbreviations: *ca* caput femoris, *cf* collum femoris, *cl* condylus lateralis, *cm* condylus medialis, *csm* crista supracondylaris medialis, *ct* crista trochanteris, *faa* facies articularis antitrochanterica, *faac* facies articularis acetabularis, *fp* fossa poplitea, *io* impressiones obturatoriae, *tf* trochlea fibularis. *Scale bar*=2 cm

Registro de Cariamiformes en Chile

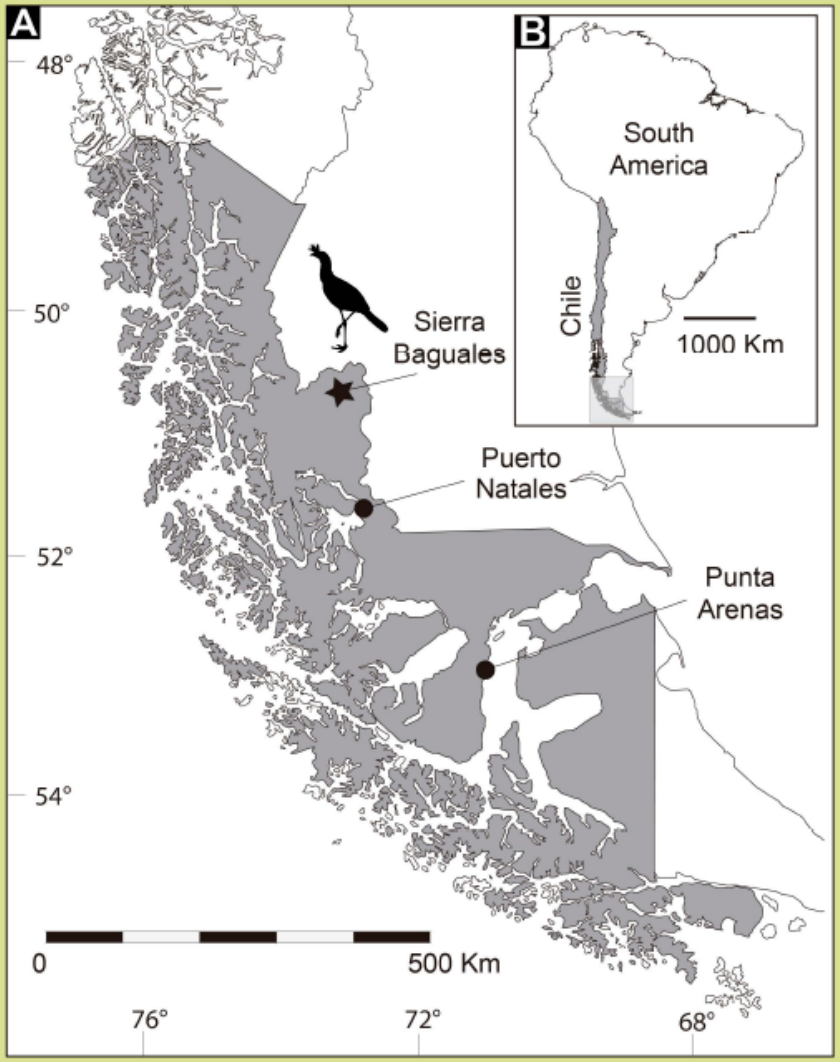

Figure 1: A) Map of the Magallanes Region indicating the locality where CPJLO154 was collected in Sierra Baguales, near to Torres del Paine. B) Map of South America showing the geographical area enlarged in A.

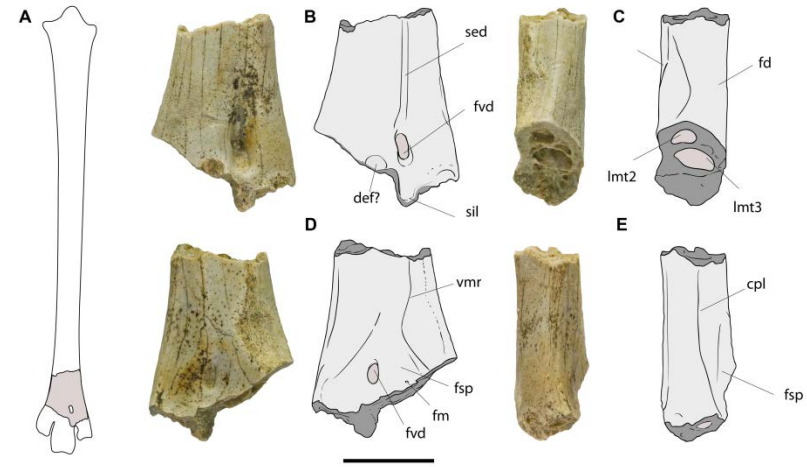

Figure 2: CPJLO154, A) anatomical position of the distal fragment of left tarsometatarsus from Santa Cruz Formation levels (Burdigalian) in Sierra Baguales. Photos and drawings of the material in B) dorsal view, C) medial view, D) plantar view, E) lateral view. **Anatomical abbreviations**: **cpl**, crista plantaris lateralis; **def?**, distal extensor fossa?; **fd**, facies dorsalis; **fm**, foramina; **fsp**, fossa supratrochlearis plantaris; **fvd**, foramen vasculare distale; **lmt2**, lumen of metatarsal 2; **lmt3**, lumen of metatarsal 3; **sed**, sulcus extensorius dorsalis; **sil**, surface of the incisura intertrochlearis lateralis; **vmr**, ventro-medial ridge. Scale bar = 10 mm.

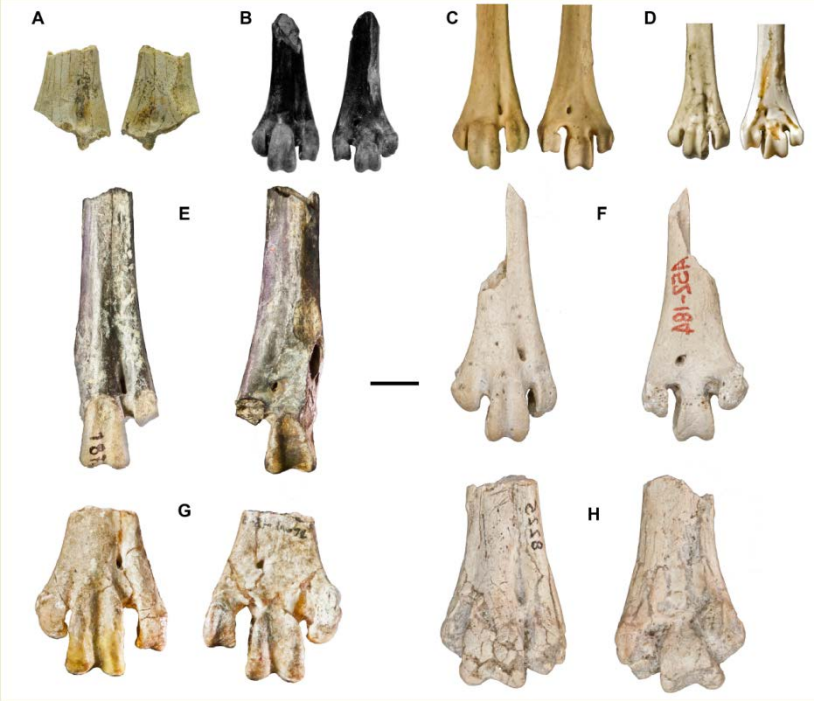

Figure 3. Comparison of the dorsal an ventral aspect of the CPJLO154 with fossil and living seriemas (Cariamidae) and gracile "terror-birds" (Phorhusracidae: Psilopterinae): A) Cariamidae indet. CPJLO154; B) *Noriegavis santacrucensis* MPM-PV 15049 (modified from Mayr and Noriega in press); C) *Cariama cristata* MNHN 5480; D) *Chunga burmeisteri*; E) *Psilopterus bachmanni* MLP 20-187; F) *Psilopterus affinis* MACN-A 52-184 (holotype, reversed for better comparison); G) *Psilopterus colzeccus* MLP 76-VI-12- 2 (holotype); H) *Procariama simplex* MACN-PV 8225 (holotype, reversed for better comparison). Scale bar = 10 mm.

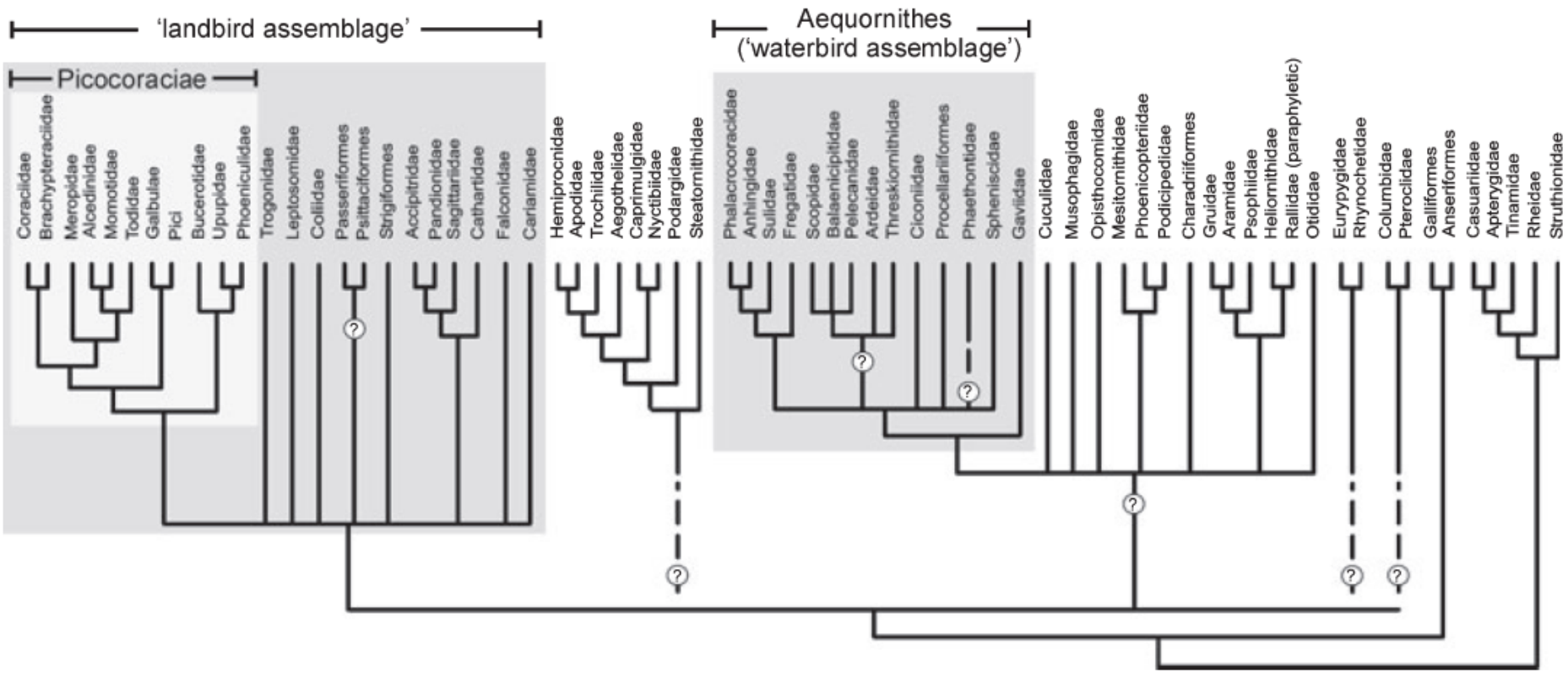

Fig. 5. Summary phylogenetic hypothesis as discussed in the present review. Question marks on dashed lines indicate that the position of a clade is uncertain, whereas question marks on continuous lines demark weakly supported clades. The shaded fields outline composition of the 'land bird assemblage' and the newly introduced terms Picocoraciae and Aequornithes ('waterbird assemblage')

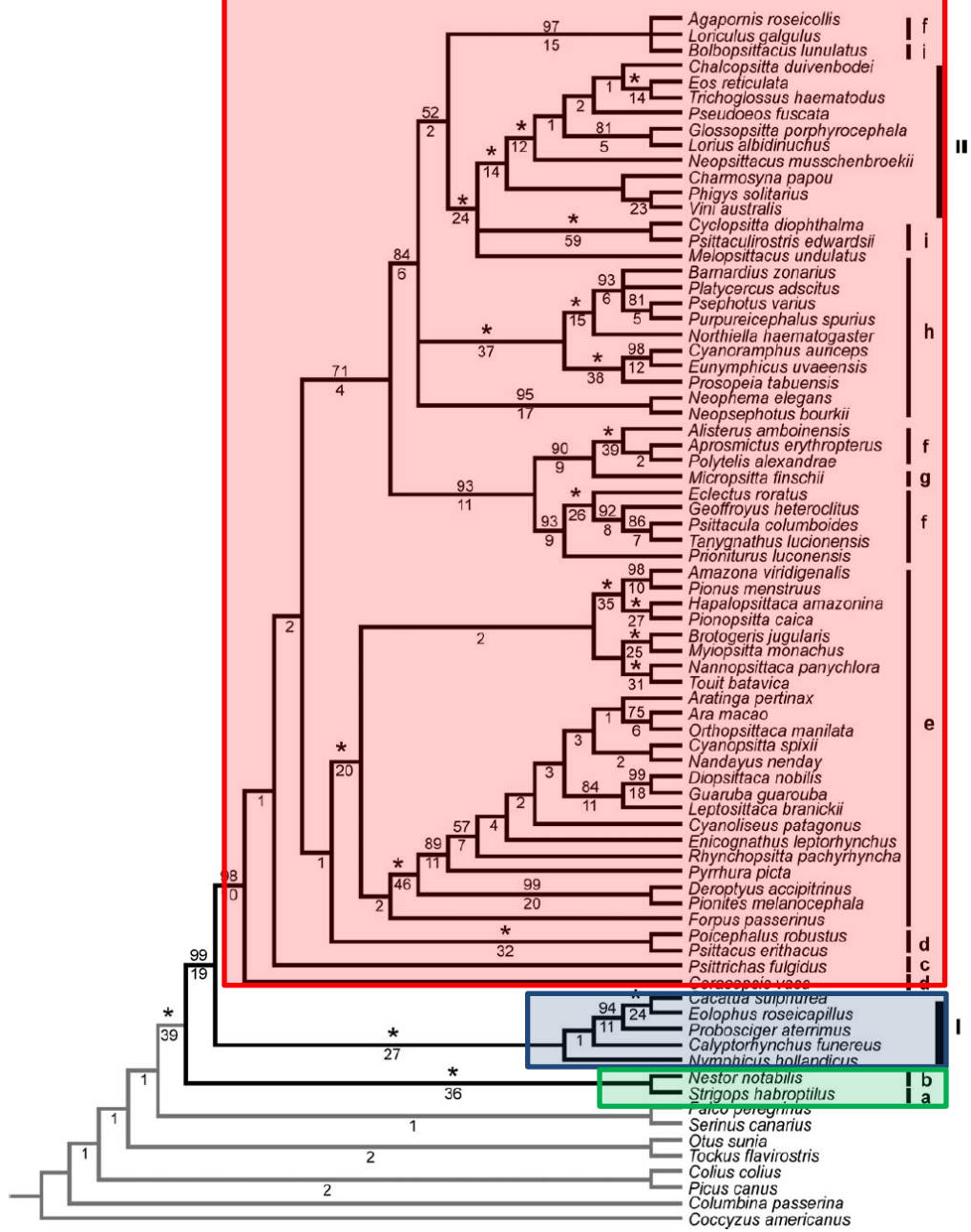

FIG. 1.—Cladogram of relationships among representatives of 69 parrot genera and 8 outgroup taxa based on a strict consensus of 4 trees obtained from combined parsimony (MP) analysis of the 4 sequence partitions (COI + ND2, TROP, TGFB2, and RDPSN) with coded gaps. MP bootstrap support values for each node are shown above the branches with values of 100% indicated by asterisks; Bremer decay index values are shown below. The classifications of Rowley (1997) and Collar (1997) are indicated by bars on the right: I) family Cacatuidae, II) subfamily Loriinae, and, within the subfamily Psittacinae, the tribes a) Strigopini, b) Nestorini, c) Psittrichadini, d) Psittacini e) Arini, f) Psittaculini, g) Micropsittini, h) Platycercini, and i) Cyclopsittacini.

Stem-Psittaciformes

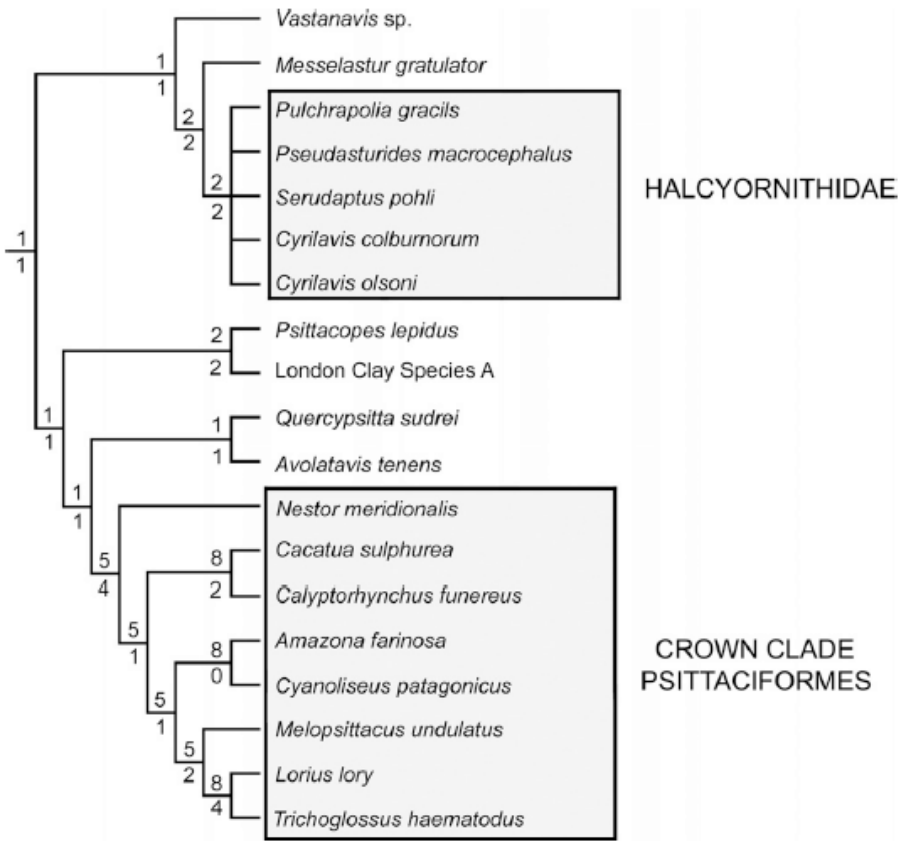

FIGURE 4. Strict consensus tree (TL = 2769 steps, RI = 0.617, RC = 0.448) from combined analysis of 106 morphological characters and sequence data from cytochrome *b*, RAG-1, and the third intron of the Z-chromosomal spindlin gene. The strict consensus tree from the analysis using only the morphological data set is congruent except that one additional branch is collapsed. Bremer support values for the combined tree are placed above the appropriate branches, and Bremer support values for the morphological tree are placed below the appropriate branches. Note that the single branch that was not recovered in the morphological analysis is indicated by a Bremer value of 0.

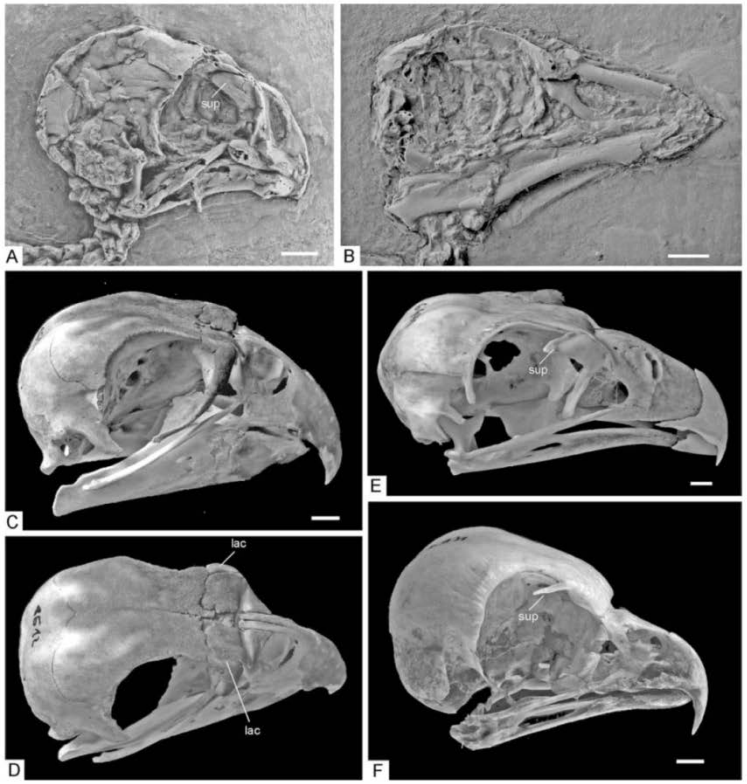

Figure 2. Skulls in comparison. **A,** *Messelastur gratulator* Peters, 1994 from the Middle Eocene of Messel (holotype, SMF-ME 2024); **B,** *Serudaptus pohli* Mayr, 2000b from the Middle Eocene of Messel (Halcyornithidae; holotype, WDC-C-MG 201a); **C, D,** Red-lored Amazon, *Amazona autumnalis* (Psittacidae), juvenile specimen in lateral (C) and dorsolateral (D) view; **E,** Crested Caracara, *Caracara plancus* (Falconidae); **F,** Hawk-Owl, *Surnia ulula* (Strigidae). Abbreviations: lac, os lacrimale; sup, processus supraorbitalis. Fossil specimens are coated with ammonium chloride. Scale bars = 5 mm.

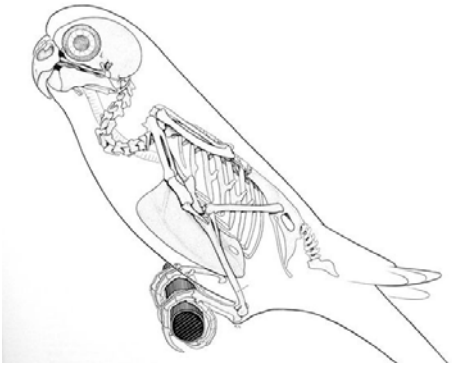

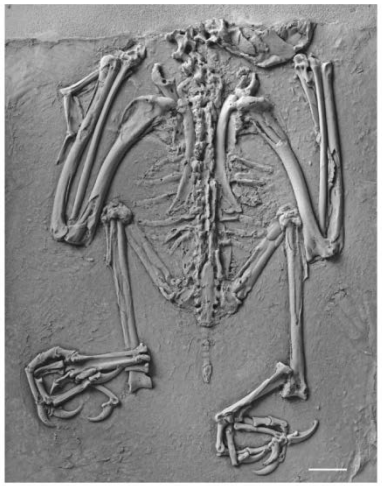

Figure 1. Postcranial skeleton of *Messelastur gratulator* Peters, 1994 from the Middle Eocene of Messel (SMF-ME 11348). Coated with ammonium chloride. Scale bar = 10 mm.

Stem-Psittaciformes

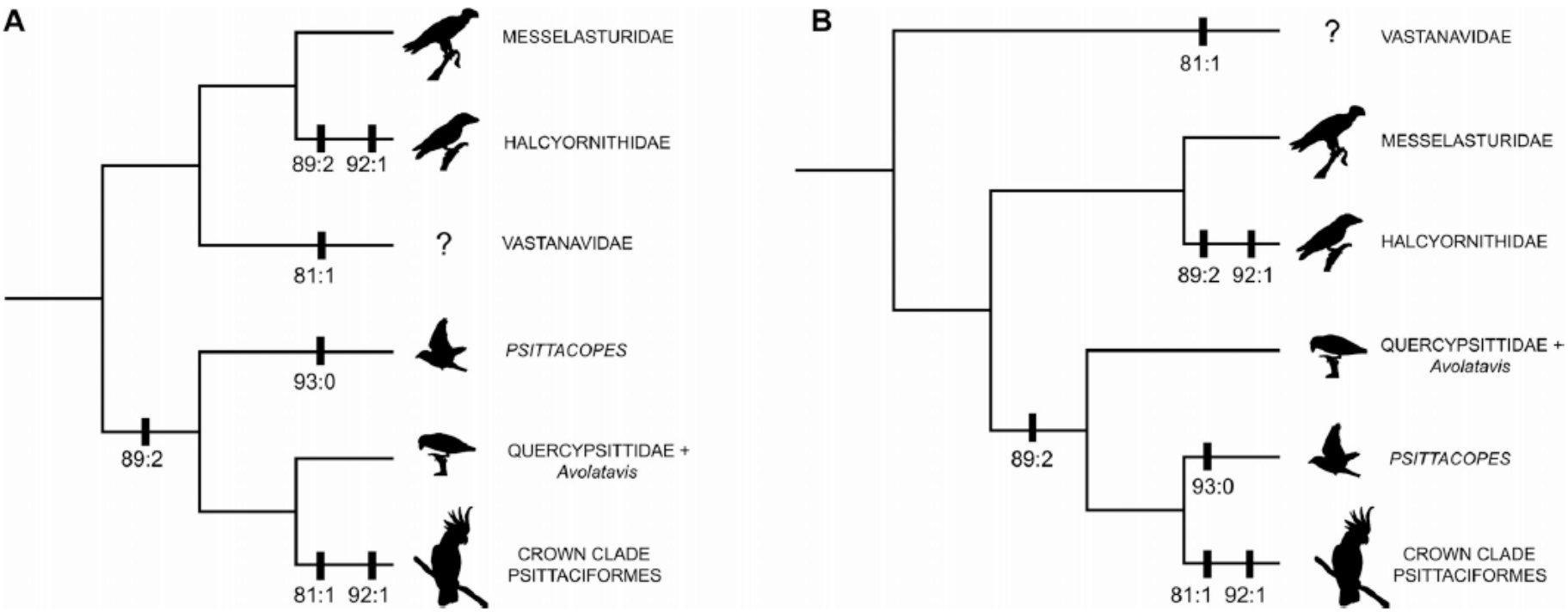

FIGURE 5. Alternate hypotheses for Pan-Psittaciformes phylogeny mapping key characters of the grasping foot that evolved multiple times within the clade. **A**, phylogeny from the analysis presented in this paper; **B**, phylogeny preferred by Mayr et al. (2010), with *Avolatavis* inserted based on results presented in this paper. Character numbers correspond to the phylogenetic matrix: **81(1)**, fossa metatarsi I shifted to medial face of tarsometatarsus; **89(2)**, presence of fully developed trochlea accessoria of metatarsal IV; **92(1)**, pedal digits III–IV robust and digit II gracile; **93(0)**, proximal 3 phalanges of digit IV subequal in length to penultimate phalanx (reversal from greatly abbreviated).

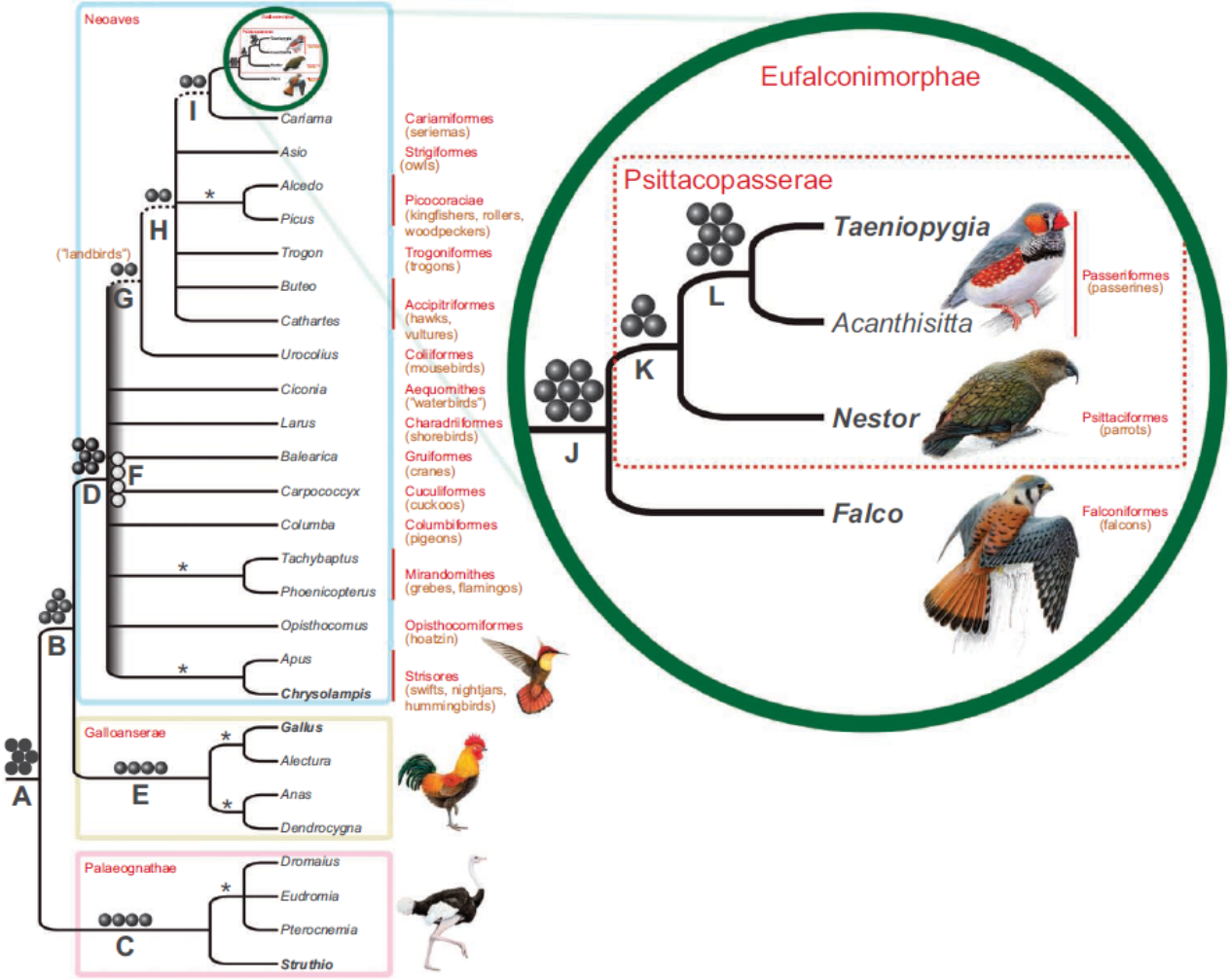

Figure 1 | Retroposon evidence for the early branching events in the avian tree of life. The tree topology is derived from our presence/absence matrix (Supplementary Table S1; Supplementary Software) utilizing maximum parsimony and considering representatives of the key avian lineages[13,14]. Black filled circles (branch A) are bird-specific retroposon insertions (exhibiting a 6-nt deletion that is found in some avian CR1s, but absent in all other avian and reptilian CR1s), and dark grey balls represent retroposon presence/absence markers that are congruent with one another. Light grey balls on grey gradient (label F) are retroposon markers that were probably inserted at the very beginning of the neoavian radiation and were subjected to incomplete lineage sorting of retroposon dimorphisms, as they exhibit presence/absence patterns that are incongruent with one another and with some of the retroposon markers on the dashed branches. Nodes without retroposon support are not collapsed (but highlighted by asterisks) if they received very strong support in nucleotide sequence analyses[12-14]. Higher-ranking taxa are in red letters (English terms in orange letters and parentheses), including the new taxa Eufalconimorphae (falcons + parrots + passerines) and Psittacopasserae (parrots + passerines), and some recently introduced superordinal groupings[14,53,54]. Bird names in bold letters belong to the nearest bird icon.

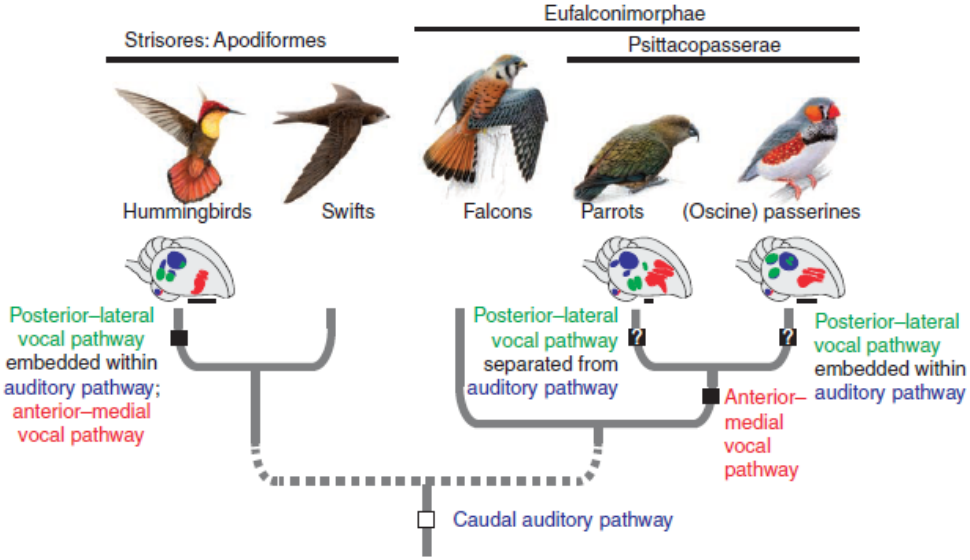

Figure 4 | Evolution of vocal learning in birds. Schematic brain drawings (adapted from Jarvis *et al.*[31]) depict the hearing- and vocalizing-induced ZENK transcription factor expressions in hummingbirds, budgerigars (parrot representatives) and songbirds (passerine representatives). Our robust phylogenetic framework implies that some traits associated with vocal learning (for example, the anterior–medial vocal pathway (red)) are potentially homologous and thus evolved as an autapomorphic trait (black square) in the psittacopasseran ancestor, but also independently in the distantly related ancestor of hummingbirds (dashed lines indicate that several neoavian lineages are not shown). Neuroanatomical studies on early branching passerines (that is, Suboscines and Acanthisittidae) are necessary to infer that the posterior–lateral vocal pathway (green, located at different brain regions in parrots and oscine passerines) is either homologous or evolved independently in the two lineages. The caudal auditory pathway (blue) is a plesiomorphic trait (white square) and was probably inherited from a common avian ancestor[32]. The putative location of the auditory pathway in falcons and swifts is not shown, as ZENK expression patterns have, to our knowledge, not yet been investigated in these birds. Scale bar, 2 mm.

Zygodactylidae

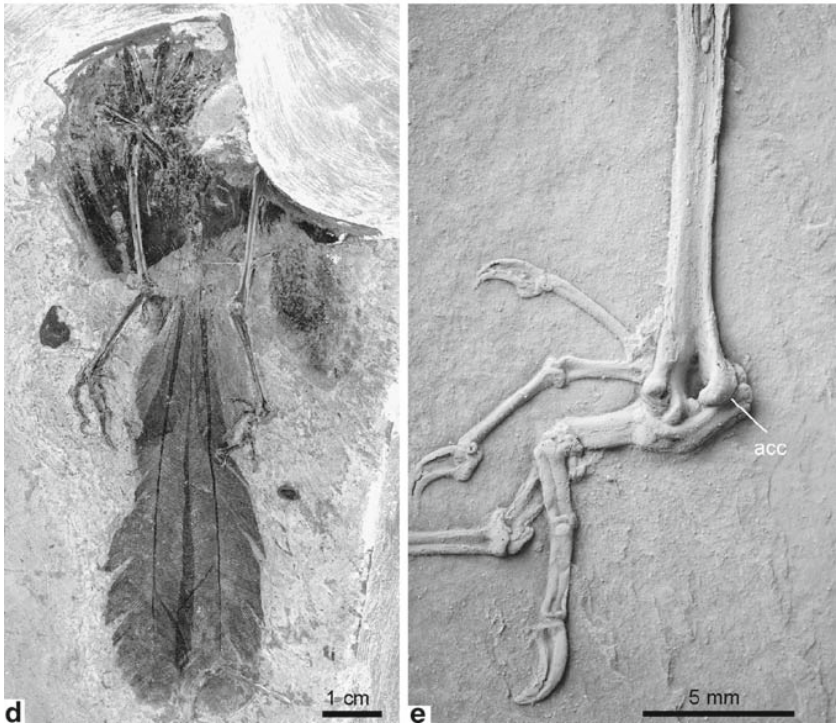

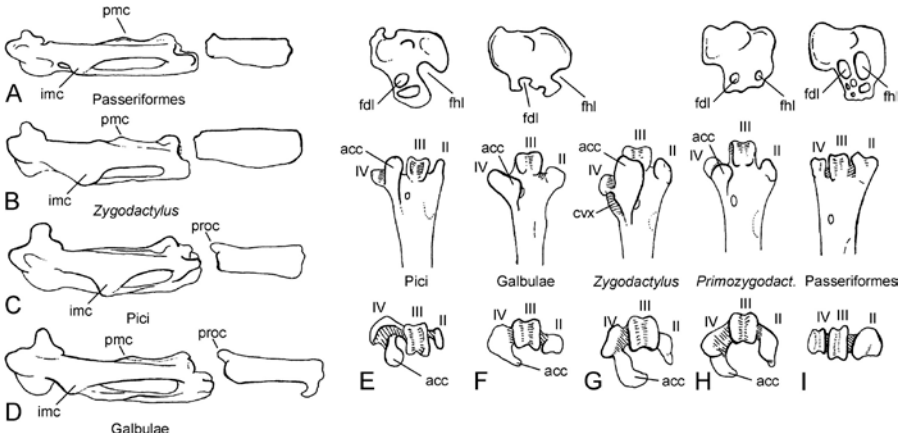

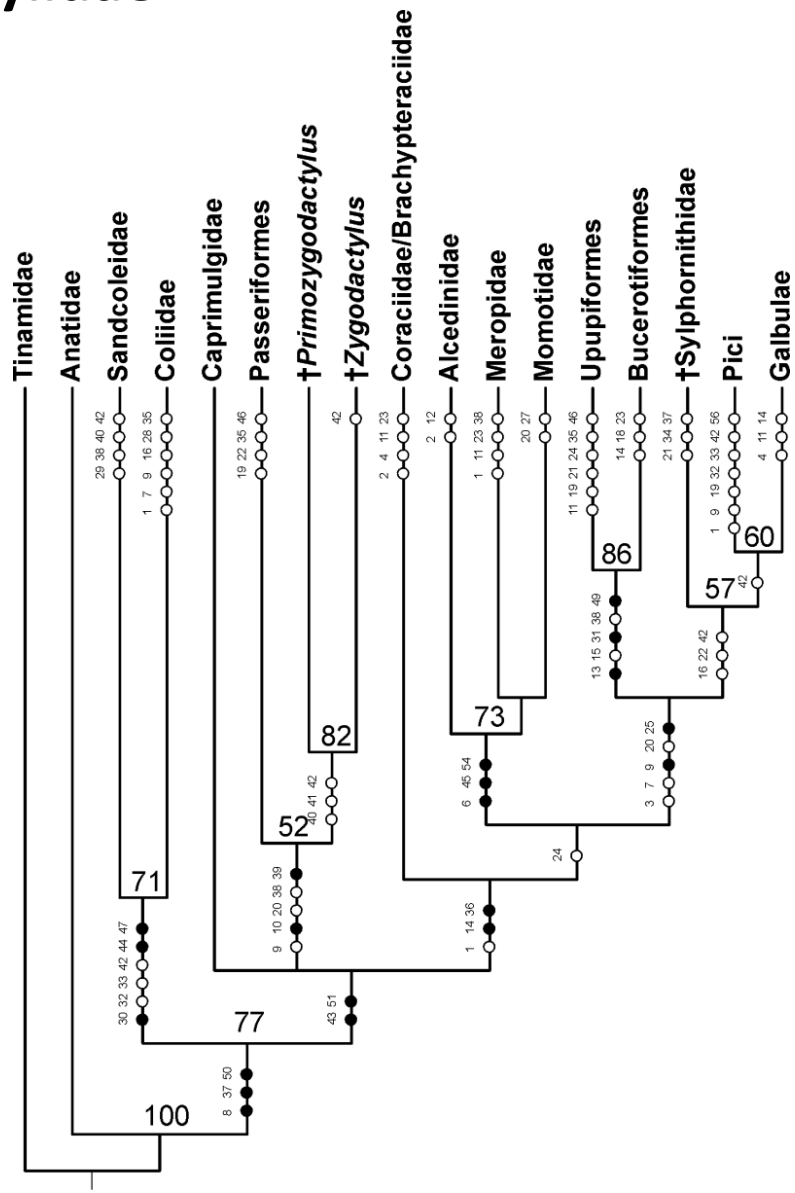

Passeriformes

Jamna szybiaki
(Oligoceno temprano)

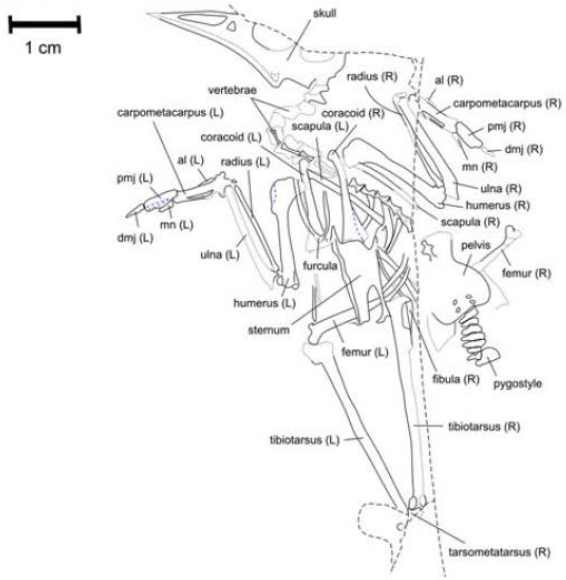

Fig. 1 *Jamna szybiaki* gen. et sp. nov., holotype, specimen MSMD Av JAM-6 from Jamna Dolna, Poland, early Oligocene (*top*) and interpretative drawing (*bottom*). Left (*L*) and right (*R*) elements are indicated. *al* Phalanx digiti alulae, *dmj* phalanx distalis digiti majoris, *mn* phalanx digiti minoris, *pmj* phalanx proximalis digiti majoris

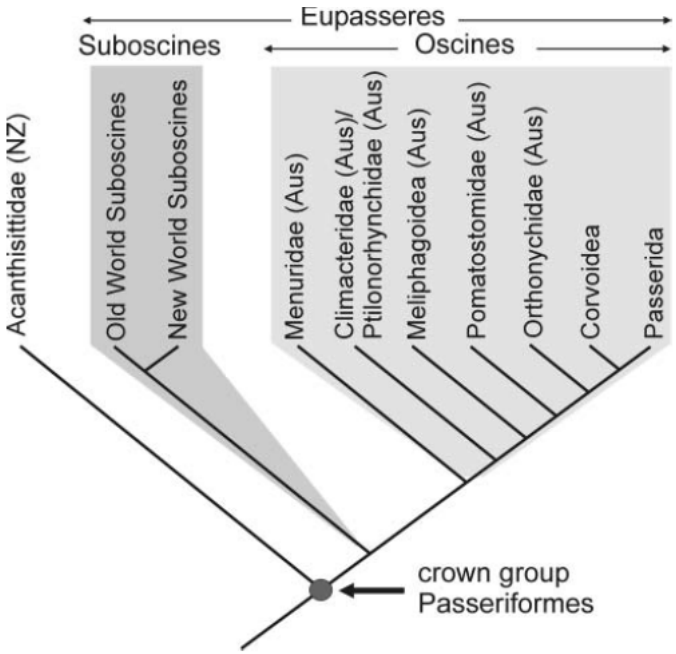

Fig. 1. Consensus phylogenetic inter-relationships of crown group Passeriformes as obtained from analyses of molecular sequence data. Taxa, which only occur in New Zealand (NZ) or Australia/New Guinea (Aus) are labelled. Note that Old World Suboscines include one New World representative, the Broad-billed Sapayoa (*Sapayoa enigma*; e.g. Fjeldså *et al.*, 2003).

Registro más antiguo de stem paserinos (Eoceno temprano)

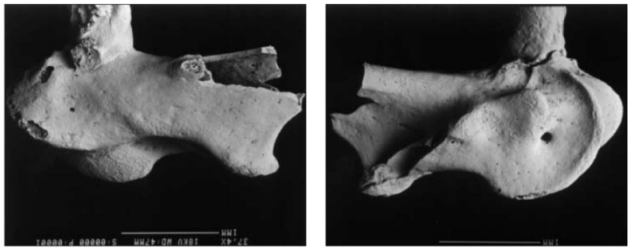

Figure 1 Proximal carpometacarpal fragment (QM F20688) from Murgon: (a) dorsal view and (b) ventral view. Line equals 1 mm.

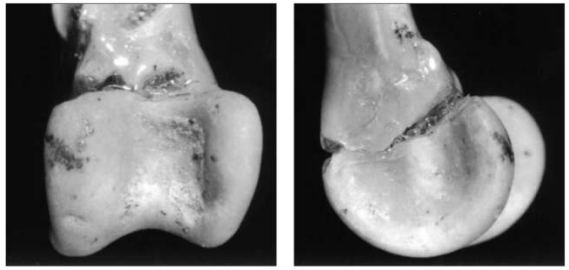

Figure 2 Distal tibiotarsal fragment (QM F24685) from Murgon: (a) cranial view ands (b) lateral view. Distal width 4.1 mm.

Origen y Radiación de Passeriformes

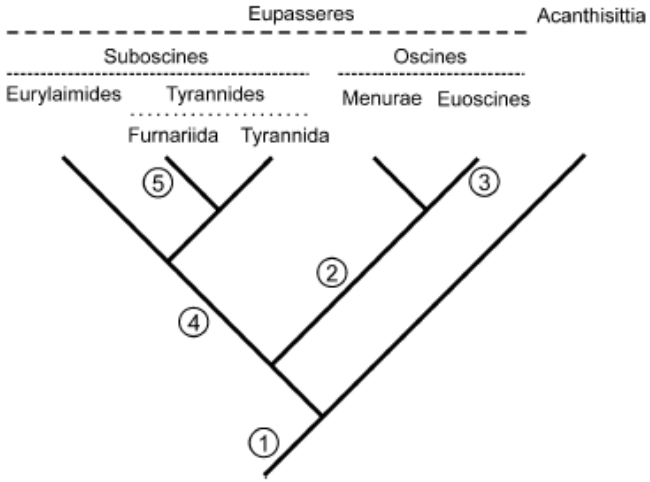

Fig. 8. Graphic representation of the provisional classification based on DNA sequence data (see Table 2). The taxonomic distribution of the morphological characters that traditionally have been used to infer relationships among basal passerines is fully consistent with this phylogenetic tree. Node 1: aegithognathous palate, "passerine" tensor propatagialis brevis, bundled spermatozoa with coiled head, enlarged hallux, and type VII deep plantar tendons (Raikow 1982). Node 2: acromyodian (oscine) syrinx (Müller 1847, Garrod 1876). Node 3: syrinx with four intrinsic muscles (Ames 1971). Node 4: stapal bone (columella) with expanded foot (Feduccia 1975). Node 5: tracheophone syrinx (Garrod 1876, Ames 1971). From Ericson et al. (2002b).

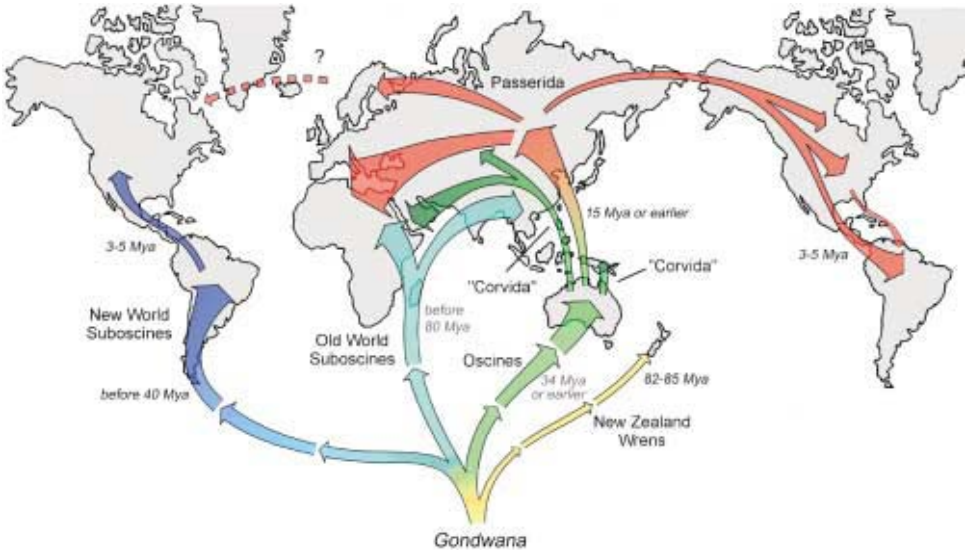

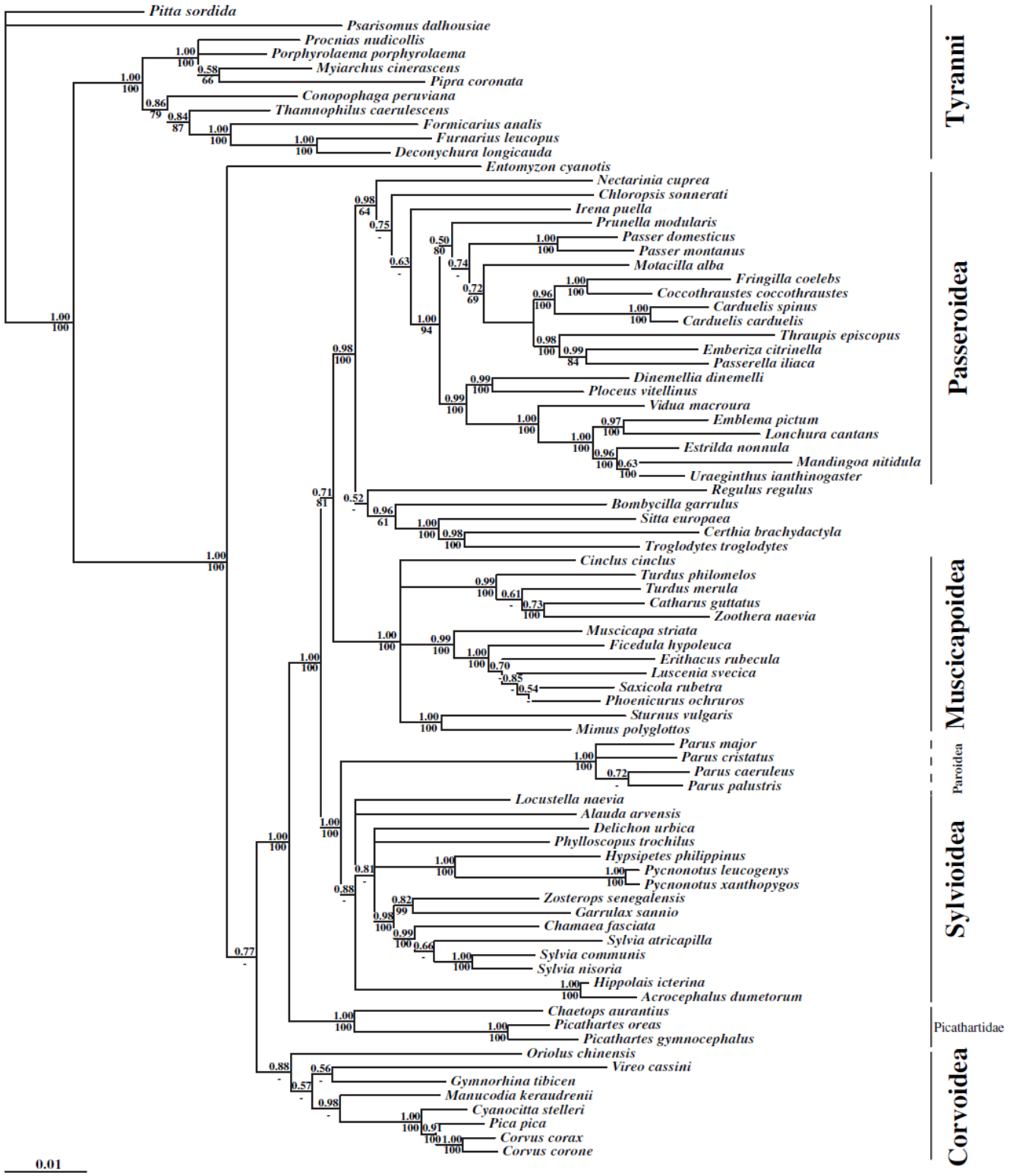

Fig. 1. Phylogenetic tree of the Bayesian analysis of the ZENK data set with Bayesian (upper value) and MP ratchet (lower value) support added at each node. Within Sylvioidea, the dashed line refers to "Paroidea".

Tyranii

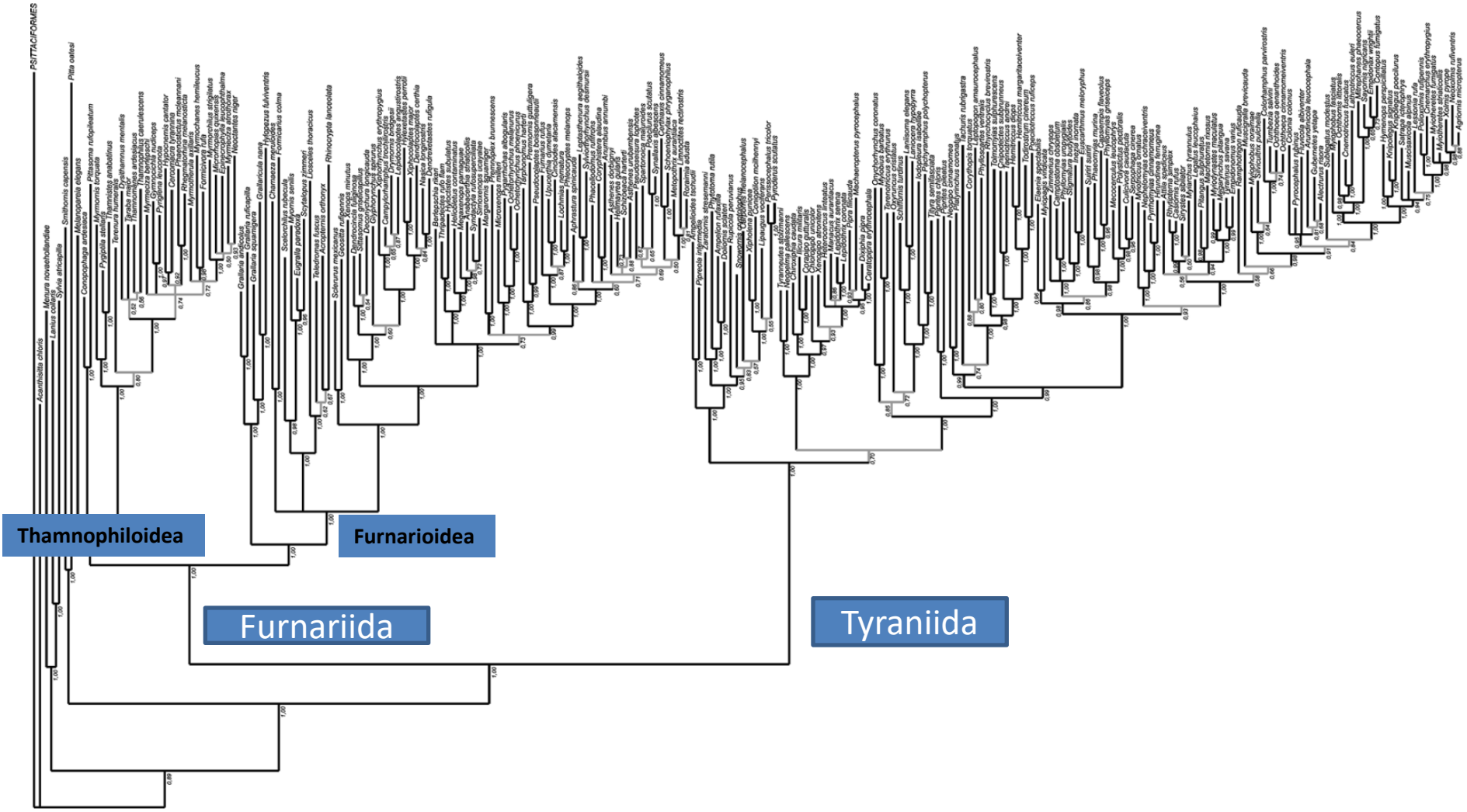
PSITTACIFORMES
Thamnophiloidea
Furnarioidea
Furnariida
Tyraniida

Diversificación de Passeriformes Calibrada temporalmente: Inconsistencia con registro fósil

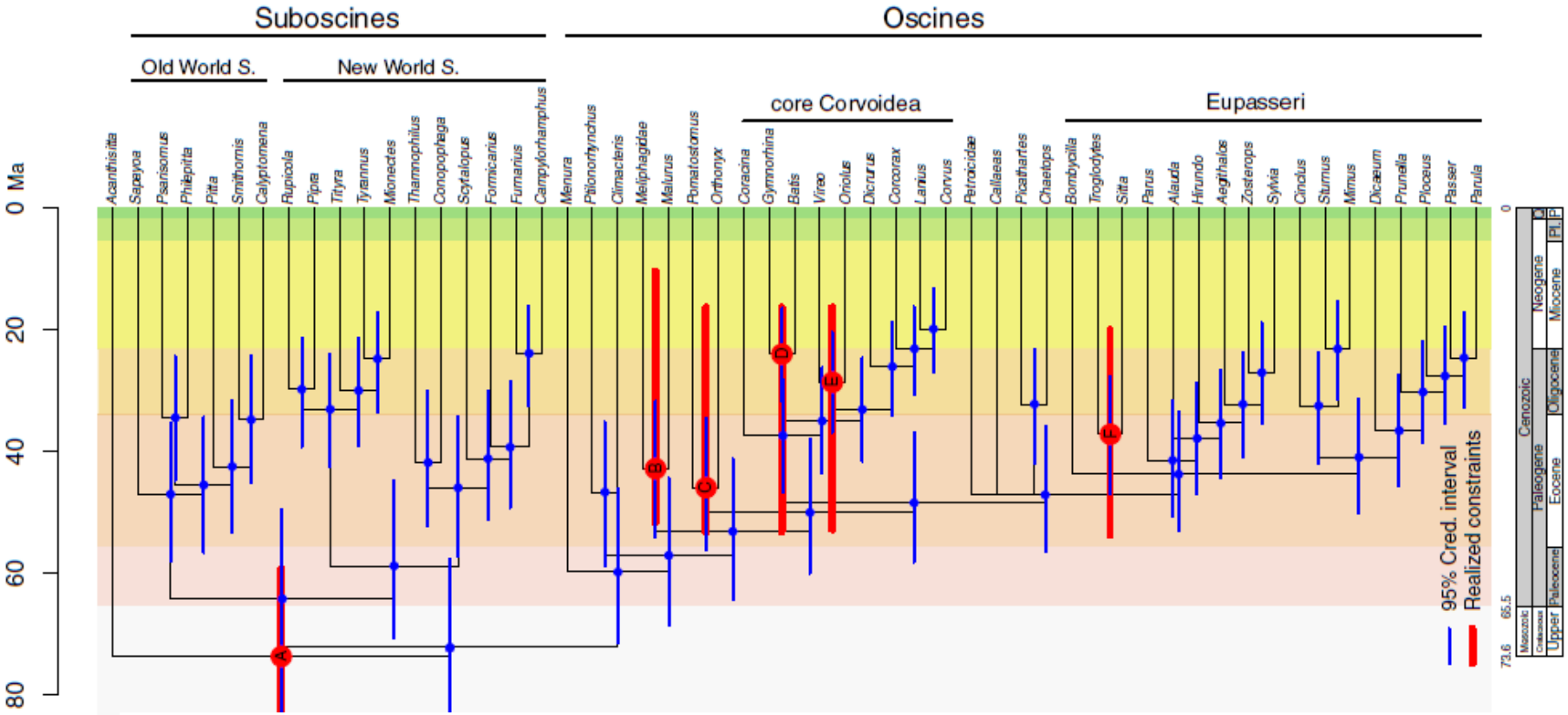

(See figure on previous page.)

Figure 1 Phylogenetic estimate of the evolutionary time-scale of passerines, with 95% credibility intervals plotted for estimated divergence times (thin blue bars). Thick red bars represent the realized age priors (95%) for the constrained nodes. Labels **A-F** indicate calibration points and fossil placements, **A**: vicariance event separating New Zealand from Antarctica, **B**: honeyeater (Meliphagidae) [44], **C**: logrunner (Orthonychidae) (JMTN, unpublished observations), **D**: crown-group cracticid (Cracticidae) [41], **E**: oriolid (Oriolidae) [42], **F**: "climbing Certhioidea" [43]. Panel below figure indicates the geological time line; Q: Quaternary, Pl.: Pliocene, P: Pleistocene.

ure 1 (See legend on next page.)

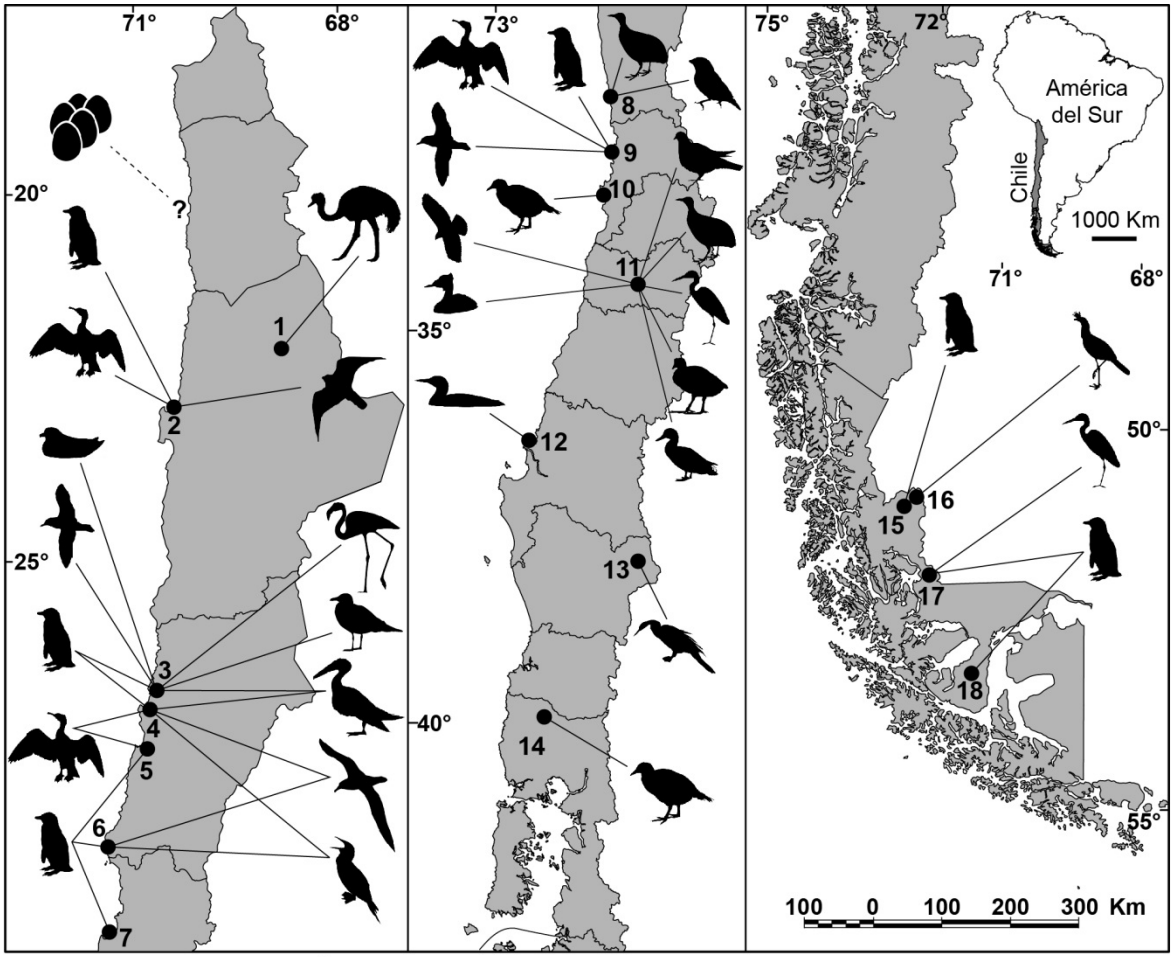

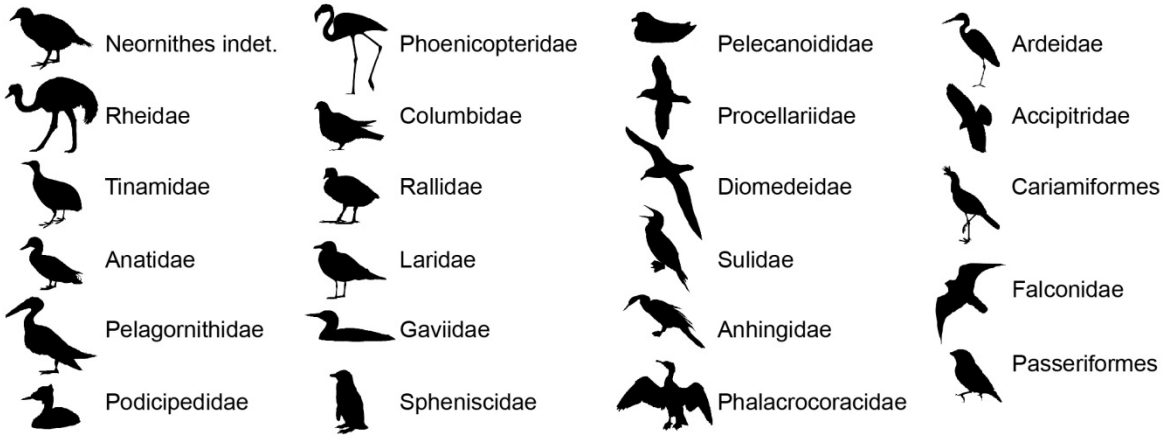

Localidades con aves fósiles en Chile

1) **Kamac Mayu**, Región de Antofagasta. Pleistoceno.

2) **Mejillones**, Región de Antofagasta. Formación La Portada (Plioceno).

3) **Cerro Ballena**, Región de Atacama. Estratos de Caldera (Pleistoceno).

4) **Bahía Inglesa**, Región de Atacama.
Formación Bahía Inglesa (Mioceno medio-Plioceno).

5) **Bahía Salada**, Región de Atacama.
Formación Bahía Inglesa (Mioceno medio-Plioceno).

6) **Chañaral de Aceituno**, Región de Atacama.
Formación Coquimbo (Mioceno medio-Plioceno).

7) **La Cantera**, Región de Coquimbo.
Formación Coquimbo (Mioceno medio-Plioceno).

8) **Quereo**, Región de Coquimbo.
Formación Quebrada Quereo (Pleistoceno).

9) **Maitencillo-Horcón**, Región de Valparaíso.
Formación Horcón (Plioceno).

10) **Algarrobo**, Región de Valparaíso. Estratos de Algarrobo (Eoceno).

11) **Laguna de Tagua Tagua**, Región de O'Higgins.
Formación Laguna de Taguatagua (Pleistoceno).

12) **San Vicente**, Región del Bíobio.
Formación Quiriquina (Maastrichtiano superior).

13) **Cerro Rucañanco**, Región de La Araucanía.
Formación Cura-Mallín (Mioceno temprano).

14) **Pilauco Bajo**, Región de Los Lagos.
Unidad no formalizada (Pleistoceno).

15) **Sierra Baguales**, Región de Magallanes.
Formación Man Aike (Eoceno medio-superior).

16) **Sierra Baguales**, Región de Magallanes.
Formación Santa Cruz (Burdigaliano).

17) **Sierra Dorotea**, Región de Magallanes.
Formación Río Turbio (Eoceno medio-superior).

18) **Río de las Minas**, Región de Magallanes.
Formación Loreto (Eoceno superior).